INNATE IMMUNE TRAINING RESTORES PRO-REPARATIVE MYELOID FUNCTIONS FOR REMYELINATION IN AGED CENTRAL NERVOUS SYSTEM

VINI TIWARI

Graduate School of Systemic Neurosciences

LMU Munich

Dissertation der
Graduate School of Systemic Neurosciences der
Ludwig-Maximilians-Universität München

26 JUNE, 2023

Supervisor: Prof. Dr. med Mikael Simons

Institute of Neuronal Cell Biology
Technical University Munich

German Centre for Neurodegenerative Diseases
(DZNE)

First Reviewer: Prof. Dr. med. Mikael Simons
Second Reviewer: Prof. Dr. Axel Imhof
External Reviewer: Prof. Dr. med. Martin S. Weber

Date of Submission: 26 June 2023
Date of Defense: 08 Feb 2024

Table of Contents

Abstract **6**

Introduction **7**

1. Macrophages in the CNS **7**

1.1. Microglia: CNS resident macrophage 7

1.2. Regulation of microglial activation in development and neurodegenerative diseases 10

1.3. Interaction of microglia with other cell types 11

1.4. Diversity of brain-associated macrophages 11

1.5. Contribution of infiltrating myeloid cells in CNS injury 12

2. Remyelination in demyelinating diseases **14**

2.1 Overview of demyelinating diseases 14

2.2 Multiple sclerosis 15

2.3 Factors limiting remyelination efficiency 15

2.4 Models to study MS 17

2.5 Role of microglia in remyelination 17

3. Epigenetic regulation and microglia plasticity **20**

3.1 Epigenetic modifications regulating microglia function 20

3.2 Epigenetic regulation in glial cells during neuroinflammation 24

4. Aging **27**

4.1 The concept of Inflammaging 27

4.2 Myeloid cells involved in Inflammaging 29

4.3 Age associated regulation of microglia 30

4.4 Priming in microglia 31

5. Innate immune memory **33**

5.1 The concept of Innate immune memory (IIM) 33

5.2 Trained immunity 35

5.3 BCG induced Trained immunity 39

5.4 Intersection of microglia priming and Trained immune response 43

6. Lipid processing in myeloid cells **44**

6.1 Myelin debris phagocytosis and degradation 44

6.2 The LXR and RXR pathway 46

6.3 The PPAR pathway 47
6.4 The SREBP pathway 47
6.5 Epigenetic regulation of lipid metabolism : Focus on HDACs 47
Hypothesis and aim of this project 50
Materials and methods 52
1. Materials 52
1.1 Consumables 54
1.2 Primers 54
1.3 Buffers and solutions 55
2. Methods 59
2.1 Animal studies 59
2.2 Immunization/Treatment 61
2.3 Lysolecithin injections 61
2.4 Histological analysis of lesioned mouse CNS tissue 62
2.5 Fluorescent in situ hybridization 63
2.6 Confocal microscopy 63
2.7 Image analysis 64
2.8 In-vitro analysis 65
2.9 Molecular biology analysis 66
2.10 Sequencing 67
2.11 Gene ontology enrichment analysis (GO analysis) 73
2.12 Statistics and reproducibility 73
Results 74
1. Single-nucleus RNA sequencing identifies differences in microglial responses in young and aged mice 74
1.1 Experimental design and quality control for snRNA sequencing 74
1.2 Characterizing the transcriptomic signature of microglia / macrophages in lesions 75
1.3 Differential expression analysis between young and aged microglia / macrophages 77
1.4 Enrichment analysis of microglia in lesions between young and aged mice 79
2. Analysis of the epigenome revealed restricted chromatin accessibility in aged microglia after demyelination injury. 80
2.1 Experimental design for ATAC seq 80
2.2 Quality control and ATAC seq analysis 80

3. Immune training with BCG alters the microglial chromatin landscape of aged mice 84

3.1 CHIP Sequencing identifies greater enrichment of H3K27ac and H3K4me3 histone marks in microglia of aged mice treated with BCG 85

4. The influence of innate immune training on microglia/macrophages by BCG 88

4.1 Myelin repair is enhanced in aged mice by BCG 88

4.2 Innate immune training by BCG improves lipid clearance by microglia and macrophages after demyelinating injury 88

4.3 BCG induces precise microglia activation upon demyelination which is necessary for lesion recovery 91

5. BCG-induced immune training modifies the transcriptome profile of cells in lesions permissive for myelin regeneration 92

5.1 Quality control of differential analysis between BCG and Saline (control) conditions 92

5.2 Transcriptomic analysis identifies genes involved in lipid metabolism and chromatin organization to be enriched in lesions of BCG treated mice 94

6. Understanding the effect of inhibiting Histone deacetylase 1 and 2 in microglia / macrophages 97

6.1 Genetic ablation of HDAC1 and HDAC2 from aged microglia improves lesion recovery 97

6.2 Genetic ablation of HDAC1 and HDAC2 from aged microglia improves lipid clearance and activation 99

7. The contribution of HDAC1,2 in innate immune training 103

7.1 Trained immune response by BCG is abolished in Cx3cr1-HDAC1,2 depleted, aged mice..... 103

Discussion 105

1. Inadequate response of myeloid cells in CNS results in failure of lesion recovery..... 107

1.1 Distinct transcriptomic signature is observed in aged mice following demyelinating injury 107

1.2 Restricted chromatin accessibility is attributed to inadequate transcriptional response in aged mice 108

2. Innate immune training restores myeloid responses in Central Nervous System..... 110

2.1 BCG can induce trained immune response in aged microglia / macrophages 110

2.2 Trained immune response is beneficial for lipid processing and lesion recovery in aged mice. 111

3. Innate immune training encompasses epigenetic regulation 113

3.1 Inhibiting HDAC1,2 in microglia promotes lesion recovery 113

3.2 Innate immune training by BCG is abolished in HDAC1,2 KO mice 114

Conclusion 115

Appendix 116

1. Summary figure 116
2. Protocols 117
3. Custom made Macros in Fiji and R scripts 135
References 136
List of figures 154
List of tables 155
List of abbreviations 156
List of publications 159
Acknowledgements 160
Affidavit / Eidesstattliche Versicherung 163
Author contributions 164

Abstract

The age-related decline in the nervous system's capacity to regenerate impairs functional recovery after demyelinating injury. When damage or inflammation occurs in the brain, microglia are the first line of defense. Recovery from demyelinating injury is hindered by age-related changes in the phenotype of microglia. There is evidence that microglial metabolic capacity is overwhelmed by myelin debris in the aged subjects, preventing tissue regeneration, but the mechanisms underlying this effect are not well understood. Many genes that are inefficiently activated in aged microglia/macrophages in a model of demyelination were found to have epigenetic modifications associated with decreased chromatin accessibility. The ability of aged mice to re-myelinate damaged tissue was restored by selectively deleting two class I histone deacetylases in microglia/macrophages. We used Bacillus Calmette-Guerin (BCG), a live-attenuated vaccine, to train the innate immune system, and detected epigenetic reprogramming of brain-resident myeloid cells and functional restoration of myelin debris clearance and lesion recovery. Further, trained microglia showed enhanced activation and improved myelin lipid metabolism in response to demyelinating injury, a process mediated at least in part by histone deacetylases. Our results provide insight into aging-associated decline in myeloid function and how this decay can be prevented by innate immune system reprogramming. In conclusion, we demonstrate that epigenetically mediated innate immune training of microglia can serve as strategy to convert microglia into pro-reparative state following demyelinating injury.

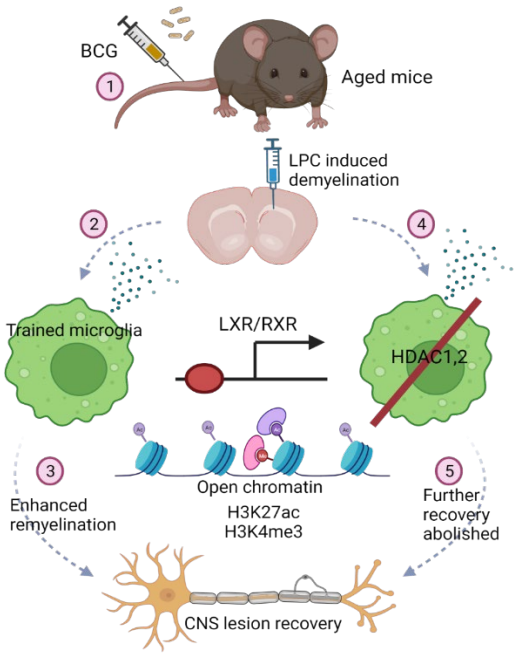

Graphical abstract

Abstract 1.1: The figure illustrates the outline of the current project

(1) When aged animals are injected with BCG, **(2)** critical histone marks such as H3K4me3 and H3K27ac (involved in trained immunological response) are increased in microglia around genes associated with lipid metabolism, inflammation, and innate immune response. **(3)** These epigenomic changes result in appropriate transcription of genes involved in inflammation resolution and lesion recovery following demyelinating damage. **(4)** To better understand the role of HDAC1,2 in innate immune training, when BCG was injected into HDAC1,2 KO and control mice, **(5)** no further enhancement in pro-regenerative functions of microglia or lesion recovery was observed, indicating that histone acetylation is required for memory induction.

Illustration created in (Biorender.com). For abbreviations, please see the list of abbreviation.

Introduction

1. Macrophages in the CNS

Microglia in the CNS parenchyma and non-parenchymal macrophages in the various CNS barriers provide immune surveillance of the CNS. When the central nervous system (CNS) is injured, circulating monocytes can also enter the area. Technological advancements in recent years have enabled a fine-grained comprehension of microglia function throughout development, homeostasis, aging, and damage. These fascinating results pave the way for more accurate process targeting and a more nuanced understanding of how microglia react in different situations.

1.1. Microglia: CNS resident macrophage

Del Hortega (1932) was the first to describe microglia, then known as oligodendrocytes, as a separate cellular component of the CNS from neurons and astrocytes. About 10% of all brain cells in mammals are microglia (Aguzzi, Barres and Bennett, 2013) because they are the resident tissue macrophages of the CNS parenchyma. Unlike CNS macrophages such as, meningeal or plexus chroideus macrophages, which are products of definitive hematopoiesis, microglia originate from erythromyeloid precursors in the yolk sac during primitive hematopoiesis (Alliot, Godin and Pessac, 1999; Ginhoux *et al.*, 2010; Kierdorf *et al.*, 2013). Microglia are specialized cells found throughout the CNS that aid in maintaining tissue homeostasis and ensuring proper CNS development and maturation. As the only type of immune cell to reside in the brain, they also make up the cellular component of the innate immune system in the central nervous system. That's why they're involved in pretty much every kind of pathology that can happen in the central nervous system (Aguzzi, Barres and Bennett, 2013).

1.1.1 Ontogeny

Recent years have provided conclusive evidence for the YS (yolk sac) ontogeny of microglia (Ginhoux and Guilliams, 2016), thanks to lineage-tracing experiments, parabiosis experiments, and neonatal BM transplantations (Ajami *et al.*, 2007; Ginhoux *et al.*, 2010; Hashimoto *et al.*, 2013). The current consensus view is that YS erythromyeloid precursors (EMPs) are the progenitors of microglia and YS macrophages, the immediate migratory precursors that colonize the embryonic brain (Kierdorf *et al.*, 2013; Gomez Perdiguero *et al.*, 2014). It has been difficult to determine the ontogeny of microglia and

central nervous system macrophages because there are at least three waves of hematopoiesis that partially overlap in timing and the tissues involved. The first wave of primitive progenitor cell generation begins at around embryonic day E7.0 in the YS blood islands (posterior plate mesoderm). Primitive hematopoiesis (Perdiguero and Geissmann, 2015; Ginhoux and Guilliams, 2016) refers to the process by which these progenitors differentiate into nucleated erythrocytes and YS macrophages without going through monocytic intermediates.

1.1.2 Development and maturation

Microscopic glial precursors / EMPs originate in the YS, where they undergo macrophage differentiation before migrating to other embryonic tissues, including the brain. Microglial precursors first appear in the cephalic mesenchyme at E9.0, and then they begin to penetrate the neuroepithelium at E9.5. This is demonstrated using Cx3cr1GFP mice, which express green fluorescent protein (GFP) under the control of the endogenous Cx3cr1 locus. Macrophage progenitors must be distributed evenly across mouse embryos, and CX3C-chemokine receptor 1 (CX3CR1) plays a key role in this process.

Microglial precursors, once inside the brain parenchyma, receive cues for differentiation from the central nervous system environment. They are highly proliferative from embryonic day 14.5 until postnatal day, when they undergo a transition from amoeboid to ramified morphology (Kierdorf *et al.*, 2013; Swinnen *et al.*, 2013; Bennett *et al.*, 2016). Microglia complete their development and begin expressing adult-signature genes by postnatal day 14. Through tightly coupled local proliferation and apoptosis, this population of cells maintains itself at constant and region-specific densities for nearly the entire lifespan of the animal (Askew *et al.*, 2017). The olfactory bulb is one of the brain regions with the fastest microglial turnover rate (an estimated 8 months for full turnover in mice). Microglia in the mouse neocortex have a median lifespan of more than 15 months, according to a recent in vivo single-cell imaging study. It appears that microglial self-renewal occurs randomly and in a region-independent fashion, but during pathology, this process switches to clonal expansion (Füger *et al.*, 2017; Tay *et al.*, 2017).

As soon as microglial precursors emerge in the YS, they begin to differentiate. Microglial homeostasis and proliferation depend on CSF1R signaling. In order to proliferate, differentiate, and survive during embryogenesis, YS macrophages require CSF1R signaling (Chitu *et al.*, 2016; Chitu and Stanley, 2017). Myeloid cell differentiation may be induced by CSF1R signaling through the activation of the myeloid lineage-determining transcription factor PU.1. Additionally, adult CNS microglia

maintenance necessitates continuous CSF1R signaling. As early as E10.25, it was shown that the colonized precursor cells begin to express microglia-specific genes like Sall1 and Sall3 (Mossadegh-Keller *et al.*, 2013; Mass *et al.*, 2016). Environnemental cues imprint microglial and macrophage tissue-specific identities (Gosselin *et al.*, 2014; Lavin *et al.*, 2014).

Microglial and macrophage identities and plasticity are regulated by a complex network of transcriptional and epigenetic mechanisms (Amit, Winter and Jung, 2015). Tissue macrophages are shaped by ontogeny and environmental cues, resulting in tissue-specific gene expression, chromatin modifications, and enhancer landscapes. Common myeloid enhancers are established by lineage-determining transcription factors like PU.1, and microglia-restricted enhancers are activated in response to incoming brain-derived signals. Myocyte-specific enhancer factor 2C (MEF2C) was hypothesized to play a role in microglial specification by analyzing consensus binding sites around enhancers that are only active in microglia (Gosselin *et al.*, 2014; Lavin *et al.*, 2014).

1.1.3 Role of microglia in CNS physiology

Time-lapse recordings suggest that microglia can actively contact other neural components, such as synaptic clefts, with their fine processes at least once every few hours, spanning the entire brain parenchyma. Microglia have been shown to play an important role in synapse remodeling and maturation during development (Paolicelli *et al.*, 2011; Hoshiko *et al.*, 2012; Schafer *et al.*, 2012).

The classical complement system is essential for the defense against pathogens and the disposal of cellular debris. Complement component C1q, complement receptor 3 (CR3), and CR5 are all expressed by microglia, but they are not the only cells that express these complement components in the brain. When the central nervous system is healthy and "sterile," complement proteins serve a much broader purpose than just fighting off bacteria and other microorganisms (Stephan, Barres and Stevens, 2012). The pruning of synapses during development, synapse loss due to disease, and cognitive decline with age are all influenced by these proteins. In both the immature and mature brain, microglia are responsible for the phagocytosis of dead, dying, and even healthy live cells. During cerebellar development, microglia produce reactive oxygen species (ROS) that promote the death of Purkinje neurons via engulfment.

1.2. Regulation of microglial activation in development and neurodegenerative diseases

The highly branched processes of mature microglia are in stark contrast to the 'amoeboid' morphology of their larger, rounder cell bodies and shorter, thicker branches that they adopt during development. Increased phagocytic activity, in addition to distinct gene expression and secretory profiles, accompany these morphological features during development. IGF1 secretion by microglia is an example of how this cell type is thought to be "developmentally activated," a state necessary for normal brain development. Microglia undergo similar morphological changes in response to immune challenge or in brain diseases, which are sometimes accompanied by the release of cytokines, chemokines, and/or trophic factors (Ueno *et al.*, 2013; Hagemeyer *et al.*, 2017). Depending on the expression of a few known markers, these polarized cells have traditionally been classified as having either a "toxic" (M1 type) or "protective" (M2 type) state. Evidence is mounting, however, that microglial polarization is not a simple linear spectrum, but rather a multidimensional process characterized by extensive overlap in gene expression (Ransohoff, 2016a). Almost all forms of neurodegeneration share a prominent feature of neuroinflammation, which is largely characterized by microglial activation (Colonna and Butovsky, 2017).

Despite the fact that microglial activation can modify disease progression, human genetics research suggests that microglial dysfunction plays a causal role in disease onset. TREM2, CD33, and CR1, all of which are expressed only by microglia in the CNS parenchyma, are prime examples of risk genes for Alzheimer's disease that have been found to be expressed exclusively by microglia (Guerreiro *et al.*, 2013). It is believed that the underlying amyloidosis-related microglial phagocytic activity is influenced by these genes (Griciuc *et al.*, 2013; Colonna and Wang, 2016). In particular, TREM2 and CD33 have been hypothesized to positively and negatively regulate -amyloid phagocytosis, respectively. Tauopathy is another characteristic of Alzheimer's disease, and it has been suggested that microglia may play a role in the dissemination of the microtubule-associated protein tau across brain regions by means of exosomes (Asai *et al.*, 2015).

Microglial dysfunction may play a role in the development and/or progression of amyotrophic lateral sclerosis (ALS), a neurodegenerative disorder characterized by the gradual death of motor neurons. Commonly mutated genes in amyotrophic lateral sclerosis include superoxide dismutase 1 (SOD1), C9orf72, and TAR DNA-binding protein (TARDBP) (Al-Chalabi, Van Den Berg and Veldink, 2016). The loss of myelin in multiple sclerosis is thought to be mediated by autoreactive T cells, making it unique among neurodegenerative diseases (Ransohoff, 2016). The strong genetic association between

MHC risk loci and multiple sclerosis suggests that myeloid cells are crucial components driving disease onset and progression (Sawcer *et al.*, 2011).

1.3. Interaction of microglia with other cell types

Microglia mediate developmental programs, maintain homeostasis, aid in tissue repair, and contribute to disease pathology by interacting with virtually all brain cell types. Insulin-like growth factor 1 (IGF1) is secreted by microglia in the postnatal mouse brain to promote the survival of developing layer V neurons before they reach their distant CNS targets. Microglia also aid in regulating axon fasciculation in the prenatal dorsal corpus callosum and have a close relationship with white-matter tracts (Ueno *et al.*, 2013; Pont-Lezica *et al.*, 2014; Schafer and Stevens, 2015; Frost and Schafer, 2016). During times of brain injury and inflammation, microglia also communicate with astrocytes. Rapid convergence of microglial processes and cell migration can be triggered by injury-associated ATP release, which in turn induces an ATP gradient derived from astrocytes and sensed by microglia via their purinergic receptor P2RY12 (Davalos *et al.*, 2005; Roth *et al.*, 2013).

Pharmacological and genetic depletion studies have shown that early postnatal microglia are essential for the development of oligodendrocyte progenitors and the subsequent myelination process. In the adult stage, microglia continue their homeostatic maintenance of the oligodendrocyte progenitor pool. Microglia promote oligodendrocyte differentiation, which speeds up remyelination in the context of lysolecithin-induced injury. Myelin is ingested by microglia, and this can lead to insoluble protein aggregates in microglial lysosomes and a loss of function. This could be a factor in the regulation of myelin turnover and the onset of senescence. Finally, microglia interact with endothelial cells, as shown by the finding that microglia mediate blood vessel fusion downstream of vascular endothelial growth factor-dependent tip cell sprouting; loss of microglia in PU.1- or CSF1-mutant mice results in reduced complexity of the brain vesicular network during early development (Fantin *et al.*, 2010; Miron *et al.*, 2013a).

1.4. Diversity of brain-associated macrophages

Parenchymal microglia and non-parenchymal macrophages found in the meninges, perivascular spaces, and choroid plexus form the bulk of the CNS's macrophage population. Although research into microglia has been extensive, interest in border-associated macrophages (BAMs) has only recently risen. The meninges are home to a wide variety of immune cells, a population that varies with age and

degenerative brain diseases. Egfl7 (a regulator of vasculogenesis) and Lyve1, the vascular endothelial hyaluronan receptor, were found to be signature genes for subdural macrophages (MHCII lo). Subdural meningeal macrophages, in contrast to their dural counterparts, are only marginally replaced by monocytes over time and can sustain themselves locally (Goldmann *et al.*, 2016; Mrdjen *et al.*, 2018; Van Hove *et al.*, 2019).

In contrast, the dural macrophage population is more rapidly replenished by monocytes as we age, likely due to a more permissive barrier than the leptomeninges and a faster turnover of the MHCII hi population. Most immune cells in the choroid plexus, called macrophages, were found in close proximity to blood vessels. Choroid plexus macrophages could be sub clustered by differential expression of MHCII as previously reported, and they shared many of the canonical BAM-markers such as Apoe, Ms4a7, and Ms4a6c. Choroid plexus macrophages showed downregulation of Mrc1 and Lyve1 in adult and aged mice, while upregulation of Cd74 (MHCII-associated gene) and Klra2 (Killer cell lectin-like receptor 2) was observed (Van Hove *et al.*, 2019; Dani *et al.*, 2021).

Kolmer's epiplexus cells are intracerebroventricular macrophages on the ventricle-facing choroid plexus. They express Sall1 but not Mrc1, resembling microglia. Epiplexus macrophages also express Apoe, Trem2, and Clec7a, similar to the "DAM" profile of neurodegenerative microglia (Deczkowska *et al.*, 2018; Munro, Movahedi and Priller, 2022).

Brain perivascular macrophages (PVMs) reside in the perivascular space, which is defined as the region surrounding brain blood vessels and extending from the abluminal side of the vascular basement membrane to the glial limitans. Together with non-fenestrated endothelial cells linked via tight junctions, mural cells, and astrocyte end feet, they make up the neurovascular unit (NVU). When put together, they form the blood brain barrier (BBB), which prevents neurotoxic substances, pathogens, and immune cells from entering the brain. Microglia are one type of tissue-resident macrophage whose ontogeny and phenotype have recently been elucidated, along with the tissue-specific roles assigned to different populations (Mastorakos and McGavern, 2019).

1.5. Contribution of infiltrating myeloid cells in CNS injury

In addition to microglia, the recruitment of blood-derived monocytes/macrophages into the central nervous system (CNS) is characteristic of MS. These cell types have traditionally been viewed as detrimental in an autoimmune context because they promote demyelination and axonal damage. Although monocytes are normally prevented from entering the central nervous system (CNS), they are

able to cross the blood-brain barrier and migrate to sites of injury in the CNS when pathological conditions exist (Lampron, Pimentel-Coelho and Rivest, 2013). Peripheral monocytes are heavily recruited to lesion areas in animal models of demyelination, and this recruitment is mediated by chemokine receptor type 2 (CCR2). It has been shown that peripheral monocytes deficient in CCR2 are unable to infiltrate the CNS in a toxin-induced model of demyelination, but this has no effect on the demyelination or remyelination process (Lampron *et al.*, 2015).

However, Ccr2+/+ mice transplanted with CCR2-deficient peripheral blood and bone marrow did not develop the same degree of functional deficits in a model of autoimmune-mediated demyelination (EAE) where monocyte infiltration was found to correlate with disease progression to the point of paralysis (Ajami *et al.*, 2011).

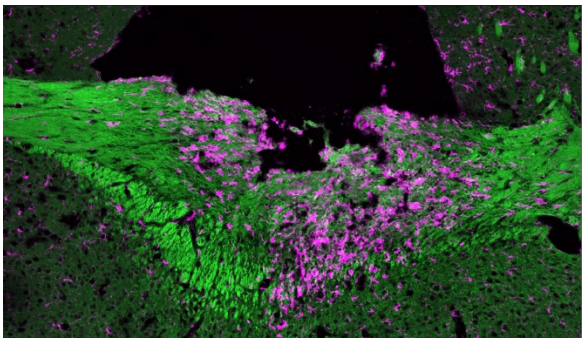

Illustration 1.5: Microglia / macrophages at the lesion site in the CNS

Activated microglia / macrophages lose their highly branched ramifications and become amoeboid in the CNS lesion site. In this picture corpus callosum is labelled with FluoroMyelin (green) and microglia/macrophages with Iba1 (magenta) and it represents 14 dpi lesion area.

2. Remyelination in demyelinating diseases

Remyelination is the process in which entire myelin sheaths are restored to demyelinated axons, reinstating saltatory conduction and resolving functional deficits. CNS remyelination, in contrast to the situation after neuronal loss or axonal damage, can be a highly effective regenerative process. The adult central nervous system is filled with a population of precursor cells called oligodendrocyte precursor cells (OPCs) that mediates this process. However, despite its efficacy in experimental models and in some clinical diseases, remyelination is often insufficient in demyelinating diseases like MS, the most common demyelinating disease and a cause of neurological disability in young adults (Smith, Blakemore and McDonald, 1979; Franklin and Ffrench-Constant, 2008).

2.1 Overview of demyelinating diseases

Demyelinating diseases of the central nervous system (CNS) are diverse and each has its own distinct cause. Inflammatory processes, viral infections, acquired metabolic disturbances, hypoxia/ischemia, and focal compression are all examples of conditions that can lead to demyelination of the nervous system. Inflammatory demyelination manifests in conditions such as multiple sclerosis, acute-disseminated encephalomyelitis (ADEM), and acute hemorrhagic leucoencephalitis (AHL). Plaque types have been further subdivided based on a combination of morphological and immunohistochemical findings in the most common of these, multiple sclerosis, which is pathologically and pathogenically heterogeneous and has been subdivided into four main subtypes (classical, acute, neuromyelitis optica, and concentric sclerosis). The JC virus causes progressive multifocal leukoencephalopathy (PML), the most common viral demyelinating disease in humans. The two most common diseases in the group of acquired metabolic demyelination are central pontine myelinolysis (CPM) and extrapontine myelination (EPM). Demyelination due to Marchiafava-Bignami disease, brought on by chronic alcoholism and malnourishment, is extremely rare. Necrosis, not demyelination, typically occurs in brain tissue in response to hypoxia or ischemia. However, there are conditions in which hypoxia or ischemia particularly harm the myelinating oligodendrocyte. Compression-induced demyelination is rarely seen in routine diagnostic neuropathology. Compression of trigeminal nerve root fibers by an overlying artery or vein near the zone of entry of the nerve root into the pons is the best documented example of compression-induced demyelination and the cause of many cases of trigeminal neuralgia (White *et al.*, 1992; Love, 2006).

2.2 Multiple sclerosis

The most common form of demyelinating disease is multiple sclerosis. Multiple genetic and environmental factors may interact to cause it. Women are twice as likely as men to develop MS. Patients typically present anywhere between the ages of 15 and 55. Multiple sclerosis can present itself in a variety of ways in the clinic. Weakness, paraesthesia, or focal sensory loss, optic neuritis, diplopia, ataxia, and vertigo are common initial symptoms. Bladder, bowel, and sex dysfunction caused by autonomic motor abnormalities are common. Seizures, psychiatric disturbances, cognitive difficulties, fatigue, depression, and pain in the muscles are some of the other possible symptoms. MRI scans often reveal lesions, and CSF oligoclonal immunoglobulin bands can be seen on electrophoresis. Neurophysiological studies frequently reveal sluggish responses to visual or other sensory elicitors. Although MS usually progresses in a relapsing-remitting pattern, it can also be progressive from the start or develop into that later. The time between relapses varies from person to person. Multiple sclerosis often has a lengthy dormant period between the onset of symptoms and the occurrence of the first relapse. Multiple sets of criteria have been proposed for the clinical diagnosis of MS, with the most widely used set currently being the McDonald et al. criteria. Brain, cerebellum, brain stem, and spinal cord can all be affected by demyelination plaques of varying sizes and shapes. There is typically extensive damage to the periventricular white matter, optic pathways, and spinal cord. Numerous classification systems have been proposed for plaques based on disease severity, progression, and the mechanisms by which they are thought to be formed into the following groups: active plaques, inactive plaques , chronic active plaques and shadow plaques (McDonald *et al.*, 2001; Love, 2006). Multiple sclerosis (MS) is thought to have a multifactorial origin, including both genetic predisposition and environmental risk factors, which together cause an inflammatory demyelinating and neurodegenerative disease. Strong associations with immune regulators like T cells, B cells, and phagocytes have been found in genetic analyses. Environmental risk factors like Epstein-Barr virus infection, vitamin D deficiency, smoking, and latitude have been uncovered through numerous systematic reviews and meta-analyses; however, no well-established risk factors exist to aid in disease prevention at this time. (Sawcer *et al.*, 2011b; Belbasis *et al.*, 2015)

2.3 Factors limiting remyelination efficiency

The effectiveness of remyelination is influenced by age, sex, and genetic background, none of which are disease-related. The efficiency of remyelination, like that of all regenerative processes, declines

with age. This decrease of the rate of occurrence likely has significant implications for disease development (which, in the case of MS, can occur over many decades). Age-related increases in the susceptibility of demyelinated axons to atrophy exacerbate the effects of slow remyelination. Reduced efficiency in both OPC recruitment and OPC differentiation underlies the age-related effects on remyelination. The decline in remyelination efficiency occurs more rapidly in males than in females, but the basis of this sex divergence is not clear. The aging effect is likely based on modifications to both the extrinsic environmental signals to which OPCs are exposed in remyelinating lesions and the intrinsic determinants of OPC behavior that occur with advancing age (Sim *et al.*, 2002; Bieber, Ure and Rodriguez, 2005; Irvine and Blakemore, 2006; Li *et al.*, 2006; Rando, 2006). Poor clearance of myelin debris and consequent persistence of myelin-associated differentiation-inhibitory proteins are caused by an impaired macrophage response in aging, which is associated with a delay in the expression of inflammatory cytokines and chemokines (Kotter *et al.*, 2006a; Zhao, Li and Franklin, 2006). In addition to delays in OPC activation, recruitment, and differentiation, which are indicative of age-associated environmental changes in remyelination, there are also changes in the expression of remyelination-associated growth factors following toxin-induced demyelination. An epigenetic change in the regulation of OPC differentiation during remyelination was recently discovered, confirming these alterations in older individuals. During OPC differentiation, histone deacetylases (HDACs) are recruited to the promoter regions of differentiation inhibitors. Aging animals have impaired HDAC recruitment, which leads to increased expression of these inhibitors, a lag in OPC differentiation, and slower remyelination as a result (Hinks and Franklin, 2000; Marin-Husstege *et al.*, 2002; Shen, Li and Casaccia-Bonnefil, 2005; Zhao, Li and Franklin, 2006). Besides these common causes, disease-specific factors also play a role in remyelination's incompleteness or failure. Multiple sclerosis provides the strongest evidence to date for the failure of remyelination. OPC recruitment, which includes proliferation, migration, and repopulating areas of demyelination, fails in multiple sclerosis lesions not due to a lack of available precursor cells but rather due to a failure of OPC recruitment. Recent research has shown that disruptions in the local expression of the OPC migration guidance cues semaphorin 3A and 3F can lead to a failure in OPC recruitment into areas of demyelination (Williams *et al.*, 2007). There is also a failure in MS caused by a lack of differentiation and maturation of oligodendrocyte-lineage cells in the demyelinated areas. Oligodendrocyte-lineage marker O4 was initially used to demonstrate the presence of OPCs in MS lesions that lacked the ability to differentiate. Inhibitory factors present in chronic demyelinated lesions may account for the failure of precursors to differentiate. One of the first pathways to be suspected was the negative regulator of OPC differentiation, the Notch-jagged pathway. Since demyelinated axons may have undergone

pathological changes during demyelination or as a result of chronic demyelination, remyelination of these axons may be more difficult than remyelination of healthy axons during development (Wang *et al.*, 1998; Wolswijk, 1998).

2.4 Models to study MS

Given that MS only affects humans and that demyelinating diseases in animals are very different from human central nervous system (CNS) diseases, it is extremely difficult to develop experimental models of MS. Transgenic mice, as well as chemically-induced, viral, and autoimmune models, are among the in vivo models developed in the course of the search for animal models of demyelination (Zhang *et al.*, 2011; Ben-Nun *et al.*, 2014; Lassmann and Bradl, 2016). Studies of myelin repair using LPC-induced demyelination are common because they mimic the demyelinated lesions seen in people with multiple sclerosis (MS) in many ways. When lysolecithin is injected into the white matter, it damages the myelin sheath and leads to the development of focal demyelinating plaques. Experimental animals such as rats, mice, cats, and rabbits have shown that the compound acts as a chemoattractant to monocytes, causing an inflammatory response. Myelin damage is rapidly followed by remyelination, as seen in other toxin-induced models of demyelination, though the rate and extent of remyelination vary with age. Microglia respond strongly and rapidly to demyelination in this model. They play a dynamic role in physiological and injury-induced remyelination. Their activation is largely confined to the lesion where the demyelination has occurred; and finally, the time course of injury and repair is well established and controlled in this model (Jeffery and Blakemore, 1995a; Blakemore and Franklin, 2008; Miron *et al.*, 2013a; Hammond *et al.*, 2014).

2.5 Role of microglia in remyelination

Throughout the process of remyelination, microglia undergo modifications to their function and gene expression. At various points in focal remyelination, different microglia/macrophage phenotypes dominate. During the beginning stages of repair, when OPCs are recruited to lesions, there is a high number of microglia with a pro-inflammatory phenotype (iNOS+, TNF+, and CD16-CD32+). At the outset of oligodendrocyte differentiation and remyelination, a regenerative phenotype (ARG1+, IGF1+, and CD206+) appears. Microglial activation is linked to a pro-remyelination state, and MSX3 expression is correlated with this state (Olah *et al.*, 2012; Voß *et al.*, 2012; Yu *et al.*, 2015). In order for OPCs to be recruited and differentiated into remyelinating oligodendrocytes, the debris left behind

by demyelination must be cleared away (Neumann, Kotter and Franklin, 2009). This process is intricate, involving uptake of debris, maturation of phagolysosomes, and recycling of cholesterol. In vivo and in vitro experiments show that microglia/macrophages internalize myelin debris and after myelin damage, microglia express genes related to phagocytosis and lysosomal pathways (Voß *et al.*, 2012; Yamasaki *et al.*, 2014; Greenhalgh *et al.*, 2018; Rawji *et al.*, 2018).

Age-related decline in remyelination is associated with deficient internalization of myelin debris in microglia / macrophages (Ruckh *et al.*, 2012). Microglia are immune cells that have been shown to express a number of receptors that control the removal and degradation of myelin debris. Microglia and CNS border-associated macrophages express high levels of the fractalkine receptor CX3CR1. Myelin debris uptake (Axl) and lipid transport and metabolism (Apoe and Lpl) are among the genes whose expression is controlled by Triggering receptor expressed on myeloid cells 2 (TREM2) signaling. Toll-like receptor 4 (TLR4), retinoid X receptor (RXR), and tyrosine protein kinase MER are a few other receptors that have been linked to myelin debris clearance. Microglia secrete numerous cytokines and growth factors that modulate the responses of cells in the oligodendrocyte lineage (Wolswijk and Noble, 1992).

Microglia, for example, express factors that directly support beneficial oligodendrocyte lineage cell responses. These factors have been identified in vivo (activin A, galectin 3, TNF, IGF1, IL-1) and in vitro (hepatocyte growth factor [HGF], CXC-chemokine ligand 12 [CCL12], and platelet-derived growth factor [PDGF]-AA) (Lloyd and Miron, 2019a).

During remyelination, microglia support OPC responses to the extracellular matrix. Matrix metalloproteinases, expressed by microglia/macrophages, degrade chondroitin sulfate proteoglycans, thereby impeding OPC recruitment and differentiation. Transglutaminase 2, secreted by microglia, cross-links laminin and stimulates OPCs' engagement with GPR56 (also called ADGRG1), a member of the adhesion G protein-coupled receptor family, to control proliferation and differentiation (van Strien *et al.*, 2011; Giera *et al.*, 2018; Pu, Stephenson and Yong, 2018). Microglia with a regenerative phenotype (CD206+) express higher levels of IGF1 and activin A than microglia with a pro-inflammatory phenotype (iNOS+, TNF+, and CD16-CD32+), suggesting that microglial activation state affects the production of regenerative factors. Myelin debris uptake and secretion of pro-

remyelination factors have been shown to be linked by studies looking at the effects of TREM2 and CSF1R signaling on microglial Igf1 expression (Miron *et al.*, 2013a; Yu *et al.*, 2015).

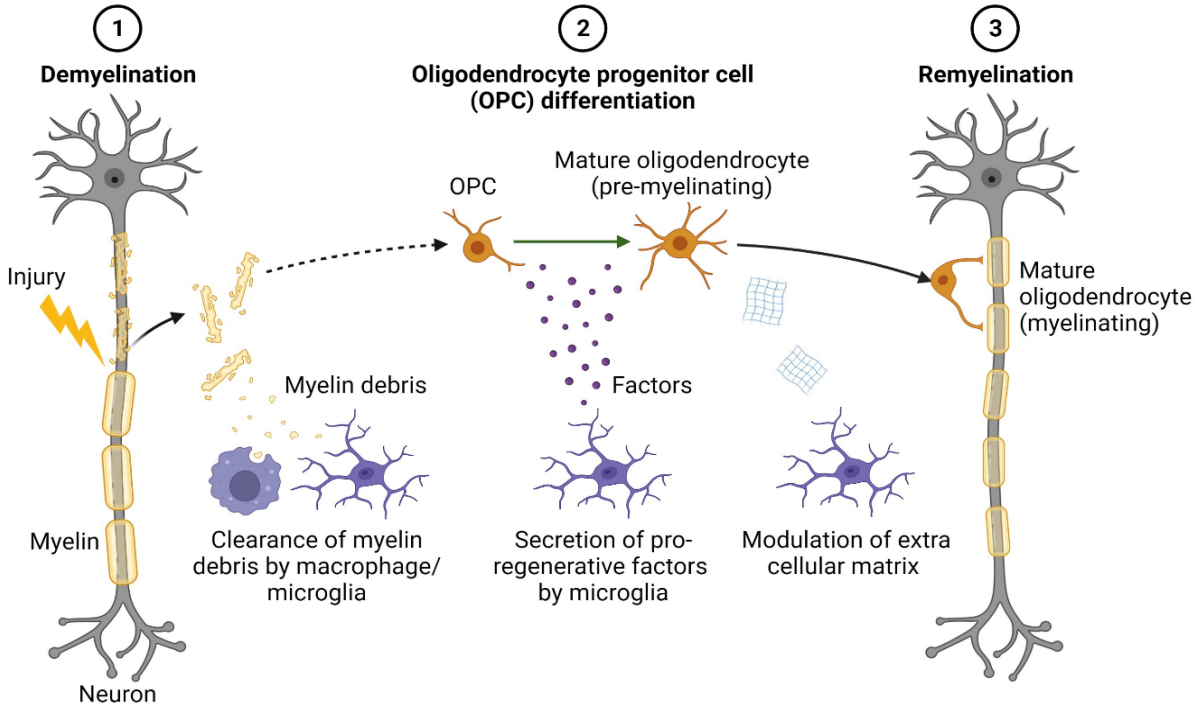

Illustration 2.5: Pro-regenerative functions of microglia

Following CNS demyelination, the usual response, at least in most experimental models, is spontaneous remyelination including OPC proliferation and differentiation. Microglia govern remyelination after demyelination in addition to maintaining oligodendrocyte precursor cell (OPC) maintenance in adults. In three ways, microglia promote remyelination by enhancing OPC recruitment and differentiation into oligodendrocytes, which make new myelin. First, they eliminate inhibitory myelin debris first by CX3CR1, TREM2 and CSF1R signaling, and then cholesterol via apolipoprotein E (APOE), LXR, ABCA1 and ABCG1. Second, pro-regenerative factors such as activin A, insulin-like growth factor 1 (IGF1), galectin 3, tumor necrosis factor (TNF), and IL-1 are secreted. Finally, they alter the extracellular matrix by secreting matrix metalloproteinases (MMPs) and TGM2.
Illustration created in (Biorender.com) from V. Miron. Adapted from (Lloyd and Miron, 2019b)*. For abbreviations please refer to list of abbreviations.*

3. Epigenetic regulation and microglia plasticity

Microglia can alter their activation state and even their identity in response to specific stimuli. Gene expression is finely modulated to control these alterations. Epigenetic modulators primarily alter the chromatin's composition and structure, resulting in this coordinated regulation. In order to direct and maintain the fidelity of target cell states, cellular and genomic reprogramming has recently been shown to rely heavily on chromatin modifications. Histone modifications (e.g., methylation, acetylation, phosphorylation), DNA methylation, and gene expression regulation by non-coding RNAs are all examples of epigenetic modifications that play an important role in normal development but can also play a role in disease (Esteller, 2008). While epigenetic modifications do not alter the cell's genome, they do play a role in defining phenotype by controlling how genes are expressed. Although microglia have been studied for nearly a century, the mechanisms leading to their activation toward a specific phenotype are not yet well understood. However, it is intuitive that epigenetic changes should contribute to the plasticity of microglia.

3.1 Epigenetic modifications regulating microglia function

Microglia plasticity and polarization toward distinct phenotypes may be regulated by a variety of epigenetic alterations, such as histone modifications, DNA methylation, or microRNA expression, and the enzymatic systems regulating these alterations. Epigenetic modifications can be used to explain the activation states of microglia in both health and disease, as well as the potential for long-lasting and even transgenerational effects of microglia, such as those seen during microglial priming/memory.

3.1.1 Histone modifications

The compaction of chromatin is regulated by the organization of histone proteins. The chromatin is made up of DNA that is tightly packed around histone proteins that are organized into nucleosomes. A nucleosome is made up of two H3-H4 dimers surrounded by two H2A-H2B dimers, forming an octameric core of histone proteins. Histone tail amino-terminal parts protrude from the nucleosome, making them accessible for post-translational modifications. Histone tail modifications and DNA methylation both play roles in controlling how easily genes can be accessed by the cell's transcription machinery. Certain amino acid residues in the histone tails can be modified by methylation, acetylation, or phosphorylation. Histone acetylation changes the accessibility of chromatin, facilitating the

recruitment of transcription-activating DNA-binding proteins to those regions. Histone acetyl transferases (HATs) are responsible for acetylating lysine residues in the histone tails or core, while histone deacetylases (HDACs) are responsible for deacetylating those same lysine residues. Depending on which amino acid is modified, methylation of a histone can either activate or repress transcription. In contrast to histone demethylases (HDMs), histone methyl transferases (HMTs) promote mono-, di-, or tri-methylation of target histone residues. Since histone acetylation was found to regulate the intensity of the inflammatory response, the use of HDAC inhibitors in inflammatory/neurodegenerative diseases has been the subject of extensive study (Blanchard *et al.*, 2002; Ito *et al.*, 2002). Recently, HDAC inhibitors have seen widespread application in treating inflammation by focusing on microglia. Valproic acid (VPA), a non-selective histone deacetylase (HDAC) inhibitor, is a drug approved by the FDA for the treatment of epilepsy and bipolar disorder. Using a model of primary human microglia and astrocytes treated with TLR3 or TLR4 ligand, researchers have investigated the use of VPA to target microglia in the context of inflammation and innate antiviral gene expression (HIV, for example). Directly affecting microglia, VPA inhibits the production of chemokine and cytokine genes, innate antiviral molecule production (such as IFN), and TLR3-TLR4 signaling pathway activation protein (Suh *et al.*, 2010). HDAC inhibition with TSA or SAHA (also known as Vorinostat) reduces cytokine expression and release following LPS induction in primary microglia cultures (Kannan *et al.*, 2013), and it also reduces LPS-induced cognitive dysfunction in the mouse brain, including weight loss, anorexia, and social withdrawal (Hsing *et al.*, 2015). Furthermore, hyperacetylation induced by TSA treatment protects neurons from damage caused by LPS and hypoxia-ischemia in female neonatal mice, which is correlated with enhanced long-term memory (Fleiss *et al.*, 2012).

Sodium butyrate (SB), like VPA and TSA, has been studied for its potential role in inflammation regulation via microglia targeting. SB has been shown to cause changes in microglia shape, with the appearance of microglial processes elongation in both inflammatory and normal conditions, as well as changes in pro-inflammatory and anti-inflammatory microglia markers (Wang *et al.*, 2018). A rapid and sustained increase in histone H4 acetylation is another effect of HDAC inhibitor treatment in microglia. LPS-induced microglia activation was also reduced in vitro when Hdac1 and Hdac2 were specifically knocked down using siRNA (Durham, Grigg and Wood, 2017).

It appears that an increase in HDAC2 expression can make up for a lack of HDAC1 when it comes to regulating the inflammatory response of microglia, demonstrating the functional redundancy between these two HDACs. It's worth noting that research suggests these two HDACs perform complementary and independent roles. Targeted deletion of Hdac1 or Hdac2 does not result in a noticeable phenotype

in the vast majority of tissues and cell types (Kelly and Cowley, 2013). Using the *Cx3cr1Cre Hdac1fl/flHdac2fl/fl* mouse model, (Datta *et al.*, 2018a) showed that in vivo gene depletion of both Hdac1 and Hdac2 had different effects on microglia at different stages of development, homeostasis, and neurodegeneration. Polycomb repressive complex 2 (PRC2) catalytic subunit, also known as Enhancer of zeste homolog 2 (EZH2), tri-methylates lysine 27 in histone H3, thereby silencing transcription (H3K27me3). H3K27me3 levels are controlled by the equilibrium between the activities of EZH2 and the histone H3K27me3 demethylase Jumonji domain containing 3 (JMJD3, also known as KDM6B). Significant and rapid upregulation of EZH2 gene expression is observed in microglia in response to pro-inflammatory stimuli like LPS-mediated TLR4 stimulation (Arifuzzaman *et al.*, 2017; Zhang *et al.*, 2018). Not only does IL-4 treatment, which encourages alternative microglial activation, increase JMJD3 expression, but so does LPS-treatment (Lee *et al.*, 2014).

EZH2's H3K27 histone tri-methyl transferase activity favors the polarization of M1 microglia while suppressing that of M2 microglia. JMJD3, on the other hand, appears to promote M2 microglia polarization while repressing M1 microglia polarization through its histone H3K27me3 demethylase activity. The transcription factors STAT1 and STAT3 have also been demonstrated to regulate JMJD3 transcription and work in tandem with it to induce the expression of pro-inflammatory genes (Przanowski *et al.*, 2014). The methylation of the lysine 4 residue of histone 3 is associated with transcribed RNA. The transcriptional activity of promoters and enhancers is correlated with their H3K27 acetylation (Creyghton *et al.*, 2010; He *et al.*, 2010; Kaikkonen *et al.*, 2013). Furthermore, Keren-Shaul et al. (2017) identified a novel type of microglia called Disease Associated Microglia (DAM), which hints at a role of H3K4me2 in microglial priming (Keren-Shaul *et al.*, 2017a). The role of histone phosphorylation in microglia is poorly understood. In the event of brain injury, the release of endogenous cannabinoids is thought to mitigate the resulting damage to neurons. Microglia have been shown to inhibit iNOS expression and NO production via the cannabinoid receptor pathway (CB1/2) and MKP-1 production via Histone H3 phosphorylation (Eljaschewitsch *et al.*, 2006). Among the many cellular processes in which Sirtuin 1 (SIRT1) participates are inflammation and aging/senescence (Gan and Mucke, 2008; Libert and Guarente, 2013). Deacetylase enzyme SIRT1 has multiple intracellular substrates, including histones (Michan and Sinclair, 2007). Microglia lose SIRT1 as they age. Decreased SIRT1 is linked not only to aging but also to Tau-mediated memory loss in mice due to increased IL-1 expression (Cho *et al.*, 2015).

3.1.2 Non-coding RNAs

Non-coding RNAs (ncRNAs), such as long non-coding RNAs (lncRNAs) and microRNAs (miRNAs/miRs), have emerged as epigenetic regulators of biological processes in microglia and play important roles in regulating the expression of certain genes (Patil, Zhou and Rana, 2014).

Indeed, distinct miRNA signatures can be used to characterize both microglial steady-state and the various microglia activation states. Using a Nano string based miRNA chip containing 600 microRNAs, researchers found that eight of these microRNAs, specifically miR-29a, mIR-29b, miR-30a, miR-99a, miR-103, miR-125b, miR-322, and miR-342, are highly expressed in unchallenged mouse microglia. In addition, it was discovered that three of those (miR-99a, miR-125b, and miR-342) were expressed uniquely by microglia compared to other immune cells. The role of the microRNA miR-155 in amyotrophic lateral sclerosis (ALS) has attracted a lot of research. MiR-155 targeting improves microglia function and increases survival in SOD1G93A mice (Butovsky *et al.*, 2013, 2015; Koval *et al.*, 2013). MicroRNAs (miRNAs) have long been known to play a role in microglia activation state regulation, but lncRNAs (long non-coding RNAs; ncRNAs longer than 200 nucleotides) have recently emerged as a new player in this field. While several lncRNAs (Qi *et al.*, 2017; Wang *et al.*, 2017; Wen, Yu and Fu, 2017) have been shown to promote neuroinflammation by encouraging M1 polarization of microglia, lncRNA GAS5 has an inhibitory effect on M2 polarization of microglia and increases demyelination (Sun *et al.*, 2017).

3.1.3 DNA methylation

DNA methylation modifies CpG dinucleotides' cytosine residues. DNA methylation in CpG islands represses gene transcription (Goll and Bestor, 2005). DNA methyltransferases (DNMTs) regulate de novo and maintenance DNA methylation. The regulation of gene expression in microglia by DNA methylation has received less attention than the effect of HDACs inhibitors on gene expression. The effects of DNA methylation in microglia have been studied from two perspectives. This epigenetic modification has been studied on two different scales: globally, by looking for shifts in total DNA methylation, and locally, by focusing on individual genes and analyzing their methylation patterns and how they affect gene expression. Microglia show global methylation changes after traumatic brain injury in a rat model (TBI) (Zhang *et al.*, 2007). Gene-specific methylation analysis has revealed that DNA methylation in aging microglia controls IL1 gene expression. Indeed, in two separate models of aging, IL1 gene hypo methylation is linked to upregulation of the cytokine production. First, the

authors hypo methylated certain CpGs on the proximal promoter of IL1 in SIRT1-deficient mice, leading to an upregulation of IL1 (Cho *et al.*, 2015). It is demonstrated that microglia activation involves a particular DNMT. Indeed, DNMT3L is upregulated following microglia activation via LPS treatment or microglia stimulation via TLR3 and TLR4 ligands, as determined by transcriptome sequencing approaches (Das, Chai, Kim, Lee, *et al.*, 2015; Das, Chai, Kim, Park, *et al.*, 2015). Emerging as critical regulators of microglia phenotype acquisition are the transcriptional and epigenetic machinery.

3.2 Epigenetic regulation in glial cells during neuroinflammation

After suffering an ischemic or traumatic brain injury, astrocytes and microglia become activated, secreting pro-inflammatory cytokines within the damaged region (Gao *et al.*, 2013; Goldmann and Prinz, 2013). In the short term, microglial activation in response to central nervous system injury has been shown to cause neuronal death (Liu *et al.*, 2007; Wake *et al.*, 2009; Prinz *et al.*, 2011). However, activated microglia appear to have a neuroprotective effect during the chronic phase of injury response. Therefore, microglia activation in response to CNS injury is both harmful and helpful. Although the secretion of pro-inflammatory cytokines like TNF- or IL1- by activated microglia has been implicated in this process, the precise pathways responsible for both the protective and deleterious effects of microglia activation in injury response are not yet well understood (Lambertsen *et al.*, 2009; Wu *et al.*, 2013). While astrocyte activation does increase the inflammatory milieu via cytokine secretion (Jensen, Massie and De Keyser, 2013), it also increases the antioxidant function of the astrocyte population and the release of nutrients to stressed neuronal cells in the damaged area (Rossi, Brady and Mohr, 2007), which results in a neuroprotective effect of astrocyte activation in physical or ischemic brain injury. When the central nervous system (CNS) sustains an acute injury, oligodendrocytes perform a remyelinating function during the chronic phase to repair the damaged areas and their surrounding myelin sheaths (Patel and Klein, 2011). Multiple studies have examined the potential role of epigenetic regulation of the injury response. One study reveals the presence of a reactive microglial subpopulation in TBI, marked by global DNA hypomethylation and suppressible by dexamethasone (Zhang *et al.*, 2007). Multiple studies using different histone deacetylase inhibitors (HDACi) show that HDACi have a neuroprotective effect in cases of acute brain injury and ischemia.

In addition, there was less of an inflammatory response and fewer activated microglia in the damaged parts of the brain, as evidenced by these reports (Hyeon *et al.*, 2007; B. Zhang *et al.*, 2008; Shein *et al.*, 2009). In addition, a neuroprotective environment was fostered by the fact that HDAC inhibition

did not dampen astrocyte activation (Xuan *et al.*, 2012). Neuroinflammation and the role of glial epigenetics There have been conflicting reports on the ability of HDAC inhibitors to attenuate microglia activation in vitro, which contrasts with the results seen in acute CNS damage. Primary microglia cultures treated with lipopolysaccharide (LPS) have been shown to respond either less activated (Kannan *et al.*, 2013) or more activated (Suuronen *et al.*, 2003) after HDAC inhibition.

An increase in histone H3K9 acetylation, which is reliant on the activity of the nuclear factor kappa B (NF-B) pathway, is induced by LPS stimulation of primary microglia (Goldmann *et al.*, 2013). Although these in vitro results appear to be at odds with one another, they are consistent with observations of microglia apoptosis in HDAC inhibitor-treated animals following acute brain injury (Chen *et al.*, 2007). This apoptosis is accompanied by increased histone H3 acetylation, which increases as HDAC inhibitor dose is increased (Shein and Shohami, 2011). Active multiple sclerosis (MS) is the most common autoimmune-mediated demyelinating inflammatory disease of the central nervous system, with peripheral leukocytes, especially cytotoxic T cells, infiltrating the inflammatory lesions (CNS). Oligodendrocytes, the cells responsible for forming the myelin sheath of axons, serve as targets of the autoimmune inflammation in the acute stages of MS and function to remyelinate demyelinated regions in the chronic stages (Lassmann, 2010; Chastain *et al.*, 2011). Astroglia and microglia, the resident immune-competent cells of the CNS, also participate in disease initiation and also in the later stages of (Emery, 2010).

Only a small number of genes have been found to be consistently hyper- or hypomethylated in MS, despite the fact that studies evaluating the role of DNA methylation in MS pathogenesis have found evidence of aberrant DNA methylation in patient samples (Baranzini *et al.*, 2010; Liggett *et al.*, 2010).It has been reported that non-diseased white matter samples of MS patient brains show an increase in histone H3 acetylation (Pedre *et al.*, 2011) and citrullination (Mastronardi *et al.*, 2006). The numbers of microglia and activated astrocytes both rose in response to H3 hyperacetylation. There was an alteration in gene expression in these white matter regions, but only a subgroup of patients showed a clear pattern of overexpression of several genes, including *Tcf7l2*, *Sox2*, and *Ids*, and there was a trend toward upregulation of HDAC8 and HDAC11 in expression of histone deacetylases in certain subgroups (Pedre *et al.*, 2011). Animal studies using the experimental autoimmune encephalomyelitis (EAE) model have shown that blocking HDAC activity improves disease symptoms, likely by preventing the activation of dendritic cells (DCs) and the polarization of T cells into Th1 or Th17 subsets (Camelo *et al.*, 2005; Ge *et al.*, 2013). Histone acetylation and specifically the function of various HDACs is a key player in the regulation of oligodendrocyte differentiation and function, so

blocking HDACs in non-inflammatory demyelinating conditions has been shown to suppress remyelination (Shen *et al.*, 2008a; Swiss *et al.*, 2011; Conway *et al.*, 2012). However, studies have shown that inhibiting sirtuin improves CNS regeneration by increasing the number of oligodendrocyte precursors after acute CNS damage (Rafalski *et al.*, 2013). However, it has not yet been demonstrated how epigenetic regulation affects astrocyte and microglia function in demyelinating disease. Based on what we know now, HDAC inhibitors have both positive and negative effects on the development of neuroinflammatory diseases, dampening the severity of symptoms during acute inflammation while also preventing the repair of previous tissue damage.

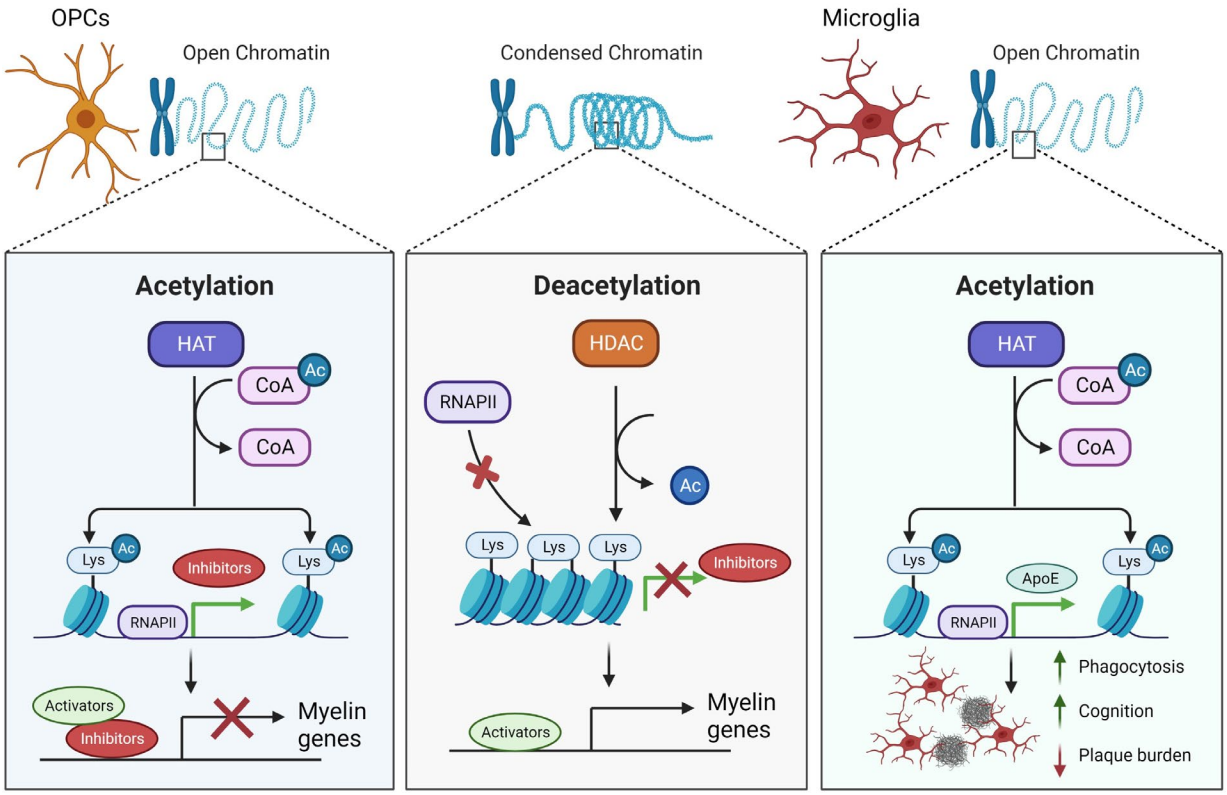

Illustration 3.2: Contrasting functions of HDACs in glial cells during neurodegeneration

In OPCs, a chromatin conformation that is permissive for inhibitor production is linked to acetylation of histones in the promoter region of differentiation inhibitors (HES5 and SOX2). Myelin genes linked to OPC differentiation are silenced by these inhibitors (left). In the process of remyelination, OPC differentiation is linked to the suppression of inhibitor gene expression and the recruitment of histone deacetylases (HDACs). As a result, myelin gene expression and OPC differentiation are enhanced. The transcriptional environment becomes more biased towards the inhibition of myelin genes as animals age due to a decrease in the recruitment of histone deacetylases (HDACs) to the promoters of the inhibitory molecules. As a consequence, OPC differentiation is disrupted and remyelination is slowed (middle). Hdac1-2 deletion from adult microglia in Alzheimer's disease model mice results in acetylation of histone residues around genes which reduces amyloid plaque burden, increases amyloid co-localization with microglia, and rescues cognitive deficits (right).
Illustration created in (Biorender.com). Adapted from (Franklin and Ffrench-Constant, 2008; Datta *et al.*, 2018a). *For abbreviations please refer to list of abbreviations*

4. Aging

Functional decline and increased mortality risk are considered hallmarks of aging (da Costa *et al.*, 2016). However, the question of whether aging is a controlled and predetermined process or the result of a random accumulation of stressor events leading to a low performance state remains contentious. In fact, cellular senescence, or the gradual and irreversible loss of proliferative capacity in cells, plays a crucial role. As a result of damage accumulation, a decline in functional reserve, and an impairment in healing capacity, the concept of aging was introduced as a response to the imbalance between stressors and compensatory mechanisms (Bektas *et al.*, 2018). Since inflammaging is characteristic of both aging tissues and age-related diseases, it is clear that the immune system plays a crucial role in both.

4.1 The concept of Inflammaging

Professor Franceschi first proposed the concept of inflammaging in 2000. Inflammaging is an evolutionary perspective on immunosenescence that attempted to use network theory to understand how stressors may influence their own feedback mechanisms and, as a result, what effects they have on aging. It is defined as an inflammatory process (low grade, clinically insignificant, chronic, systemic) that occurs in the absence of infection, which is a fundamental feature of aging (Franceschi *et al.*, 2000).

Inflammaging results from a combination of factors. When looking at the causes of inflammaging, senescence was initially viewed as a major factor. The Hayflick replicative senescence model proposes that after a certain number of cell divisions, cells become resistant to proliferation and cell death due to consumption of the cell defense leading to decrease in telomere length. Once thought to be metabolically dormant, senescent cells have instead been shown to be highly inflammatory contributors to the aging process (inflammaging). Inflammaging may be caused, in part, by the microbiome if dysbiosis or pathobionts develop anywhere in the organism. Mitochondrial metabolic changes associated with aging may also play a role in the development of inflammaging. Importantly, inflammaging may result from age-related immune system activation at the fundamental level. (Hayflick and Moorhead, 1961; Fulop *et al.*, 2021).

4.1.1 The role of adaptive immunity in inflammaging

The adaptive immune response is the most advanced and complex form of the immune system. This is because its immune system (which is clonotypic) can remember individual pathogens. Thymic involution is a major contributor to the alterations in the adaptive immune system that occur with age (Bonilla and Oettgen, 2010; Thomas, Wang and Su, 2020). The decline of naive T cells may account for the age-related rise in the prevalence of some diseases, such as infections and cancers. Senescent or worn-out cells increase in number with age and release a flood of inflammatory cytokines and mediators. (P. Chou and B. Effros, 2013; Callender et al., 2018). Other cells will be stimulated to increase their metabolic activity while remaining immunologically inactive by these proinflammatory factors.

There are likely many undiscovered processes at work behind T-cell dysfunction, such as age-related alterations to cell membranes. Rigidification of the membrane prevents the normal formation of the immune synapse, a prerequisite for a proper cellular response (Larbi et al., 2006; Mayya et al., 2019).

Also, impaired with age is the transport of signaling molecules within the immune synapse. Loss of all CD-28 expression results in a decline in IL2 production and altered immunometabolic capabilities in T cells, among other consequences (Vallejo, 2005). Another change is a switch in metabolism from the more efficient oxidative phosphorylation to the much less efficient aerobic glycosylation(McGuire, 2019; Yanes et al., 2019). As T cells age, their mTOR signaling pathways change, preventing them from efficiently making the switch and supplying the necessary energy (Liu and Sabatini, 2020). Therefore, the accumulation of the phenotypic, functional, signaling pathway, and metabolic changes that occur with age results in a change in T cell function. It was also reported recently that $CD8^+$ T cells contribute in triggering IFN-responsive cell states in the aging white matter (Kaya *et al.*, 2022).

4.1.2 The role of innate immunity in inflammaging

The innate immune system is surprisingly complex. Neutrophils, monocytes, macrophages, NK cells, and a few other cell types that aren't always well defined make up this arm of the immune system. These cells leave their normal quiescent state and become increasingly activated in response to stress (Beutler, 2004; Fulop et al., 2016, 2021). There are three primary roles played by the innate immune system. The first is to maintain a clearing function that prevents and lessens the severity of any and all

harm brought on by external and internal threats. The second is using soluble mediators like IL-12 to prime the adaptive immune system. All phagocytic cells perform the third function, which is antigen presentation (most importantly the dendritic cells). Phagocytic cell functions decline with age. This is especially true of their chemotactic phagocytic, antigen-presenting, and killing abilities. (Solana *et al.*, 2012; Hazeldine and Lord, 2015a; Müller, Di Benedetto and Pawelec, 2019; Goldberg, Shaw and Montgomery, 2020). Also, crucial to the proper operation of the innate immune system are the so-called danger recognition receptors and pattern recognition receptors (PRRs). Some of the most crucial are the NOD-like receptors (NLR), RIG-like receptors (RLR), and toll-like receptors (TLR). (Kumar, Kawai and Akira, 2011; Gong *et al.*, 2019). Their respective signaling pathways guarantee a suitable cellular response. Both the total number of these receptors and the pathways they use to transmit signals may alter with age. (Shaw, Goldstein and Montgomery, 2013; Bailey *et al.*, 2019; De Maeyer and Chambers, 2021a). One of the most significant discoveries regarding the innate immune system is that aging causes a constant activation of cells, resulting in an increase in the production of proinflammatory mediators such as free radicals and proinflammatory cytokines. But when prompted, they are unable to properly respond by ramping up their protective capabilities (Fulop *et al.*, 2021).

4.2 Myeloid cells involved in Inflammaging

There is great diversity among myeloid cells, each of which contributes to inflammaging in its own unique way under specific pathophysiological circumstances. (Hazeldine and Lord, 2015b). This age-related increase in low grade, chronic, and systemic production of inflammatory mediators (i.e. inflammaging) feeds the immunosenescence process because innate immune cells are still relatively functional in the and represent the main source of inflammatory mediators in response to challenging events (Fulop *et al.*, 2018; Franceschi, Santoro and Capri, 2020). Aging alters the number and function of myeloid innate immune cells, including neutrophils, monocytes/macrophages, myeloid derived suppressor cells (MDSCs), and dendritic cells. The intrinsic immunosenescence of these cells, along with their chronic abnormal activity in response to the aging-associated perturbations of organismal homeostasis, is the primary regulator and effector of the inflammaging process (Bleve *et al.*, 2022).

Numerous in vivo and in vitro studies have demonstrated that the chemotactic capability of neutrophils from elderly subjects is impaired. In fact, cells isolated from elderly individuals migrate significantly less in response to chemotactic agents, such as the bacterial products for formyl- methionine- leucine-phenylalanine (fMLP). Additionally, their responses to LPS and myelopoietic GM-CSF are altered. There is also a significant decrease in the surface expression of the FC receptor CD16. Aged

neutrophils from mice exhibited an increase in membrane fluidity as a result of a decrease in cholesterol and an increase in phospholipids (Alvarez *et al.*, 2001; Fulop *et al.*, 2004). Macrophages are not the only participants in inflammaging; however, it is generally accepted that monocytes and macrophages are the key initiators of this process. Important cells of the innate immune system, macrophages consist of a heterogeneous population that varies in phenotype and behavior depending on their location and the pathophysiological conditions they encounter. These cells sense environmental and senescent signals. NAD+ synthesis in macrophages declines with age and becomes more pronounced during immune responses, impairing macrophage effector function and resulting in an increase in proinflammatory functions (Minhas *et al.*, 2019; De Maeyer and Chambers, 2021b). MDSCs (Myeloid Derived Suppressor Cells) are a heterogeneous population of myeloid cells in their immature stages that appear during a chronic pathological state. Researchers have found that the number of circulating MDSCs rises with age in both humans and mice. MDSC proliferation and activation are promoted by pro-inflammatory cytokines released by senescent cells and tissues. Through their immunosuppressive activity, MDSCs dampen both the innate and adaptive immune responses (Consonni *et al.*, 2019). Dendritic cells (DCs) are the main antigen-presenting cells for naive T cells, making them an important link between the innate and adaptive immune responses. Increased IL-6 and Tnfa production by aged DCs is indicative of their role in inflammaging. In contrast, traditional DCs isolated from aged mice showed diminished capacity to elicit CD8+T cell cytotoxic responses (Agrawal and Gupta, 2011; Rodrigues *et al.*, 2021).

4.3 Age associated regulation of microglia

The central nervous system changes with age; the neuroinflammatory state is primarily caused by dysregulated activation of microglia, the CNS's innate immune cells and the primary producers of reactive oxygen species. (Cornejo and von Bernhardi, 2016). Microglia become more activated and are distributed irregularly across multiple cortical and subcortical regions as we age. They also change in appearance, becoming more granular due to increased phagocytic inclusions and displaying a wider variety of cell morphologies with shorter, simpler processes. In addition, aging slows both the processing speed and the cell-dynamics in response to tissue injury (Vaughan and Peters, 1974; Schuitemaker *et al.*, 2012; Tremblay *et al.*, 2012; Hefendehl *et al.*, 2014; von Bernhardi, Eugenín-von Bernhardi and Eugenín, 2015). Age-related phenotypic changes in microglia suggest that, rather than being in an over-activated state, aged microglia are dysregulated and lack the ability to mount a normal immune response. (Sheng, Mrak and Griffin, 1998; von Bernhardi, 2007; von Bernhardi *et al.*, 2015).

Increased expression of mRNA for inflammatory (Tnf-a, IL6, IFN-y, etc.) and decreased expression of anti-inflammatory (*IL-10, Tgf-β*, etc.) cytokines is a hallmark of activated microglia, which is also seen in aged mice (Vaughan and Peters, 1974; Godbout *et al.*, 2005; Frank *et al.*, 2006; Sierra *et al.*, 2007a).

A pathological microglial phenotype that is less protective and more cytotoxic may be induced by age, according to recent RNA sequencing studies that point to an altered microglial "sensome" induced by age (Von Bernhardi, Tichauer and Eugenín, 2010; Von Bernhardi, Tichauer and Eugenín-von Bernhardi, 2011; Yan *et al.*, 2014). Microglia change epigenetically as they age as well. An increased level of histone methylation, exacerbating the reactive microglial inflammatory response, is caused by a decrease in the histone H3K27me3 demethylase Jumonji domain 3 (Jmjd3) in the midbrain of aged mice. Recent evidence also indicates that CpG sites on the Il1b promoter are hypomethylated in aged microglia, leading to increased Il1b expression. Microglial activation and the neuroinflammation it causes in the aged brain appear to be supported by epigenetic changes that occur with age in microglia. (Tang *et al.*, 2013; Cho *et al.*, 2015). Aged microglia also express elevated levels of membrane markers including TLR1, TLR2, TLR4, TLR5, MHCII, Cd11b, and CD14 (Perry, Matyszak and Fearn, 1993; Letiembre *et al.*, 2007). Microglia have been linked to the pathology and progression of multiple neurodegenerative disorders, including prion diseases, multiple sclerosis, amyotrophic lateral sclerosis, Huntington's disease, pick's disease, and HIV-associated dementia. Age-induced microglial dysfunction appears to play a significant role in the onset of age-related neurodegenerative diseases such as Parkinson's and Alzheimer's. (Cornejo and von Bernhardi, 2016).

4.4 Priming in microglia

Microglia develop a 'primed' phenotype as they age, which is defined by an exaggerated and uncontrolled inflammatory response to an immune stimulus (Perry and Holmes, 2014). In a mouse model of prion disease, it was first observed that microglia were 'primed' by prior pathology to become permissive to exaggerated responses after a secondary inflammatory stimulus. This model featured significant synaptic degeneration in the brain, an increase in the number of local resident microglia compared to non-diseased controls, and an increase in microglial lysosomal and phagocytic activity. The term "priming" was first used to describe increased immune responsiveness after an initial inflammatory stimulus in the field of macrophage biology (Pace *et al.,* 1983). In this instance, the increased response of peritoneal macrophages to LPS after priming with IFNg was characterized by increased IL-1β and inducible nitric oxide synthase (iNOS) production compared to unprimed mouse

macrophages; this phenotype was replicated in primed microglia challenged with LPS (Cunningham *et al.*, 2005). Other mouse and rat models subsequently exhibited similar findings. including aging (Godbout *et al.*, 2005), stress (Frank *et al.*, 2007), accelerated aging with DNA damage (Raj *et al.*, 2014), Wallerian (axonal) degeneration (Palin *et al.*, 2008a), experimental auto-immune encephalomyelitis (EAE; a model for multiple sclerosis; MS (Ramaglia *et al.*, 2012), neurotoxin models of Parkinson's disease (PD) (Godoy *et al.*, 2008), and transgenic models of Alzheimer's disease (AD) pathology (Yin *et al.*, 2017).

Microglial gene expression profiles were compared across multiple mouse models of neurodegenerative disease (amyloid precursor protein (APP) transgenics and SOD1 mutant transgenics) and aging using weighted gene co-expression network analysis (WGCNA) (Holtman *et al.*, 2015a). Primed microglia showed a decrease in so-called 'homeostatic microglial signature genes' and an enrichment in KEGG pathways related to antigen presentation, lysosomes, and phagosomes. *Apoe, Axl, Clec7a, Itgax,* and *Lgals3* were among the upregulated genes in primed microglia (Keren-Shaul *et al.*, 2017a). These genes were later found to be part of a so-called disease associated microglia (DAM) signature. In addition, the DAM signature included a reduction in expression of several homeostatic genes that were also downregulated in primed microglia (*Tmem119, P2ry12*, and *Cx3cr1*). Hence, there is substantial overlap between the molecular signatures of 'primed' microglia and 'damage-associated microglia. However, it is essential to note that the primed profile associated with aging microglia does not refer to an enhanced immune response at baseline, but rather to an exaggerated inflammatory response to an immune challenge/stimulus (Cunningham *et al.*, 2005). Priming of microglia has been studied extensively in the context of systemic inflammation and neurodegenerative diseases.

5. Innate immune memory

Innate immune memory is a concept that has been around for a while, positing that even the innate immune system has some form of memory. Because of metabolic and epigenetic changes at the cellular levels, the involved cells become significantly more capable of fighting the aggression each time the innate system meets a new challenge. However, this chain reaction cannot continue indefinitely without consequences. The flip side of this idea is the permanent paralysis of cells, which means they no longer react to stimuli and become nonfunctional.(Kleinnijenhuis *et al.*, 2012a; Arts, Joosten and Netea, 2016; Van Der Heijden *et al.*, 2018; Ciarlo *et al.*, 2020; Domínguez-Andrés *et al.*, 2020; Netea *et al.*, 2020a).

5.1 The concept of Innate immune memory (IIM)

It is well known that the adaptive immune system in mammals is capable of forming immune memories that protect the host from re-infection with the same pathogen. Myeloid cells and other innate immune cells have been shown to be capable of immune memory responses (Netea *et al.*, 2015, 2016) in recent years. In this case, a first immune stimulus elicits widespread reprogramming of cells, and the same cells show enhanced or reduced responsiveness in mice and humans even after a latent period of up to a few months (Kleinnijenhuis *et al.*, 2012a; Wendeln *et al.*, 2018). There are two types of IIM states: immune training and immune tolerance. These two types of IIM states cause either increased or decreased immune responses in response to secondary stimulation (mostly assessed by cytokine release).

The concept of "immune training" was first used to describe the phenomenon of "cross-protection" (Netea *et al.*, 2016a). The protective effects of a first stimulus with the tuberculosis vaccine Bacillus-Calmette-Guerin (BCG) against a subsequent lethal infection with *Candida albicans* in animal models (Kleinnijenhuis *et al.*, 2012b; Saeed *et al.*, 2014a) and against infection with a yellow fever virus vaccine strain in human volunteers (Arts *et al.*, 2018a) are examples of training effects in vivo. Tolerance to immune responses can be induced, for instance, by administering LPS at a septic dose to mice and humans. In particular, β-glucan, a component of BCG that mimics its training effects, can be used to reduce immunosuppression in monocytes after human volunteers undergo experimental sepsis (Shalova *et al.*, 2015; Novakovic *et al.*, 2016). As a result, IIM states remain potentially modifiable in response to additional inflammatory signals.

5.1.1 Microglia manifest innate immune memory

Recent research has shown that immune stimulation can permanently alter microglial function. Microglial responses and function were found to be altered upon exposure to a second inflammatory stimulus (e.g., poly-I:C) in adulthood (as evidenced by, e.g., transcriptomic analyses) in studies where pregnant mice (termed' maternal immune activation', MIA) or neonatal animals were exposed to inflammatory stimuli (including LPS, the viral mimetic poly-I:C, and live bacteria and viruses) (Bilbo, 2010; Mattei *et al.*, 2017).

Long-term reprogramming of the immune system in the brain has been observed in adult mice, according to other studies. Wallerian (axonal) degeneration, for instance, can activate microglia in the optic tract and the superior colliculus after experimental optic nerve crush in mice. In this case, transcriptional profiling has shown that microglia can revert to their basal state after 28 days; however, microglia still show elevated IL-1 production and phagocytic responses in the optic nerve and superior colliculus in response to peripheral LPS challenge, in comparison to LPS-treated animals without axonal injury (Palin *et al.*, 2008b).

Mice infected with an attenuated strain of *Salmonella typhimurium* responded to intracerebral LPS injection 4 weeks later with increased histological staining intensity of microglial activation markers (e.g., CD11c and CD68) compared with mice that had not been infected. New evidence for IIM in adult microglia has been reported, adding to the existing body of research. In particular, a single injection of LPS (0.25 mg/kg from Escherichia coli) into the i.p. vein of 2- to 4-month-old mice suppressed IL-1β release in the brain in response to a second i.p. injection of LPS for up to 32 weeks (Püntener *et al.*, 2012; Schaafsma *et al.*, 2015).

Recent research shows that different numbers of LPS injections lead to different immune reprogramming of microglia in adult mice, which is consistent with a previous study using similar LPS injection protocols. For example, a single intraperitoneal injection of LPS (0.5 mg/kg from S. typhimurium) led to immune training 1 day later, while 4 consecutive injections of LPS (at the same dose) led to immune tolerance in the brain, as shown by increased and suppressed production of several cytokines, respectively. Furthermore, the acute immune training effect was abolished in mice lacking histone deacetylases 1 and 2 (Hdac1/2) or Tak1 (an activator of NF-kB signaling), indicating that microglia were the primary drivers of these acute alterations (Wendeln *et al.*, 2018).

Since IIM in microglia appears to share functional and phenotypic similarities with peripheral myeloid cells in mouse models, this suggests that IIM in microglia may also have a major impact on brain health and disease.

5.2 Trained immunity

The term "trained immunity" refers to the functional reprogramming of innate immune cells over the long term that occurs in response to exogenous or endogenous insults and results in a different response to a subsequent challenge following a period of inactivity. In order to impart time- and context-specific responses, it is possible to modify the secondary response to the subsequent non-specific stimulus so that the cells respond more or less strongly than to the primary response. Rather than being a specific transcriptional or functional programme, it is important to emphasize that trained immunity represents the concept of long-term adaptation of innate immune cells to a variety of stimuli (such as β-glucan, LPS, or the bacillus Calmette-Guérin (BCG) vaccine (Netea *et al.*, 2020a).

Trained immunity is mediated not by gene recombination but by epigenetic reprogramming of transcriptional pathways, in contrast to adaptive immune responses. The trained immunity immunological phenotype has been shown to last at least 3 months and up to 1 year, while heterologous protection against infections induced by live vaccines can last up to 5 years. Despite this, adaptive immune memory that is specific to a particular epitope is more long-lasting and difficult to erase than trained immunity. Recent research, however, has hinted at effects that can be felt across generations by way of trained immunity. (Netea *et al.*, 2016a, 2020a).

There are a number of key ways in which acquired immunity is distinct from the conventional immunological memory of adaptive immunity. It is carried out by a series of cellular populations that are distinct from one another in terms of their developmental history and effector roles. Myeloid cells, monocytes, macrophages, natural killer cells, and dendritic cells make up the bulk of these cells. Even innate lymphoid cells (ILCs) differ in function from conventional immune memory cells. Features of trained immunity can also be found in non-hematopoietic cells, such as epidermal stem cells. Epidermal stem cells have an interesting epigenetic memory, as some of its characteristics can be detected months after inflammation has subsided. (Netea *et al.*, 2020a; Vetvicka, Sima and Vannucci, 2021).

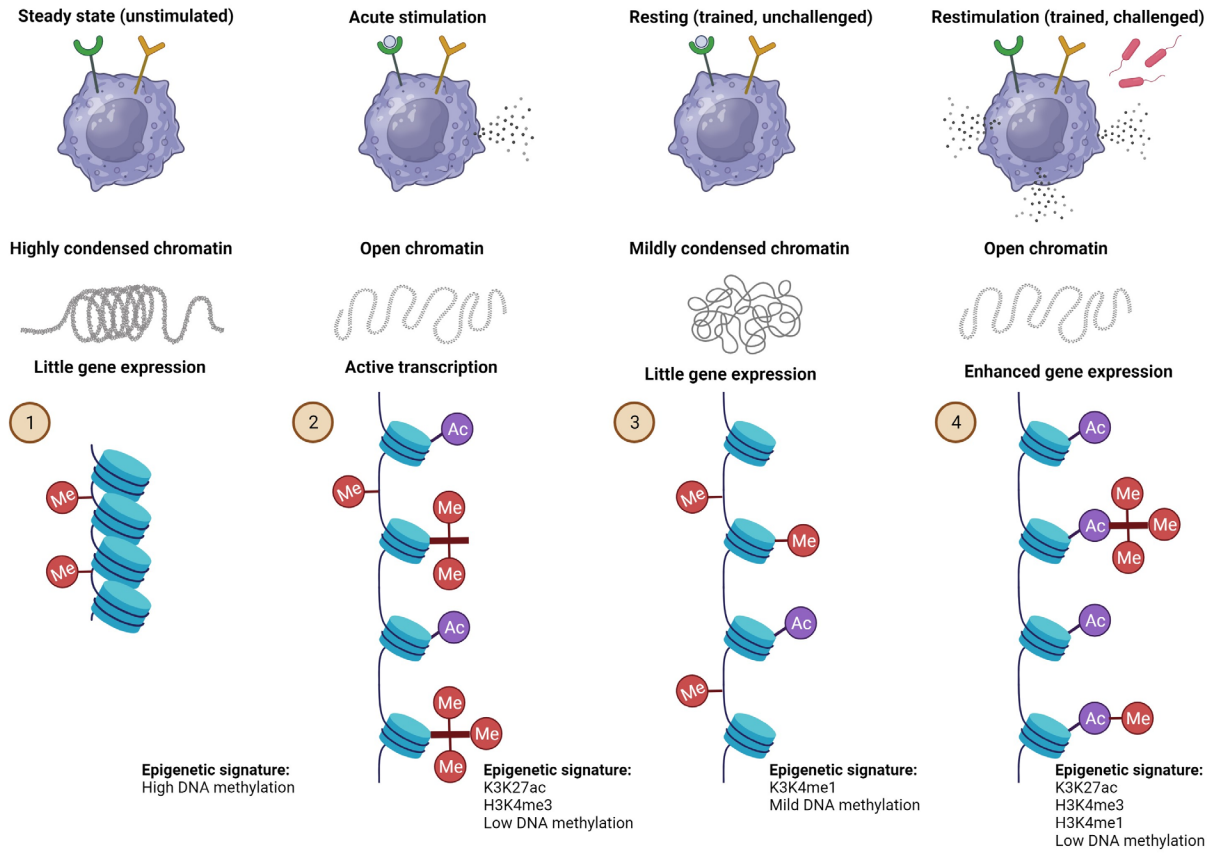

Illustration 5.2: Epigenetic reprogramming in trained immunity

(1) The cells during steady or unstimulated state **(2)** After innate immune cells are stimulated, transcription and expression of proinflammatory factors are facilitated by the unfolding of chromatin as a result of changes in DNA methylation state. **(3)** Even when the stimulus is no longer present, these alterations persist to some extent. The recruitment of transcription factors and the expression of genes following a secondary challenge is accelerated and improved as a result **(4)** Unstimulated cells, acutely stimulated cells, resting "trained" cells, trained cells that have been restimulated, are all depicted in the illustration along with their corresponding chromatin states and epigenetic signature. Histone 3 lysine 27 acetylation; histone 3 lysine 4 methylation; histone 3 lysine 4 trimethylation (abbreviated as H3K4me3, H3K4me2, and H3K4me1). *Illustration created in (Biorender.com). Adapted from* (Netea *et al.*, 2020a)*. For abbreviations please refer to list of abbreviations*

5.2.1 Epigenetic and metabolic reprogramming in Trained immunity

By inducing a trained immune phenotype in innate immune cells, these cells can respond to subsequent triggers with enhanced, more rapid, or qualitatively different transcriptional responses. There is evidence that multiple regulatory layers converge, including changes in chromatin organization at the level of the topologically associated domains (TADs), transcription of long non-coding RNAs (lncRNAs), DNA methylation, and reprogramming of cellular metabolism, to account for the altered responsiveness of a defined subset of inflammatory genes. Numerous studies have shown that

activation of innate immune cells can alter their long-term responsiveness through the implementation of trained immunity programmes, leaving a 'epigenetic scar' at the level of stimulated genes. The question of how an epigenetic scar is selectively directed to specific locations in the genome, such as the promoters of stimulated genes or distant regulatory elements, is inherent to the existence of such a scar. Key epigenetic marks that occur alongside trained immunity include the accumulation of histone 3 lysine 4 trimethylation (H3K4me3) marks at the promoters of stimulated genes and the acquisition of histone 3 lysine 27 acetylation (H3K27ac) marks at distal enhancers (marked with histone 3 lysine 4 methylation, H3K4me1) (Netea *et al.*, 2020a). Several groups of innate immune genes are partitioned into TADs (Topologically associated domains) and interact within multigene complexes, as shown by studies employing Hi-C (a technique for analyzing chromatin interactions). Recent research has shown that the structure of TADs facilitates the proximity of a group of lncRNAs known as "immune gene-priming lncRNAs" (IPLs) to transcriptionally poised innate immune genes before the transcriptional activation of these genes. To enable the epigenetic activation and training of highly responsive innate immune genes, IPLs take advantage of preformed 3D looping contacts to bring the H3K4me3 histone-modifying complex close to their promoters. These genes are responsive to β-glucan training and can respond rapidly and robustly (in a population-wide sense) because an IPL was inserted into the mouse preformed chemokine TAD (Fanucchi *et al.*, 2019).

An essential unanswered question concerns the mechanism by which the H3K27ac mark is targeted to particular distal enhancer marks (carrying H3K4me1 epigenetic marks). According to data obtained from mouse HSCs, acetylation drives the opening of specific TADs following BCG exposure, and the acquisition of open chromatin, as measured by assay for transposase-accessible chromatin using sequencing (ATAC-seq), begins in HSCs. When HSCs are differentiated into specialized myeloid and lymphoid lineage cells, the precise locations of these marks are maintained, at least in part (Kaufmann *et al.*, 2018).It remains to be formally analyzed and established whether or not the H3K4me1 marks established in the HSC lineage are maintained in terminally differentiated myeloid cells and whether or not the gain and loss of H3K27ac occurs in response to exposure to LPS tolerization and β-glucan priming. The central mystery of how trained immunity is reliably maintained concerns the transmission of these marks through DNA replication and the cell cycle (Natoli and Ostuni, 2019).

HSCs maintain H3K4me1 and H3K4me3 marks throughout the cell cycle via some unknown mechanism. MicroRNAs may also be involved in these processes, both in their induction and their regulation. It was discovered that miR-155 plays a crucial role in adaptive NK cell responses to MCMV infection by regulating targets like NOXA and SOCS1 (Zawislak *et al.*, 2013; Lu *et al.*, 2015). The

ability to respond to stimuli that induce trained immunity, such as BCG, has been linked to changes in DNA methylation patterns, according to recent studies. Specifically, in comparison to those classified as non-responders, those who show increased containment of *M. tuberculosis* replication after BCG vaccination exhibited a widespread loss of DNA methylation among promoters of genes belonging to immune pathways (Verma *et al.*, 2017).

Epigenetic reprogramming of innate immune cells and their progenitors is dependent on cellular metabolism, which plays a crucial mediating role in this process. Since it is well known that metabolites can regulate the activity of chromatin-modifying enzymes, rewiring the metabolism of innate immune cells or their progenitors will govern the flexibility and epigenetic reprogramming of these cells in the context of acquired immunity (Donohoe and Bultman, 2012a; Norata *et al.*, 2015; Domínguez-Andrés, Joosten and Netea, 2019a; Penkov *et al.*, 2019). AKT, mTOR, and hypoxia-inducible factor 1 (HIF1) all play a role in the increased aerobic glycolysis that characterizes monocytes that have been trained with β-glucan. Consistently, inhibiting the AKT-mTOR-HIF1 pathway reverses the effects of vaccination. In addition, the metabolic reprogramming of monocytes toward aerobic glycolysis is functionally necessary for BCG-induced trained immunity to develop enhanced responsiveness to subsequent stimulation (Cheng *et al.*, 2014; Arts *et al.*, 2016).

Crosstalk between glycolysis and glutaminolysis in trained immunity was discovered in subsequent studies using integrated metabolomic and transcriptomic analyses of human β-glucan-trained monocytes. By decreasing the activity of KDM5 histone demethylases, the tricarboxylic acid cycle (TCA) metabolite fumarate affects epigenetic reprogramming in trained monocytes. Furthermore, the activity of innate immune cells is affected in different ways by the various TCA intermediates. For instance, the H3K27 demethylase JMJD3 mediates the epigenetic reprogramming by which α-ketoglutarate encourages anti-inflammatory activation of macrophages. When administered after classical LPS-mediated or IFN—mediated activation of macrophages, α-ketoglutarate promotes endotoxin tolerance (Arts, Novakovic, *et al.*, 2016; Liu *et al.*, 2017). However, in mouse bone marrow-derived macrophages, LPS-induced succinate controls a proinflammatory HIF1-IL-1 pathway. By blocking succinate dehydrogenase-mediated oxidation of succinate to fumarate, the metabolite itaconate, whose concentration is highly upregulated in LPS-activated macrophages, exerts anti-inflammatory activity. In macrophages, itaconate has an anti-inflammatory effect by preventing LPS-induced NF-kappa B induction and bolstering the activity of the anti-inflammatory transcription factor NRF2. This latter itaconate-induced change does not involve NRF2, but rather activating transcription

factor 3 (ATF3) (Tannahill et al., 2013; Cordes et al., 2016; Lampropoulou et al., 2016; Bambouskova et al., 2018; Mills et al., 2018).

Interestingly, β-glucan inhibits the expression of immune-responsive gene 1 (IRG1) protein, the enzyme responsible for itaconate generation, thereby counteracting the tolerance that itaconate induces in human monocytes through the induction of trained immunity. Increased expression of succinate dehydrogenase is a result of β-glucan-mediated inhibition of IRG1, which is consistent with fumarate accumulation in β-glucan-trained monocytes. As a result, the endotoxin tolerance-inducing effects of itaconate, an antagonist of succinate dehydrogenase, are reversed following β-glucan-induced trained immunity, along with increased succinate dehydrogenase activity and accumulation of fumarate. (Arts, Novakovic, *et al.*, 2016; Domínguez-Andrés *et al.*, 2019). One of the most notable characteristics of β-glucan-trained monocytes is their increased cholesterol synthesis. Fluvastatin, an inhibitor of 3-hydroxy-3-methylglutaryl coenzyme A (HMG-CoA) reductase, suppresses acquired immunity in human primary monocytes. Mevalonate, a metabolite produced during cholesterol biosynthesis, accumulates to achieve this effect. Through activation of the insulin-like growth factor 1 receptor and mTOR signaling, mevalonate can initiate monocyte training. Not only do mature myeloid cells benefit from β-glucan-induced training, but so do their progenitors (hematopoietic stem and progenitor cells, or HSPCs) (Bekkering *et al.*, 2018).

Accumulation of cholesterol esters and lipids with more saturated acyl chains is associated with the long-term myelopoiesis bias conferred to HSPCs by β-glucan-induced training. HMG-CoA reductase inhibition reduces β-glucan-induced HSPC expansion and myelopoiesis. The upregulation of CD131, the common -subunit of the IL-3/GM-CSF receptor, may promote a myelopoiesis bias as a result of the increased cholesterol levels in HSPCs that occur as a result of innate training. Consistent with these results, it has been found that a lack of the ATP-binding cassette transporter ABCA1 in HSPCs increases CD131 expression and myelopoiesis in the bone marrow (Yvan-Charvet *et al.*, 2010; Murphy *et al.*, 2011; Mitroulis *et al.*, 2018).

5.3 BCG induced Trained immunity

The *Mycobacterium bovis* strain attenuated through serial passage was used to create the Bacillus Calmette-Guérin (BCG) vaccine. In 1908, Albert Calmette and Camille Guérin at the Pasteur Institute in Lille first isolated *Mycobacterium bovis* from a glycerol bile potato medium. They found that the

strain, which they named BCG , protected the body from attack by the virulent *Mycobacterium tuberculosis* after serially passaging it from 1908 to 1921 (Petroff and Branch, 1928). In 1924, BCG production went into mass production, and after widespread intradermal injection vaccination, its benefits were discovered to extend beyond tuberculosis prevention. Autopsy research conducted by Pearl in 1928 revealed a low rate of cancer among tuberculosis patients (Pearl, 1928). Subsequent epidemiological studies demonstrated that BCG could reduce infant mortality regardless of whether or not the child had tuberculosis (LEVINE and SACKETT, 1946; Ferguson and Simes, 1949; ROSENTHAL *et al.*, 1961). This generated a lot of interest and provided a novel perspective on investigating BCG's potential role in other diseases. Studies in the years following BCG inoculation have shown that BCG-inoculated mice can prevent infections like *Plasmodium* (Clark, Allison and Cox, 1976), *Schistosoma mansoni* (Civil, Warren and Mahmoud, 1978), providing further evidence for BCG induced non-specific protection. In 1988, (Bistoni *et al.*, 1988) demonstrated that cytotoxic T cells and B lymphocytes do not play a key role in the protection against *C. albicans* infections by vaccinating athymic mice against the fungus. This protective effect was not due to T or B cells, suggesting that BCG may provide immunity without relying on adaptive immunity.

In 2003, (Garly *et al.*, 2003) demonstrated that BCG vaccination in West African children could reduce morbidity from infections other than tuberculosis, thereby lowering overall mortality. BCG has been hypothesized to provide broad immunity, making it effective against a wide range of infections; however, more research is needed to determine how this happens. Monocytes (Mo), macrophages (M), natural killer cells (NK), dendritic cells (DC), and neutrophils were thought to mediate these nonspecific protective effects until 2011. Immune memory was shown to be a feature of innate host defenses, as demonstrated by (Netea *et al.*, 2016b). This characteristic is referred to as "trained immunity" (Netea, Quintin and Van Der Meer, 2011a) . An epigenetic change at the level of histone methylation (H3K4me3) mediated by NOD2 was shown to be the mechanism by which BCG enhances innate immune responses in a 2012 study that combined in vivo and in vitro experiments (Kleinnijenhuis *et al.*, 2012a). Epigenetic regulation of monocyte-to-macrophage differentiation and trained immune pathways was first shown to be important by (Saeed *et al.*, 2014a). Additionally, (Cheng *et al.*, 2014b) demonstrated that keeping trained immunity active requires a metabolic switch to aerobic glycolysis. Metabolism and epigenetic modification are intertwined, and positive feedback loops may enhance trained immunophenotypes, according to a 2016 study that examined the connection between epigenetics and metabolism-induced trained immunity (Arts, Carvalho, *et al.*, 2016b). Considering that mature innate immune cells (e.g., monocytes) have a short lifetime in

circulation compared to the duration of trained immunity, a study demonstrated that BCG-induced HSC reprogramming changes the transcriptional patterns of hematopoietic stem cells (HSCs) and multipotent progenitor cells (MPPs) in the bone marrow (Mitroulis *et al.*, 2018b). By reprogramming hematopoietic stem cells (HSCs) with BCG, trained monocytes/macrophages can persist in vivo and offer enhanced protection (Kaufmann *et al.*, 2018). This extends the trained immune mechanism to the level of HSCs. It's been 100 years since BCG was first used to treat and prevent tuberculosis, but the vaccine's effectiveness varies from patient to patient. Preventing widespread tuberculosis is the primary indication for administering BCG to children (Trunz, Fine and Dye, 2006). BCG has anti-cancer properties as well. In 1959, Old LJ. et al. demonstrated that BCG inhibited tumor growth by stimulating the immune system and slowed tumor progression. (Old, Clarke and Benacerraf, 1959; Han and Pan, 2006). Non-muscle invasive bladder cancer has traditionally been treated with BCG therapy (Larsen *et al.*, 2020). Several different viruses can be inhibited by BCG's antiviral properties. To prevent infection by yellow fever attenuated vaccine strains in humans during experimental infection, BCG was shown to induce genome-wide epigenetic reprogramming in monocytes (Arts *et al.*, 2018b). This reprogramming may be essential for the protective function of IL-1 produced by monocytes. In the case of autoimmune disorders, BCG may also be extremely useful. Hyperglycemia in patients with advanced type 1 diabetes has been shown to decrease after BCG inoculation (Kühtreiber *et al.*, 2018).

BCG may also have some effects on a wide variety of other diseases. For instance, BCG reduces human malaria infection in some volunteers (Palin *et al.*, 2008a), and BCG immunotherapy for bladder cancer is associated with a significantly reduced risk of Alzheimer's disease and Parkinson's disease (Klinger *et al.*, 2021). Surprisingly, there is not enough proof that BCG vaccination can prevent malaria (Rodrigues *et al.*, 2007; Witschkowski *et al.*, 2020). Furthermore, BCG can hasten the development of chronic inflammatory disorders (Li *et al.*, 2022). This demonstrates that trained immunity has both beneficial and detrimental effects on the treatment of cancer, viruses, and autoimmune diseases.

5.3.1 BCG and Multiple Sclerosis (MS)

The potential modulation of T-cell-mediated immunity by BCG has been shown to have a beneficial effect on the activity of multiple sclerosis (Ristori *et al.*, 2018). Relapsing-remitting multiple sclerosis patients had less MRI activity after a single dose of BCG vaccine, according to a phase two clinical trial (Paolillo *et al.*, 2003). BCG vaccination delayed the onset of a second demyelinating episode by five years in people with clinically isolated syndrome, suggesting that the vaccine has long-lasting effects. Antibodies against BCG antigenic proteins have been found to be less tightly bound in MS

patients compared to healthy and disease control subjects in retrospective studies (Ristori *et al.*, 2014a; Cossu *et al.*, 2017). The BCG vaccine's protective effects against MS have been studied predominantly in the experimental autoimmune encephalomyelitis (EAE) model (Cossu *et al.*, 2021).

Injecting C57Bl/6J female mice with BCG intraperitoneally six weeks prior to myelin oligodendrocytes glycoprotein (MOG) - induced EAE reduced the clinical severity of the disease in a dose-dependent manner (Sewell *et al.*, 2003). Active BCG infection decreased the number of interferon gamma (IFNg)+ CD4+ cells and spinal cord demyelination by diverting MOG-specific cells to granulomas in the spleen and liver. It was shown that intracerebral infection with BCG is more effective than intraperitoneal infection at producing the desired suppressive effect (Lee *et al.*, 2008). Live BCG Pasteur strain injected intracerebrally suppressed MOG-specific IFNy+CD4+ and IL17+CD4+T cells and reduced mononuclear cell infiltration in the spinal cord, preventing EAE development in C57BL/6J mice. BCG's suppressive effect on EAE was not due to Foxp3+CD4+ T cells, but rather to Il-17+ CD4+ T cells in an IFNg-independent fashion. Consistent with previous research using a murine EAE model in which mycobacterial antigen-specific T cells are not induced (cell wall skeleton (CWS)-EAE), these results were observed in this study (Lee *et al.*, 2008; Matsuzaki *et al.*, 2021a). Vaccinating C57Bl/6J mice intraperitoneally with the BCG Tokyo 172 strain 6 days after inducing CWS-EAE reduced disease severity by decreasing the number of MOG-specific Il-17+ CD4+ T cells in the central nervous system (CNS) and increasing their number in the draining lymph nodes. These results confirmed that BCG inhibits Th17 responses in the central nervous system via a mechanism involving the restriction of peripheral trafficking of encephalitogenic T cells. C57Bl/6J mice with MOG-induced EAE were treated with subcutaneous injections of BCG that had been inactivated by extended freeze drying, demonstrating an immunomodulatory effect (Lippens *et al.*, 2018; Matsuzaki *et al.*, 2021a). The levels of TNF-alpha and Il-1B were reduced after receiving BCG treatment, which reduced disease severity and facilitated symptom recovery. The expression of suppressive IL-10 secreted by regulatory T cells was linked to BCG's ability to inhibit encephalitogenic T cells both systemically and locally in the central nervous system. Similarly, immunization with the BCG Moreau-Rio de Janeiro strain, followed by boosters with a vaccine containing the mycobacterial heat shock protein (HSP) gene, significantly suppressed IL-10 and IFNg levels induced by myelin basic protein in Lewis rats, thereby modulating the host immune response. BCG's ability to increase T cell apoptosis is being investigated as a potential mechanism by which it suppresses autoimmunity during infection. Mice that had been infected with the BCG Pasteur strain had less severe EAE than controls when subjected to a passive transfer model of the disease. Increased peripheral apoptosis in MOG-specific CD4+T cells was observed in BCG-

infected mice (O'Connor, Wittmer and Dalton, 2005; Zorzella-Pezavento *et al.*, 2013; Lippens *et al.*, 2018)

5.4 Intersection of microglia priming and Trained immune response

In order to answer the question of whether or not a primed microglial state (as observed in chronic neurodegenerative diseases and aging (Holtman *et al.*, 2015) resembles the molecular profile of microglia trained by a single i.p. injection of LPS in mice (Wendeln *et al.*, 2018), further research into the molecular pathways and mechanisms of the effects of different primary and secondary stimuli (with differing strength, duration, etc.) and their various combinations is required.

Some homeostatic genes (e.g., *Tmem119, P2ry12*, and *Cx3cr1*), as well as most DAM genes in one gene module, were upregulated in microglia isolated from WT and APP transgenic mice treated with i.p. LPS 6 months earlier (either 1x or 4x), as well as from APP control mice. This module partially reflects a primed microglial gene expression network because it is rich in pathways related to the lysosome, the phagosome, and oxidative phosphorylation. However, there appears to be little overlap between trained microglia and microglia primed in models of chronic brain disease for example, in mouse models of Alzheimer's disease (AD), amyotrophic lateral sclerosis (ALS), and accelerated aging; furthermore, both profiles are significantly different from those of microglia isolated from mice with a 'acute post-LPS transcriptional profile (Holtman *et al.*, 2015b; Wendeln *et al.*, 2018).

6. Lipid processing in myeloid cells

The majority of the brain's dry weight is made up of white matter that is myelin-enriched (Hamilton *et al.*, 2007). Myelin, is composed of roughly 43% phospholipid (PL), 28% glycosphingolipid, and 28% cholesterol by weight. Normal brain functions rely on tightly regulated lipid metabolism in the central nervous system. As a result of their insolubility in water, lipids like cholesterol and triglycerides must be transported with Apo proteins to form an emulsion that can then be pumped through the extracellular milieu and/or the peripheral circulation to reach other cells. A hydrophobic core of neutral lipids like CEs (Cholesterol esters) and TGs (Triglycerides) is surrounded by an amphipathic monolayer of PLs (phospholipids), free cholesterol, and apolipoproteins to form lipoproteins (Loving and Bruce, 2020). This chapter thus discusses the transcriptional and signaling pathways that regulate macrophage phagocytosis of myelin debris, as well as the processing of the lipids contained within such debris.

6.1 Myelin debris phagocytosis and degradation

Cholesterol plays a crucial role in the cell membranes of neurons in the brain. The central nervous system accounts for 23% of the body's total cholesterol content, the vast majority of which is found in the cell membranes of neurons and myelin (Hamilton *et al.*, 2007). The accumulation of myelin debris that results from the destruction of myelin in neuroinflammatory diseases can stimulate microglial phagocytosis, directly inhibit remyelination, and propagate a pro-inflammatory response (Calder, 2015; Kopper and Gensel, 2018). Myelin debris is recognized by microglia and MDMs through the use of scavenger receptors such as SRII and complement receptors such as CR3 (Smith, 2001; Takahashi, Rochford and Neumann, 2005). Phosphoinositide 3-kinase (PI3K)-dependent signaling pathways are activated by these receptors, leading to actin filament rearrangement and phagocytic uptake of myelin debris.

The lysosome is responsible for breaking down ingested lipids into free cholesterol and free fatty acids. Endoplasmic reticulum (ER) re-esterification of free cholesterol to cholesterol fatty acid esters allows cholesterol to be stored in the cytosol in lipid droplets, contributing to the "foam" of foam cells. The other option is for free cholesterol to be effluxed out of the cell via the plasma membrane. The accumulation of cholesterol in cells activates a number of transcription factors (TFs) including the liver X receptor and (Lxra, Lxrb), the retinoid X receptor (Rxr), and the peroxisome proliferator-activated

receptor (Ppar) family members Ppar-α and Ppar-γ (Klappacher and Glass, 2002; Maxfield and Tabas, 2005; Duffy and Rader, 2009).

The transcriptional regulation of expression of cellular cholesterol efflux proteins like ApoE and ATP-binding cassette transporters (ABCs) is mediated by the heterodimerization of ligand-bound LXR and retinoid X receptor (RXR) (Zhao and Dahlman-Wright, 2009). Cholesterol is incorporated into ApoE-containing high-density-lipoprotein (HDL)-like particles, and the efflux of cholesterol is mediated by ABCA1 and ABCG1 (Hirsch-Reinshagen *et al.*, 2004).

There are two alternative pathways for passive efflux of free cholesterol: aqueous diffusion and SR-BI-mediated facilitation of diffusion (Phillips, 2014). It is well established that CSF cholesterol is elevated in MS patients, most likely as a result of impaired cholesterol elimination. Hence, Cholesterol clearance is an important function of microglia (Van De Kraats *et al.*, 2014; Lavrnja *et al.*, 2017; Cantuti-Castelvetri *et al.*, 2018).

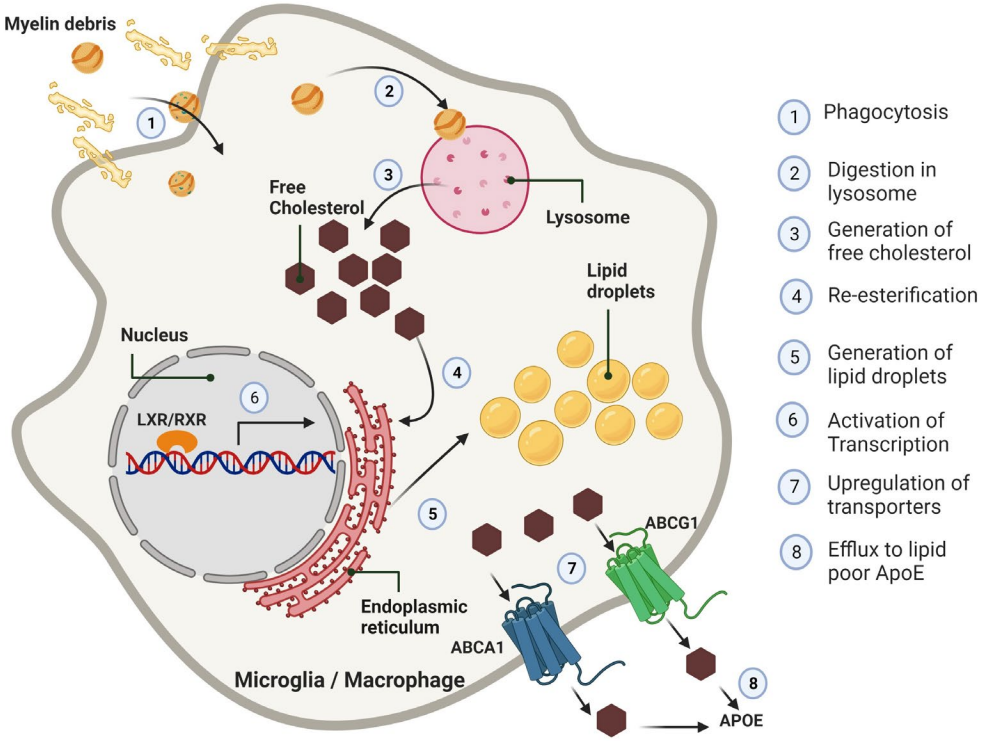

Illustration 6.1: Overview of lipid metabolism in microglia / macrophages

Myelin lipid fragments and oxidized lipoproteins are taken up through micropinocytosis, phagocytosis, and scavenger receptor-mediated processes in macrophages. After the lysosome breaks down the ingested lipids, free cholesterol and fatty acids are produced. As cellular cholesterol builds up, several transcription factors, including PPAR, LXRs, and RXRs become active. These transcription factors then control the expression of their target genes, which include transporters like

ABCA1 and ABCG1 that control the efflux of free cholesterol and scavenger receptors. A different possibility is passive outflow of free cholesterol.
Illustration created in (Biorender.com). For abbreviations please refer to list of abbreviations

6.2 The LXR and RXR pathway

Liver X receptors (LXRs) are transcription factors that respond to oxysterol ligands and serve primarily as cholesterol sensors. Macrophages can acquire oxysterols from ingested oxLDL or produce them endogenously by modifying cholesterol. LXRs regulate reverse cholesterol transport, which is perhaps their most well-known role (see above). By controlling the expression of the cholesterol efflux transporters ABCA1 and ABCG1, LXRs lower cellular cholesterol levels in macrophages. LXR signaling not only upregulates the expression of cholesterol efflux transporters, but it can also upregulate the expression of cholesterol receptor apolipoproteins like ApoE and ApoC. (Costet *et al.*, 2000; Repa *et al.*, 2000; Schwartz, Lawn and Wade, 2000; Venkateswaran *et al.*, 2000; Laffitte *et al.*, 2001).

Mice deficient in ApoE only in macrophages are more prone to developing atherosclerosis (Curtiss, 2000), demonstrating the significance of apolipoproteins in macrophage cholesterol efflux. LXRs function in macrophages to lower cholesterol by increasing production of lipoprotein remodeling proteins such as LPL. Several studies have linked LXRs to the regulation of glucose metabolism and innate and adaptive immune responses, in addition to their role in lowering cholesterol levels. The latter is represented in macrophages by LXR activation that suppresses inflammatory mediators like iNOS and Cox2 (Zhang *et al.*, 2001; Joseph *et al.*, 2003; Castrillo and Tontonoz, 2004).

Some of the most well-known genes that LXR interacts with are:

- *Abca1* and *Abcg1*: Cholesterol efflux is mediated by the ABC-type transporters abca1 and abcg1, which move free cholesterol from the cytoplasm of the cell to lipoproteins. ABCG1 effluxes cholesterol into APOE-containing lipoproteins, whereas ABCA1 preferentially binds to APOA1-containing lipoproteins that are low in lipids.
- *Apoa1* and *Apoe*: To form lipoproteins, remove cholesterol from the body, and transport cholesterol in reverse, apolipoproteins A1 and E (Apoa1 and Apoe) are essential (Cummins and Mangelsdorf, 2006).
- *Srebp1c*: Increased fatty acid synthesis and other lipogenic gene expression is mediated by the transcription factor Srebp1c (Hong and Tontonoz, 2014).

- *Npc1* and *Npc2*: Npc1 and Npc2 are proteins that control the movement of cholesterol within cells (Rigamonti *et al.*, 2005).

6.3 The PPAR pathway

The nuclear hormone receptor superfamily called peroxisome proliferator-activated receptors (PPARs) plays an established role in lipid metabolism through its family of transcription factors. Homodimerization with RXRs activates PPARs, just as it does LXRs (Gearing *et al.*, 1993). The family includes PPARα, which is linked to lipid metabolism in the liver and heart, PPARβ, which is expressed ubiquitously, and PPARγ, which is highly expressed in adipose tissue and is required for adipocyte differentiation. PPARγ, a fatty acid receptor, has been shown to play a significant role in cholesterol metabolism. Lipid accumulation in macrophage cells in atherosclerotic plaques has been shown to be controlled by PPARγ. To do this, it controls the expression of cholesterol efflux genes like ABCA1 and ABCG1 and scavenger receptors involved in lipid uptake like CD36 and SR-A, by activating LXR (Ricote *et al.*, 1998; Tontonoz *et al.*, 1998; Chawla *et al.*, 2001; Chinetti *et al.*, 2001). Because of this role, decreased or absent PPARγ expression in macrophages is linked to elevated risk of atherosclerosis and insulin resistance (Odegaard *et al.*, 2007).

6.4 The SREBP pathway

Cholesterol and lipid synthesis are controlled by SREBPs, which are encoded by the genes Srebf1 and Srebf2. Leucine zipper TFs are a subfamily of basic helix-loop-helix TFs. SREBPs are kept in the endoplasmic reticulum by intracellular cholesterol, desmosterol, and oxysterols; however, when these levels drop, SREBPs are released into the nucleus, where they bind to sterol regulatory elements (SREs) and induce gene transcription, resulting in increased cholesterol and fatty acid synthesis. The accumulation of newly synthesized sterols then inhibits the cleavage and exit of the ER-bound SREBPs, creating a negative feedback loop. Deleting the genes Insig1 and Insig2 that keep SREBP in the ER is harmful because it leads to lipid accumulation, which has been linked to lipotoxicity in alveolar macrophages (Plantier *et al.*, 2012).

6.5 Epigenetic regulation of lipid metabolism: Focus on HDACs

Histone deacetylases (HDACs) are classified into the sirtuin protein family and the histone deacetylase family based on the presence of a conserved deacetylase domain and the requirement for specific

cofactors. Class I deacetylases include HDAC1, 2, 3, and 8, while class II includes HDAC4, 5, 6, 7, 9, and 10, and class IV includes HDAC11. All deacetylases are zinc-dependent amidohydrolases. Class II enzymes are further subdivided into IIa and IIb subgroups based on the domain compositions of their active sites. Class III histone deacetylases (HDACs) include the sirtuin proteins, which rely on the cofactor nicotinamide adenine dinucleotide (NAD) to carry out their catalytic activity. There are 18 reported mammalian HDACs, which can be broadly categorized as described above (Park and Kim, 2020).

Recently it has been reported that chromatin-remodeling events regulate lipid metabolic homeostasis. It was discovered that inhibiting class I HDACs is a novel mechanism for controlling ApoE expression and secretion in astrocytes (Dresselhaus *et al.*, 2018). Inhibition of histone deacetylase has also been shown to control lipid homeostasis in a mouse model of Amylotropic lateral sclerosis (Burg *et al.*, 2021).

Histone deacetylase 9 (HDAC9) has been linked to lipid metabolism, atherosclerosis progression, and macrophage polarization via histone acetylation changes at target genes (Cao *et al.*, 2014). HDAC9 risk alleles are associated with increased HDAC9 expression in human monocytes/macrophages and atherosclerotic plaques in humans. (Asare *et al.*, 2020) utilized in vitro assays, in vivo genetic mouse models, including Hdac9 deficient (*Hdac9-/-*) mice, and therapeutic interventions to investigate the mechanisms underlying HDAC9's involvement in atherosclerosis and vascular inflammation. Experiments with bone marrow transplantation were used to evaluate the effects of Hdac9 hematopoietic deficiency. *Apoe-/-* mice that received bone marrow from *Hdac9-/-* mice had smaller and fewer atherosclerotic lesions than mice that received bone marrow from wild-type (*Hdac9+/+*) mice. (Knutson *et al.*, 2008) demonstrated in another study that HDAC3 deletion disrupts normal lipid homeostasis. Mice lacking liver-specific Hdac3 exhibit hepatomegaly due to hepatocyte hypertrophy, as well as altered carbohydrate and lipid metabolism.

The enzyme cholesterol 7-hydroxylase (CYP7A1) plays a crucial role in cholesterol homeostasis because it acts as a rate-limiting checkpoint in the process of hydroxylating cholesterol at the 7 position. Hypercholesterolemia with elevated LDL cholesterol levels is seen in patients with a homozygous deletion mutation in CYP7A1, as shown by research by (Mitro *et al.*, 2007). It has been shown that CYP7A1 and bile acid synthesis play a vital role in regulating cholesterol levels in the body. Bile acids act as a negative feedback regulator on the CYP7A1 gene's transcription. In response to bile acids, HDAC7 moves from the cytoplasm to the nucleus and is then recruited to the promoter of the CYP7A1

gene in a sequence that includes HDAC3, HDAC1, SMRT, and NCoR1. This repressor complex mediates histone deacetylation, which blocks the recruitment of transcriptional factors that normally inhibit CYP7A1. Serum LDL-fraction cholesterol is reduced and CYP7A1 expression is induced when HDAC inhibitors are given to LDL receptor deficient (Ldlr-/-) mice, a genetic model of hypercholesterolemia (Mitro *et al.*, 2007).

Several lines of evidence have accumulated in recent years suggesting that sirtuins act as energy sensors and regulators in various metabolic tissues, thereby influencing metabolic processes such as energy metabolism and insulin sensitivity. Among the sirtuin family, SIRT1 and SIRT3 action in lipid metabolism is the most studied and well characterized. SIRT1 is a positive regulator of liver X receptors (LXRs), as shown by (Li *et al.*, 2007), who showed that SIRT1 deacetylates LXRs at lysine K4 in a loop region adjacent to the ligand activation domain. This led the authors to speculate that SIRT1 might play a role in maintaining healthy cholesterol levels. The ATP-binding cassette transporter (Abca1) is critical for HDL synthesis and reverse cholesterol transport, and SIRT1 is the LXR target gene that activates its transcription.

Hypothesis and aim of this project

In previous studies, we observed that remyelination in aged animals is limited due to inadequate activation and cholesterol clearance by microglia / macrophages. Stimulation of the LXR pathway in aged mice promoted cholesterol efflux by microglia and MDMs and improved myelin regeneration after toxin-induced demyelination (Cantuti-Castelvetri *et al.*, 2018). However, the underlying mechanisms behind inadequate gene expression in microglia/macrophages necessary for resolving the inflammation are unknown. Immune function declines with age due to immunosenescence, but in addition to this, a gain-of-function occurs in the form of a pro-inflammatory state known as inflammaging (Fulop *et al.*, 2018).

Hypothesis: We hypothesized that the activation of trained immunity in microglia/macrophages of aged mice, through an innate immune training protocol using BCG, would modulate the epigenetic regulation and enhance the efficiency of remyelination after toxin-induced demyelination. Furthermore, we proposed that the epigenetic rigidity resulting from chromatin architecture disruptions contributes to the limited adaptive responses following central nervous system (CNS) injury, ultimately leading to remyelination failure in aged animals.

Aim: The aim of this study was to investigate the influence of trained immunity on the function of microglia in the context of demyelination and remyelination in aged mice.

Specifically, we aimed to:

1. Assess the response of microglia to demyelinating injury in aged animals through combined transcriptomic and epigenomic analysis.
2. Examine the efficiency of remyelination in aged mice following the activation of trained immunity using a mouse model of toxin-induced demyelination.
3. Investigate the epigenetic regulation modulated by trained immunity in microglia/macrophages of aged mice, focusing on the chromatin architecture disruptions and their impact on adaptive responses after CNS injury.
4. Gain a deeper understanding of the cellular and molecular mechanisms underlying remyelination failure in aged animals, potentially identifying new targets for remyelination-promoting therapies.

By addressing these objectives, we aimed to contribute to the existing knowledge on the role of trained immunity and epigenetic regulation in microglia function, with implications for developing novel therapeutic strategies to enhance remyelination in aging and age-related neurodegenerative disorders.

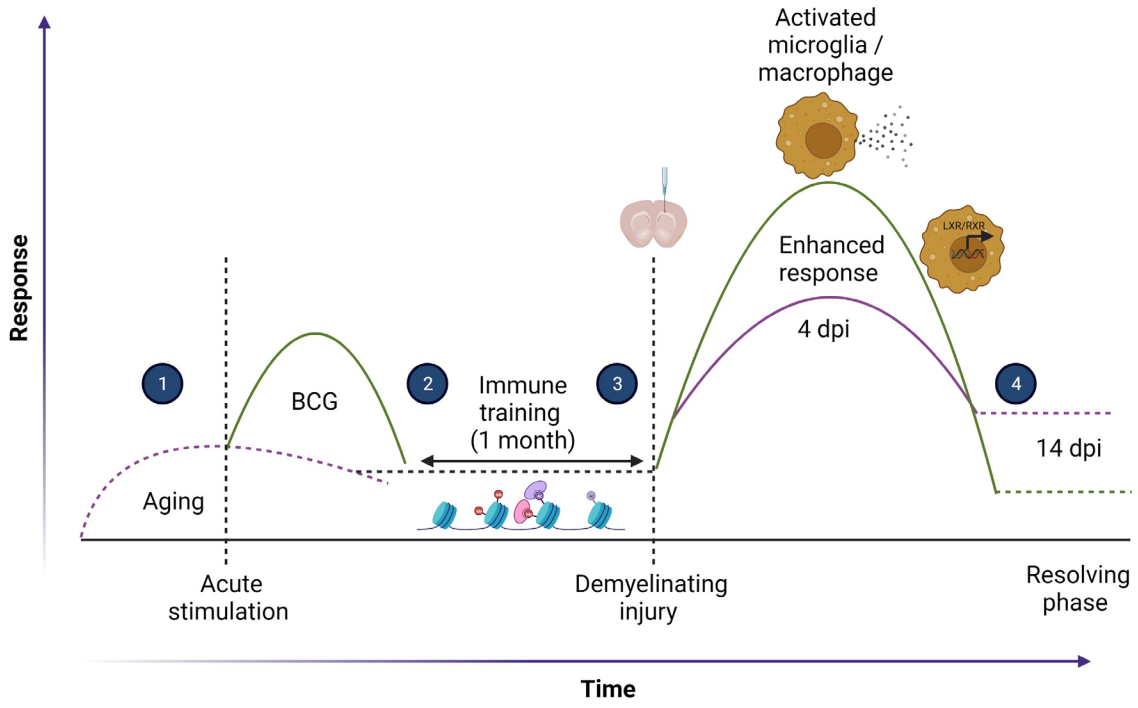

Hypothesis 1.1: Illustration to explain the working hypothesis

(1) Inflammaging, a part of the aging process, is characterized by a low-grade inflammatory condition that is harmful to the precise microglia / macrophage activation necessary for inflammation resolution and lesion recovery.

(2) We tested the hypothesis that peripheral stimulation of aged mice with BCG could instruct microglia and macrophages.

(3) After a month of primary stimulation, LPC-induced demyelinating damage was used as secondary stimulation to examine the impact of trained immune response on microglia response and lesion repair.

(4) We expected the microglia response to demyelinating damage is enhanced by training with BCG, thus leading to more effective lesion repair.

Materials and methods

1. Materials

Table 1: Resource table

REAGENT or RESOURCE	SOURCE	IDENTIFIER
Antibodies		
Rabbit anti-IBA1	Wako	Cat# 019-19741, RRID:AB_839504
Chicken anti-IBA1	Synaptic systems	Cat# 234 009, RRID:AB_2891282
Guinea pig anti-IBA1	Synaptic systems	Cat# 234 308, RRID:AB_2924932
Rat anti-MAC2	Bio legend	Cat# 125402, RRID:AB_1134238)
Rat anti-MHCII	Thermofisher Scientific	Cat# 14-5321-81,RRID:AB_467560)
Rabbit anti-PLIN2	Novus Biologicals	Cat#NB11040877,RRID:AB_787904
Rabbit anti-OLIG2	Millipore	Cat# AB9610, RRID:AB_570666)
Mouse anti-APC-CC1	Millipore	Cat# OP80, RRID:AB_2057371
Rat anti-CLEC7A	InvivoGen	mabg-mdect,RRID:AB_2753143
Rat anti-LAMP1	Santa Cruz Biotechnology	Cat# sc-19992, RRID:AB_2134495
Rabbit anti- Histone (H3K4me3)	Diagenode	Cat# C15410003, RRID:AB_2924768
Rabbit anti- Histone (H3K27ac)	Diagenode	Cat# C15410196, RRID:AB_2637079
Alexa Fluor 555	Thermofisher Scientific	Cat# A-21422, RRID:AB_2535844
Alexa Fluor 555	Thermofisher Scientific	Cat# A-21428, RRID:AB_2535849
Alexa Fluor 647	Thermofisher Scientific	Cat# A-21244, RRID:AB_2535812
Alexa Fluor 647	Thermofisher Scientific	Cat# A-21450, RRID:AB_141882
Alexa Fluor 647	Jackson ImmunoResearch	Cat# 712605150,RRID:AB_2340693)
Bacterial strain		
BCG (Bacillus Calmette Guérin) (RIVM strain)	Medac GmbH	N/A
Chemicals, peptides, and recombinant proteins		
FluoroMyelin	Thermofisher Scientific	Cat# F34651
DAPI	Thermofisher Scientific	Cat# D1306
Tamoxifen	Sigma	Cat# T5648
4- Hydroxy-Tamoxifen	Sigma	Cat# H7904
L-α-lyso-Lecithin (Lysolecithin)	Sigma-Aldrich	Cat# L4129
Critical commercial assays		
Invisorb Spin Tissue Mini Kit	Invitek	Cat# 1032100300
Adult tissue dissociation kit	Miltenyi Biotech	Cat# 130-107-677
RNeasy Plus Mini kit	QIAGEN	Cat# 74134
Superscript III First strand Synthesis	Thermo fisher Scientific	Cat# 18080051
RNAscope Multiplex Fluorescent v2 assay	Advanced cell Diagnostics	Cat# 323100
Chromium Next Gen Single Cell 3' HT kit v3.1	Illumina	Cat# 1000348
iDeal ChIP-seq kit for Histones	Diagenode	Cat# C01010059
High Sensitivity NGS Fragment Analysis Kit	Agilent	Cat# DNF-474
DNA Clear & Concentrator TM-5 kit	Zymo-research	Cat# D4014

IP-Star® Compact Automated System	Diagenode	Cat# B03000002
MicroPlex Library Preparation Kit v3 /96 rxns	Diagenode	Cat# C05010002
Qubit™ dsDNA HS Assay Kit	Thermofisher Scientific	Cat# Q32854
Deposited data		
Raw and analyzed data	N/A	GEO (GSE230187, GSE230190, GSE230191, GSE230480)
Experimental models: Organisms/strains		
Mouse : C57BL/6JRj	JANVIER labs, France	N/A
Mouse: *Cx3cr1*^{creERT2}*x Hdac1,2*^{flox}	Datta et al., 2018	N/A
Mouse: *Hdac9*^{flox}	Asare et al., 2020	N/A
Oligonucleotides		
Primers	Table 2 and 3	N/A
Software and algorithms		
R	https://www.r-project.org/	RRID:SCR_001905
R studio	https://www.rstudio.com/	Version 4.2 and 4.3
LIGER	Welch et al., 2019	RRID:SCR_018100
Cell ranger	10x genomics	v(6.1.0); RRID:SCR_017344
Doublet finder	McGinnis et al., 2019	v(2.0.2); RRID:SCR_018771
scCustomise version(1.1.1)	Marsh, 2023	https://github.com/samuel-marsh/scCustomize
Seurat	Satija et al., 2015	v(4.0.6; 4.4.0); RRID:SCR_016341
Galaxy	https://usegalaxy.eu/	RRID:SCR_006281
IGV	Robinson et al., 2011	RRID:SCR_011793
Cutadapt	Martin, 2011	RRID:SCR_011841
Bowtie2	Langmead and Salzberg, 2012	RRID:SCR_016368
BAM tools	Barnett et al., 2011	RRID:SCR_015987
Picard tools	http://broadinstitute.github.io/picard	RRID:SCR_006525
Deep tools	Ramírez et al., 2014	RRID:SCR_016366
MACS2	Zhang et al., 2008	RRID:SCR_013291
Csaw	Lun and Smyth, 2016	https://doi.org/10.1093/nar/gkv1191
FindMotifsGenome tool	Heinz et al., 2010	http://homer.ucsd.edu/homer/motif/
STAR	Dobin et al., 2013	RRID:SCR_004463
Feature counts	Liao et al., 2014	RRID:SCR_012919
Deseq2	Love et al., 2014	RRID:SCR_015687
Gene ontology (GO) enrichment analysis	http://www.geneontology.org	RRID:SCR_002811
Revigo	Supek et al., 2011	RRID:SCR_005825
Cytoscape	https://cytoscape.org/	RRID:SCR_003032
Graph Pad Prism	https://www.graphpad.com/	RRID:SCR_002798
Image Lab Software	Bio-Rad	RRID:SCR_014210
ImageJ (Fiji)	Schindelin et al., 2012	RRID:SCR_002285
Adobe Illustrator	https://www.adobe.com/	RRID:SCR_010279
Code for calculating the lesion volume	Bosch et al., 2022	https://github.com/lenkavaculciakova/lesion_volume

Other		
Nuclei EZ Prep lysis buffer	Millipore Sigma	Cat# NUC101
OptiPrep™ Density Gradient Medium	Millipore Sigma	Cat# D1556
UltraPure SSPE, 20X	Thermofisher Scientific	Cat# 15591043
PKD buffer	QIAGEN	Cat# 157014133
Tween-20	Bio-Rad	Cat# 1610781
RNase inhibitor	Takara-Bio	Cat# 2313A
Oligo dT25 magnetic beads	Invitrogen	Cat# 61005
Cell Lysis Buffer (10X)	Cell Signalling Technology	Cat# 9803
Proteinase K solution	QIAGEN	Cat# 19131
RNAscope Probe-Mm-Tnf-a,	Advanced cell Diagnostics	Cat# 311081
RNAscope Probe-Mm-Il1b-C2	Advanced cell Diagnostics	Cat# 316891-C2
RNAscope Probe-Mm-Abca1	Advanced cell Diagnostics	Cat# 522251
RNAscope Probe-Mm-Abcg1-C2	Advanced cell Diagnostics	Cat# 422221-C2
RNAscope Probe-Mm-Nr1h2	Advanced cell Diagnostics	Cat# 563261
RNAscope 3-Plex Negative Control Probe_Mm	Advanced cell Diagnostics	Cat# 320871
RNAscope 3-plex Positive Control Probe_Mm	Advanced cell Diagnostics	Cat# 320881

1.1 Consumables

Greiner bio-one (Germany), Falcon (Becton Dickinson Labware Europe, France), Omni lab (Germany), neo Lab (Germany), VWR (Germany), Sarstedt (Germany), Millipore (Germany), Fine Science Tools (Germany), Science Services (Germany), and Eppendorf were some of the suppliers for the consumables used in this study.

1.2 Primers

Primers were prepared by adding the corresponding volume of Tris-EDTA buffer to the lyophilized powder and mixing thoroughly. Both the forward and reverse primer of one same primer pair were combined with water (40 µL F primer, 40 µL R primer, 720 µL ddH2O) to achieve a concentration of 5 µM of each primer.

Table 2: Sequence details of all primers used for genotyping

Gene name		Sequence (5'- 3')
Cx3cr1	F R Specific	CCTCTAAGACTCACGTGGACCTG GACTTCCGAGTTGCGGAGCAC GCCGCCCACGACCGGCAAAC
Hdac1	F R	CCTGTGTCATTAGAATCTACTT GGTAGTTCACAGCATAGT ACTT
Hdac2	F R	CCCTTTAGGTGTGAGTACAT AACCTGGAGAGGACAGCAAA

Table 3: Sequence details of all primers used for RT-qPCR analysis

Gene name		Sequence (5'- 3')
Hdac1	F R	CCTGTGTCATTAGAATCTACTT GGTAGTTCACAGCATAGT ACTT
Hdac2	F R	CCCTTTAGGTGTGAGTACAT AACCTGGAGAGGACAGCAAA
Apoe	F R	CTGACAGGATGCCTAGCC TCCCAGGGTTGGTTGCTTTG
Abca1	F R	TGTCTGAAAAAGGAGGACAGTG TGTCACTTTCATGGTCGCTG
Abcg1	F R	CAGACGAGAGATGGTCAAAGA TCAAAGAACATGACAGGCGG
Cyc1	F R	ATGGGGAGATGTTCATGCGG CTGAGGTCAGGGGGTAAGC

1.3 Buffers and solutions

1.3.1. For Lysolecithin injections

1.3.1.2 Lysolecithin solution

Under a laminar flow hood, 25 mg of lysolecithin (LLC) (L4129, Sigma-Aldrich, Germany) was mixed with 2.5 mL of sterile 1X PBS to create a 1% solution (10010-056, Thermo Fisher Scientific, Germany). For 15 minutes, the solution was sonicated at 40 kHz in an ultrasonic cleaner to ensure full dissolution. Aliquots of 20 µL were made of the solution and kept at -20°C until use. Each thawed aliquot was used only once before being thrown away. The solution was stored at 37 degrees Celsius while in use to avoid precipitation.

1.3.1.2 Monastral blue solution

A solution of 3% Monastral blue (274011, Sigma-Aldrich, Germany) was prepared by dissolving 1.5 g Monastral blue in 50 mL of dH2O. The solution was then filtered through a Whatman filter paper and autoclaved. Just before injection into the brain, we added 0.2 µL Monastral blue solution into 20 µL of LLC solution.

1.3.1.3 Mouse anesthesia and analgesia

An MMF solution containing 0.5 mg medetomidine/kgBW, 5.0 mg midazolam/kgBW, and 0.05 mg fentanyl/kgBW was injected intraperitoneally into mice to render them unconscious before CNS injections. Subcutaneous injections of AFN solution (2.5 mg atipamezol/kgBW, 1.2 mg naloxon/kgBW, and 0.5 mg flumazenil/kgBW) were used to reverse anesthesia in mice. An intraperitoneal injection of 100 µL of 10% ketamine and 2% xylazine rendered the mice unconscious prior to their euthanasia by perfusion. On the day of surgery, as well as on days 1 and 3, mice received an injection of 0.05 mg buprenorphine/kgBW to alleviate postoperative pain.

1.3.2 For histological analysis of mouse tissue

1.3.2.1 Paraformaldehyde solution for histology

Paraformaldehyde (PFA) 16% stock solution was prepared by dissolving 80 g PFA (158127, Sigma Aldrich, Germany) in 450 mL dH2O at 65ºC, while stirring for 15 to 20 minutes. Then, droplets of 5 NaOH (6771.1, Roth, Germany) were added until the solution became clear. Afterwards, 50 mL 10X PBS were added and the pH was adjusted to 7.4. Finally, dH2O was added until the final volume of 500 mL (to compensate for evaporation). Aliquots of the solution were then stored at -20ºC. The working solution of 4% PFA in PBS was prepared by diluting 50 mL of PFA stock solution in 150 mL of 1X PBS, filtering the resulting solution with a Steritop 0.22 µm filter system (SCGPT01RE, Merck Millipore, Germany) and storing it at 4 ºC.

1.3.2.2 Sucrose solution

To cryoprotect tissues before freezing, a 30% sucrose solution was prepared by mixing 15 g of sucrose (S0389, Sigma-Aldrich, Germany) in 50 mL of 1X PBS.

1.3.2.3 10X Phosphate Buffer Solution (PBS)

10X PBS was prepared by dissolving the following in 1L ddH2O:

- 80 g NaCl (3957.2, Roth, Germany)
- 2 g KCl (6781.1, Roth, Germany)
- 18.05 g Na2HPO4•2H2O (1.06580.1000, Merck Millipore, Germany)
- 2.4 g KH2PO4 (3904.1, Roth, Germany)

The pH was adjusted to 7.4 and the solution stored at RT. To prepare 1X PBS, 10X PBS was diluted 10 times with ddH2O, the pH value was re-adjusted to 7.4, and the solution was stored at RT.

1.3.2.4 Blocking and staining solution for immunohistochemistry

The blocking solution for immunohistochemistry was prepared by mixing the following in 500 mL of 1X PBS:

- 12.5 mL bovine calf serum (BCS) (SH30073.03HI, GE Healthcare Life Sciences, USA)
- 12.5 g bovine serum albumin (BSA) (A2153, Sigma-Aldrich, Germany)
- 12.5 mL fish gelatin (G7765, Sigma-Aldrich, Germany)

The solution was aliquoted and kept at -20°C. To prepare the staining solution, I diluted the blocking solution 1:4 in 1X PBS.

1.3.2.5 Citrate buffer for antigen retrieval

Citrate buffer was prepared by diluting 2.941 g of tri-sodium citrate dehydrate (C6H5Na3O7•2H2O, 1.06448.0500, Merck Millipore, Germany) in 1L of ddH2O. The pH value was adjusted at 6.0 using HCl.

1.3.2.6 Mowiol solution

Mowiol was used as the mounting medium after immunocytochemistry and immunohistochemistry. The solution was prepared by stirring 2.4 g mowiol (0713.2, Roth, Germany), 6 g glycerol (65518,

Sigma-Aldrich, Germany) and 6 mL ddH2O for several hours at RT. After addition of 12 mL 0.2 M Tris-HCl (pH 8.5), the solution was incubated at 60°C for 10 minutes and then centrifuged at 4,000 g for 15 min. Finally, mowiol was aliquoted and kept at -20°C until further use.

1.3.3 For other purposes

1.4.3.1 Tris-HCl Buffer

To prepare Tris-HCl Buffer, 60.57 g of Tris Base (A1379,5000AppliChem, Germany) were dissolved into 350 mL of ddH2O by stirring. Then, under pH monitoring, 12 M HCl (258148, Sigma-Aldrich, Germany) was added until the pH reached a pH value of 7.4. Finally, ddH2O was added to fill up to 500 mL and the solution was filtered and stored at 4°C.

1.3.3.2 Tris-EDTA Buffer

A solution of 10 mM Tris-EDTA Buffer was prepared by combining the following:

- 5 mL of 1M Tris (A1379.5000, AppliChem, Germany) pH 8
- 1 mL of 0.5M EDTA (AM9261, Invitrogen, Thermo Fisher Scientific, Germany pH 8
- 496 mL ddH2O

The solution was autoclaved to sterilize.

1.3.3.3 TBS and TBST buffers

1X TBS Solution was prepared by dissolving the following in 800 mL of ddH2O:

- 6.05 g Tris (A1379.5000, AppliChem, Germany)
- 8.76 g NaCl (3957.2, Roth, Germany)

The pH value was adjusted 7.6 with 1 M HCl. The volume was then filled up to 1L with ddH2O. Once prepared, TBS is stable at 4°C for 3 months. To prepare TBST, 1 mL of Tween 20 (8.22184.0500, Merck Millipore, Germany) was added to 1 L of 1X TBS.

1.3.3.4 TAE Buffer for agarose gels

A 10X TAE Buffer was prepared by combining the following in 1L of ddH2O:

- 48.4 g Tris base (A1379.5000, AppliChem, Germany)

- 11.4 mL Acetic acid (3738.4, Roth, Germany)
- 20.0 mL 0.5 M EDTA (AM9261, Invitrogen, Thermo Fisher Scientific, Germany)

The pH value was adjusted to 8.5.

2. Methods

The purpose of this section is to provide a detailed overview of the research techniques employed in this project. Section 2 of the Appendix contains detailed protocols outlining all the steps to be taken for several of the following techniques.

2.1 Animal studies

Mice were housed in the animal facility of the German Centre for Neurodegenerative Diseases (DZNE), Munich, in a standard, pathogen-free, 12-hour light-dark cycle and with ad libitum access to food and water. The animal facility maintained a temperature of 20 to 22°C and 40 to 60% humidity. All C57BL/6J mice were imported from JANVIER laboratories. The heterozygous mouse line for *Hdac1,2* (*Cx3cr1*$^{creERT/het}$*Hdac1*$^{wt/fl}$*Hdac2*$^{wt/fl}$) was provided by Marco Prinz (Freiburg University), which was further bred in the DZNE mouse facility to generate a homozygous line for *Hdac1,2* (*Cx3cr1*$^{creERT/het}$*Hdac1*$^{fl/fl}$*Hdac2*$^{fl/fl}$). All animal studies complied with the ARRIVE (Reporting of in vivo experiments) guidelines, the German animal welfare law, and were approved by the institutional animal use and care committee in DZNE in agreement with the district government of Upper Bavaria, Germany.

2.1.1 HDAC1,2 depletion in microglia/macrophages

In *Cx3cr1*$^{creERT/het}$*Hdac1*$^{fl/fl}$*Hdac2*$^{fl/fl}$ mice, the activation of Cre recombinase (under the control of Cx3cr1 promoter was induced by tamoxifen (T5648, Sigma-Aldrich). The stock solution of 20mg/ml was prepared in corn oil. 12-month-old mice were administered 200 µL of tamoxifen solution via intraperitoneal injection thrice, separated by 48 hours. As control animals, tamoxifen injected (*Cx3cr1*$^{creERT/wt}$*Hdac1*$^{fl/fl}$*Hdac2*$^{fl/fl}$) and (*Cx3cr1*$^{creERT/het}$*Hdac1*$^{wt/wt}$*Hdac2*$^{wt/wt}$) animals were used. A mixed proportion of males and females were used for this study.

2.1.2 Genotyping

The tissue lysis and DNA extraction from mouse tissue for genotyping was performed with the Invisorb Spin Tissue Mini Kit (1032100300, Invitek, Germany) according to the manufacturer's instructions.

Genotyping of the transgenic lines was performed in a standard PCR reaction with 2-5 µL of extracted DNA using the primers described in section 1.3 of Materials and Methods, a Biometria TRIO thermocycler (Analytik Jena, Germany) and according to the following instructions.

Table 4: The following thermocycler steps were performed to amplify the *Cx3cr1* ^{creERT2}gene

Step	Temperature(°C)	Time	Notes
1	94	5 minutes	
2	94	30 seconds	
3	58	45 seconds	
4	72	45 seconds	Repeat step 2-4 for 35 cycles
5	72	5 minutes	
6	10		

The genotype was decided based on the presence of bands of different molecular weight:

- 304 bp: mutant, cre/cre
- 304 bp and 750 bp: heterozygote, cre/wt
- 750 bp: wild-type, wt/wt

Table 5: The following thermocycler steps were performed to amplify the *Hdac1* ^{flox} gene

Step	Temperature(°C)	Time	Notes
1	94	5 minutes	
2	94	30 seconds	
3	58	30 seconds	
4	72	1 minute	Repeat step 2-4 for 40 cycles
5	72	5 minutes	
6			

The genotype was decided based on the presence of bands of different molecular weight:

- 900 bp: mutant, flox/flox
- 900 bp and 850 bp: heterozygote, flox/wt
- 850 bp: wild-type, wt/wt

Table 6: The following thermocycler steps were performed to amplify the *Hdac2* ^{flox} gene

Step	Temperature(°C)	Time	Notes
1	94	5 minutes	
2	94	30 seconds	
3	58	30 seconds	
4	72	1 minute	Repeat step 2-4 for 40 cycles
5	72	5 minutes	
6			

The genotype was decided based on the presence of bands of different molecular weight:

- 850 bp: mutant, flox/flox
- 850 bp and 700 bp: heterozygote, flox/wt
- 700 bp: wild-type, wt/wt

2.1.3 Agarose gel electrophoresis

The PCR products were run for 1 hour and 10 minutes on a 1% agarose or 1.5% (Seakem LE Agarose, 50004, Lonza, US) gel at 125 V with a Powerpac HC (Biorad, USA). For DNA labelling in the gel, we used GelRed (41003-1, Biotium, USA) and A 100 bp or 1000 bp ladder (SM0241, Thermo Fisher Scientific, Germany) was added to interpret the results.

2.2 Immunization/Treatment

2.2.1 BCG Immunization

BCG (RIVM strain -closely related to *M. bovis* BCG Pasteur 1173P2 strain) was reconstituted in 50ml 0.9% NaCl solution on ice. To prevent the degradation of CFU (Colony forming units) due to the sensitivity of BCG-bacteria, BCG suspension was used within 6-7 hours after reconstitution maintaining the efficacy and potency. 12 months old C57Bl/6J mice were intravenously (i.v.) injected with 200µl of reconstituted BCG containing $8x10^5$-$12x10^6$ CFU. The control mice received 200µl of 0.9% NaCl solution (i.v.). After one month of immunization, further experiments were executed. Wild-type C57Bl/6J male mice and a mixed proportion of male and female mice for $Cx3cr1^{creERT/het}Hdac1^{fl/fl}Hdac2^{fl/fl}$ were used for this section of the study.

2.3 Lysolecithin injections

2.3.1 The lysolecithin model of de and re-myelination

In this study, we make ample use of the LLC model of remyelination. LLC is a demyelinating chemical that non-specifically disrupts lipids by integrating into cellular membranes and increasing cell membrane permeability (Plemel *et al.*, 2018). Administration of LLC into white matter tracts such as the corpus callosum or the spinal cord white matter through a stereotactic injection creates a focal demyelinated lesion. In this model, noticeable demyelination occurs within hours after the injection, significant demyelination lasts for 7 to 10 days, until the repair process of remyelination follows demyelination. Remyelination is maximal between 14 to 21 dpi and requires rapid clearance of

damaged myelin by microglia and macrophages (Jeffery and Blakemore, 1995b). The LLC injection causes a disruption of the blood-brain barrier, thereby promoting the infiltration of MDMs into the demyelinating lesion.

2.3.2 Methodology

LPC injections were performed according to an established protocol described in (Bosch-Queralt *et al.*, 2022). The following coordinates for injections were used: Injection site 1: X = −1/+1, Y =+1.10, Z = −2.30 → −2.25, Injection site 2: X = −1/+1, Y = −0.10, Z = −1.45 → −1.40, Injection site 3: X = −0.55/+0.55, Y = −1.22, Z = −1.45→ −1.40. For volumetric calculations, site 2 was used. Sites 1 and 3 were used additionally when considerable amounts of demyelinated white matter were needed for –omics studies. 1µL of LPC was injected at 150nL/minute (1 lesion) and 250nL/minute (multiple lesions). Mice were monitored for 3-4 days' post-surgery for any physiological changes.

2.4 Histological analysis of lesioned mouse CNS tissue

2.4.1 Tissue preparation

To prepare samples for immunohistochemistry, mice were anesthetized with an intraperitoneal injection of 10% ketamine/2% xylazine and perfused intracardially with 4% paraformaldehyde (PFA) with a peristaltic pump (Peri-Star PRO, World Precision Instruments). The brain was removed, postfixed in 4% PFA overnight, and cryoprotected in 30% sucrose in PBS. The tissue was embedded in Tissue-Tek O.C.T (4583, Sakura Europe, Germany), frozen on dry ice, and kept at −80°C until sectioning.

For sectioning of the injected brains, a cryostat (CryoStar NX70, Thermo Scientific) was used to cut 16-µm-thick coronal sections, which were directly mounted on Superfrost Plus slides (10149870, Thermo Scientific, Germany) serially. The presence of monastral blue identified the lesions. All sections were kept at −20°C until further processing.

2.4.2 Immunohistochemistry

For staining, the sections were dried at 37 °C for 30 minutes, rinsed with 1× PBS, and permeabilized for 10 min in 1× PBS containing 0.3% Triton X-100. To prevent non-specific binding, sections were incubated for 1 hour with a blocking solution (2.5% bovine serum albumin, 2.5% fish gelatin, and 2.5%

fetal calf serum in 1× PBS). Primary antibodies were diluted in staining solution (25% of blocking solution in 1× PBS) and incubated overnight at 4°C except for Plin2 staining, where the staining solution was supplemented with 0.05% saponin additionally. The next day, sections were further incubated with primary antibodies for 1 hour at RT, washed with 1× PBS, and subsequently incubated with secondary antibodies (1:500) for 2 hours. After washing with 1× PBS, the sections were incubated with FluoroMyelin (1:400, F34651, Invitrogen) and DAPI (1: 1,000) in 1×PBS for 15 minutes. Finally, sections were washed in distilled water and then mounted with mowiol. For stainings with antibodies produced in mice, the Fab fragment-blocking step (715–007–003, Jackson ImmunoResearch) was performed before adding the blocking solution. All steps were performed at room temperature (RT) unless stated otherwise. For CC1 and perilipin2 staining, heat-induced antigen retrieval was accomplished using (Sodium citrate buffer-10mM Sodium citrate, pH 6.0) before blocking. The primary and secondary antibodies used were the following: IBA1 rabbit (1:1000), IBA1 chicken (1:400), IBA1 guinea pig (1:500), MAC2 rat (1:400), MHCII rat (1:100), PLIN2 rabbit (1:200), Olig2 rabbit (1:250), APC-CC1 mouse (1:100), Alexa Fluor 555 anti-mouse (1:500), Alexa Fluor 555 anti-rabbit (1:500), Alexa Fluor 647 anti-rabbit (1:500), Alexa Fluor 647 anti-Guinea pig (1:500) and Alexa Fluor 647 anti-rat (1:500).

2.5 Fluorescent in situ hybridization

The RNAscope Multiplex Fluorescent v2 Assay (Advanced Cell Diagnostics Inc.) was performed according to the manufacturer's instructions for fixed frozen tissue. Brain sections (16-µm-thick) were hybridized with the respective mRNA probes: RNAscope Probe-Mm-Tnf-α; RNAscope Probe-Mm-Il1β-C2, RNAscope Probe-Mm-Abca1; RNAscope Probe-Mm-Abcg1-C2 and RNAscope Probe-Mm-Nr1h2 all from Advanced Cell Diagnostics. Additionally, the negative control probe (RNAscope 3-Plex Negative Control Probe) and the positive control probe (RNAscope 3-plex Positive Control Probe_Mm) were used in some sections to assure the specificity and the sensitivity of the signal. The target probes were also combined with immunofluorescence for IBA1 to determine which cells express the genes of interest.

2.6 Confocal microscopy

All images were acquired using confocal microscopy either with a Leica SP5 confocal (20x/0.75 NA air, 63x/1.40NA oil) or the Zeiss LSM 900 (20x/0.8 M27 air, 40x/1.1 W Korr UV-VIS- IR water,

63x/1.2 Imm Korr DIC M27-Oil). Additionally, the navigator function of Zeiss was used using (10X/0.30 M27-Air). The different fluorophores were stimulated sequentially using the following laser lines: 405 nm for DAPI, 488 nm for Alexa Fluor 488 (AF488), 561 nm for Alexa Fluor 555 (AF555), and 633 nm for Alexa Fluor 647 (AF647). For reflection^{+} microscopy, the reflected light using the Leica SP5 confocal microscope was used in parallel to imaging the fluorophores as previously described. In Leica SP5, the scanning speed was set to 600 Hz and the bit depth to 16 Bit. The pixel size was variable, but the format of the images was either 512x512 or 1024x1024 pixels, with either 1X or 2X zoom. The pinhole was kept at 1 AU, except in the cases where it was necessary to collect more light, Furthermore, a 2X or a 4X line average was used to increase the signal to noise ratio. The tiles of a tile scan were stitched automatically using the Leica Application Suite AF software (Leica Microsystems, Germany), at the settings of low speed and high precision, and without smoothing the signal between tiles. To control for possible effects of the monastral blue dye on the stainings, the transmitter light from the laser line 633 nm was also collected. This way, the accumulations of blue dye could be observed, and its signal ignored during manual quantification of myelin- and crystal-loaded cells. In Zeiss LSM 900, the scanning speed was set to 8 lps with a bit depth of 16 Bit. The pixel size was 2.50 µm and the format of the images was 1024 x 1024 pixels with 2x line averaging. The pinhole was kept at 1AU. The tiles of a tile scan were stitched automatically using the ZEN software (Zeiss, Germany), at the settings of low speed and high precision, and without smoothing the signal between tiles. All settings were kept constant throughout the imaging of one same experiment and were kept similar among similar analysis in different experiments.

2.7 Image analysis

To quantify the demyelination volume and the IBA1^{+} volume, the area of demyelination shown by negative FluoroMyelin staining and the area of clustered IBA1^{+} cells, respectively, was measured in consecutive sections of a lesion, which were separated by a known distance. The lesion volume was then calculated according to the truncated cone volume formula in an automated fashion using IPython 2.7. as described in (Bosch-Queralt *et al.*, 2022). For the quantification of myelin-loaded IBA1^{+} cells, crystal-loaded IBA1^{+} cells, MAC2^{+}IBA1^{+} cells, MHCII^{+}IBA1^{+} cells, CC1^{+} cells, and foam cells, the cells were counted manually in high magnification images of the lesion using the Cell Counter plug-in in Fiji (Schindelin *et al.*, 2012). The pictures were coded so that the analysis would be blinded. The quantifications of lipid-loaded microglia, MHCII^{+} microglia, MAC2^{+} microglia *Tnf*$^{+}$*Il1ß* $^{+}$ mRNA in microglia were performed by counting manually in the images acquired. For quantifying the *Abca1*,

Abcg1 and *Nr1h2* mRNA particles in the fluorescence in situ hybridization, the positive particles were quantified in the mask created by the IBA1$^+$ signal in an automated fashion using Fiji.

2.8 In-vitro analysis

2.8.1 Myelin purification

Myelin was isolated from 8-week-old C57BL/6J mouse brains were homogenized by sonication in 10 mM HEPES buffer (pH 7.4). The homogenate was layered on a sucrose gradient of 0.32 M and 0.85 M sucrose and centrifuged at 25,000 rpm for 38 minutes with a SW32Ti rotor (Beckman Coulter, Germany). The crude myelin fraction was carefully isolated from the interface and subjected to three rounds of osmotic shock by dissolving it in ddH2O and centrifuging first at 25,000 rpm, then at 10,000 rpm for 18 minutes. The resulting pellet was again laid on a sucrose gradient and the same procedure was repeated to purify myelin. The yield of myelin was calculated by measuring the total amount of protein with the Bradford assay (500-0006, Bio-Rad, USA). Before addition to the cell culture media, myelin was re-suspended by passing the solution through a 25G needle. For further details on buffer preparation, please refer to the protocol in the section 2 of the Appendix.

2.8.2 Preparation of L929-conditioned media

L929 cells are a fibroblast cell line derived from mouse adipose tissue. They secrete MCSF, a factor that is essential for microglia survival and growth in culture after isolation, thus; we normally used L929-conditioned media to culture our microglia. To prepare L929-conditioned media, cells from the L929 cell line were cultured in the DMEM containing 10% BCS (SH30073.03HI, GE Healthcare Life Sciences, USA), 1 mM sodium pyruvate (11360039, Thermo Fisher Scientific, Germany), GlutaMAX™ (35050038, Thermo Fisher Scientific, Germany) and 1% penicillin/streptavidin (15070063, Thermo Fisher Scientific, Germany), and split 3 times to obtain a large-scale L929 culture in 175-cm² flasks. The confluent cells were incubated for 2 weeks. Then, the conditioned medium was collected, passed through a 0.22 µm vacuum filter (S2GPU05RE, Merck Millipore, Germany) and the aliquots were stored at -20 °C.

2.8.3 Bone marrow derived macrophages (BMDM) isolation

Both femoral bones from adult mice were isolated, disinfected with 70 % ethanol, and put into ice cold 1x DPB. Bones were cut at both ends and flushed with 2.5 mL cold 1x DPBS per bone with a syringe and 25G needles to extract bone marrow. The bone marrow suspension was further centrifuged at 1000 rpm for 10 minutes. The pellet was resuspended in BMDM/Serum/L929 and 5 x 10^5 cells were plated per sterile and untreated 10cm-diameter tissue culture dish, containing 10 mL BMDM –Media. Cells were cultivated at 37°C with 5% $C0_2$ v/v. After 3 days, 5 ml of BMDM media (supplemented with serum and L929) were added and after another 7 days, media was changed completely to 10mL BMDM media. BMDMs were then cultivated until a sufficient number of cells was reached. BMDMs were then harvested with 2ml Accutase (Innovative cell technologies Inc.) detachment solution per dish for 5-10 min at 37°C. Detachment was stopped with 8ml complete media per dish and cell suspension was centrifuged at 1000 rpm for 10 min. Cells were then resuspended in BMDM media and plated for the experiments. For in-vitro recombination of cells, to achieve a knockout of the floxed gene, 4 – hydroxyl tamoxifen (4-OHT) was added to cells in culture at a final concentration of 4µM. BMDMs received 4 –OHT on day 1 and were cultured with the compound until scheduled complete media change (day 10) for BMDMs.

2.9 Molecular biology analysis

2.9.1 Microglia isolation from adult mice

Mice were anesthetized with an intraperitoneal injection of 10% ketamine/2% xylazine and perfused intracardially with ice-cold 1XPBS with a peristaltic pump (Peri-Star PRO, World Precision Instruments). Primary microglia were isolated from adult mice brains using an Adult Brain dissociation kit (cat_-130-107-677, Miltenyi Biotech). Myelin debris and red blood cell removal were performed according to the manufacturer's instructions. Then $Cd11b^+$ cells were labeled using magnetic beads and isolated using a magnetic column. The cells were further processed and used for different assays.

2.9.2 RNA isolation by RT-qPCR

Total RNA was isolated from primary microglia ($CD11b^+$) cells from adult mouse brains following the manufacturer's instructions of the RNeasy plus mini kit (74134, QIAGEN). The RNA was reverse

transcribed with the superscript III first-strand synthesis system (18080051, Invitrogen) using 100ng to 1µg of total RNA. Quantitative PCR was performed using the Power Up SYBR Green Master Mix (A25742, Applied Bio systems) on a Light Cycler 480 Real-time PCR system (Roche). All qPCR reactions were run in triplicate.

2.10 Sequencing

2.10.1 Single nucleus RNA sequencing (snRNA seq)

2.10.1.1 Sample preparation and sequencing

The mice were perfused intracardially with ice-cold- IX PBS with a peristaltic pump (Peri-Star PRO, World Precision Instruments). The lesioned white matter was dissected from young and aged C57Bl/6J mice on ice using a stereomicroscope (Leica S9E number 10446339). The isolated white matter was flash-frozen in liquid N_2 and stored (-80°C) until further processing. The frozen white matter tissues were homogenized in the cold Nuclei EZ Prep lysis buffer (Millipore Sigma) in a 2ml Dounce grinder, followed by clean-up using OptiPrep™ Density Gradient Medium (Millipore Sigma) (Corces *et al.*, 2017). The nuclei recovered from the interface of 29% and 35% of the OptiPrep medium were examined and counted using Trypan Blue staining in a hemocytometer. The nucleus suspension of each sample was used for snRNA-seq preparations. Single-nucleus RNA-seq libraries were prepared using Chromium Next Gen Single Cell 3' v3.1 Reagents following the manufacturer's instruction (10X Genomics). The libraries were pooled and sequenced on the NovaSeq 6000 sequencer (Illumina). n = 3 biological replicates per condition were analyzed.

2.10.1.2 Data analysis

Raw sequencing data in fastq format were aligned to *Mus musculus*(mm10) reference genome, quantified, and filtered using 'cell ranger-count (10x genomics, version 6.1.0). Doublet analysis was performed using the 'Doublet Finder' R package (v.2.0.2) (McGinnis, Murrow and Gartner, 2019). The filtered matrix file was further processed using LIGER (Linked inference of Genomic Experimental Relationships) (Welch *et al.*, 2019) using R version (4.2.2) , where replicates from each condition were merged. The datasets were normalized and scaled to account for differences in sequencing, efficiency, and variance between the cells. Integrative non-negative matrix factorization

(iNMF) was performed on normalized datasets with the following parameters (K=20, λ=5, threshold 1e-6, max iters-30) followed by joint clustering of cells by quantile normalization and Louvain clustering algorithm (resolution-0.25) in LIGER. Two dimensional representations were generated using uniform manifold approximation and projection (UMAP) as implemented in Liger with the following parameter settings: ('min. dist = 0.3', 'n.neighbors = 30', 'cosine' distance metric). To determine the gene markers for all clusters and for comparing the expression within different datasets, the 'runWilcoxin' function was used with (padj <0.05). As for cell-type identification, a high-quality single-cell RNA-seq of mouse brain dataset served as a reference for our dataset (Rosenberg *et al.*, 2018). The expression profiles of differentially expressed genes were determined by the 'plotgene' function in Liger. For visualizing the QC/alignment metrics of sequencing data and for plotting density and dot plots of gene expression, scCustomise version (1.1.1) was used (Marsh, 2023). To determine the cell proportion in each microglia, cluster and for plotting heat maps of differentially expressed genes, Seurat (version 4.0.6) was used.

2.10.2 Assay for Transposase -Accessible Chromatin using sequencing (ATAC-seq)

2.10.2.1 Sample preparation and sequencing

$CD11b^+$ cells were isolated from lesioned brains of mice by MACS as described above and were cryopreserved with 5% DMSO in Mr. frosty container at -80°C (to allow the slow cooling rate to minimize cell lysis) until further processing. Cells (stored at -80°C) were thawed for 2 min at 37°C and then mixed with ice-cold PBS (1:1), followed by centrifugation at 3000 rpm for 5 min at 4°C. Cell pellets were then re-suspended in ice-cold PBS, and cell viability was assessed with Trypan Blue staining. After counting, 20000 viable cells were transferred into a separate tube and centrifuged at 3000 rpm for 7 min at 4°C. ATAC-seq protocol was performed according to the original procedure by (Buenrostro *et al.*, 2013) with some modifications included for the frozen cells according to (Fujiwara *et al.*, 2019). Briefly, cell pellets were re-suspended in ice-cold lysis buffer (10mM Tris-Cl, pH 7.4, 10 mM NaCl, 3mM $MgCl_2$, and 0.1% (v/v) Igepal CA-630) and immediately spun down for 10 min at 500rcf at 4°C. The supernatant was discarded, and cell nuclei were re-suspended in the transposition reaction containing 2µl TDE1 (Nextera Tn5 enzyme), 10µl of 2x TD reaction buffer, and 8µl of H_2O. The reaction was incubated at 37°C for 30 min with gentle shaking (300 rpm). Subsequently, DNA was purified with the ZymoResearch DNA Clear & Concentrator TM-5 kit (Cat. No. D4014) and eluted in 10µl of elution buffer (10mM tris-Cl pH 8). DNA was stored at -20°C. The library of transposed

DNA fragments was prepared and 10µl of eluted transposed DNA was mixed with 10µl of nuclease-free water, 2.5µl of 25µM PCR primer 1, 2.5µl of 25µM Barcoded PCR Primer 2 (Ad1 and Ad2 PCR primer sequences as in (Buenrostro *et al.*, 2013)

and 25µl of NEBNext High-Fidelity 2x PCR Master Mix (NEB). The reaction was incubated for 5 min at 72°C, 30 secs at 98°C, followed by five cycles of 10 sec at 98°C, 30 sec at 63°C, and 1 min at 72°C. qPCR was then performed to determine the additional number of PCR cycles required for the final library. The profiles of libraries were assessed with the Bioanalyzer2100. The ATACseq libraries were sequenced at 2x76bp paired-end on HiSeq 1500. Each profile was sequenced in two separate lanes. n = 2 replicates per condition were analyzed.

2.10.2.2 Data analysis

FastQC was used to check the quality of raw fastq files. Trimming of Nextera transposase adapters and reads <20 bp with quality cutoff 20 was done using Cutadapt (Martin, 2011). The trimmed fastq files were aligned to the mm10 genome using bowtie2 (Langmead and Salzberg, 2012). The mapped reads were further filtered for mitochondrial reads, reads that are not properly paired and with low mapping quality (phred scale >=30) using BAM tools (Barnett *et al.*, 2011). Duplicate reads were removed using the Picard tool (Mark Duplicates). Insert sizes were checked with a paired-end histogram to visualize the fragment length distribution (an indicator for the quality of ATAC seq). The aligned BAM files were converted to BED format. Peak calling was performed using MACS2 (Y. Zhang *et al.*, 2008) using the settings ('- -nonmodel - - shift-100 - -extsize 200'). The minimum FDR cutoff was set to 0.05, and `no broad regions ´ was set for peak detection. Detection of differential binding sites was done using csaw (Lun and Smyth, 2016). FDR correction was applied on significant p values =<0.05. Visualization of coverage and peaks was performed on Bigwig files using the plot Heatmap of DeepTools (Ramírez *et al.*, 2014) and the Integrative Genome Viewer (IGV) (Robinson *et al.*, 2011). The replicates in each condition were merged using the Bigwig merge to generate a combined bigwig file for each condition. Motif analysis was done using the FindMotifsGenome tool (Heinz *et al.*, 2010) of HOMER on the Galaxy platform (https://usegalaxy.eu/).

2.10.3 Bulk -RNA sequencing

2.10.3.1 Sample preparation and sequencing

RNA was isolated from PFA-fixed OCT-embedded frozen brain sections using the method that digest proteins to free cross-linked RNA. In brief, frozen brain sections (16 µm) were taken out of -80°C and incubated at RT for 5 min, avoiding drying out. 50 µl RNA isolation buffer per sample was prepared and kept on ice, containing 40 µl of PKD buffer (157014133, QIAGEN) with 10 µl proteinase K solution (19131, QIAGEN). The target brain sections (lesion white matter tissue) were covered with 50 µl isolation buffer and incubated at room temperature for 30 sec. Four lesion tissue sections were scratched from each slide and condition (aged mice C57Bl/6J treated with saline or BCG) using a stereomicroscope (Olympus SZ51 Model number 1111260100). The brain lysate was collected by pipetting with 200µl tips, snap-frozen in liquid nitrogen, and stored at -80°C until further processing using the method described in (Ji *et al.*, 2023). Samples were thawed at RT for 3 min, then vortexed and spun down, followed by the incubation of samples at 56°C for 4 h in a thermal cycler with the lid set at 66°C, checking hourly if the sample was dissolving. After the incubation, vortexing and spinning down the samples, they were transferred into pre-cooled 1.5 ml tubes on ice. Prepared oligo dT25 magnetic beads (61005, Invitrogen) with three washes of 1x hybridization buffer (HB), which contains 2x SSPE (Life Technologies, Cat#15591-043), 0.05% Tween-20 (1610781, Bio-Rad), 0.05% RNase Inhibitor (2313A, Takara). Resuspend the beads with half of the original volume in 2x HB for later usage. 10 µl washed dT25 beads (0.1 mg) was added into each sample to reverse cross linked samples and heated the samples at 56°C for one minute. Placed the samples on ice after 10 min incubation at room temperature to allow mRNA hybridization. Then washed the beads two times in 100 µl of ice-cold 1x HB, followed by a subsequent wash using ice cold 1x PBS with 0.1% RNase Inhibitor inside. Removed PBS and resuspended with 15 µl RNase-free water. Incubated the sample-beads mixture at 80°C for two minutes to elute mRNA, then immediately pelleted on a room temperature magnet. Rapidly removed the supernatant containing mRNA and transfer to a new tube and store at -80°C. 1ng mRNA from each sample was taken and continued with the Smart-seq2 protocol as described in (Safaiyan *et al.*, 2021; Kaya *et al.*, 2022). Libraries were sequenced 2x150 reads base pairs (bp) paired-end on DNBSEQ Sequencing System (BGI) to a depth of $8x10^6$-$30x10^6$ reads/sample. n = 6 biological replicates per condition were analyzed.

2.10.3.2 Data analysis

FastQC was used to check the quality of fastq files. Low-quality reads and adapters were trimmed using Cutadapt (Martin, 2011)using the following parameters (reads <20 bp with quality cutoff 20). The trimmed FASTQ files were mapped to the mm10 reference genome using STAR (Dobin *et al.*, 2013). The mapped reads (of lesion tissue sections) belonging to the same slide were merged using the merge BAM files tool in Galaxy version 4. To quantify the number of reads mapping to the exons of each gene, Feature counts was used (Liao, Smyth and Shi, 2014). Further, to compare the expression of single genes between different conditions, differential analysis was performed using Deseq2 (Love, Huber and Anders, 2014). The minimum FDR cutoff was set to 0.05 for further analysis. Additionally, for visualization of gene expression over samples between conditions, a heatmap was plotted of the computed z-scores using Galaxy version 4.11 (https://usegalaxy.eu/).

2.10.4 Chromatin immunoprecipitation sequencing (Chip-seq)

2.10.4.1 Sample preparation and sequencing

CD11b^{+} cells were isolated from the brains of aged mice treated with saline or BCG by MACS, as described above. The isolated cells were fixed with formaldehyde solution (Cat no. 28906, Thermo Scientific) at a final concentration of ~1 % for 10 min, followed by quenching using Glycine (Cat. No. 10002113, Th. Geyer) at a concentration of 1.25M for 5 minutes at RT to stop fixation. The cross-linked cells were gently washed with ice-cold HBSS (Cat. No. 14175-053 Thermofisher Scientific) containing protease inhibitor cocktail -25X (PIC) (Cat No. C12010013 Diagenode) and were stored at (-80° C) until further processing. Diagenode ChIP-seq/ChIP-qPCR Profiling service (Diagenode Cat# G02010000) prepared the chromatin using the iDeal ChIP-seq kit for Histones (Diagenode Cat# C01010059). The cell nuclei were lysed, and chromatin was sheared using a Bioruptor® Pico sonication device (Diagenode Cat# B01060001) combined with the Bioruptor® Water cooler for 8 cycles using a 30'' [ON] 30'' [OFF] settings. Shearing was performed in 0.2ml Bioruptor® Pico Microtubes with the following cell number: 1 million in 100µl. An aliquot of this chromatin was used to assess the size of the DNA fragments obtained by High Sensitivity NGS Fragment Analysis Kit (DNF-474) on a Fragment Analyzer™ (Agilent). ChIP was performed manually following the protocol of the kit as mentioned above. Chromatin corresponding to 94ng was immunoprecipitated using the

following antibodies and amounts: H3K4me3 (Diagenode C15410003, Lot A8034D) and H3K27ac (C15410196, Lot A1723-0041D). Chromatin corresponding to 1% was set apart as input. qPCR analyses were made to check ChIP efficiency using KAPA SYBR® FAST (Sigma-Aldrich) on LightCycler® 96 System (Roche). IPs with a negative control isotype (IgG) were also performed in parallel. Libraries were prepared using IP-Star® Compact Automated System (Diagenode Cat# B03000002) from input and ChIP'd DNA using MicroPlex Library Preparation Kit v3 /96 rxns (Diagenode Cat# C05010002) with 24 UDI for MicroPlex v3 - Set I (Diagenode Cat# C05010008). Optimal library amplification was assessed by qPCR using KAPA SYBR® FAST (Sigma-Aldrich) on Light Cycler® 96 System (Roche) and by using High Sensitivity NGS Fragment Analysis Kit (DNF-474) on a Fragment Analyzer™ (Agilent). Libraries were then purified using Agencourt® AMPure® XP (Beckman Coulter) and quantified using Qubit™ dsDNA HS Assay Kit (Thermo Fisher Scientific, Q32854). Finally, their fragment size was analyzed by High Sensitivity NGS Fragment Analysis Kit (DNF-474) on a Fragment Analyzer™ (Agilent). Libraries were pooled and sequenced with paired-end reads of 50bp length on an Illumina Novaseq 6000 n = 2 independent replicates per condition were used for each histone mark. Each replicate was a pool of 3 animals.

2.10.4.2 Data analysis

Quality control of sequencing reads was performed using FastQC. The raw reads with a phred score > 30 were further used to align to the mm10 genome using bowtie2 (Langmead and Salzberg, 2012). Duplicate reads were removed using the Picard tool (Mark Duplicates). Quality control of Chip-seq preparation was done by determining the correlation between samples (a method to know if Chip-seq samples are more enriched than input samples using multiBamSummary and QC modules of Deep tools plot correlation (Ramírez *et al.*, 2014). To detect the enriched regions marked by H3K4me3 and H3K27ac marks, peak calling was performed using MACS2 (Y. Zhang *et al.*, 2008) normalized to the input (control) using the parameters –(create_model - - mfold (5-50) - -bw 300'). The minimum FDR cutoff was set to 0.05, and `no broad regions ´ was selected for peak detection. Detection of differential binding sites was done using csaw (Lun and Smyth, 2016). FDR correction was applied on significant p values =<0.05. To find the genes enriched for H3K4me3 and H3K27ac marks out of genes common for (snRNA and ATAC), the bed file of 833 genes was prepared from the UCSC table browser, and differential binding was performed using Csaw. Visualization of coverage and peaks was performed on Bigwig files using the plot Heatmap of DeepTools and the Integrative Genome Viewer (IGV)

(Robinson *et al.*, 2011). The replicates in each condition were merged using the Bigwig merge to generate a combined bigwig file for each condition.

2.11 Gene ontology enrichment analysis (GO analysis)

Gene ontology (GO) enrichment analysis was done using (http://www.geneontology.org/) database (Harris *et al.*, 2008) using the annotation dataset – GO biological process complete and a reference list of *Mus musculus* species. Fisher's exact test with FDR correction was applied to report statistically significant enriched terms. Revigo (Supek *et al.*, 2011) and Cytoscape (version 3.9.1) were used for enrichment maps of GO-enriched terms.

2.12 Statistics and reproducibility

Data values are represented as mean ± SD. Statistical analysis was performed with Graph Pad Prism (Graph Pad Software). The number of animals used for the experiments is indicated as a single bubble in all graphs or shown in the methodology. Normality tests (for e.g. Shapiro -Wilk test) were used to confirm the normal distribution of our data. Thus, a two-tailed Welch's t-test or Mann Whitney test was applied to compare the two groups. For measuring statistical differences in RT-qPCR results, the $-2^{\Delta\Delta Ct}$ value was employed, and the $-2^{\Delta\Delta Ct}$ values were subjected to the test. A P value of ≤ 0.05 was considered significant in all cases. Three to five brain sections were quantified per mouse to account for variability within the biological sample. For all experiments, 12-15 months aged mice and 3 months aged young mice were taken except snRNA and ATAC seq, where 15-20 months aged mice were used.

Results

First, we characterized the transcriptome and epigenome of microglia/macrophages in aged mice and young mice after demyelinating injury. Second, we analyzed the trained immune response of microglia / macrophages in promoting remyelination in aged mice upon BCG (Bacillus Calmette Guerin) immunization. Then, we explored the possible epigenetic mechanisms in microglia promoting remyelination in aged mice based on the transcriptomic profile of lesions of mice treated with BCG. Finally, we provided evidence that age associated decline in regeneration capacity could be elevated by BCG induced training of microglia involving epigenetic reprogramming which promotes precise activation and functioning of microglia, which is essential for oligodendrocyte differentiation and remyelination upon demyelinating injury.

1. Single-nucleus RNA sequencing identifies differences in microglial responses in young and aged mice

1.1 Experimental design and quality control for snRNA sequencing

Previous studies have demonstrated that diverse microglial activation responses are triggered in demyelinated mouse lesions. While young mice can recover from demyelinating injury much more rapidly, remyelination in aged mice is frequently impeded by poor microglia activation (Cunha *et al.*, 2020a) and insufficient myelin debris and lipid clearance (Safaiyan *et al.*, 2016; Cantuti-Castelvetri *et al.*, 2018). To examine how microglia tailor their responses differently in young and aged mice following demyelinating injury, we used an injury model of LPC-induced demyelination, a well-known model to study myelin repair, where microglia play a dynamic role in physiological and injury-induced remyelination (Jeffery and Blakemore, 1995a; Miron *et al.*, 2013b) and characterized the microglial response, utilizing single-nucleus RNA-sequencing (snRNA-seq), a highly effective and sensitive method for revealing transcriptomic cell-to-cell variation of microglia in the normal and diseased brain. (Masuda *et al.*, 2019; Zhou *et al.*, 2020; Morabito *et al.*, 2021) White matter tracts, including the corpus callosum, optical tracts, and medial lemniscus, were removed from the brains of lesioned young and aged mice for snRNA seq based on 10x genomics. Our study focused on the time period (4 –7) days post-lesion induction, during which microglia are particularly active, and the lesion is shifting from the myelin debris clearance phase to the remyelination initiation phase (Hammond *et al.*, 2019).

Schematic representation of the snRNA-seq experiment and downstream bioinformatic analyses.

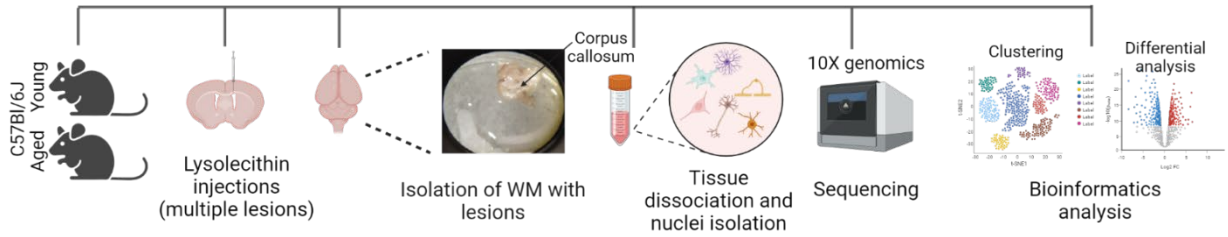

After quality control and filtering, we obtained aged (35,696) and young (30,930) single-nuclear transcriptomes. **(Figure 1.1 B -G)**. To ensure the validity of our study, we applied batch correction methods to the data of snRNA seq using integrative non-negative matrix factorization (iNMF) to reduce dimensionality while simultaneously eliminating batch effects (Welch *et al.*, 2019). In addition, the cell type composition was analyzed using unsupervised Uniform Manifold Approximation and projection (UMAP) analysis and Louvain clustering algorithm to the batch corrected transcriptomic datasets. The cell type identities were confirmed by the expression of canonical cell type marker genes **(Figure 1.1 A)** which identified 19 different clusters in both young and aged datasets.

1.2 Characterizing the transcriptomic signature of microglia / macrophages in lesions

To focus on microglia, we subsetted four microglia clusters **(Figure 1.3 A)** composed of total aged (5,792) and young (6,093) nuclei respectively **(Figure 1.1 B)**. Differential marker gene expression revealed that the microglia clusters displayed distinct expressions among themselves. Cluster 1 microglia expressed genes (*Slco2b1, Cfh, Cxcl10, and Ccl4*) involved in the heme analog import, interferon response, and inflammation pathways. Microglia Cluster 2 displayed upregulation of genes involved in pathways such as phagocytosis and inflammation, akin to axon tract-associated microglia (ATM) (*Gpnmb, Lgals3, Ms4a7, Mdfic*) (Hammond *et al.*, 2019). Microglia Cluster 3 expressed genes (*Zfp536, St6galnac3, Map7, Dscaml1*) involved in neuron projection development, glycosphingolipid metabolism, and retinoic acid signaling pathway, whereas microglia cluster 4 expressed genes (*Top2a, Diaph3, Knl1, Mki67*) involved in proliferation **(Figure 1.2 A, B).**

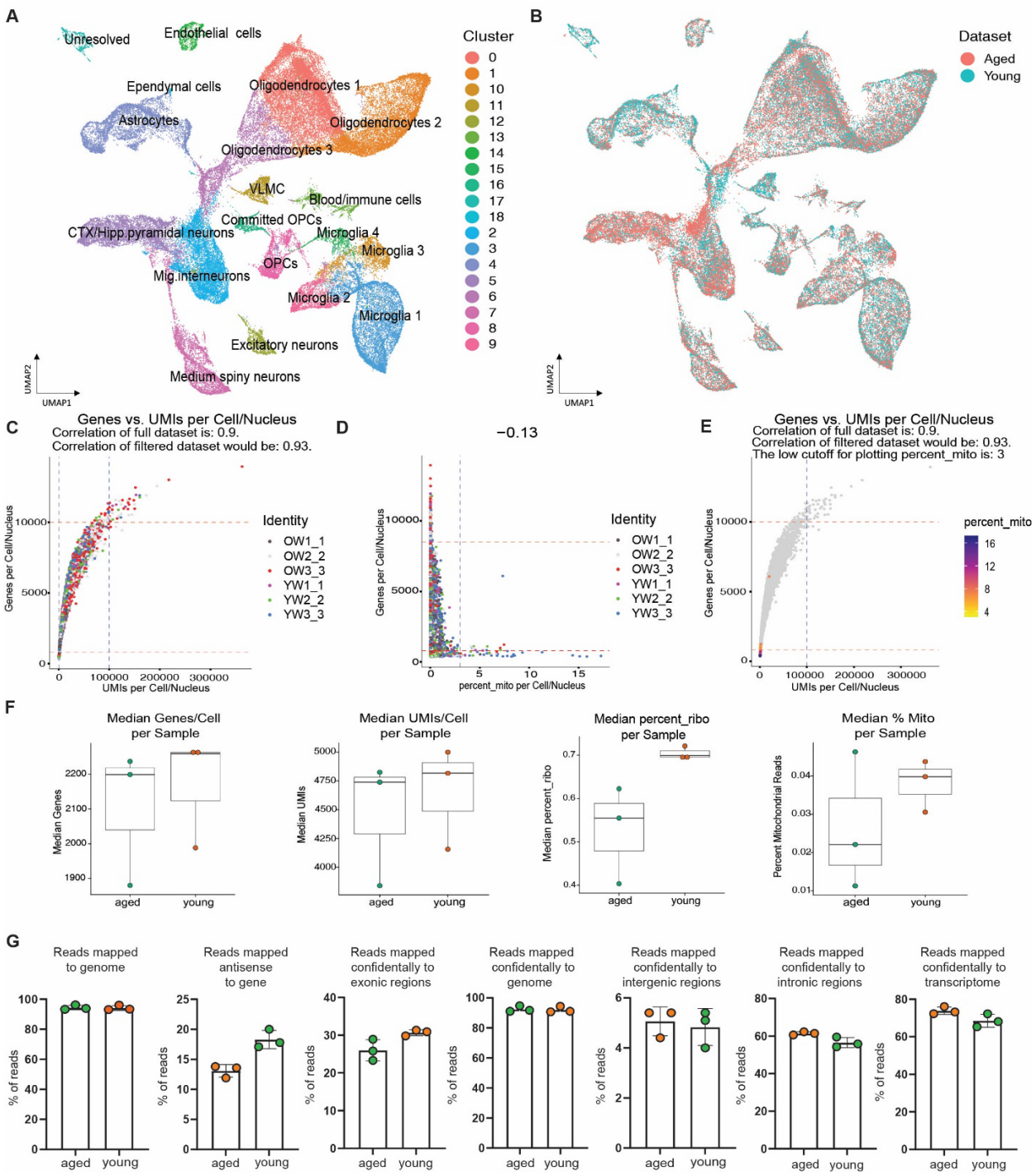

Figure 1.1: Quality control analysis of snRNA seq experiment

(A) UMAP plots of all cell types identified in the snRNA-seq dataset where dots correspond to individual nuclei profiled where each cell type cluster is color coded, identifying 19 different clusters.

(B) UMAP plot divided by total nuclei profiled in young (30,930) and aged (35,696) datasets.

(C, D) Scatter QC plot of genes vs. UMI per cell/nucleus and genes vs. percent mitochondria per cell/ nucleus with added visualization of potential cutoff thresholds and correlation after filtering in all the replicates of aged (OW1_1, OW2_2, OW3_3; n=3) and young (YW1_1, YW2_2, YW3_3; n=3) datasets respectively.

(E) Scatter QC plot of genes vs. UMI per cell /nucleus indicating the percent of mitochondrial reads with a cutoff of 3.
(F) Boxplots indicating the median genes, UMIs per cell/sample, and percent ribosome and percent mitochondria per sample in each dataset.
(G) Bar plots indicating the QC of sequencing and alignment metrics in both young and aged datasets.
See also Table 1.

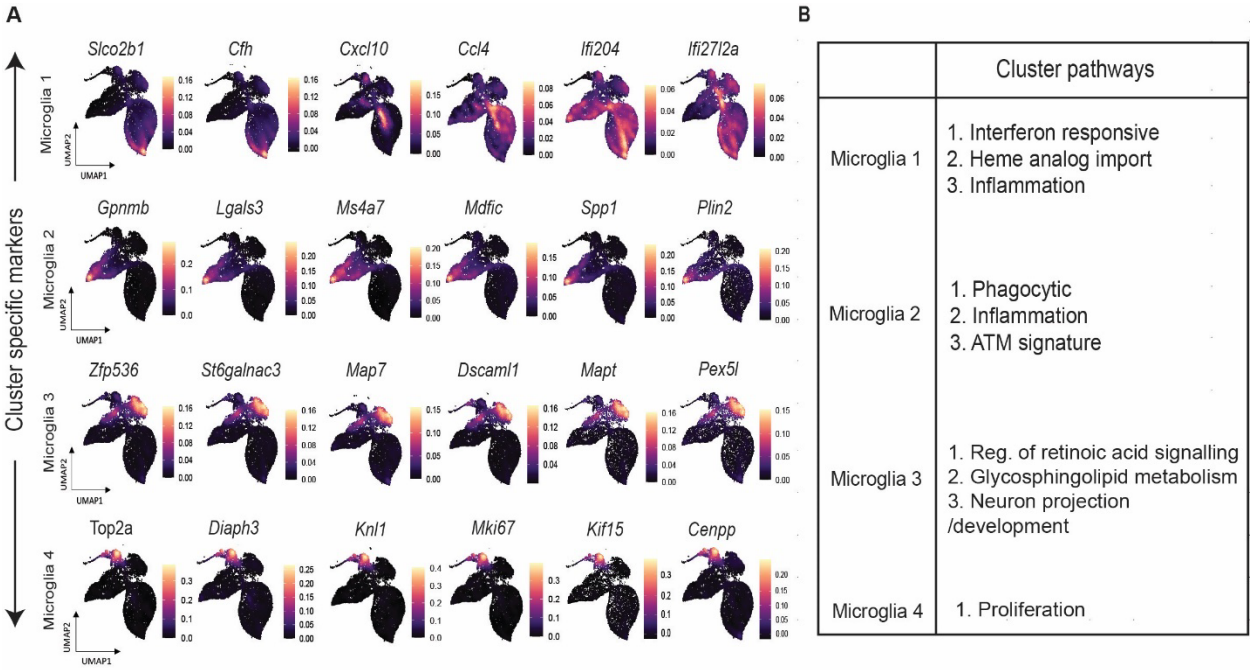

Figure 1.2: Characterization of microglia clusters
(A) Density plots of top differentially expressed genes in each microglia cluster, FDR <0.05, logFC>3.0, based on Kernel gene-weighted density separating them into distinct clusters.
(B) Functional annotation of each microglia cluster by GO terms FDR<0.05.

1.3 Differential expression analysis between young and aged microglia / macrophages

Intriguingly, all microglia clusters shared a DAM / IRM (Disease associated / Injury responsive) microglia signature with relatively higher average expression in Clusters 1 and 2, indicating that the microglia response to injury is preserved **(Figure 1.3 D)**. (Keren-Shaul *et al.*, 2017b; Hammond *et al.*, 2019). To identify distinct populations of microglia in young and aged datasets, cell proportion percentages were calculated for each cluster of microglia; however, no significant differences were observed **(Figure 1.3 C)**. Nevertheless, differential expression (DEG) analysis revealed unambiguous gene expression differences between young and aged microglia We identified, for example, *Apoe*, a factor known to have pro-regenerative properties, as one of the most differentially transcribed genes in cluster 1, 2, and 3 microglia with higher expression in young compared to aged. **(Figure 1.3 E)**.

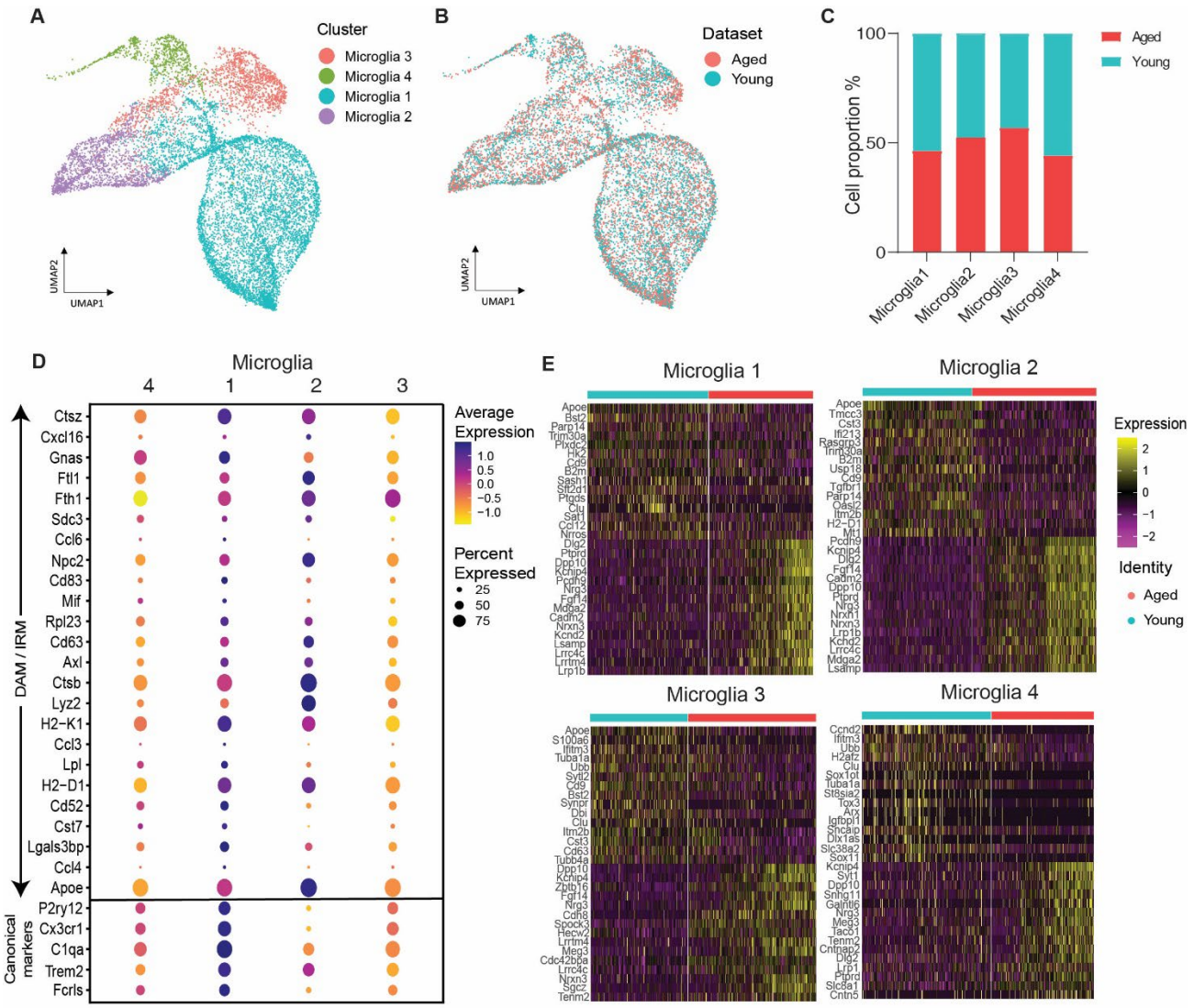

Figure 1.3: Single-nucleus RNA-seq to examine distinct cellular response in young and aged white matter (WM) after demyelinating injury

(**A**) UMAP visualization of microglia clusters in which dots correspond to individual nuclei profiled with snRNA-seq.

(B) UMAP visualization of microglia clusters divided by young (6,093 nuclei) and aged (5,792 nuclei) datasets.

(C) Distribution of microglia clusters between young (cyan) and aged (red) mice.

(D) Dot plot of average expression of DAM/IRM and canonical marker genes in all four clusters of microglia.

(E) Heatmap of top 15 differentially expressed genes between young and aged mice in each microglia cluster, FDR<0.05, Fold enrichment > 1.5.

1.4 Enrichment analysis of microglia in lesions between young and aged mice

Gene ontology analysis revealed microglia in aged mice were enriched for pathways such as: nervous system development, synapse assembly, homeostatic process, cell-cell adhesion, etc., whereas microglia in young mice were enriched for pathways such as cell migration, innate immune response, glial cell differentiation, macrophage activation, lipid response etc. (FDR <0.05) **(Figure 1.4. A, B)** indicating that a deficient transcriptional response of microglia to demyelinating injury in aged mice is responsible for insufficient activation and myelin lipid clearance, which is a bottleneck for lesion recovery and inflammation resolution.

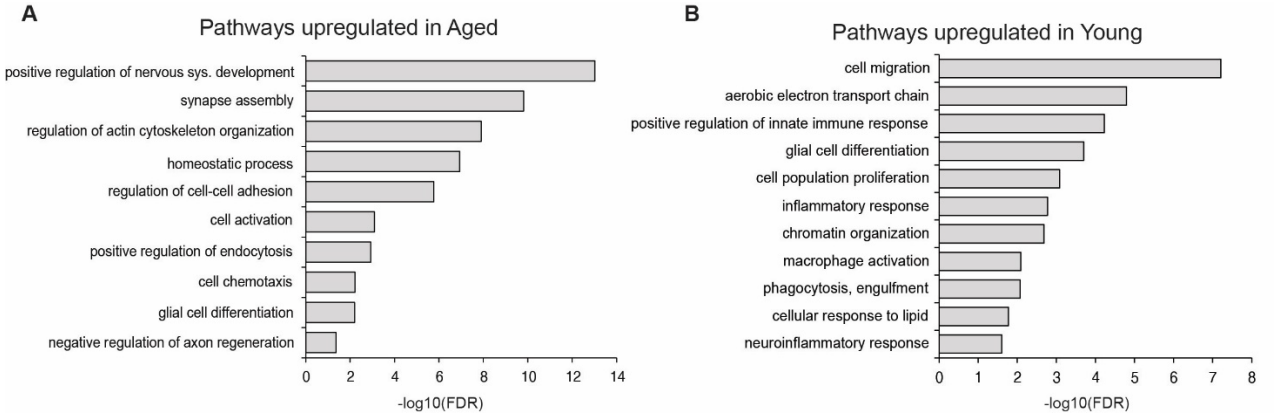

Figure 1.4: Distinct microglia response in young and aged mice post demyelinating injury
(A, B) Gene ontology (GO) term enrichment analysis depicting ten terms for biological process (A) upregulated in aged and (B) upregulated in young microglia clusters using Fisher's exact test and Benjamin-Hochberg FDR correction.

2. Analysis of the epigenome revealed restricted chromatin accessibility in aged microglia after demyelination injury.

It is evident from previous studies that modulation of gene expression is highly regulated through the remodeling of chromatin, the complex of DNA, and histone proteins around which DNA wraps (Kornberg, 1974). Transcriptional regulation requires the repositioning of the nucleosomes around promoters and enhancers, thereby making chromatin accessible to transcription factors. (Boeger *et al.*, 2003; Lee *et al.*, 2004; Henikoff, 2008; Radman-Livaja and Rando, 2010).

2.1 Experimental design for ATAC seq

We hypothesized that the impaired function of microglia/macrophages in aging following demyelinating injury might be due to chromatin in-accessibility, which prevents the effective binding of the transcription factors (TFs) to the promoter of the genes involved in pathways such as activation, innate immune response and response to lipid metabolism thereby resulting in poor recovery. To investigate, we performed Bulk ATAC (Assay for Transposase -Accessible Chromatin) sequencing on Cd11b+ cells isolated from the brains of young and aged mice (4-7) days after lesion induction (Buenrostro *et al.*, 2013).

Schematic representation of the ATAC-seq experiment on CD11b^{+} cells isolated from lesioned white matter (WM) of young and aged mice.

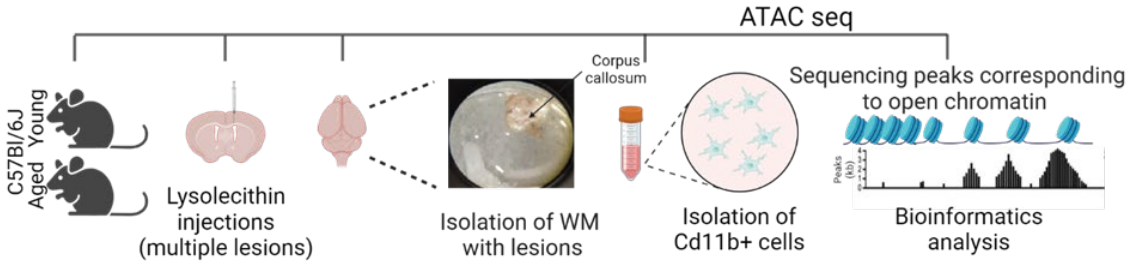

2.2 Quality control and ATAC seq analysis

Fragment length distribution of samples revealed distinct peaks at around 50bp, 200bp, 400bp, and 600bp, respectively, ensuring the quality and downstream analysis **(Figure 2.2 A)**. Interestingly, we observed a higher landscape of open chromatin regions in young mice compared to aged around ±1Kb of transcription start site (TSS). Differential analysis revealed fewer differential accessible regions DARs in aged (3,345) than in young (18,579) (FDR <0.05, logFC>1). **(Figure 2.2 B, C)**.

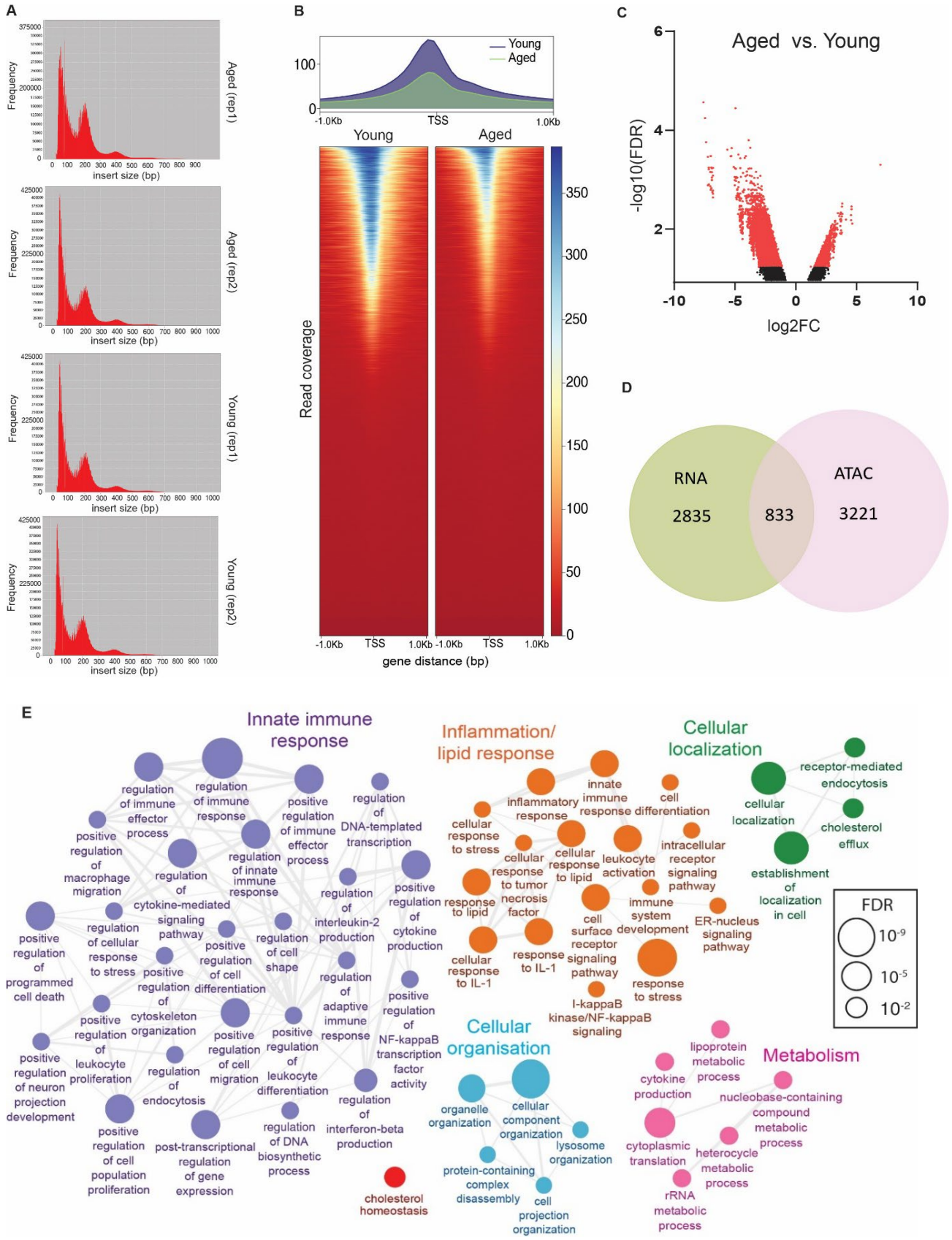
A
Frequency
insert size (bp)
Aged (rep1)
Aged (rep2)
Young (rep1)
Young (rep2)
B
Young
Aged
TSS
-1.0Kb
1.0Kb
Read coverage
gene distance (bp)
C
Aged vs. Young
-log10(FDR)
log2FC
D
RNA
2835
833
ATAC
3221
E
Innate immune response
Inflammation/ lipid response
Cellular localization
Cellular organisation
Metabolism
FDR
10-9
10-5
10-2

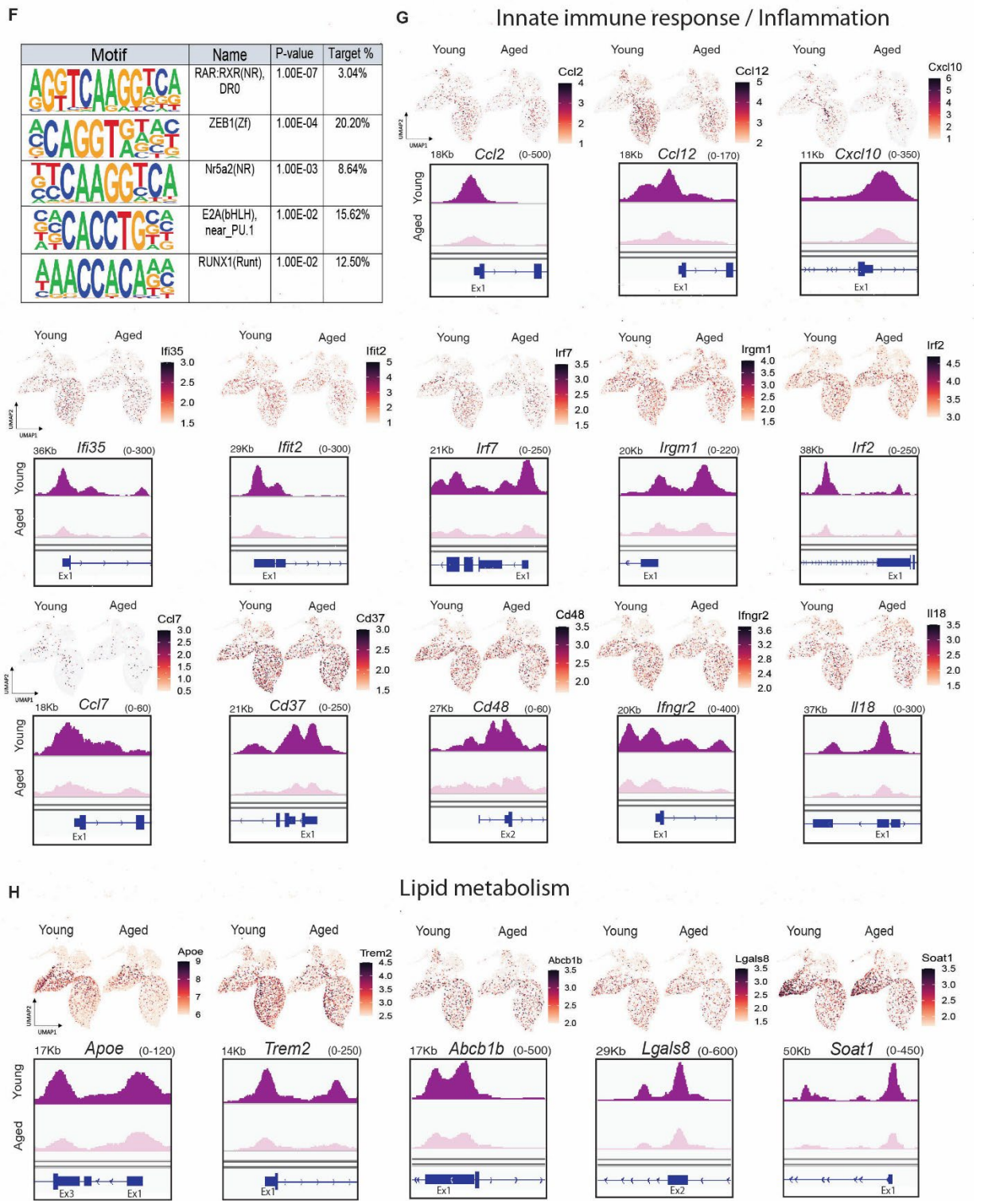

Figure 2.2: Epigenomic analysis of young and aged microglia after demyelinating injury
(A) Paired-end histogram indicating the fragment length distribution of each replicate (rep 1 and rep 2) in young and aged datasets of ATAC-seq experiment.

(B) Plot profile depicting the mean signal intensity at 1Kb around TSS (transcription start site) and heatmap summarizing the coverage of genomic reads with a color code from red (no coverage) to blue (maximum coverage) at 1Kb around TSS between young and aged microglia
(C) Volcano plot of differentially accessible regions (DARs) in aged compared to young microglia, FDR<0.05.
(D) Venn diagram indicating common genes between snRNA and ATAC-seq datasets that are downregulated in aged microglia due to poor accessibility.
(E) Enrichment map of biological pathways downregulated in aged due to poor accessibility, using Fisher's exact test and Benjamin-Hochberg FDR correction.
(F) Motif enrichment analysis of the common set of genes identified between snRNA and ATAC seq datasets that are downregulated in aged mice due to poor accessibility.
(G, H) Feature plots indicated normalized expression of selected genes involved in (G) Innate immune /inflammation (H) lipid response in each microglia cluster along with accessibility profile showing the coverage of genes around the promoter region. The first exon for each gene is indicated below. FDR<0.05.

DARs were further filtered for introns and unannotated regions, resulting in (4,054) regions inaccessible in aged. Further, to determine if the deficient transcription is due to poor chromatin accessibility, we compared the genes that were downregulated in aged microglia in single nuclear RNA seq with the regions that are inaccessible in aged in ATAC seq and found that 833 genes were shared between these two datasets, indicating that ~30% of genes that are poorly transcribed were due to chromatin in-accessibility in aged microglia upon demyelinating injury. Enrichment analysis of shared genes uncovered innate immune response, lipid response, cellular localization, organization, and metabolism as the major cluster of pathways downregulated in aged mice due to poor accessibility. (FDR <0.05) **(Figure 2.2 D, E)**.

Open chromatin can influence transcription via TFs, which aid transcription by recognizing and binding to specific DNA sequences known as Motifs (D'Haeseleer, 2006). We performed motif enrichment analysis using Homer on shared genes and discovered the following motifs to be underrepresented in aged: RAR: RXR (p-val :1.00E-07), Nr5a2 (p-val :1.00E-03), which are involved in lipid metabolism and cholesterol transport as well as ZEB1(p-val :1.00E-05), E2A_near PU.1(p-val :1.00E-02), Runx1(p-val :1.00E-02) which are involved in immune response, microglia proliferation, and differentiation. Therefore, deficient myelin lipid clearance and inadequate activation in aged mice following demyelinating injury could be attributed to inadequate transcription of genes due to reduced accessibility of chromatin around promoters **(Figure 2.2 F, G, H)**.

3. Immune training with BCG alters the microglial chromatin landscape of aged mice

In the CNS, resident microglia provide innate immunity. They are essential for immune surveillance, development, and plasticity (Nimmerjahn, Kirchhoff and Helmchen, 2005). However, it is known that microglia develop an inflammatory phenotype as they age, reducing their ability to mount an appropriate physiological response following CNS injury. Consequently, persistent neuroinflammation in the CNS hinders CNS recovery (Sierra *et al.*, 2007b; Perry, Nicoll and Holmes, 2010; Norden and Godbout, 2013; Niraula, Sheridan and Godbout, 2016). Significant clinical and experimental evidence suggests that the innate immune system can acquire non-specific immunological memory, also known as trained immunity, due to epigenetic and metabolic reprogramming of innate immune cells. (Netea, Quintin and Van Der Meer, 2011b; Donohoe and Bultman, 2012b; Saeed *et al.*, 2014b; Domínguez-Andrés, Joosten and Netea, 2019b). Trained immunity may play an essential role in mitigating the effects of immunosenescence. In light of the fact that microglia are known to interpret and propagate inflammatory signals in the periphery, we wondered whether they could be trained (Ek *et al.*, 2001; Perry, 2007; Wendeln *et al.*, 2018; Neher and Cunningham, 2019). Bacillus Calmette- Guérin (BCG), a vaccine commonly used against tuberculosis, was utilized for this study. BCG has been extensively studied to provide heterologous effects, secondary infection protection, and amelioration of certain neurodegenerative diseases (Ristori *et al.*, 2014b; Zuo *et al.*, 2017; Arts *et al.*, 2018a; Matsuzaki *et al.*, 2021b). This is mediated by the epigenetic reprogramming of innate immune cells, which involves the deposition of specific chromatin marks H3K27ac and H3K4me3, resulting in chromatin unfolding and transcription facilitation. (Kleinnijenhuis *et al.*, 2012b; Arts, Carvalho, *et al.*, 2016a).

To determine if peripheral stimulation of BCG can alter the chromatin landscape and induce a trained immune response in microglia, we analyzed microglia ($Cd11b^{+}$) cells isolated from mice treated with BCG or saline for the following histone marks H3K4me3 and H3k27ac using Chip sequencing.

Schematic representation of the ChIP-seq experiment on $CD11b^{+}$ cells isolated from aged mice treated with BCG or saline.

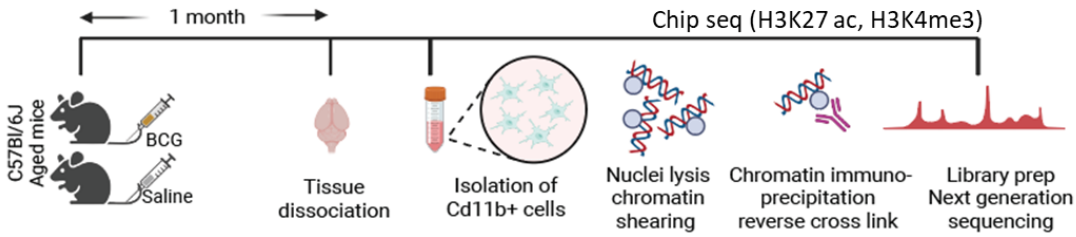

3.1 CHIP Sequencing identifies greater enrichment of H3K27ac and H3K4me3 histone marks in microglia of aged mice treated with BCG

Interestingly, we observed greater enrichment of H3K27ac and H3K4me3 marks in microglia of BCG-treated mice compared to controls after determining the correlation between immunoprecipitated and input samples **(Figure 3.1 A, B)**. The genes enriched for the H3K27ac mark were involved in pathways: differentiation, migration, innate immune response, and lipid metabolism, while the genes enriched for H3K4me3 were involved in inflammation and interferon response, respectively **(Fig 3.1 C, D)**.

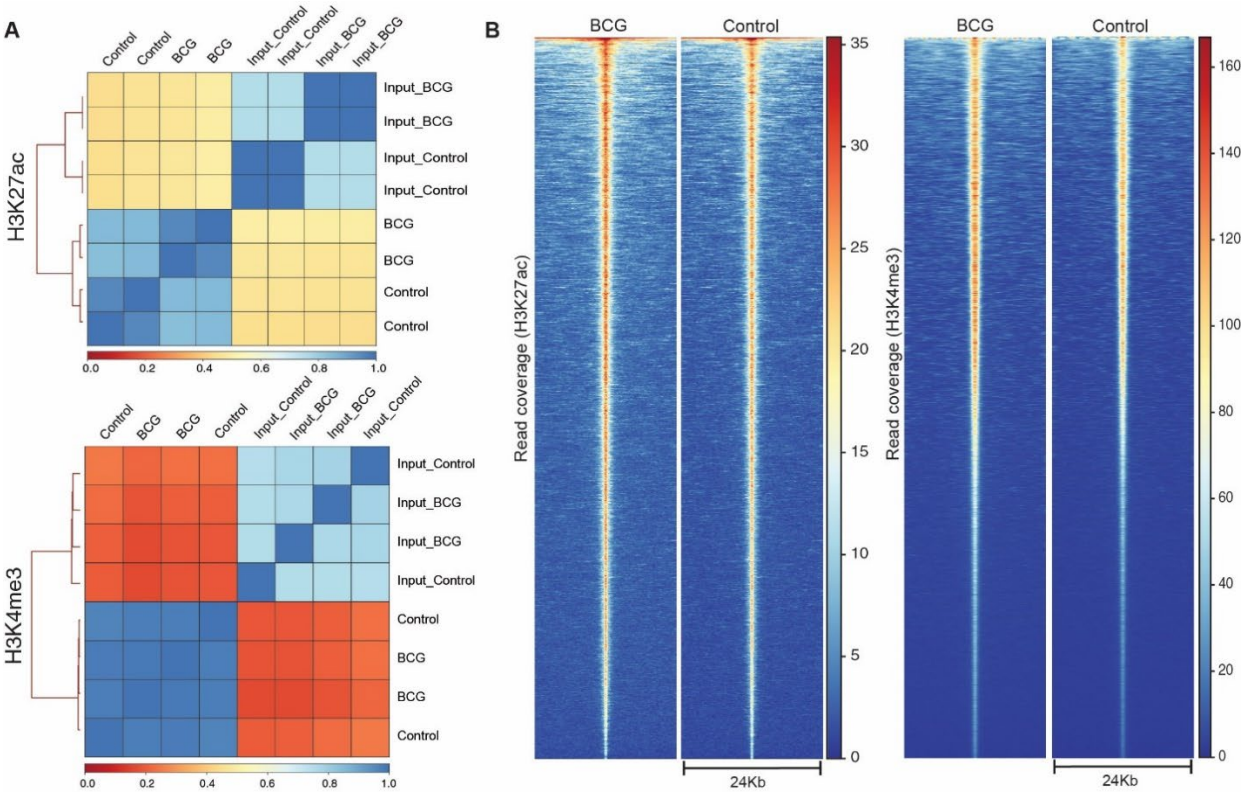

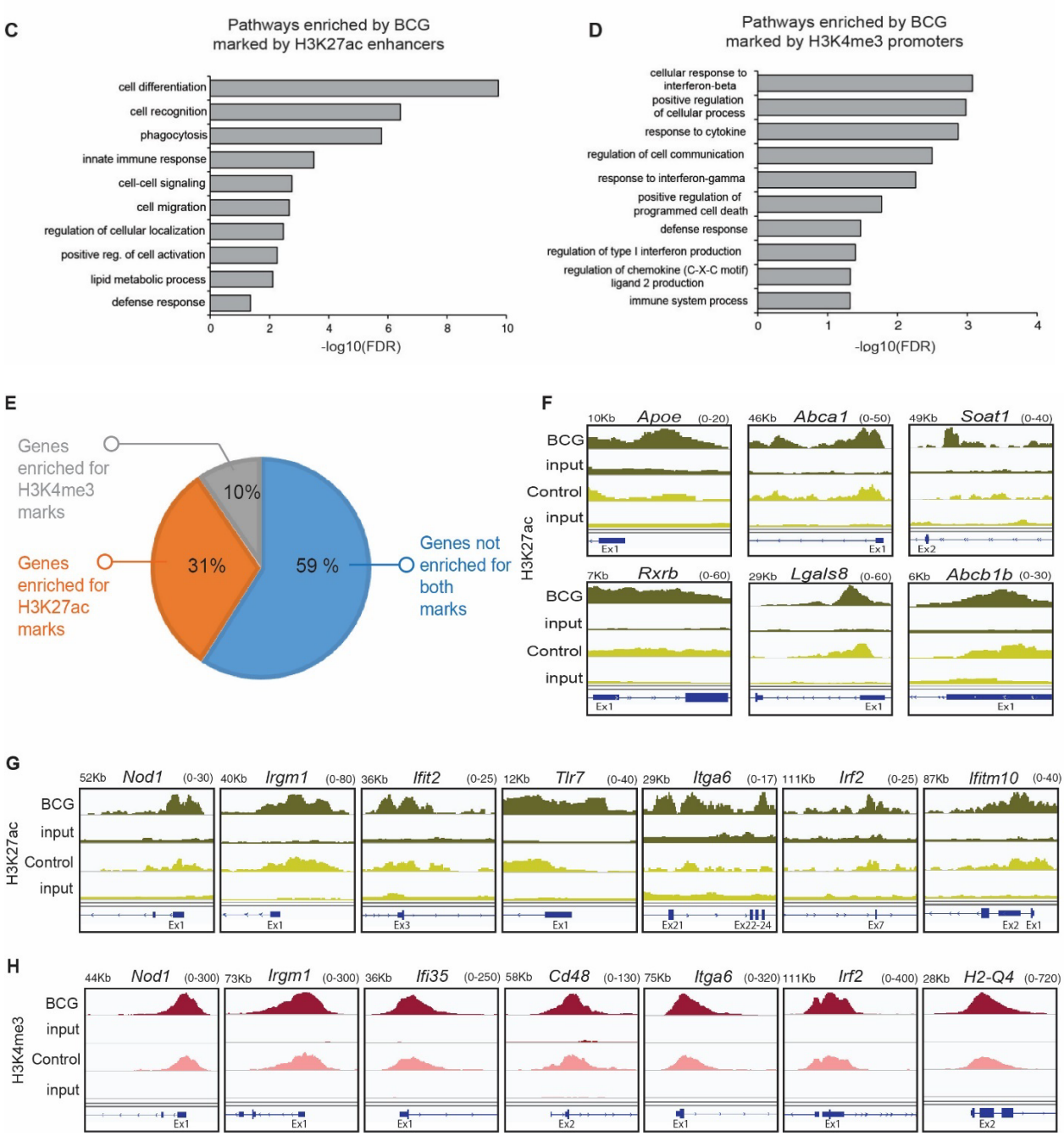

Figure 3.1: H3K27ac and H3K4me3 epigenetic marks are enriched in the microglia of aged mice treated with BCG

(A) Correlation plot indicating pairwise Pearson correlation between the replicates of Chip and input, respectively, for H3K27ac and H3K4me3 read densities.

(B) Heatmaps of epigenetic marks specifying enrichment of H3K27ac (around enhancers) and H3K4me3 (around promoters) between BCG and control, where rows are genomic regions from -12 to +12kb around the center of the peaks.

(C, D) GO term enrichment analysis depicting ten terms for biological process (C) enriched for H3K27ac marks and (D) enriched for H3K4me3 marks in aged mice treated with BCG using Fisher's exact test and Benjamin-Hochberg FDR correction.
(E) Pie chart representing the percentage of genes enriched for H3K27ac and H3K4me3 marks after BCG treatment out of the common set of genes in snRNA and ATAC seq.
(F, G, H) Coverage plots of (F, G) H3K27ac marks and (H) H3K4me3 and input for the differentially regulated genes in control (saline) and BCG-treated mice. The exon for each gene is indicated below, FDR<0.05.

To determine if the enrichment of these key histone marks was also on the poorly transcribed genes after demyelinating injury, we performed differential analysis between BCG and control on the shared set of genes between (snRNA and ATAC) for H3K27ac and H3K4me3 histone marks. Interestingly, we found that 31% of genes were enriched for H3K27ac marks, including those involved in lipid metabolism (*Apoe, Abca1, Soat1, Rxrb*) and innate immune response (*Nod1, Irgm1, Ifit2, Tlr7, Itga6, Irf2, Ifitm10*) whereas 10% of genes were enriched for H3K4me3 marks which were mostly involved in inflammation and interferon response (*Nod1, Irgm1, Ifi35, Cd48, Itga6, Irf2, H2-Q4)* (FDR<0.05). **(Figure 3.1 E-H)**. Taken together, our data indicate that BCG-induced immune training can alter the chromatin landscape in microglia for H3K27ac and H3K4me3 histone marks on poorly transcribed genes after demyelinating injury.

4. The influence of innate immune training on microglia/macrophages by BCG

To examine the role of BCG-inducing training in CNS lesion recovery, we used the aforementioned injury model of LPC in BCG- or saline-treated mice at 4 and 14 dpi following lesion induction. Microglia are the dominant population in this model, as only a small number of monocyte-derived macrophages enter lesions from the periphery (Lloyd *et al.*, 2019; Plemel *et al.*, 2020).

Schematic representation of BCG treatment and experimental timeline in aged mice.

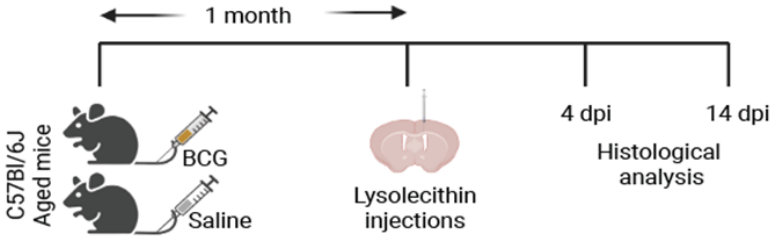

4.1 Myelin repair is enhanced in aged mice by BCG

We measured the size of lesions with FluoroMyelin labeling and quantified microglia with anti-IBA1 antibodies. At 4 dpi, demyelinating lesions were of similar size in BCG and saline-treated mice, and comparable volumes of the lesions were occupied by IBA1^{+} microglia, showing that lesion formation was unaltered **(Figure 4.1 A, B)**. However, when lesion sizes were analyzed at 14 dpi, we observed that lesion volume decreased in BCG-treated mice, and there was a reduction in Iba1+ cells, pointing to enhanced lesion recovery **(Figure 4.1 C, D)**. Moreover, assessment of oligodendrocytes using antibodies against anti-adenomatous polyposis coli (APC), clone CC1, revealed a higher percentage of mature CC1+ oligodendrocytes in lesions of BCG-treated mice 14 days after injection **(Figure 4.1 E, F)**. Thus, BCG treatment reduced inflammation and enhanced lesion recovery after demyelinating injury in aged mice.

4.2 Innate immune training by BCG improves lipid clearance by microglia and macrophages after demyelinating injury

Microglia/macrophages are crucial in removing myelin lipid debris and promoting a regenerative response following demyelination (Kotter *et al.*, 2006b; Huang *et al.*, 2010; Cantuti-Castelvetri *et al.*,

2018; Bogie *et al.*, 2020). Consequently, we investigated whether a BCG-induced trained immune response promotes myelin-debris clearance and lipid processing by microglia in lesions 14 days' post-injection. Reflection microscopy, a hybrid of fluorescence confocal microscopy and laser reflection, allowed us to discover fewer Reflection^{+} IBA1^{+} cells in the lesions of BCG-treated animals. We observed less LAMP1 labeling in microglia colocalizing with myelin debris and reflection^{+} material in

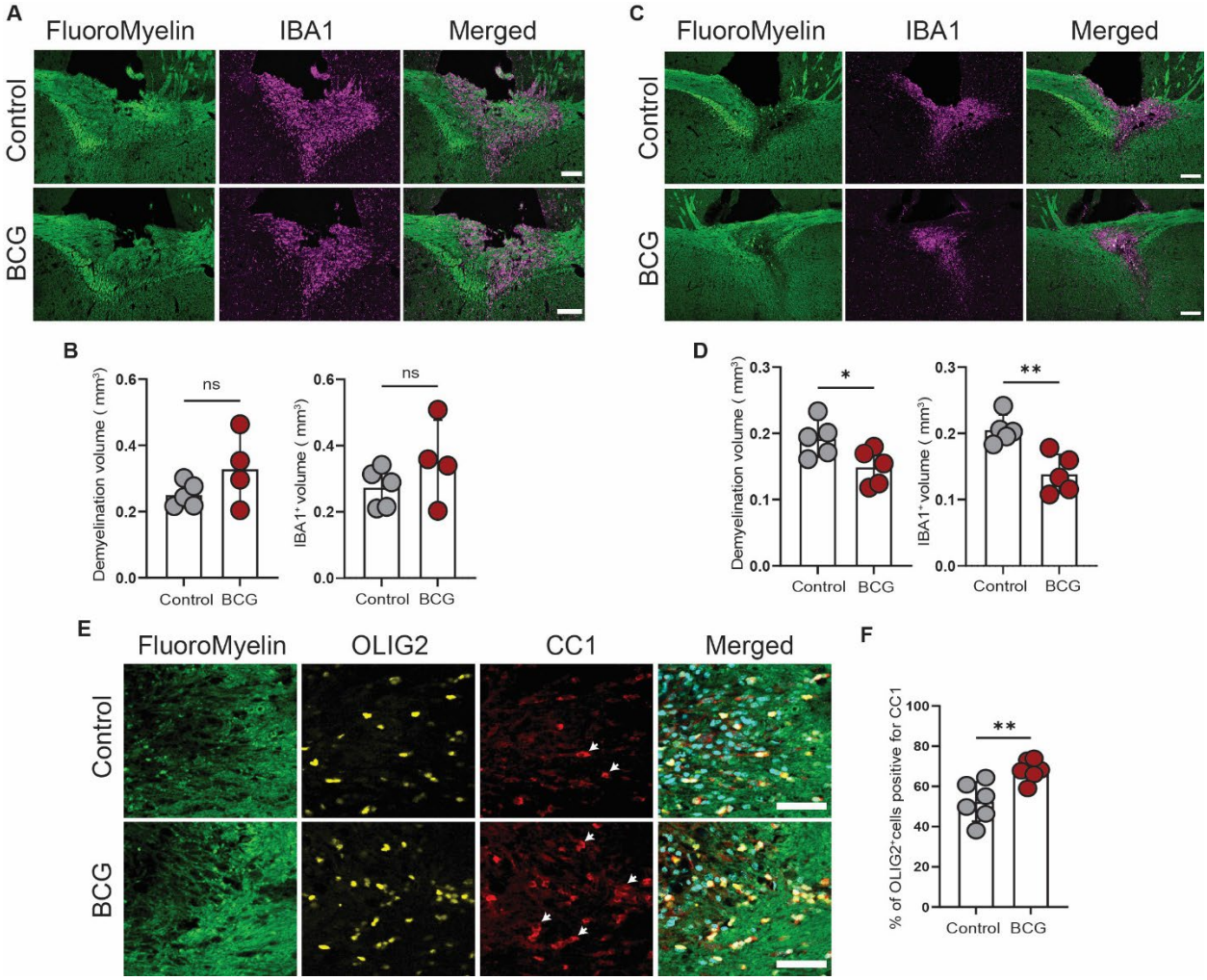

Figure 4.1: BCG immunization promotes lesion recovery after demyelinating injury in aged mice
(A) Images of corpus callosum lesions in 12 months aged mice treated with BCG or saline at 4 dpi. Scale bar, 200µm.
(B) Quantification of lesion volume and IBA1^{+} volume at 4 dpi.
(C) Images of corpus callosum lesions in 12 months aged mice treated with BCG or saline at 14 dpi. Scale bar, 200µm.
(D) Quantification of lesion volume and IBA1^{+} volume at 14 dpi.
(E) Images of the demyelinated lesions in the corpus callosum at 14 dpi exemplifying the numbers of CC1^{+}OLIG2^{+} cells at the demyelination/remyelination edge. White arrows indicate CC1^{+}OLIG2^{+} cells. Scale bar, 50 µm.
(F) Quantification of the percentage of OLIG2^{+} cells positive for CC1

All data are mean ± SD; *P<0.05, **P<0.01, ***P<0.01, ns-not significant, two-tailed Welch's *t*-test or Mann Whitney test, n numbers are indicated in the figure; each dot represents one mouse.

14 dpi lesions of BCG-treated animals **(Figure 4.2 A, C, E)**. In addition, we quantified the number of IBA1$^+$ microglia harboring myelin debris, which we labeled with FluoroMyelin, and observed that lesions from BCG-treated mice had fewer myelin-laden microglia than those from saline-treated mice as well as less Plin2$^+$ Iba1$^+$ microglia in BCG treated mice **(Figure 4.2 A, B, D, F)** suggesting that there is less cholesterol overloading of microglia after inducing demyelinating injury in BCG-treated mice, pointing to improved lipid processing and myelin clearance.

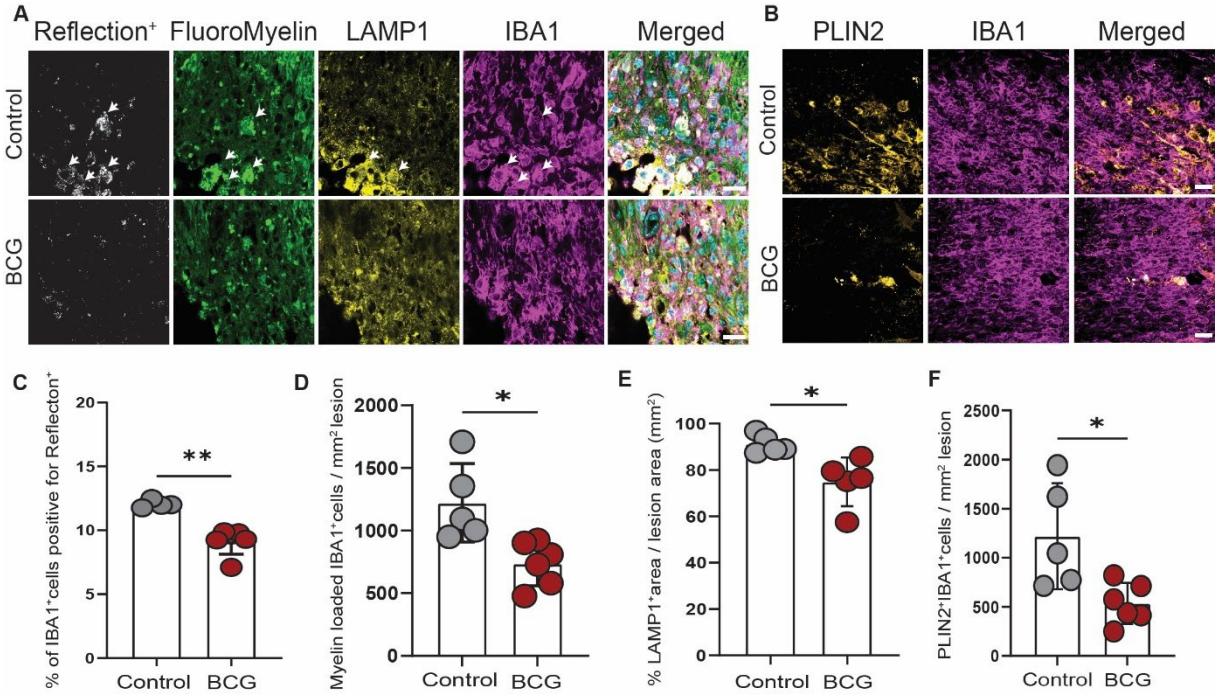

Figure 4.2: BCG immunization promotes lesion recovery after demyelinating injury in aged mice
(A) Images demonstrating refection microscopy and accumulation of myelin debris in LAMP1$^+$IBA1$^+$ cells in demyelinated lesions at 14 dpi. Scale bar, 50 µm. White arrows point to reflection$^+$ myelin-debris accumulation within LAMP1$^+$IBA1$^+$ cells.
(B) Images of demyelinated lesions at 14 dpi demonstrating PLIN2$^+$ signal within IBA1$^+$ cells, Scale bar, 50 µm.
(C, D, E) Quantification of the percentage of (C) IBA1$^+$ cells positive for reflection, (D) myelin loaded (FluoroMyelin$^+$) IBA1$^+$ cells per mm^2 of lesion and (E) percentage of lesion area occupied by LAMP1$^+$ signal at 14 dpi.
(F) Quantification of PLIN2$^+$IBA1$^+$cells per mm^2 of lesion at 14 dpi.
All data are mean ± SD; *P<0.05, **P<0.01, ***P<0.01, ns-not significant, two-tailed Welch's *t*-test or Mann Whitney test, n numbers are indicated in the figure; each dot represents one mouse.

4.3 BCG induces precise microglia activation upon demyelination which is necessary for lesion recovery

One of the possible explanations for improved lipid processing could be enhanced microglia activation at earlier time points after demyelination (Franklin and Ffrench-Constant, 2017; Cunha *et al.*, 2020a). We used immunohistochemistry to examine microglia reactivity and activation at 4 dpi in BCG-treated mice versus controls. Surprisingly, we found a higher percentage of MHCII $^{+}$IBA1^{+} and MAC2 $^{+}$IBA1 $^{+}$cells in the lesions of BCG-treated mice **(Figure 4.3 A, B)**. Also, it is known from previous studies that BCG-induced training increases Tnf and Il1b cytokines in monocytes and macrophages (Kleinnijenhuis *et al.*, 2012b; Moorlag *et al.*, 2019). To validate that in microglia, we checked for Tnf-a and Il1ß mRNA particles post-demyelinating injury at 4 dpi and found that there were more Tnf-a^{+} Il1ß$^{+}$ mRNA particles in Iba1^{+} cells in BCG-treated mice **(Figure 4.3 C-F)**. Hence, BCG-induced training improved remyelination in aging by increasing pro-inflammatory activation in microglia after demyelinating injury, which was essential for myelin lipid clearance and inflammation resolution.

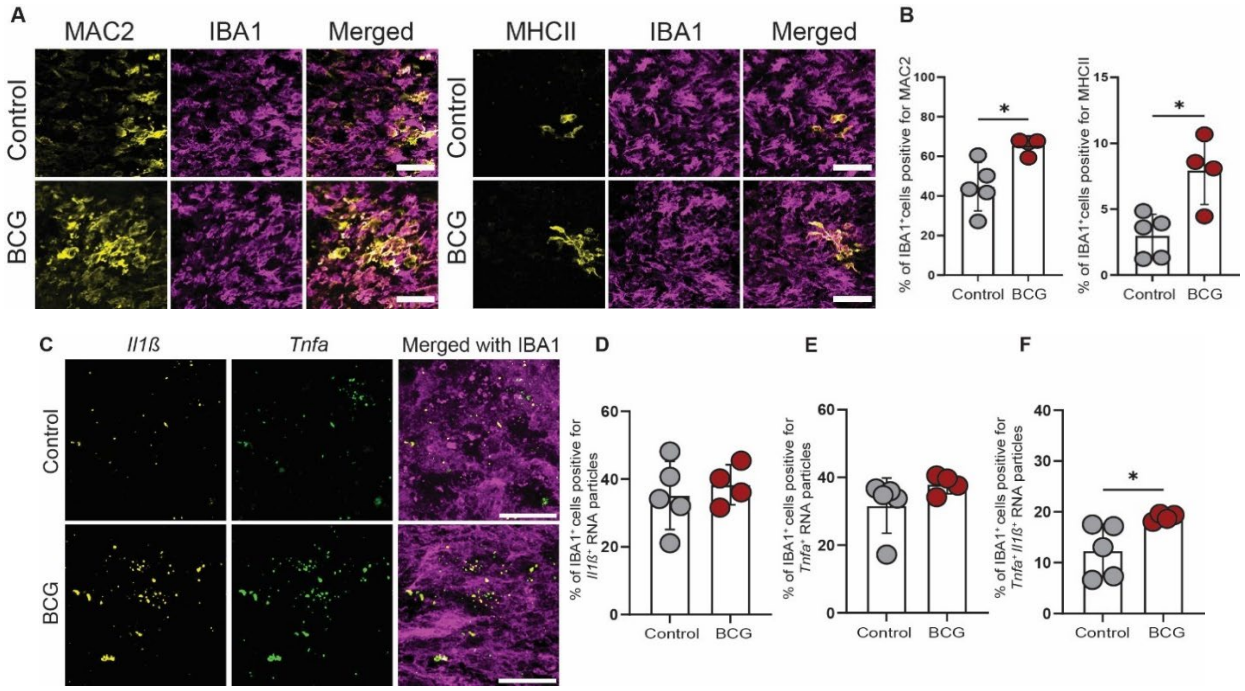

Figure 4.3 BCG treatment increases activation and cytokine expression after demyelinating injury
(A) Images of MAC2^{+}IBA1^{+} and MHCII^{+}IBA1^{+} cells in the demyelinated lesions at 4 dpi. Scale bar, 50 µm
(B) Quantification of the percentage of MAC2+IBA1+ and MHCII+IBA1+ cells over IBA1+ cells in the demyelinated lesion at 4 dpi.
(C) Images of corpus callosum lesions in 12 months aged mice treated with BCG or saline at 4 dpi, demonstrating the *IL-1ß* (yellow) and *Tnf-a* (green) mRNA particles accumulating within IBA1^{+} cells Scale bar, 20µm.
(D, E, F) Quantification of the number (%) of *IL-1ß* and *Tnf-a* mRNA particles within IBA1^{+}cells.
All data are mean ± SD; *P<0.05, two-tailed Welch's *t*-test, *n* numbers are indicated in the figure; each dot represents one mouse.

5. BCG-induced immune training modifies the transcriptome profile of cells in lesions permissive for myelin regeneration

For transcription factors (TFs) to access the chromatin and initiate gene transcription, chromatin modifications such as the deposition of histone marks H3K27ac and H3K4me3 must occur. We performed transcriptomic analysis of 14 dpi lesions in BCG- or saline-treated mice to determine if immune training of microglia by BCG led to the transcription of genes involved in myelin repair.

5.1 Quality control of differential analysis between BCG and Saline (control) conditions

Samples clustered into their respective experimental groups, as shown by principal component analysis (PCA) and a heatmap of the distance matrices between the samples **(Figure 5.1 A, B)**. To estimate the significance of expression differences between the two groups, we performed differential analysis **(Figure 5.1 B, D, E, G)** and found that 993 genes upregulated and 614 genes downregulated in BCG condition compared to saline(control), FDR <0.05 **(Figure 5.1 C, F)**.

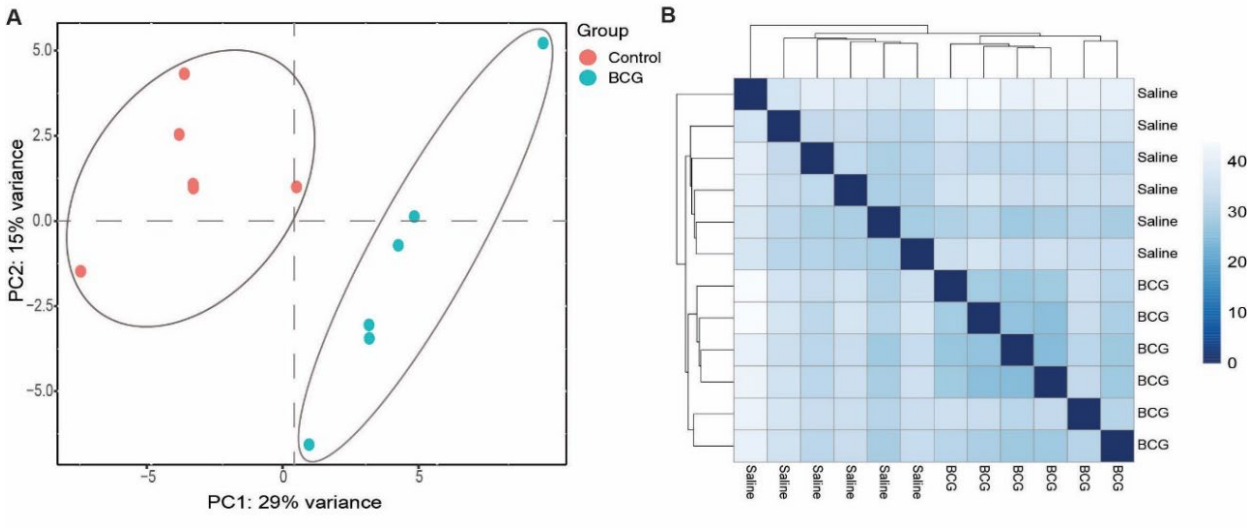

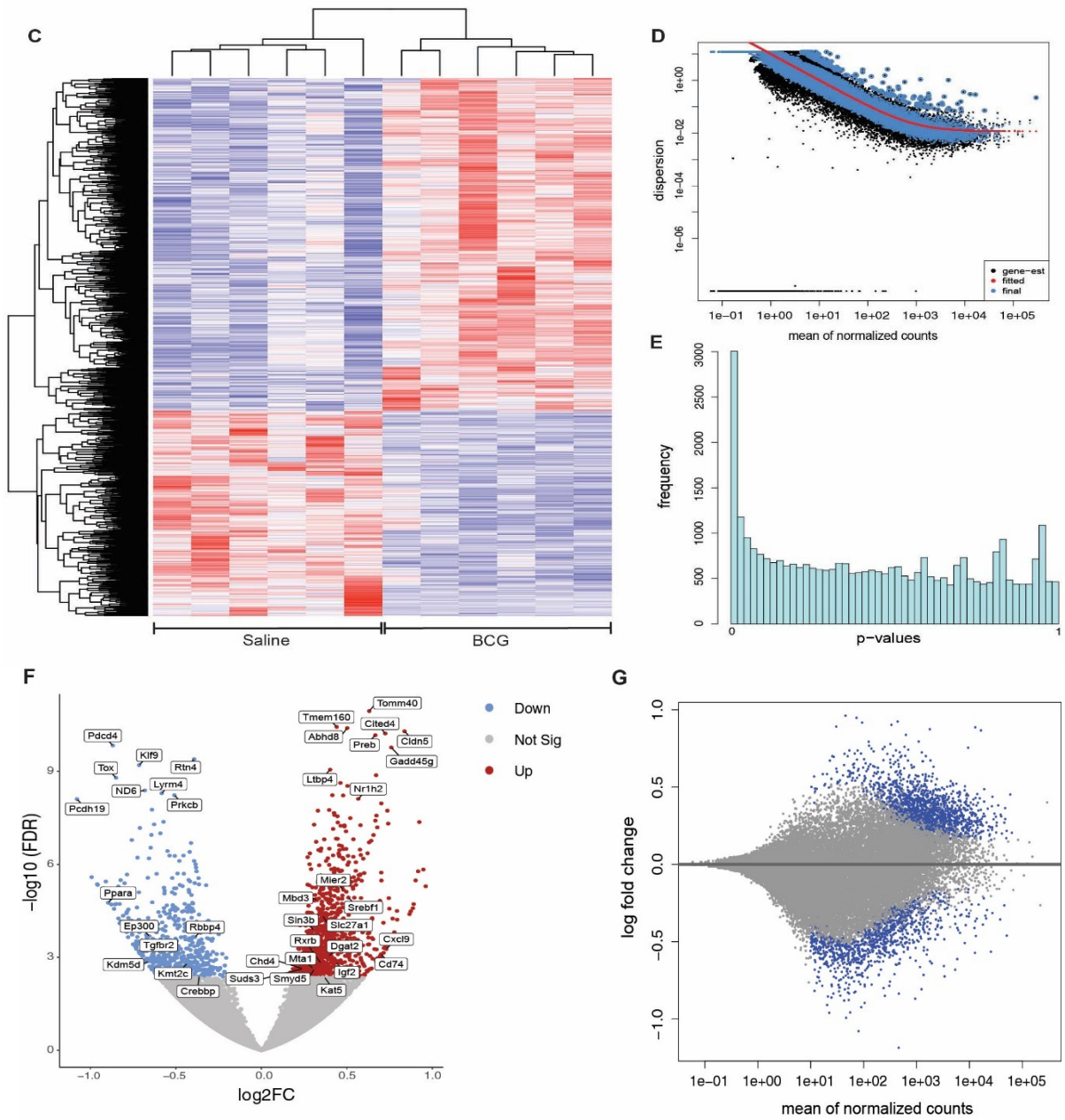

Figure 5.1: Quality control of differential analysis between BCG and Saline (control)

(A) Principal component analysis (PCA) of RNA-seq normalized read counts from BCG and control group where each replicate is plotted as an individual data point.

(B) Heatmap of the sample-to-sample distance matrix (with clustering) based on the normalized counts, indicating an overview of similarities and dissimilarities between samples: the color represents the distance between the samples. Dark blue means shorter distance, i.e., closer samples given the normalized counts.

(C) Heatmap of differentially expressed genes over samples of BCG and control indicating z-score.

(D) Scatter plot of dispersion vs. mean of normalized counts, indicating the dispersion estimates: gene-wise estimates (black), the fitted values (red), and the final maximum a posteriori estimates used in testing (blue).

(E) Histogram of *p*-values for the frequency of genes in comparison between BCG and control

(F) Volcano plot of differentially expressed genes in BCG-treated mice lesions compared to control mice, FDR<0.05.

(**G)** MA plot displaying the global view of the relationship between the expression change of conditions (log ratios, M), the average expression strength of the genes (average mean, A), and the ability of the algorithm to detect differential gene expression. The genes that passed the significance threshold (adjusted p-value < 0.1) are colored in blue.

5.2 Transcriptomic analysis identifies genes involved in lipid metabolism and chromatin organization to be enriched in lesions of BCG treated mice

Gene ontology analysis identified lipid metabolism, chromatin modification, aerobic respiration, and cellular localization as the key differentially regulated pathways (Fold enrichment-1.0-6.0; FDR<0.05) **(Figure 5.2 A)**. Among the differentially expressed genes, upregulated in lesions of BCG-treated mice, were two lipid sensing nuclear receptors, *Nr1h2* (liver X receptor A) and *Rxrb* (Retinoid X Receptor Beta), previously implicated in remyelination (Huang *et al.*, 2010; Cantuti-Castelvetri *et al.*, 2018). Since, the reverse cholesterol pathway with *Abca1*, and *Abcg1* as key molecules is under control of these nuclear receptors (Fielding and Fielding, 1995), we analyzed *Nr1h2, Abca1* and *Abcg1* expression using RNA in situ hybridization and found higher expression in microglia/macrophages of BCG compared to control **(Figure 5.2 B-F)**. Furthermore, genes involved in histone acetylation and deacetylation were shown to be differentially expressed in samples of BCG-treated mice. For example, we discovered upregulation of *Kat5*, a histone acetyltransferase, and differential regulation of *Sin3b, Chd4, Mbd3, Mier2, Mta1, Rbbp4,* and *Suds3,* all of which are known to regulate the activity of Histone deacetylase (HDAC 1 and 2) by forming a core repressor complex (Seto and Yoshida, 2014) **(Figure 5.2 G)**.

Earlier research has shown that while HDACs are essential for downregulating oligodendrocyte differentiation inhibitors (Shen *et al.*, 2008b), depleting HDAC1, 2 in microglia can lessen amyloid plaque burden and improve cognition (Datta *et al.*, 2018) and that in microglia-specific HDAC1,2 KO mice, the immune response by LPS is nearly abolished (Wendeln *et al.*, 2018). Therefore, we reasoned if epigenetic regulation by HATs and HDACs is the key driver in modulating the chromatin landscape of microglia/macrophages, thereby regulating the transcription of genes involved in myelin repair.

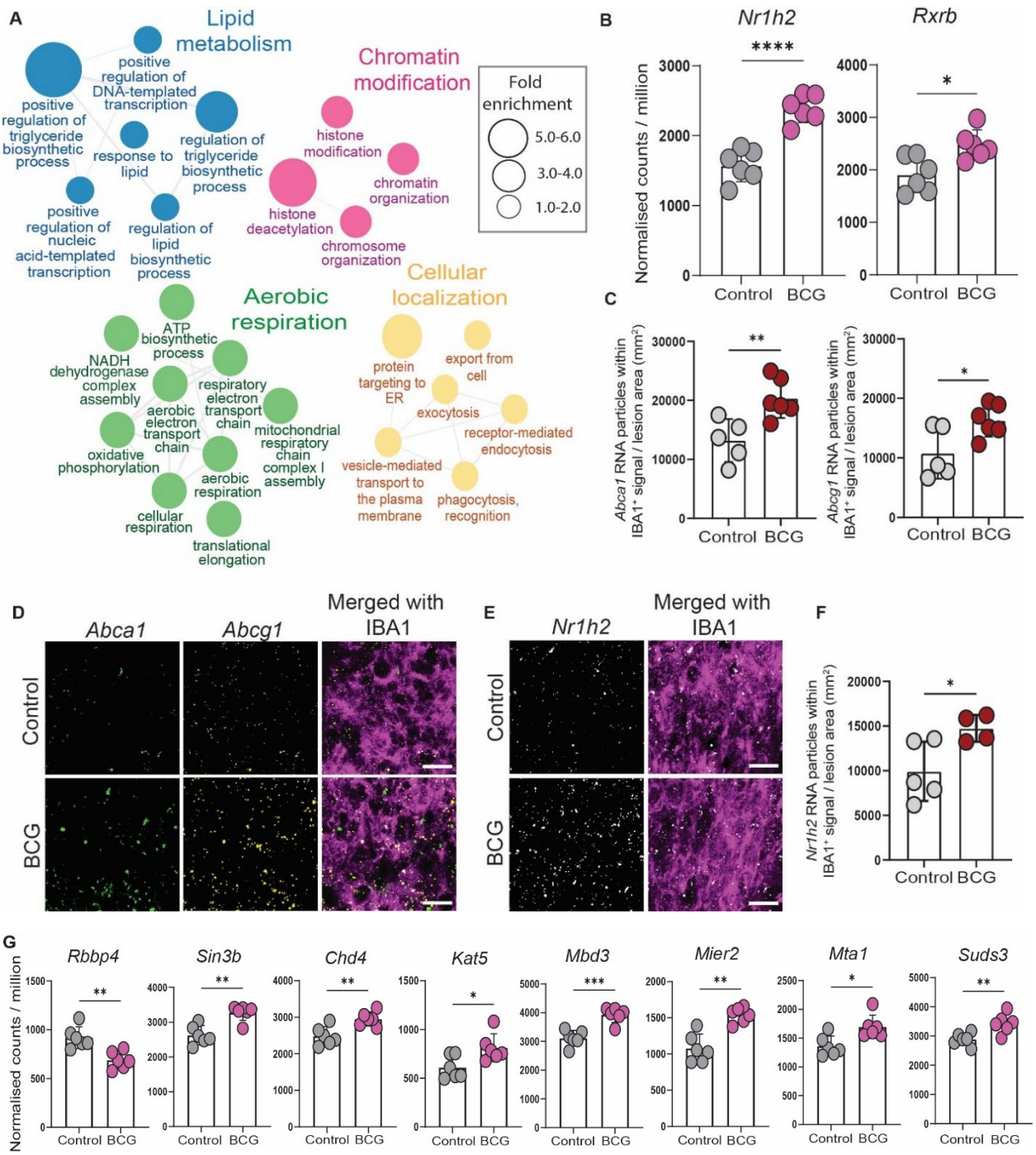

Figure 5.2: Differential transcriptomic analysis of lesions isolated from BCG-treated mice vs. control

(A) Enrichment map of biological pathways enriched in BCG-treated aged mice compared to control, using Fisher's exact test and Benjamin-Hochberg FDR correction.
(B) Bar plots designating normalized counts/million of differentially expressed genes, FDR <0.05.
(**C**) Quantification of *Abca1* and *Abcg1* particles accumulating within IBA1+ cells per mm^2 of lesion area.
(D) Images of the lesioned corpus callosum of control and BCG-treated mice at (14 dpi) demonstrating *Abca1*(green) and *Abcg1* (yellow) particles accumulating within $IBA1^+$cells (magenta) visualized by RNA *in-situ* hybridization, Scale bar 20 µm.

(E) Images of the lesioned corpus callosum of control and BCG-treated mice at (14 dpi) demonstrating *Nr1h2* (white) particles accumulating within IBA1^{+}cells (magenta) visualized by RNA *in-situ* hybridization, Scale bar 20 µm.
(**F**) Quantification of Nr*1h2* particles within IBA1+ cells per mm^2 of lesion area.
All data are mean ± SD; *P<0.05, **P<0.01, ***P<0.01, two-tailed Welch's *t*-test; n numbers are indicated in the figure; each dot represents one mouse.
(G) Bar plots designating normalized counts/million of differentially expressed genes, FDR <0.05.

6. Understanding the effect of inhibiting Histone deacetylase 1 and 2 in microglia / macrophages

To determine if inhibiting HDACs in microglia could be a strategy for improving insufficient activation and lesion repair in aged mice, tamoxifen-inducible microglia/macrophage-specific mutant mouse line for *HDAC1,2* was generated by crossing *Cx3cr1*^{CreERT2} mice with mice carrying floxed alleles of HDAC*1 and HDAC2* to obtain *Cx3cr1*^{CreERT2}:*HDAC1*$^{fl/fl}$ *HDAC2*$^{fl/fl}$ (HDAC1,2 KO) mice (Datta *et al.*, 2018a).

Schematic representation of experimental paradigm in *Cx3cr1*$^{creERT/het}$*Hdac1*$^{fl/fl}$*Hdac2*$^{fl/fl}$ aged mice.

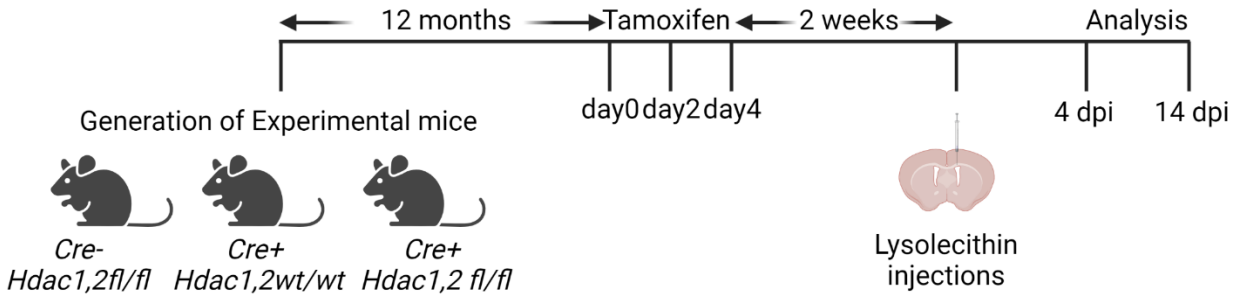

6.1 Genetic ablation of HDAC1 and HDAC 2 from aged microglia improves lesion recovery

First, we confirmed the deletion of *HDAC1,2* at 2 weeks after tamoxifen treatment by analyzing the expression of the microglia transcript by RT–qPCR **(Figure 6.1 A)**. Next, we induced demyelinating lesions and examined mice at 4 and 14 dpi to identify potential changes in lesion recovery. However, when lesions were analyzed at 14 dpi, we observed improved lesion recovery and a decrease in IBA1^{+} cells in HDAC*1,2KO*(Cre+) mice versus control mice(Cre-) **(Figure 6.1 B, C, E)**. Furthermore, quantification of oligodendrocytes using anti-adenomatous polyposis coli (APC) clone CC1 revealed a higher number of mature CC1+ oligodendrocytes in HDCA1,2 KO (Cre+) mouse lesions at 14 dpi **(Figure 6.1 D, F)**.

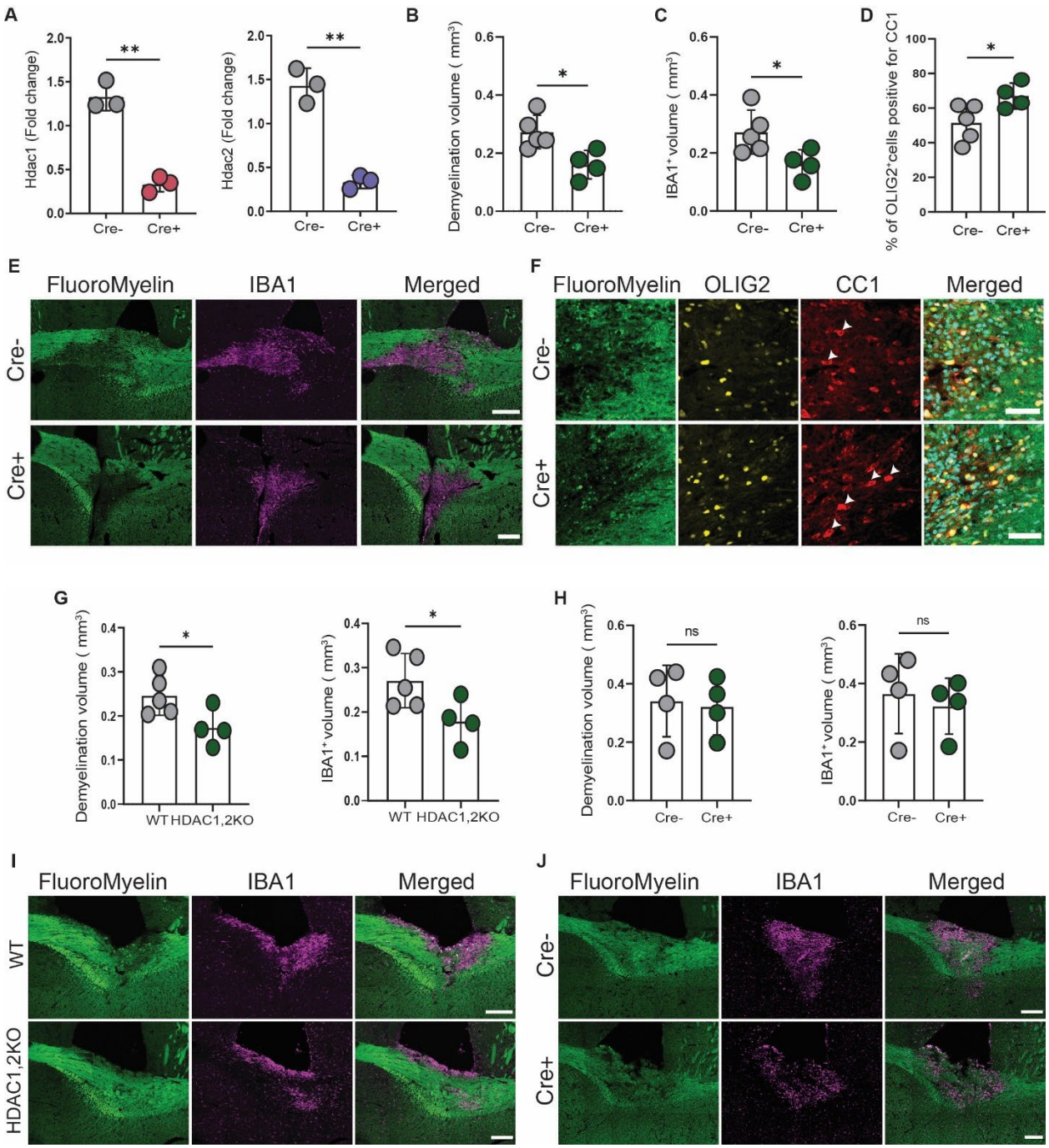

Figure 6.1 HDAC1,2 depletion in microglia improves remyelination in aged mice
(A) Quantitative PCR analysis of *Hdac1* and *Hdac2* in CD11b$^+$ cells isolated from Cre- and Cre+ mice two weeks after tamoxifen induction.
(B, C, D) Quantification of lesion volume and IBA1$^+$ volume and percentage of OLIG2$^+$ cells positive for CC1, at 14 dpi.
(E) Images of corpus callosum lesions in 12 months aged Cre- (Control) and Cre+ (knockout) mice at 14 dpi. Scale bar, 200µm.

(F) Images of the demyelinated lesions in the corpus callosum at 14 dpi exemplifying the numbers of $CC1^{+}OLIG2^{+}$ cells at the demyelination–remyelination edge. White arrows indicate $CC1^{+}OLIG2^{+}$ cells. Scale bar, 50 µm.
(G) Quantification of lesion volume and $IBA1^{+}$ volume at 14 dpi.
(H) Quantification of lesion volume and $IBA1^{+}$ volume at 4 dpi.
(I) Images of corpus callosum lesions in 12 months aged WT (*Cx3cr1*$^{creERT/het}$*Hdac1*$^{wt/wt}$*Hdac2*$^{wt/wt}$) and HDAC1,2 KO (*Cx3cr1*$^{creERT/het}$*Hdac1*$^{fl/fl}$ *Hdac2*$^{fl/fl}$) mice at 14 dpi.
(J) Images of corpus callosum lesions in 12 months aged Cre- (Control) and Cre+ (knockout) mice at 4 dpi. Scale bar, 200µm.
All data are mean ± SD; $^{*}P<0.05$, $^{**}P<0.01$, $^{***}P<0.01$, two-tailed Welch's *t*-test; n numbers are indicated in the figure; each dot represents one mouse.

At 4 days post-injection, there were no differences in demyelination or the number of IBA1+ cells **(Figure 6.1 H, J)**. It is known that TAM inducible Cre induction can also lead to enhanced activation and phagocytosis (Sahasrabuddhe and Ghosh, 2022). To rule out the effect of Cre+ and validate if the effect is because of HDAC1,2 depletion, we used an additional control *Cx3cr1*$^{creERT/het}$*HDAC1*$^{wt/wt}$*HDAC2*$^{wt/wt}$ (WT) along with *Cx3cr1*$^{CreERT/het}$*HDAC1*$^{fl/fl}$ *HDAC2*$^{fl/fl}$ (HDAC1,2KO) and checked for lesion recovery at 14 dpi. Interestingly, we observed lower demyelination volume and reduction in IBA1+cells, thus validating that improved lesion recovery is due to HDAC1,2 depletion and not just Cre+ induction. **(Figure 6.1 G, I)**.

6.2 Genetic ablation of HDAC1 and HDAC 2 from aged microglia improves lipid clearance and activation

Immunohistochemistry also revealed less accumulation of myelin debris within lysosomes of microglia co-labelled with FluoroMyelin and Iba1. Using reflection microscopy, we found decreased $Reflection^{+}$ material in $Iba1^{+}$ cells in lesions of HDAC1,2 KO(Cre+) mice. Also, microglia in 14 dpi lesions of HDAC1,2 KO(Cre+) displayed less LAMP1 labeling, colocalized with both $reflection^{+}$ myelin debris and lower $Plin2^{+}$ $Iba1^{+}$cells at 14 dpi (**Figure 6.2 A-F**) indicating that there is less cholesterol overloading of microglia after inducing demyelinating injury in HDAC1,2KO(Cre+) mice, pointing to improved lipid processing and myelin clearance. To validate if increased cholesterol efflux is behind better myelin clearance we checked for mRNA particles for *Abca1 and Abcg1* and found higher expression of *Abca1* and *Abcg1* in microglia /macrophages of HDAC1,2 KO compared to control **(Figure 6.2 K-L)**. To understand if improved lipid processing and lesion recovery are attributed to the initial activation of microglia, we

examined microglia activation at 4 dpi by immunohistochemistry, using antibodies against MHCII and MAC2. Surprisingly, we detected higher percentages of MHCII+IBA1+ and MAC2+IBA1+ cells in lesions of HDAC1,2 KO mice (Figure 6.2 G-J).

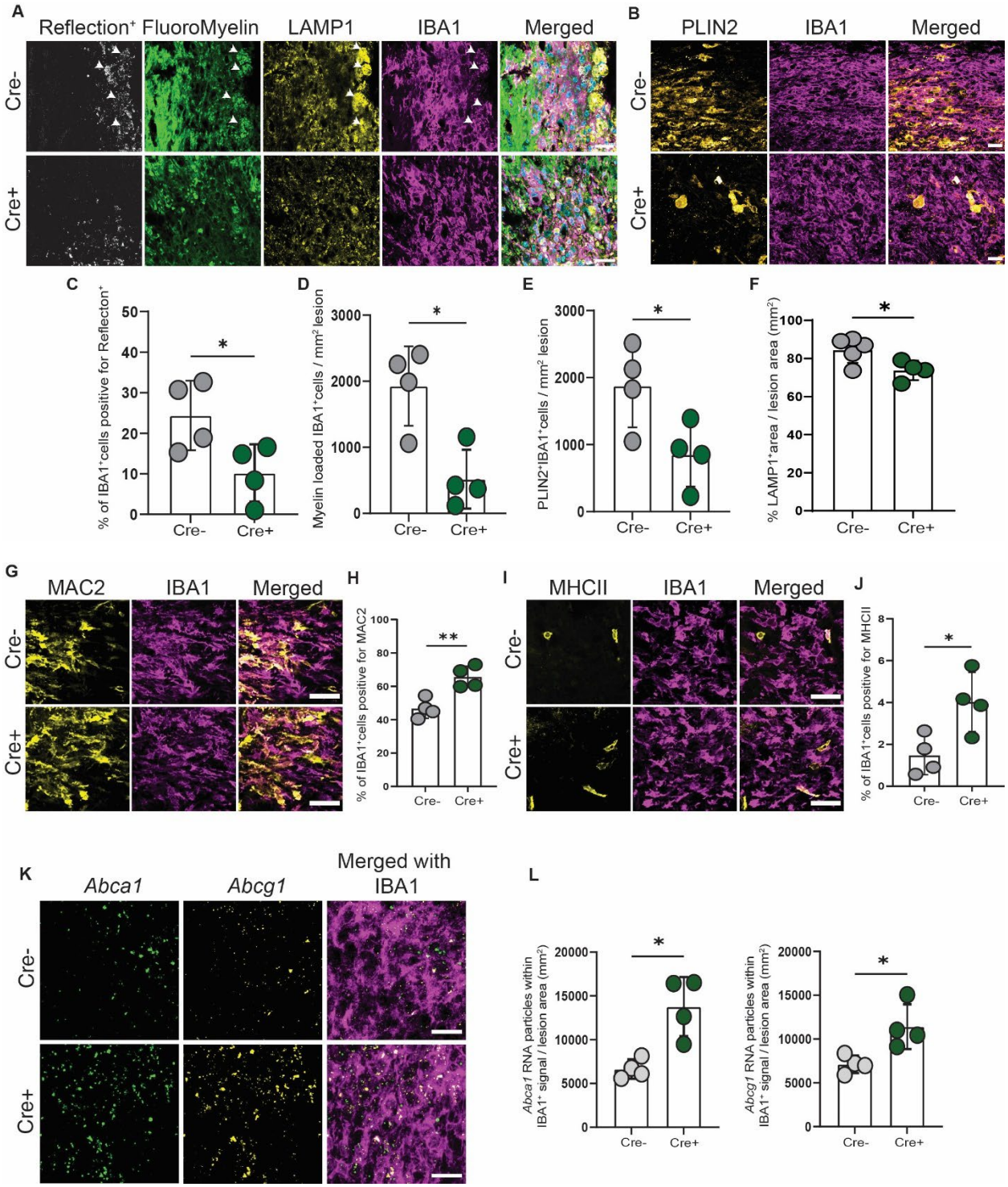

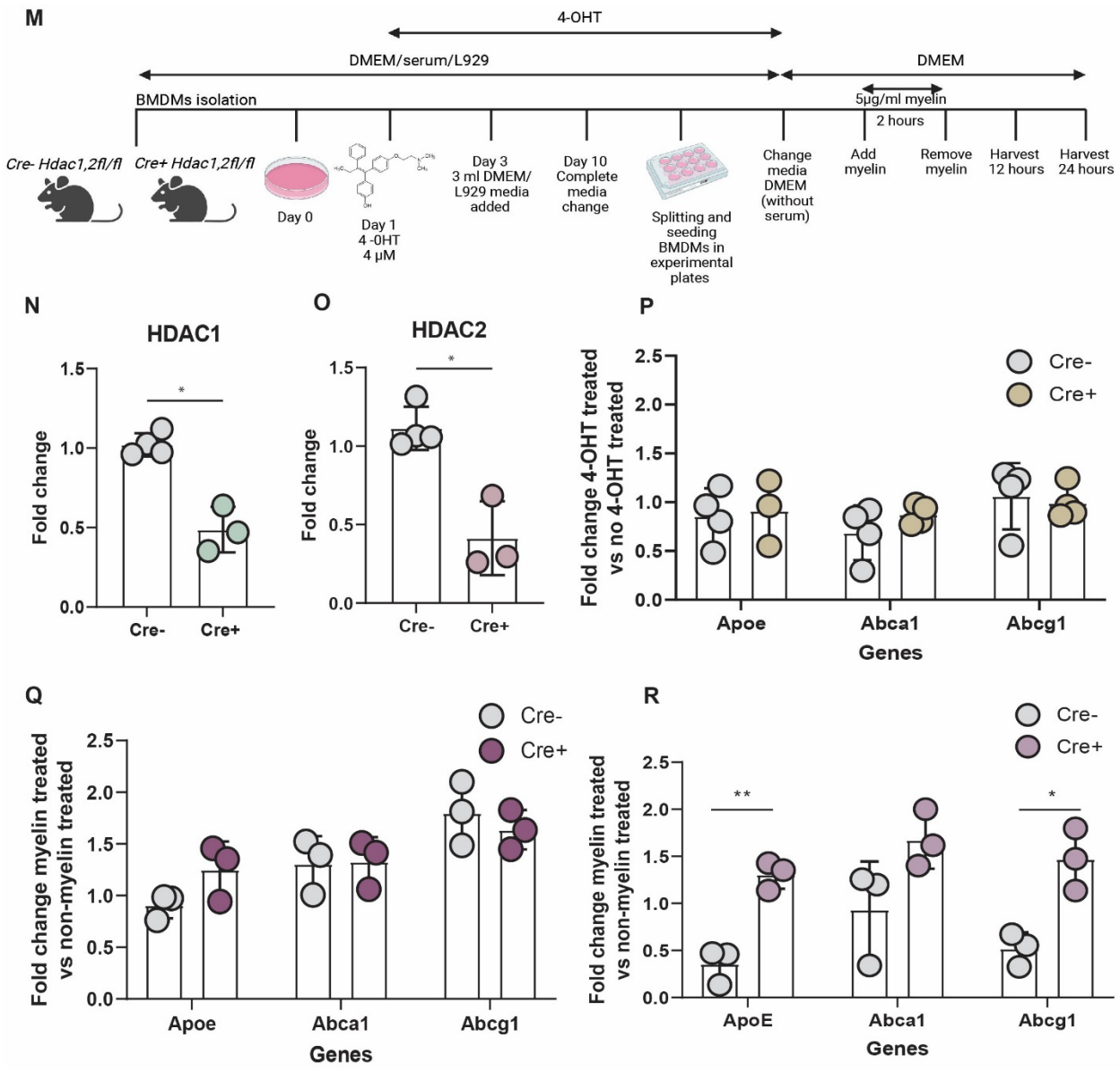

Figure 6.2: Genetic ablation of HDAC1 and HDAC 2 from aged microglia improves lipid clearance and activation

(A) Images demonstrating refection microscopy and accumulation of myelin debris in LAMP1$^+$IBA1$^+$ cells in demyelinated lesions at 14 dpi. Scale bar, 50 µm. White arrows point to reflection$^+$ myelin-debris accumulation within LAMP1$^+$IBA1$^+$ cells.

(B) Images of demyelinated lesions at 14 dpi demonstrating PLIN2$^+$ signal within IBA1$^+$ cells, Scale bar, 50 µm.

(C, D, E, F) Quantification of the (C) percentage IBA1$^+$ cells positive for reflection, (D)myelin-loaded (FluoroMyelin$^+$), (E) PLIN2$^+$IBA1$^+$ cells per mm^2 of lesion and (F)percentage of lesion area occupied by LAMP1$^+$ signal and at 14 dpi.

(**G**) Images of MAC2$^+$IBA1$^+$ cells in the demyelinated lesions at 4 dpi. Scale bar, 50 µm.

(**H**) Quantification of the percentage of MAC2$^+$IBA1$^+$ cells over IBA1$^+$ cells in the demyelinated lesion at 4 dpi.

(**I**) Images of MHCII$^+$IBA1$^+$ cells in the demyelinated lesions at 4 dpi. Scale bar, 50 µm.

(**J**) Quantification of the percentage of MHCII^{+}IBA1^{+} cells over IBA1^{+} cells in the demyelinated lesion at 4 dpi.
(K) Images of the lesioned corpus callosum of Cre- and Cre+ mice at 14 dpi demonstrating *Abca1* (green) and *Abcg1* (yellow) particles accumulating within IBA1^{+} cells (magenta) visualized by RNA *in-situ* hybridization, Scale bar 20 µm.
(L) Quantification of *Abca1* and *Abcg1* particles within IBA1^{+}cells per lesion area.
(M) Experimental paradigm for isolating BMDMs from Cre-and Cre+ animals and for checking reverse cholesterol genes upon myelin treatment
(N, O) Quantitative PCR analysis of (N) *Hdac1* and (O) *Hdac2* in BMDMs isolated from Cre- and Cre+ mice 10 days after 4-hydroxy tamoxifen (4-OHT) tamoxifen treatment in-vitro.
(P) Quantitative PCR analysis of *Apoe, Abca1* and *Abcg1* genes in BMDMs isolated from Cre- and Cre+ mice 10 days after 4-hydroxy tamoxifen (4-OHT) tamoxifen treatment in-vitro.
(Q) Quantitative PCR analysis of *Apoe, Abca1* and *Abcg1* genes in BMDMs isolated from Cre- and Cre+ mice 12 hours after myelin treatment in-vitro for 2 hours.
(R) Quantitative PCR analysis of *Apoe, Abca1* and *Abcg1* genes in BMDMs isolated from Cre- and Cre+ mice 24 hours after myelin treatment in-vitro for 2 hours.
All data are mean ± SD; $^{*}P<0.05$, $^{**}P<0.01$, $^{***}P<0.01$, two-tailed Welch's *t*-test; n numbers are indicated in the figure; each dot represents one mouse.

Thus inhibiting HDAC1,2 in microglia increases acetylation of the genes involved in lipid processing and myelin clearance, thereby improving inflammation and lesion resolution post-demyelinating injury. Additionally, we used an in vitro system to confirm our findings in which we isolated BMDMs (Bone Marrow Derived Macrophages) from adult Cre- and Cre+ mice and used 4-OHT (Hydroxy- Tamoxifin) to induce HADC1,2 knockout in cell culture before myelin treatment to examine the effect of HDAC1,2KO on reverse cholesterol genes **(Figure 6.2 M)**. By examining the expression of the HDAC1 and HDAC2 transcripts by RT-qPCR, we first verified the deletion of HDAC1,2, 10 days after 4-OHT treatment **(Figure 6.2 N, O).** After tamoxifen induction, we found no alterations in the transcript levels of the *Apoe, Abca1, or Abcg1* genes, indicating that HDAC1,2 KO is not responsible for inducing the reverse cholesterol genes in the absence of injury or myelin debris. However, after myelin treatment, we saw that the genes *Apoe, Abca1*, and *Abcg1* were induced **(Figure 6.2 P)**. Twelve hours after myelin treatment, we did not notice any differences in the reverse cholesterol genes transcripts between Cre- and Cre+ mice **(Figure 6.2 Q)**. However, after 24 hours of myelin treatment, we noticed higher mRNA transcripts for the *Apoe* and *Abcg1* genes in Cre+ mice **(Figure 6.2 R)**., indicating that HDAC1,2 depletion in macrophages can result in long-term induction of reverse cholesterol genes, which is crucial for cholesterol clearance and inflammation resolution.

7. The contribution of HDAC1,2 in innate immune training

Next, we wished to determine the contribution of HDAC1 and HDAC2 in microglia/macrophages in the BCG-induced immune training effect. We induced the knockout by tamoxifen administration administered BCG or saline to 12-months-aged HDAC1,2 KO or control mice, injected LPC into the corpus callosum to induce demyelinating lesions and examined mice at 14 dpi to identify potential changes in lesion recovery.

Schematic representation of BCG or saline treatment in Cx3cr1creERT/hetHdac1fl/flHdac2fl/fl and Cx3cr1creERT/wtHdac1fl/flHdac2fl/fl aged mice.

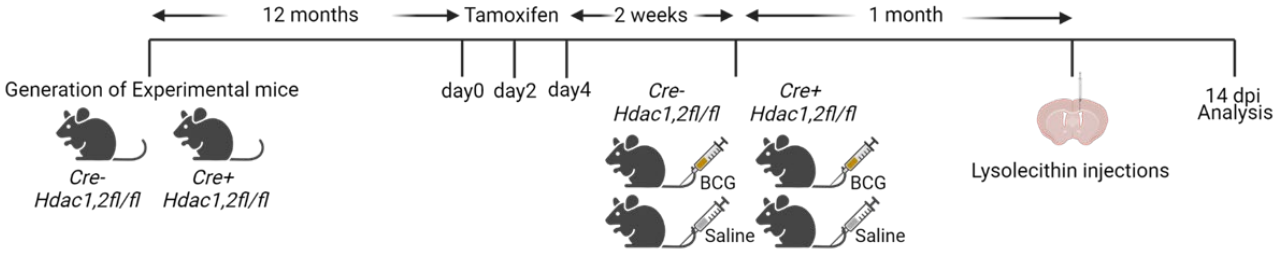

7.1 Trained immune response by BCG is abolished in Cx3cr1-HDAC1,2 depleted, aged mice

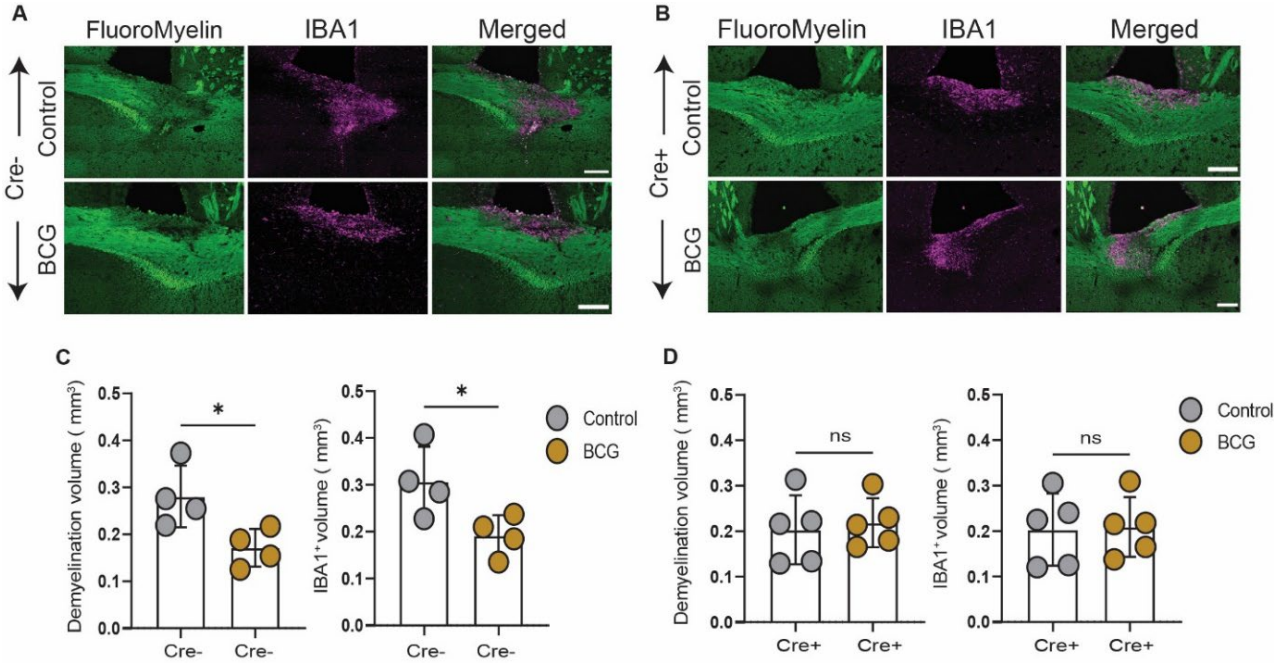

Figure 7.1: Trained immune response by BCG is abolished in Cx3cr1-HDAC1,2 depleted, aged mice

(A) Images of corpus callosum lesions in Cre- mice treated with BCG or saline at 14 dpi. Scale bar, 200µm.
(B) Images of corpus callosum lesions in Cre+ mice treated with BCG or saline at 14 dpi. Scale bar, 200µm.
(C) Quantification of lesion volume and $IBA1^+$ volume in Cre- mice treated with BCG or saline at 14 dpi.
(D) Quantification of lesion volume and $IBA1^+$ volume in Cre+ mice treated with BCG or saline at 14 dpi.
All data are mean ± SD; $^*P<0.05$, $^{**}P<0.01$, $^{***}P<0.01$, ns-not significant, two-tailed Welch's *t*-test, n numbers are indicated in the figure; each dot represents one mouse.

When Cre- mice were administered BCG as opposed to saline, remyelination was enhanced, as seen by decreased demyelination and Iba1 infiltration volume **(Figure 7.1 A, B)**. When Cre+ mice were treated with BCG or saline, there was no further improvement in remyelination, as demonstrated by the absence of a difference in demyelination volume and Iba1 infiltration volume between BCG and control conditions **(Figure 7.1 C, D)**. Together, these results show that BCG-induced immune training is abolished by ablation of HDAC1/2.

Discussion

Our research aims to clarify the mechanisms by which microglia's regenerative abilities decline with age. Aged microglia are defective in activating the transcriptional responses required for myelin debris clearance, which are controlled by the nuclear lipid-sensing LXR/RXR pathway in the presence of a demyelinating lesion high in cholesterol and fatty acids derived from myelin debris (Cantuti-Castelvetri et al., 2018).

We investigated the transcriptomic and epigenomic mechanisms by which aging modifies microglia's pro - repair functions following CNS demyelinating injury. We found that the transcriptomic profile of microglia in aged mice was different from that of microglia in young mice. Genome-wide analysis of chromatin accessibility revealed that a significant number of the uninduced genes in aged microglia/macrophages have epigenetic changes associated with chromatin inaccessibility, with the greatest differences being found in genes involved in innate immune function and lipid metabolism. Our findings lend credence to the hypothesis that epigenomic changes associated with aging are a major contributor to diminished central nervous system (CNS) repair capacity.

We utilized the classical model of innate immune training by BCG (Bacillus Calmette Guerin) and found that myelin repair was enhanced in the aging nervous system. We used BCG as an approach to train immunity, because of its preference for cells of the immune system, in particular those of the myeloid lineage. Mice treated with BCG showed enrichment for H3K4me3, H3K27ac histone marks on the genes that were downregulated in aged microglia due to poor accessibility. This resulted in precise activation and up regulation of genes involved in lipid metabolism and cholesterol clearance which was essential in inflammation resolution. On transcriptomic analysis of lesions of mice treated with BCG, interestingly we found enrichment of chromatin modifying genes which were known to regulate HDAC1/2. Using myeloid-specific knockout of HDAC1/2 to increase histone acetylation and to enhance chromatin accessibility, we were able to restore microglia function and improve lesion recovery in aged mice.

Microglia/macrophage-specific deletion of Hdac1/2 re-stored pro-regenerative lipid clearance function, suggesting that epigenetic alterations, and in particular histone acetylation levels, contribute to poor responsiveness of microglia towards demyelinating injury in aging. We also found that BCG vaccination was able to enhance pro-regenerative functions of microglia in aged mice, but not in those lacking HDAC1/2.

Our findings can be summarized into three major conclusions that will be separately discussed. In first part we discuss the mechanisms of altered responsiveness of microglia / macrophages in aged mice following demyelinating injury. In second part we highlight the importance of innate immune training of microglia /macrophages as a method to improve remyelination and finally we conclude with the epigenetic modifications in innate immune training and targeting histone deacetylases as a method to improve microglia response upon demyelinating injury in aging.

1. Inadequate response of myeloid cells in CNS results in failure of lesion recovery

1.1 Distinct transcriptomic signature is observed in aged mice following demyelinating injury

The ability to regenerate after a demyelinating injury in the nervous system is impaired with age (Franklin and Ffrench-Constant, 2017). Demyelinated mouse lesions have been shown to elicit a wide variety of microglial activation responses. Remyelination in aged mice is frequently hampered by poor microglia activation (Cunha *et al.*, 2020b) and insufficient myelin debris and lipid clearance, while young mice can recover from demyelinating injury much more quickly (Safaiyan *et al.*, 2016; Cantuti-Castelvetri *et al.*, 2018).

Disease-associated microglia (DAM), which are phagocytic in nature, appear in neurodegenerative diseases like Alzheimer's disease (Keren-Shaul *et al.*, 2017b); in contrast, a signature of microglia called IRM (Injury responsive microglia) has been reported in aging that overlaps with DAM (Hammond *et al.*, 2019).

Using single nucleus RNA sequencing(snRNA-seq), we identified four distinct clusters of microglia in aged and young mice post demyelinating injury. The subpopulations of microglia shared a DAM / IRM signature with relatively higher expression in clusters 1 and 2, in addition to other distinct gene expression involving in interferon response and heme analog import (cluster 1), phagocytosis and inflammation (cluster 2), and proliferation (cluster 4) etc. Additionally, we discovered a previously unreported cluster of microglia (Cluster 3) that was involved in neuron projection development, glycosphingolipid metabolism, and the retinoic acid signaling pathway in both young and aged mice.

We did not find statistically significant differences in the cell proportion of microglia clusters between young and aged mice, we did find a trend in cluster 3 and Cluster 4 microglia. Hence, we further re-clustered the microglia subpopulation and identified age specific clusters (data not reported).

We observed unambiguous DEG differences between young and aged microglia. For instance, we found that Apoe, a factor with pro-regenerative properties, is highly expressed in young compared to aged and is one of the most differentially transcribed genes in cluster 1, 2, and 3 microglia. This indicates that changes in transcriptional expression in microglia begin at an earlier stage of the aging curve, leading to a more impaired response as age advances.

Upregulated pathways in aged microglia were found to be distinct from those in young microglia through a combination of gene ontology analyses. Hence, the failure to resolve inflammation and recover from lesion is primarily due to an altered transcriptional response of microglia and macrophages.

1.2 Restricted chromatin accessibility is attributed to inadequate transcriptional response in aged mice

Among the many factors that control transcription is the chance encounter of transcription factors with upstream promoter and enhancer DNA regions. A promoter is a region of DNA that must be therefore accessible so that it can be read by transcription factors and RNA polymerase to facilitate gene transcription.

In order to examine cell-type-specific epigenomic dysregulation in neurodegeneration, such as in human Alzheimer's disease, previous research has demonstrated the use of multi-omic approaches employing both single nucleus ATAC seq and single nucleus RNA seq (Morabito *et al.*, 2021). Complex disease mechanism identification necessitates comprehensive knowledge of epigenetic and transcriptomic gene regulatory systems specific to different cell populations. Single-cell chromatin accessibility is a challenging data modality to work with due to its inherent sparsity, but it can provide important insights into disease.

Since we found no statistically significant differences in cluster proportions between young and aged microglia using snRNA seq, we decided to use bulk ATAC Seq to look for changes in microglial and macrophage accessibility following demyelinating injury. We found that after demyelinating injury, microglia and macrophages in aged mice had decreased chromatin accessibility in comparison to those in young mice.

After performing differential analysis, we identified all of the genes in each cluster of microglia that were downregulated in aged mice. When we compared these downregulated genes to all of the inaccessible regions in aged microglia (FDR 0.05), we made an interesting discovery: ~30% of the genes downregulated in aged microglia were a result of restricted chromatin accessibility. Gene enrichment analysis of the common set of genes reveled that innate immune response and lipid metabolism to be the key pathways altered in aged microglia due to chromatin inaccessibility.

Hence, age associated epigenetic changes microglia / macrophages is the underlying reason behind inadequate transcription of genes in aged mice after demyelinating injury.

2. Innate immune training restores myeloid responses in Central Nervous System

2.1 BCG can induce trained immune response in aged microglia / macrophages

The anti- tuberculosis vaccine, Bacillus Calmette-Guerin (BCG), is a well-known immune modulator that offers broad protection from heterologous infections by inducing innate immune memory, also known as "trained immunity."

We used the (RIVM) strain of BCG to examine its impact on the CNS myeloid responses and regeneration in aged mice. Intravenous administration was used because it has been well-studied for its efficacy in inducing a trained immune response via epigenetic regulation in peripheral myeloid cells (Arts, Carvalho, *et al.*, 2016a). Another potential effect of BCG vaccination via intravenous inoculation is a systemic infection with mycobacteria. Mycobacteria, when administered intravenously, invade or are phagocytosed by macrophages in the recipient's lungs, liver, spleen, and lymph nodes. In addition to causing hepatosplenomegaly, this infection ultimately causes granulomas, which are macrophage-lymphocyte interaction sites, to form in the host tissue (Smrkovski, 1981). As a result of this interaction, cell-mediated immune responses to other antigenic stimuli are often augmented. This route of administration has been extensively studied to prevent the progression of EAE, as it reduces the number of interferon gamma (IFNg)+ CD4+ cells in spinal cord demyelination by diverting MOG-specific cells to granulomas in the spleen and liver.

When innate immune cells are activated, transcription and expression of proinflammatory factors are facilitated by the unfolding of chromatin as a result of changes in DNA methylation status. After the stimulus is no longer present, all of these alterations disappear, but only to a certain extent. Because of this, transcription factor recruitment and gene expression can be sped up and improved following a secondary challenge with a different stimulus. Numerous studies have shown that activating innate immune cells results in an 'epigenetic scar' at the level of stimulated genes, altering the cells' responsiveness in ways that can be seen in trained immunity programs. Acquiring histone 3 lysine 27 acetylation (H3K27ac) marks at distal enhancers (marked with histone 3 lysine 4 methylation (H3K4me1) and consolidating histone 3 lysine 4 trimethylation (H3K4me3) marks at the promoters of stimulated genes are two key epigenetic marks that accompany trained immunity (Netea *et al.*, 2020a).

CHIP sequencing confirmed a trained immune response in the brain's innate immune cells by revealing an enrichment of H3K4me3 and H3K27ac histone marks in CD11b+ cells of aged mice treated with

BCG compared to Saline. There may be a trained immune response in favor of CNS regeneration, as 31% of the total down-regulated genes in aged mice due to restricted chromatin accessibility were enriched by H3K27ac, primarily involved in innate immune response/lipid response, and 10% of those were enriched by H3K4me3 marks, primarily involved in inflammation/interferon response.

The central nervous system (CNS), the peripheral circulation, and the immune system in particular, are known to have a mutually dependent relationship. Given that BCG is unable to cross the blood-brain barrier, it is possible that the neuroimmune milieu is altered as a result of a peripheral cytokine response that alters the microglia signature. Alternatively, we speculate that BCG vaccination alters the activation status of peripheral T lymphocytes, which in turn induces changes in the secretion of cytokines and neurotrophins in the brain.

Interestingly, effect of BCG vaccination are sex specific. It has been reported that Estrogen can inhibit the production of cytokines however it does not influence the induction of trained immunity in females on the other hand males respond quickly to BCG (de Bree *et al.*, 2018). Therefore, it would be interesting to study the effects of BCG immunization on CNS regeneration in both sexes.

2.2 Trained immune response is beneficial for lipid processing and lesion recovery in aged mice

Our data showed that BCG-treated mice exhibited enhanced lesion recovery compared to control animals, as indicated by reduced demyelination, increased oligodendrocyte differentiation, and decreased Iba1^{+} infiltration volume. In addition, microglia/ macrophages in BCG-treated could mount precise activation during a demyelinating injury, a process crucial to the resolution of inflammation. Previous research has shown that a possible mechanism of failure in aged mice is impaired cholesterol efflux by microglia and macrophages. In fact, stimulation of LXR pathway in aged mice, led to better lipid clearance by microglia and macrophages and enhanced remyelination (Cantuti-Castelvetri *et al.*, 2018). Transcriptomic analysis of isolated lesions from BCG- or saline-treated mice revealed upregulation of two master regulators involved in cholesterol efflux and lipid metabolism, *Nr1h2* and *Rxrb*.

Moreover, RNA scope analysis showed that microglia/macrophages have elevated levels of the *Nr1h2* and *Rxrb* transcripts. However, because this immunization was not cell-specific, we must take into account its potential impact on non-target cells. Astrocytes, for instance, are the brain's primary

regulators of lipid homeostasis. They are the primary source of lipids and cholesterol, supplying the brain's oligodendrocytes and neurons via LXR-dependent reverse cholesterol transport (Courtney and Landreth, 2016). In addition, myelination impairments in LXR-deficient mice show that the LXR pathway regulates myelination (Wang *et al.*, 2002). Similar to how LXR agonists control the expression of myelin-related genes, they also stimulate the differentiation of oligodendrocytes (Shackleford et al., 2013). Hence, it is plausible that the effects from systemic BCG immunization stem not only from the beneficial effects on microglia and macrophages but also on other glial cells.

Transcripts involved in chromatin organization and histone deacetylation, such as *Sin3b, Chd4, Mbd3, Mier2, Mta1, Rbbp4, and Suds3*, were enriched in BCG-treated mice. These proteins are known to regulate the activity of Histone deacetylase (HDAC 1 and 2) by forming a core repressor complex (Seto and Yoshida, 2014). Interestingly, using several different genetic models, researchers found that HDAC1 and HDAC2 perform complementary and distinct roles in a variety of cell types and developmental contexts. In the developing vertebrate brain, HDAC functions are essential for oligodendrocyte differentiation. By increasing the levels of *Olig2* in the zebrafish genome, HDAC1 plays a critical role in OPC specification. Ablation of both HDAC1 and HDAC2 in oligodendrocyte lineage cells in mice prevents OPC proliferation and differentiation in the central nervous system (CNS), but ablation of either gene alone does not. This suggests functional redundancy between HDAC1/2 in mammalian OPC development. The use of different phylogenetically distant model organisms, such as zebrafish and mammals, suggests that the functional redundancy of HDAC1/2 may be species-specific (Cunliffe and Casaccia-Bonnefil, 2006; Ye *et al.*, 2009; LeBoeuf *et al.*, 2010).

While Transcriptional profiling is an effective approach to provide biological insight and rapid, unbiased screening of nearly whole transcriptomes to reveal the most promising biomarkers, it is mostly concerned with differentially expressed genes (DEGs) and does not consider clusters of highly correlated genes, which may be responsible for specific features of interests.

Weighted gene co-expression network analysis (WGCNA) is a bioinformatics application for exploring the relationships between different gene sets (modules), or between gene sets and clinical features. The WGCNA describes the correlation patterns between genes and provides straightforward biologically functional interpretations of gene network modules (Langfelder and Horvath, 2008). In our current study, this analysis could shed light on the correlation between expression patterns of genes involved in chromatin organization / histone modifications with respect to other glial cells.

3. Innate immune training encompasses epigenetic regulation

3.1 Inhibiting HDAC1,2 in microglia promotes lesion recovery

We hypothesized that targeting Histone deacetylases would be a strategy to restore the myeloid responses in favor of myelin repair based on our previous findings of restricted chromatin accessibility after demyelinating injury in aged mice and enrichment of histone /chromatin modifying genes after BCG immunization in lesions.

Previous research has shown that HDAC1/2 function in microglia depends on both time and context. Depletion of HDAC1/2 during development results in impaired proliferation and increased apoptosis induction, but adult microglia do not require HDAC1/2 for homeostatic maintenance. Microglial phagocytosis of amyloid plaques is enhanced and genes involved in debris clearance (*Apoe, Axl*, and *Flt1*) are induced in a mouse model of Alzheimer's disease when HDAC1/2 is absent in microglia (Datta *et al.*, 2018b). Inhibiting class I HDACs has been also identified as a novel mechanism for regulating *Apoe* expression and secretion in astrocytes (Dresselhaus *et al.*, 2018).

Using myeloid-specific knockout of HDAC1/2 to increase histone acetylation and to enhance chromatin accessibility, we were able to restore microglia function and improve lesion recovery in aged mice. We show that microglia/macrophage-specific deletion of Hdac1/2 re-stored pro-regenerative lipid clearance function, suggesting that epigenetic alterations, and in particular histone acetylation levels, contribute to poor responsiveness of microglia towards demyelinating injury in aging.

Our data at a glance seemed unexpected as the potential role of inhibiting Class II HDACs such as Histone deacetylase 9 (HDAC9) has been linked to lipid metabolism, atherosclerosis progression, and macrophage polarization via histone acetylation changes at target genes (Cao *et al.*, 2014; Asare *et al.*, 2020) .We examined the potential role of HDAC9 KO in lesion recovery of aged mice. However, we did not see any significant differences in lesion volume and Iba1^{+} filtration volume (data not shown).

The use of constitutive HDAC9 KO mice may account for the lack of an effect on lesion recovery, but we cannot rule out the beneficial response of microglia-specific tamoxifen-inducible Cx3cr1 HDAC9 KO mice in lesion recovery. Unfortunately, the generation of such mice was outside the scope of this project.

3.2 Innate immune training by BCG is abolished in HDAC1,2 KO mice

In order to understand the contribution of HDAC1,2 in innate immune training. We examined the effect of BCG immunization on lesion recovery in both KO as well as control animals. We found that BCG vaccination was able to enhance pro-regenerative functions of microglia in aged mice, but not in those lacking HDAC1/2. Our work was in line with a previous study showing that peripherally applied injections of low-dose lipopolysaccharides induces acute immune training of microglia in wild-type but not in mice with a microglial-specific HDAC1/2 deletion (Wendeln *et al.*, 2018), suggesting that acetylation status of histones are required for inducing memory.

Inhibitors of histone deacetylase (HDACs) have recently found widespread use in treating inflammation by targeting microglia. In this study, the impact of sodium butyrate on remyelination was examined by my colleague Dr. Mar Bosch Queralt in aged mice and she observed that animals given the compound in their water supply 5 days prior to the induction of a lesion had better lesion recovery which was consistent with a prior study showing that butyrate inhibited demyelination and promoted remyelination in an organotypic slice culture while also promoting oligodendrocyte differentiation (Chen *et al.*, 2019). Similar to research into the effects of Sodium butyrate (SB), VPA and TSA have also been investigated for their potential to regulate inflammation by targeting microglia. However, HDAC inhibition-based therapeutic approaches may have off-target effects and interfere with other cell types which can have detrimental effects.

For this reason, we used BCG as an approach to train immunity, because of its preference for cells of the immune system, in particular those of the myeloid lineage. However, we cannot exclude the possibility of the BCG to affect other cell types. In the future, it will therefore be crucial to design CNS cell targeted therapies with adequate standardization of dosage, treatment duration, permeability through the blood brain barrier, etc. and determine the precise molecular pathways that lead to long-term modulation of microglial responses.

Conclusion

Our findings support the hypothesis that epigenomic changes associated with aging contribute to impaired pro-regenerative functions of microglia in the aged subjects, and we show proof-of-concept that innate immune training of microglia can reverse these changes and enhance microglial pro-regenerative functions following demyelinating injury. These findings are consistent with the theory that aging is characterized by an aberrant epigenetic state (Calvanese *et al.*, 2009; Copray *et al.*, 2009; López-Otín *et al.*, 2013; Pal and Tyler, 2016).

The different influences of age on microglia should be taken into account. Immune function declines with age due to immunosenescence, but in addition to this, a gain-of-function occurs in the form of a pro-inflammatory state known as inflammaging (Franceschi *et al.*, 2018). David Sinclair's 2019 "information theory of aging" postulates that age-related cellular deterioration is found on the gradual loss of epigenetic information over time, analogous to a scratched vinyl record.

Our results provide supporting evidence that epigenetic rigidity resulting from chromatin architecture disruptions limits adaptive responses following central nervous system (CNS) injury. The inflammatory profile of microglia in the aging brain is elevated, and this is linked to a "sensitized" or "primed" phenotype (Perry and Holmes, 2014). Microglia that have been thus primed are much more reactive to a subsequent inflammatory stimulus (Perry, 2007). Acute damage to the central nervous system, such as demyelination, inhibits microglia from fully activating, leading to impaired cholesterol efflux and lipotoxicity. Even though phagocytes are sent to the damaged area, they lack the ability to activate the full complement of repair mechanisms. Therefore, age is not synonymous with unresponsive microglia. Instead, we propose that aging creates a condition of microglia rigidity in which they lose their ability to mount a precisely adjusted injury response.

Finally, we conclude that trained immunity in microglia/macrophages is critically important. Reprogramming the innate immune system in old age to facilitate the recovery of the central nervous system without inducing maladaptive hyper inflammatory states will be a formidable challenge.

Appendix

1. Summary figure

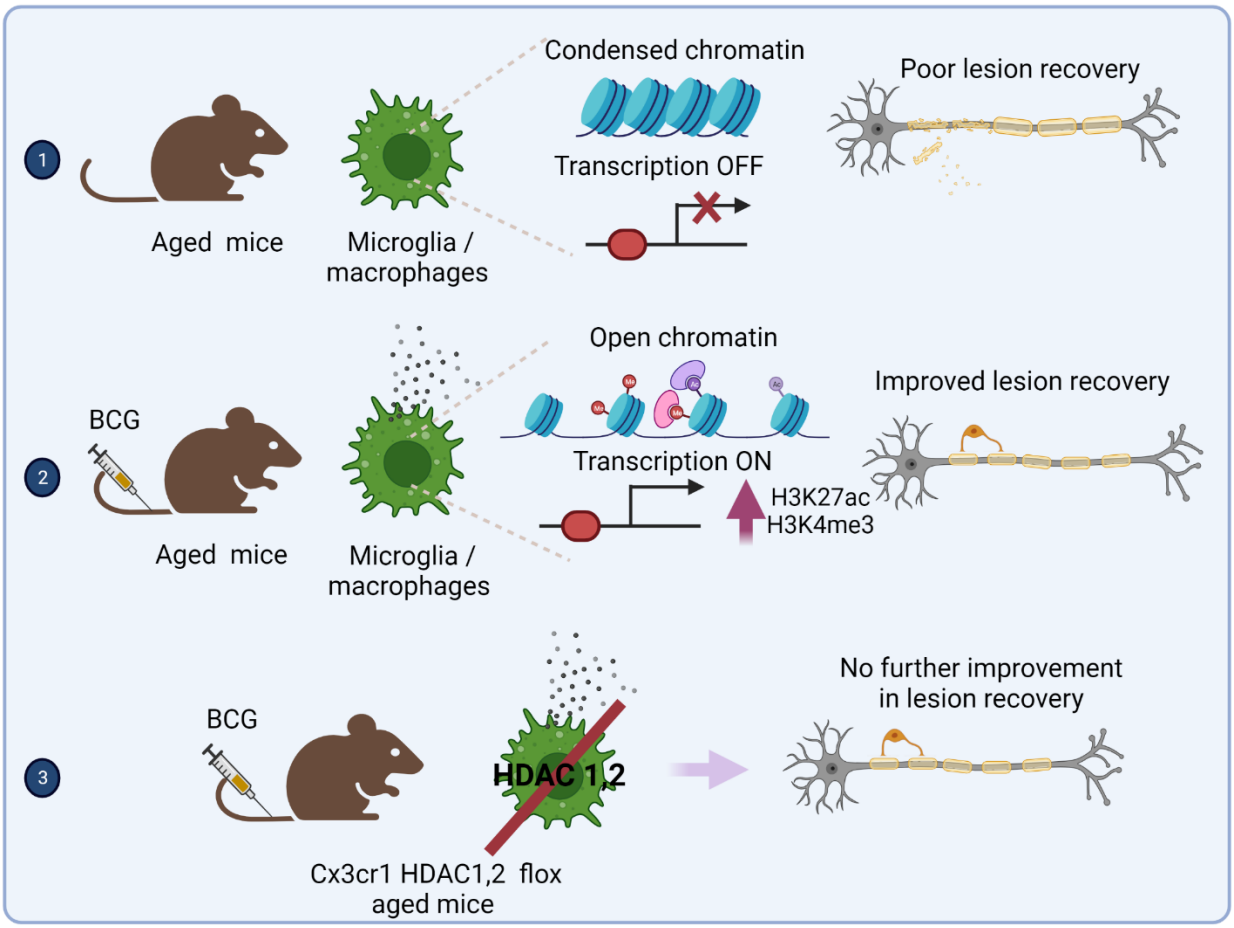

Appendix 1.1: Innate immune training of microglia restores CNS lesion recovery in aged mice

This figure illustrates the summary of the current study in a nutshell

(1) In aged mice a deficient transcriptional of microglia/macrophages upon demyelinating injury is due to restricted chromatin accessibility **(2)** Innate immune training by BCG resulted in gain of key histone marks H3K4me3 and H3K27ac histone marks (involved in trained immune response) around genes involved in lipid metabolism, innate immune response and inflammation. Upon demyelinating injury, these epigenomic modifications results in adequate transcription of genes involved in inflammation resolution and lesion recovery. **(3)** To understand the contribution of HDAC1,2 in innate immune training, BCG was injected in HDAC1,2 KO mice and control, however no further enhancement in pro-regenerative functions of microglia or lesion recovery was observed, suggesting that acetylation status of histones are required for inducing memory.

Illustration created in (Biorender.com). For abbreviations, please see the list of abbreviations

2. Protocols

Here, we describe the detailed protocols of the most commonly used techniques of this study

DNA isolation and PCR for genotyping

Lysis with Invisorb Spin Tissue Mini Kit (Refer the manual for more information)

PROTOCOL

- Prewarm the needed amount of elution buffer up to 52°C.
- Transfer the starting material into a 1.5 ml reaction tube (not provided). (A mechanical disruption or a cutting of the material will increase the lysis efficiency).
- Add 400 µl Lysis Buffer G and 40 µl Proteinase S and vortex thoroughly.
- Incubate the reaction tube at 52°C until the lysis is complete under constant shaking. For material that is difficult to lyse we recommend to vortex the tube several times and the lysis was continued overnight.
- Centrifuge for 3 min at 11.000 x g (11.000 rpm) to spin down non lysed material. Transfer the supernatant into a new 1.5 ml tube.
- Add 200 µl Binding Buffer A and vortex for 10 sec. Keep it for 5 min at RT.
- Place a Spin Filter into a 2.0 ml Receiver Tube. Transfer the suspension onto the Spin Filter and incubate for 1-2 min. Close Spin Filter and centrifuge at 13.500 x g (12.000 rpm) for 3 min.
- Discard the filtrate and place the Spin Filter again into the Receiver Tube.
- Add 550 µl Wash Buffer, close Spin Filter and centrifuge at 11.000 x g (11.000 rpm) for 1 min. Discard the filtrate, place the Spin Filter again into the Receiver Tube.
- Repeat the washing step once. Discard the filtrate, put the Spin Filter back into the Receiver tube and remove the residual Ethanol by final centrifugation for 4 min at maximum speed.
- Place the Spin Filter into a 1.5 ml Receiver Tube and add 50 µl of the pre-warmed elution Buffer. Incubate for 3 min at room temperature. Centrifuge for 1 min at 11.000 x g (11.000 rpm), Repeat the step 10 by adding 50 ul of pre-warmed buffer onto the spin filter.
- The eluate contains ready to use DNA, avoid repeat freezing and thawing of DNA, therefore make a working stock and store it 4 deg (it is stable for several weeks).
- Store the DNA for a longer time at -20 deg C.

Mix for PCR Cx3cr1:

25 µL dream Taq Green PCR Master Mix (2X)
0.2 µL of each primer (original concentration 100 uM, final concentration 0.4 uM) X µL DNA; To 50µL with nuclease-free Water

Component	For one well
Dream Taq Green	25 µL
Primer CX3CR1cre Mainz fw (double amount)	0.4 µL
Primer CX3CR1cre Mainz rev wt	0.2 µL
Primer CX3CR1cre Mainz spec 1	0.2 µL
Water	19.2 µL
DNA	5 µL in each well

Mix for PCR HDAC1:

0.1 µL of each primer (final concentration 100 uM) x µL DNA
10mM dNTPs - 0.5 µl

Component	For one well
Dream Taq Buffer 10X	2.5 µL
Primer HDAC1 fw	0.1 µL
Primer HDAC1 rev	0.1 µL
Dream Taq polymerase	0.2 µL
Water	19.6 µL
DNA	2 µL in each well

Mix for PCR HDAC2:

1 µL of each primer (final concentration 10 uM) x µL DNA
10mM dNTPs - 0.5 µl

Component	For one well
Dream Taq Buffer 10X	2.5 µL
Primer HDAC2 fw	1 µL
Primer HDAC2 rev	1 µL
Dream Taq polymerase	0.2 µL
Water	17.8 µL
DNA	2 µL in each well

Agarose gel electrophoresis

For Cx3cr1 - run 1 % agarose gel; 0.1 % gel red; 150 V; 1 hour
For HDAC1 and HDAC 2 - run 21.5 % agarose gel; 0.1 % gel red; 90-100V; 2 hours Load 4 µl of PCR product + 0.8 µl of DNA loading dye (purple gel 6X) HADC
Load 5 µl of PCR product + 1 µl of DNA loading dye (purple gel 6X) HADC2

Standard IHC fluorescence

All procedures are performed in RT unless otherwise stated

Day 1:

Incubate slides 30' at 37°C (bacterial incubator, must be DRY). This brings slides to RT and makes the sections stick even more on the glass slide.

1. Wash with PBS 3x10'
2. Permeabilization - wash with PBS+0,3% Triton X100 for 10'.
3. Wash 2x5' with PBS
4. Draw liquid blocker line with pap pen and let dry for 5 seconds before dipping it again into a solution (do not do this step before triton – even if they say that the pen resists… it doesn't!)
5. Incubate with mouse Fab fragments if any of the primary antibodies are produced in mouse, 1:100 in PBS, 1h, then wash 3x5' in PBS.
6. Incubate with **Blocking solution** (ready made in lab, PBS+2.5% BSA, 2.5% FCS and 2.5% fish gelatin – no triton because it messes up with lipid stainings. Add triton if better infiltration required and not looking for lipid stainings) for 1h – careful with timing when you have many slides!
7. Dip slides once in PBS
8. Prepare Primary Antibody in **Staining solution** (25% of Blocking Solution – no triton because it messes up with lipid stainings. Add triton if better infiltration required and not looking for lipid stainings).
9. Incubate Primary Antibody overnight at 4°C

Day 2:

1. Take slides out of fridge and incubate primary antibody for 1h
2. Wash 3x10' with PBS (each staining separately)
3. Dilute Secondary Antibody in Staining Solution
4. Incubate Secondary Antibody for 2h (alternatively: Overnight at 4° C)
5. Wash 3x10' with PBS (each staining separately)
6. Prepare Fluoromyelin and DAPI in PBS
7. Incubate Fluoromyelin and DAPI for 15'
8. Wash with PBS 3x10' (important washing step)
9. Dip once in H2O to remove salts
10. Dry
11. Mount with Mowiol
12. Dry
13. Check staining

L929 cell line preparation

Cells are kept in 10% DMSO in the media (which depends on the cell line). DMSO protects the membranes, but it is toxic so we should get rid of it before plating the cells.
Serum helps cells recover after thawing, makes it easier to plate them and expand them so that they recover well. L929 are fibroblasts (they will form nice epithelia), and they are tumor cells, so they accumulate mutations.

Solutions:

- Media: DMEM+ 1% P/S + 1% Sodium Pyruvate → filtrate sterile (because sodium pyruvate is common stock).
- Add serum just before use, 10% (5mL serum, 45 mL medium) – into a separate aliquot (50 mL) of medium, not into the stock bottle – avoid contamination.

Pre do:

1. Warm up media

Protocol:

2. Take frozen tube from liquid N2 storage: our rack is n. 7! Tube is labelled "L929 cells, P(X)" – this X will be the number of passages already undergone by this line.
3. Thaw cells by shaking tube in 37°C until it is liquid (water bath should not touch the lid).
4. Transfer cells (2 mL) to a 15 mL tube.
5. Add 9 mL warm media very slowly – by reclining pipette on the wall of the tube (not surface but more deep inside) and going at low speed.
6. Spin down at 300 x g for 10' at RT – intention: get rid of all the DMSO.
7. We plate in flasks (orange cap with filter. If it did not have holes with the filter, it would be necessary to keep the lid lose so that cells get the correct CO_2 concentration.
8. Label flasks with my name, the cell's name and the passage number (freezing and thawing counts as one passage as well!
9. We obtain a bit pellet from the centrifuge. Discard supernatant with pump.
10. Resuspend pellet in 1 mL new media and then add 9 mL more.
11. Put the 10 mL with the cells in the flask (10 mL/flask, 30mL/flask in the bigger ones). Pipette again more media into the same plastic pipette to completely wash cells off the pipette.
12. Check cells under microscope and decide whether they are too many and we therefore have to put them in a bigger flask or not.
13. Shake flasks a little – avoid touching neck.
14. To the incubator!
15.

To passage cells 1 to 4:

1. Remove media of the flask.
2. Add 5 mL for small, 10 mL for big flask of media without serum (with pyruvate) – this will wash serum off
3. Close and shake
4. Remove this 5 or 10 ml
5. Add 1.5 mL for small, 3 mL for big flask of Trypsin + EDTA mix, shake strongly
6. Hit repeatedly with the hand surface to de-attach the cells. Have a look under the microscope to confirm that cells are floating.
7. Add 2-3 volumes of media with serum (5 mL for small, 10 mL for big flask)
8. Flush on the wall of the flask to detach cells
9. Transfer all liquid to 15 mL tube
10. Centrifuge 300x for 10', resuspend in 1 mL of media
11. Prepare media + FCS
12. Prepare 4 flasks and label them. Add 12 mL for small, 30 mL for big flask of media in each flask
13. Add 250 µL of the resuspended stuff in each flask.

The cells should be passaged again 1:4. Then:

- Wait until 100% confluence and change the media.
- Wait 1 week.
- Collect the medium, filter it, aliquot in 10 mL aliquots and keep frozen.
-

To freeze cells:

Freeze them when they have around 70% confluence (never at 100% because they would downregulate their proliferation machinery). Each cell line has its specific properties – check instructions online.
We leave the cells in medium for around one week and collect the medium they produce, which we use at 10-20% in the medium for microglia.

Myelin isolation protocol

Materials

- Waste Bottle
- 10 and 25 mL pipettes (many)
- Centrifuge tubes (Beckman Coulter, REF 326823)
- 20 mL syringes
- Big needles (green)
- Ice bucket
- Rack for 50 mL falcons
- HEPES Buffer, sucrose solutions, sterile filtered
- ddH2O sterile filtered
- glass vase to balance (100 mL vase)
- Filter tips 1 mL and p20
- Ultracentrifuge
- Rotor and buckets for µUltracentrifuge (SW32Ti in BMC).
- Forceps
- Pipette P1000 and P20

Before starting

- Prepare **Buffers**: filtrate sterile in cell culture hood
    - 10 mM HEPES (1 mol=238.31 g) in ddH20 → 2.38 g HEPES in 1 L ddH2O

- Prepare **Sucrose solutions** in different molarities, in the Buffer just prepared. Place in ice once done. Prepare fresh every time, maximum keep 1-2 days at 4°C.
    - 0.35 M sucrose (1 mol = 342.3 g) → 29.95 g for 250 mL, 59.9 g for 500 mL
    - 0.85 M sucrose (1 mol = 342.3 g) → 72.74 g for 250 mL, 145.48 g for 500 mL

** do not dissolve in full volume of buffer. If, e.g. preparing 100 mL, just fill it up with buffer until 50 mL. Then, when shaked, the sucrose dissolves and makes it increase in volume. Once dissolved, add buffer volume up to 100 mL.

- Filter some ddH2O (approx. 1.5 L needed for 6 big tubes)
- (In BMC!) Fill tubes up with EtOH to make them more sterile and wash them. Remove EtOH after a while and re-use it. Dry tubes well with Kimtech tissue.

Brain extraction and tissue homogenization

1. Use adult male mice (we used 8 wo mice).
2. Dislocate head and cut off. Remove brain and spinal cord.
3. (optional) Wash brain and spinal cord in PBS in a culture dish in order to remove blood.
4. Possible: freeze brains on dry ice if later use predicted. 3 brains and 2 spinal cords per each tube.
5. Add HEPES solution (2 mL) to the tube with brains under cell culture hood
6. Homogenize tissue: perform with sonicator (3rd floor). Button to turn on is in the front lower part. Recall program 13, press "start" to run. Program takes 40s. Check for pieces, and run again if there are still some.
7. Keep tubes on ice.

Myelin from non-myelin separation

9. Turn on centrifuge, turn vacuum on and set temperature to 4°C.
10. Make sure to clean tubes with EtOH before using them.
    They are plastic, in theory not reusable, but we reuse them as long as they do not have cracks.
11. Add 15 mL of 0.35 M sucrose into each tube.
12. Cut needle tip so that it is not sharp (clean scissors in EtOH).
13. Fill tubes up with 15 mL of 0.85 M sucrose from the bottom of the tube, using a long needle and a big syringe (approx. 20 mL syringe), thereby creating a gradient. Perform slowly and with great care not to mix the two phases. Handle the tubes with care from here on in order to avoid mixing.
    *** Ensure that syringe is full of liquid before inserting it into the tube and insert the liquid, in order to avoid bubbles.*
14. Transfer tubes to buckets with forceps.
    *** avoid scratching buckets with forceps - changes weight!*
15. Add the 2 mL of homogenate on top of the tube by laying pipette tip on the side of the tube.
16. Weight buckets with tube inside and without lid. Weigh one, add 1 mL of 0.35M sucrose to this one, then zero balance, and then adjust all others. Balance all tubes by adding 0.35 M sucrose on the top of the tube so that all tubes have the same weight (only ±0.01 g is allowed).
    *** if we over-adjust and add too much liquid, we can always remove a bit and transfer it into another tube (as long as all myelin is the same).*
17. Close lids by turning and pressing until number of lid and bucket are in front of each other.
18. Centrifuge at 25000 rpm (for SW32Ti) for 38' at 4ºC.
    - Acceleration: set to slow.
    - Deceleration: set to slow.
19. Collect white interphases (as shown in figure) into new tubes (same tubes as before, also cleaned). To do so, aspirate the myelin part by staying with the pipette tip at the surface of the myelin phase and rotating slowly.

Washing steps

20. Fill tubes up with ice-cold ddH20 (pipette up and down a bit if liquid is not homogenous) - water osmotically breaks myelin membranes.
21. Again, place tubes in the buckets and balance them.
22. Centrifuge for 18' at 4ºC at 25000 rpm (for SW32Ti). Acceleration and deacceleration set at max.

23. Discard supernatant with 25 mL pipette and pipette boy. Be careful because the pellet is quite loose – there will be more washing steps, so it is better to keep some water in there than to lose pellet!
24. Add 2 mL of ice-cold ddH20 in each tube and resuspend pellet thoroughly with the 1 mL pipette. Add water until almost full, dry tubes and transfer to buckets, and balance all tubes.
25. Centrifuge for 18' at 4ºC at 10000 rpm (for SW32Ti). Acceleration and deacceleration set at fast. Repeat steps 22-24.

Myelin purification

- Discard supernatant with 25 mL pipette and pipette boy. Be careful because the pellet is still quite loose.
- Resuspend in 2 mL 0.35 M sucrose in each tube.
- Fill another round of tubes up with 15 mL of 0.35 M sucrose.
- Then add 0.85 M sucrose from the bottom of the tube, using a long needle and a big syringe (approx. 20 mL syringe), thereby creating a gradient. Perform slowly and with great care not to mix the two phases. This time it is a bit harder to see the two phases but it is still manageable. Handle the tubes with care from here on in order to avoid mixing.
- Add the re-suspended myelin on top of the tubes by laying pipette tip on the side.
- Centrifuge at 25000 rpm (for SW32Ti) for 38' at 4ºC.
    - Acceleration: set to slow.
    - Deceleration: set to slow.
- Again, aspirate the white interphase that contains the purified myelin and transfer into new tube. To do so, collect the myelin interphase with the 1 mL pipette. At this point, myelin is sticky and it sticks to the walls of the tube, so be careful to get it all.
- Fill in tube with ice-cold ddH2O – first only 2 mL to mix with myelin, then fill tube up.
- Transfer tubes into buckets, balance buckets.
- Centrifuge for 18' at 4ºC at 25000 rpm (for SW32Ti). Acceleration and deceleration set at maximum.
- Discard supernatant by decantation.
- Add 2 mL of ice-cold ddH20 in each tube and resuspend pellet thoroughly with the 1 mL pipette. Add water until almost full, dry tubes and transfer to buckets, and balance all tubes.
- Centrifuge for 18' at 4ºC at 10000 rpm (for SW32Ti). Acceleration and deacceleration set at fast.
- Discard pellet with 25 mL pipette and pipette boy – pellet is quite loose!
- Repeat steps 37-39.
- Keep pellets on ice, cover tubes with Para film cleaned with Ethanol, go back to lab.
- Resuspend pellet in 500 µL of 4ºC HEPES Buffer under the hood. Pool all myelin in one 15 mL tube. Add 500 µL of HEPES Buffer more to the tubes to really clean them and get all the myelin.
- Use 27G needle to break the remaining myelin pieces.
- Freeze myelin at -20˚C (if you want to go home and sleep. Otherwise, simply continue).

Myelin protein quantification

- Thaw myelin and sonicate it (Program 13, twice). This resuspends really all pieces.
- Use BSA for creating the standardized curve in HEPES Buffer. Create different concentrations of BSA (1, 0.8, 0.6, 0.4, 0.2, 0.1, 0.05 mg/ml) and transfer 10 µL of each into a flat 96-well plate, in triplicates.
- Transfer 10 µL Hepes Buffer into also three of the wells.
- Dilute myelin 1:3 in a separate tube and also transfer 10 µL in plate.
- Add 200 µL of Bio-Rad Protein Assay Dye Reagent Concentrate, diluted 1:5 in ddH2O.
- 3'-4' of incubation with the dye
- Measure concentrations in the Höglinger Lab and extrapolate in curve using regression line. Take care that R^2 is high enough (more than 0.9!).
    - Omega software – magda user – run
    - Plate out, put plate in, plate in
    - Manage protocol – Bradford – edit
    - Wavelength 595 – set up layout
    - Start measurement – recheck – confirm
    - Say yes to "no concentration values"
    - The program runs, then finishes when noise stops. Plate out!
    - Where is it saved? In Mars – Exit Omega to enter Mars
    - Open Mars (Omega Data Analysis) – magda – run
    - Ignore error
    - Double click to open the last run program (make sure it is the date and time correct)
    - Have raw and blank correct options
    - Export excel and save

*** Take into account that proteins degrade over time so the concentration might have to be re-checked!*

Comments

Be always VERY SAFE when using an Ultracentrifuge:

- Balance tubes to the ±0.01 g.
- Fill tubes up as much as possible – leave approximately 2-3 mm free in the small SW60 tubes, and approx. 5 mm in the big SW20 tubes.
- Fill up first tube balance with 1 mL more of solution, then all tubes have less weight and liquid has to be added to reach the wanted weight – makes balancing easy.
- Move rotor always with its base, because it is really not balanceable without it. Put it into the centrifuge in a straight fashion (without the base of course).

- Each rotor has its buckets, make sure you use the correct ones!
- Keep numbers: bucket to lid and to position in the rotor.
- Double check correct positioning of tubes in rotor by pulling them downwards and sideward.
- Switch vacuum off every time we want to open the ultracentrifuge, and on again once it is closed.
- Double check correct positioning of rotor in centrifuge by assuring that we hear the click and by turning the rotor manually.
- Decrease the acceleration and deceleration of the rotor when working with gradients so as to avoid initial or final mixing of tube content.
- Stay in the room until the centrifugation reaches 3000 rpm to ensure that everything runs smoothly.
- Turn tubes open with the help of forceps in order to avoid breaking lid hook.
- Protocol can be stopped anytime you have a pelleted, by adding a bit of buffer and freezing it in dry ice.
- The more diluted myelin is, the better the yield and the quality are going to be.

How does the centrifuge work?

1. On: side switch
2. Pull handle and slide open lid
3. Put in the rotor with the buckets
4. Close
5. Set up speed, time and temp (press enter after entering the value)
6. Set up accel and deccel
7. Pres start (vacuum starts automatically)
8. To finish: press vacuum to turn it off, wait until there is no number under vacuum which means there is no vacuum, then open lid again and remove rotor
9. Leave lid open when finished?

RNA isolation Protocol

Performed on:
Samples:

Observations:

- Always read the Rneasy plus mini kit protocols before starting
- Centrifuge always at 20-25°C
- The centrifuge has no 15'' option, so all centrifugations are minimum 30'' long
- Very low ratios of A260/230 are normal because of some component of the RLT buffer that stays there – not a problem for qPCR.
- Kit: RNeasy Plus Mini
- After centrifugation, carefully remove the RNeasy spin column from the collection tube so that the column does not contact the flow-through. Be sure to empty the collection tube completely.

Prepare the kit

- I added 44 mL of 100% Ethanol (the one super pure for RNA!) to the RPE Buffer.
- Considering the samples, you have on that day, prepare an aliquot of the buffer RLT Plus with Beta-mercaptoethanol (B-ME, C2H6OS, ART Nr 4227.3 Roth) In this case, I had 8 samples, and 600 µL per sample are needed → 5 mL of RLT+50 µL of B-ME.
- Prepare the 70% Ethanol necessary: 10 samples + 350 µL 70%EtOH/sample =3500 µL →prepare 6 mL of 70% Ethanol, using the 100% Ethanol for RNA and the RNase-free water (4.2 mL of 100% EtOH, 1.8 mL of RNase free water)

Isolate RNA – RNeasy Plus mini kit

Maximal amount of starting material:

- Animal tissue: 30 mg
- Animal cells: 10^7
- Yeast: $5x10^7$
- Plant tissues: 100mg
- Filamentous fungi: 100mg

Disrupt and homogenize tissue:

- Add 350 µL of **RLT Buffer** into each tube - re-suspend sample.
  Note: use 600 µL of RLT Buffer for 20 to 30 mg of tissue, use 350 µL of RLT Buffer for less than 20 mg of tissue.
- Set the P1000 Pipette to 350 µL and pipette up and down the RLT Buffer containing the sample, so that you homogenize the sample. Pipette also up and down against the wall of the tube to really dissociate the tissue.
- Transfer all the liquid onto a **QIAshredder spin column** placed in a 2 ml collection tube (supplied), and centrifuge for 2 min at maximum speed.
- Remove the column and cover tube with the lids. Make sure that the tubes are labelled. **Centrifuge the lysate** for 3 min at maximum speed.
- Carefully remove the "supernatant" by pipetting and transfer it to a **gDNA Eliminator spin column** placed in a 2 mL collection tube (supplied).
- Centrifuge for 30s at 12000 g. Discard the column, save the flow-through.

Isolate RNA

- Add 350 µL of 70% EtOH to flow-through. Mix and immediately transfer (all liquid (700 µL) and any precipitate) onto an **RNeasy spin column** placed in a 2 mL collection tube (Supplied).
- Centrifuge 15s at 12000 g.
- Discard flow-through. Add 700 µL **Buffer RW1** to the RNeasy spin column.
- Close the lid gently and centrifuge for 15'' at 12000 x g to wash the spin column membrane.
- Discard the flow-through. Reuse the collection tube in next step. Add 500 µL **Buffer RPE** to the RNeasy spin column.
- Close the lid gently and centrifuge for 15'' at 12000 x g to wash the spin column membrane.
- Discard the flow-through. Reuse the collection tube in next step. Add 500 µL **Buffer RPE** to the RNeasy spin column. Close the lid gently, and centrifuge for 2 min at 12000 x g to wash the spin column membrane.
  The long centrifugation dries the spin column membrane, ensuring that no ethanol is carried over during RNA elution. Residual ethanol may interfere with downstream reactions.
- Optional (DO IT!): Place the RNeasy spin column in a new 2 ml tube and centrifuge at full speed for 1 min.
  Perform this step to eliminate any possible carryover of Buffer RPE, or if residual flow-through remains on the outside of the RNeasy spin column after step 9.
- Place the RNeasy spin column in a new 1.5 mL collection tube (supplied, looks like a normal one). Add 30µL **RNase- free water directly** (means making sure that the drop goes onto the membrane and not to the side of the tube) to the spin column membrane. Incubate for 5 min.
  Note: The volume of elution depends on the amount of RNA expected. You can use between 30 to 50 µL - use less volume when less RNA is expected!
- Centrifuge for 1 min at 12000 x g to elute the RNA.

Note: careful when placing tubes in centrifuge – lids of 1.5 mL tubes should not overlap or they will break! Split in two centrifugation rounds if necessary.

- Use the eluate from step 16-17 to **elute again the RNA from the membrane** by simply aspiring the elute and adding it again directly to the spin column membrane. Incubate again for 5 min and centrifuge for 1 min at 12000g.
  Note: you can either use the same elute or another volume of water – again, depending on RNA concentration wanted.

Determine the RNA yield

We use the Nano Drop Spectrophotometer for determining RNA yield. This is based on Absorbance.
Absorbance at 260nm provides total nucleic acid content, while absorbance at 280 nm determines sample purity. Since free nucleotides, RNA, ssDNA and sdDNA absorb at 260 nm, they all contribute to the total absorbance of the sample.

- 230 nm – chemicals
- 260 nm – chemicals
- 280 nm – proteins
-

Procedure

16. The sensor is very sensitive, so do not touch it directly (not even with the pipette tip).
17. Wash the Nano drop sensor: Put 1 µL of RNase free water on top of the sensor, close the Nano drop and open again, wipe with a tissue (both parts, "lid" too!!). Do this three times.
18. Open Software: Nano drop 2000, choose nucleic acid. Choose RNA as sample and write sample name.
19. Run blank: add 1 µL of RNase free water to the sensor and run the blank.
20. Measure sample: pipette up and down the sample with the RNA, and add 1 µL of the RNA sample onto Nanodrop detector.
21. Wash the sensor 1x or 2x between samples.
22. When finished, wash the Nanodrop sensor again just like in step 2.
23. At software: reports, export → save file to USB Stick.

Results:

1. Ratio A260/A280 of around 2 is considered pure (more nucleic acids than proteins).
2. Ratio A260/A230 should also be around 2 (more nucleic acids than chemicals) – in trizol isolation method this is going to be worse than in the column method.

Save the file that the software gives you by exporting the project – select all samples - and combine it in an excel file! Aliquot the samples in 2 small red tubes, each with approx. 13 µL of liquid

The art of producing cDNA

Performed:

Samples:

First-strand cDNA Synthesis

Using SuperScript III First-Strand Synthesis System for RT-PCR – see the protocol online for more details.

Material:

- SuperScript III First-Strand Synthesis System for RT-PCR, cat 18080-051, Invitrogen (kept -20°C)
- RNase ZAP to clean surfaces
- Autoclaved 1.5 mL tubes
- Sterile filter tips all sizes
- Epi Rack

Details of kit:

1. Made to detect targets from 100 bp to >12 kb.
2. Amount of starting material required can vary from 1 pg to 5 ug of total RNA (we normally use 1 ug), or 1 pg to 500 ng of poly(A)⁺RNA. For >5 ug total RNA, increase reaction volumes and amount of SuperScript III RT proportionally.
3. Small amounts of genomic DNA in the RNA preparation may be amplified along with the target cDNA. Ig your application requires removal of all genomic DNA from your RNA preparation, we recommend using DNase I, Amplification Grade (catalog n. 18068-015).
4. Primers:
    - Random hexamers: it is the most typical. Most nonspecific priming method, typically used when the mRNA is difficult to copy in its entirety and when you want to screen for many genes. With this method, al primers confer specificity during PCR. To maximize the size of cDNA, you should determine the ratio of random hexamers to RNA empirically for each RNA preparation. However, for most applications 50 ng of random hexamers per 5 ug total RNA is adequate.
    - Oligo(dT): more specific priming method, used to hybridize to 3' poly(A) tails, which are found in the vast majority of eukaryotic mRNAs. Since poly(A)+ RNA constitutes approximately 1% to 2% of total RNA, the amount and complexity of cDNA is considerably less than with random hexamers. This is recommended when performing RT-PCR for new mRNA targets, because the product it produces is more consistent. However, one has to be careful because since the primers bind the poly A, the polymerase will start at the poly A, and there might be many base-pairs separating the polyA from the actual coding sequence, and if the polymerase falls off the RNA before it has reached the coding sequence, this coding sequence will actually not get converted to cDNA!
      One can also do a mix of random hexamers + oligo(dT)20.
    - Gene-specific primer: then you basically only convert to cDNA your gene of interest. Most specific.

Preparation:

- Ice bucket with ice
- Transfer all tubes of the kit into the ice to thaw – it takes a while! Exception: RNase OUT and the Superscript III RT, which should stay at -20°C until just before use (and when you do need them, keep them in the yellow container for frozen samples).
- Transfer tubes with RNA to the ice.
- Mix and briefly centrifuge each component before use. You can vortex, EXCEPT: enzymes, DNA, RNA and primers, which should NEVER be vortexed.
- Clean with RNase ZAP: bench, hands, pipettes, epi rack, lids of tubes before opening them (spray RNase ZAP on tissue and use that to wipe tubes, pipettes and so on).
- Calculate amount of RNA to be added: normally, Ludo adds 1 ug of RNA.
- Prepare heater at 65°C

Protocol:

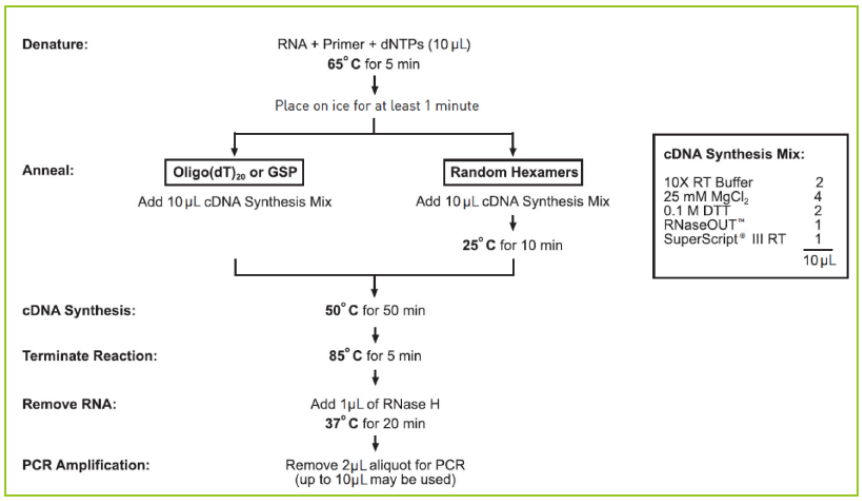

- RNA calculations: We want to add between 100 ng and 1 ug of total RNA into the reaction → make calculations. Anyway, it is not so important to be very precise with the amount of RNA added in the beginning because the qPCR already controls the initial amount – you can control for the initial differences in material quantity. Simply try to keep it constant.
- Combine the following in an autoclaved 1.5 mL tube:

Component	Amount / tube	For test samples:	For control samples:
Up to 5 ug total RNA	*n* µL		
Primer*	1 µL		
10 mM dNTP mix	1 µL		
DEPC-treated water	To 10 µL		

*Use Random Hexamers. There are other options, but the random hexamers is best for our application.

- Incubate the tubes at 65°C for 5', then place on ice for at least 1 min. Change the thermoblock to 50°C.
- Prepare the following **cDNA Synthesis Mix**, adding each component in the indicated order. MIX WELL!

Component	Amount 1x	For Today *(+RT)*	For Today (-RT)
10X RT buffer	2 µL		
25 mM MgCl2	4 µL		
0.1 M DTT	2 µL		
RNase OUT (40 U/µL)	1 µL		
SuperScript III RT (200 U/µL)	1 µL		-
DEPC-treated water	1 µL	-	

- Add 10 µL of cDNA Synthesis Mix to each RNA/primer mixture, mix gently (up and down, don't vortex) and incubate as follows:
  - Random hexamer primed: 10 min at 25˚C (on the bench), followed by 50 min at 50˚C. Prepare block at 85˚C.
  - Oligo(dT)20 or GSP primed: 50 min at 50˚C.
- Terminate the reactions at 85°C for 5'. Chill on ice for 5'. Prepare block at 37°C.
- Collect the reactions by brief centrifugation. Add 1 µL of RNase H to each tube and incubate the tubes for 20 min at 37°C.
- cDNA synthesis reaction can be stored at -30°C to -10°C or used for PCR immediately (keep on ice if wanted to use for PCR, simply put into the freezer if you want to store it).

Controls:

It is generally better to have your own tissue for positive control. This should be RNA from tissue you know definitely has the genes. Also on this control RNA and in one of the samples, a non-RT control should be added. * For First Strand cDNA synthesis of transcripts with high GC content, see Invitrogen protocol.

Control Reactions

The control RNA provided with this system consists of total HeLa RNA (10 ng/µL). The sense and antisense control primers provided with this kit are designed from the human β-actin gene and produce a 353-bp RT-PCR product.

Sense primer: 5'-GCTCG TCGTC GACAA CGGCT C-3'

Antisense primer: 5'-CAAAC ATGAT CTGGG TCATC TTCTC-3'

Use the following protocol for both plus and minus RT control reactions:

1. Dilute the total HeLa RNA to 100pg/µL with DEPC-treated water.
2. Prepare the RNA/primer mixtures in sterile 0.2- or 0.5-mL tubes as follows:

Component	+ RT Control	– RT Control
Diluted total HeLa RNA (100 pg/µL)	1 µL	1 µL
Oligo(dT)$_{20}$	1 µL	1 µL
10 mM dNTP mix	1 µL	1 µL
DEPC-treated water	7 µL	7 µL

3. Incubate the samples at 65°C for 5 min, then place them on ice for at least 1 min. Collect the contents by brief centrifugation and add the following:

Component	+ RT Control	– RT Control
10X RT buffer	2 µL	2 µL
25 mM $MgCl_2$	4 µL	4 µL
0.1 M DTT	2 µL	2 µL
RNaseOUT™ (40 U/µL)	1 µL	1 µL
SuperScript® III RT (200 U/µL)	1 µL	—
DEPC-treated water	—	1 µL

4. Mix the tubes gently and collect the reactions by brief centrifugation.
5. Incubate the samples at 50°C for 50 min.
6. Terminate the reactions at 85°C for 5 min. Chill on ice.
7. Collect the reactions by brief centrifugation. Add 1 µL of RNase H to each tube and incubate for 20 min at 37°C.
8. Prepare a PCR mixture for each control reaction. For each control reaction, add the following to a 0.2-mL tube sitting on ice:

Component	Volume
DEPC-treated water	38.1 µL
10X PCR buffer minus Mg^{++}	5 µL
50 mM $MgCl_2$	1.5 µL
10 mM dNTP mix	1 µL
Control sense primer (10 µM)	1 µL
Control antisense primer (10 µM)	1 µL
cDNA from control RNA	2 µL
Taq DNA polymerase (5 units/µL)	0.4 µL
Final volume	50 µL

9. Mix the contents of the tube. Centrifuge briefly to collect the reaction components.
10. Place reaction mixture in preheated (94°C) thermal cycler. Perform an initial denaturation step: 94°C for 2 min.
11. Perform 40 cycles of PCR:

Denature	94°C for 15 sec
Anneal	55°C for 30 sec
Extend	68–72°C for 1 min

Note: For slow-ramping thermal cyclers, follow manufacturer's directions.

12. Upon completion, maintain reactions at 4°C.
13. Analyze 10 µL of each reaction, using agarose gel electrophoresis and ethidium bromide staining. For the + RT Control, a 353-bp band, corresponding to at least 25 ng of product, should be visible. For the – RT Control, the same band should be ≤50% in intensity when compared to the + RT Control.

qPCR particularities

General protocol for: Power-up SYBR Green Master Mix - **always check** the User Guide before starting

Guidelines:

1. Use 1-10 ng single-stranded cDNA or 10-100 ng gDNA per reaction
2. Four replicates of each reaction are recommended (we sue 3)
3. Reaction mixes can be prepared depending upon experimental requirements. Scale the components according to the number of reactions and include 10% overage
4. If using smaller reaction volumes, scale all components proportionally. Reaction volumes less than 10 µL are not recommended.
5. Using no template control (NTC) reactions can be used to identify PCR contamination. NTC reactions contain all reaction components except sample and therefore should not return a Ct value → this we do with the no RT control!

Before you begin:

1. Clean bench with EtOh
2. Thaw all components in ice – SYBR Green Master Mix, Primer Mixes and cDNA. Takes a long time! Sometimes leave at RT for a bit and move back to ice…. Important is, that none of the components stays for too long at RT.
3. Prepare the cDNA: dilution 1:10 recommended, but one can modify it a bit in case of very small RNA amounts.
4. Keep the SYBR green and any tubes made with that covered – protect fluorescence.
5. Mix absolutely very tube before use by pipetting up and down the whole volume.

Set up the PCR reactions:

- Prepare the appropriate number of reactions, plus 10% coverage (10 µL/well for 384 well-plate):
  - For optimal performance in Fast and Standard modes, use 300-800 nM for each primer - we used 300 nM in the first testings and worked.
  - Use 1-10 ng cDNA or 10-100 ng gDNA for each reaction

Component	Volume (10 µL/well)	Volume (20 µL/well)
PowerUp™ SYBR™ Green Master Mix (2X)	5 µL	10 µL
Forward and reverse primers[1]	Variable	Variable
DNA template + Nuclease-Free Water[2]	Variable	Variable
Total	**10 µL**	**20 µL**

reaction

- Centrifuge briefly in case of any liquid on the tube walls, then mix thoroughly by pipetting up and down the whole volume **right before use**.
- Transfer the appropriate volume of each reaction to each well of an optical plate (9 µL/well for 384 well plate) – to the wall
- Transfer 1 µL of the corresponding cDNA to each well – put tip all the way to bottom of well.
- Cover plate and centrifuge with a plate centrifuge (AG Haass) for 1 minutes at 1000 rpm. PCR can be performed on the reaction plate up to 24h after completing the set-up, when stored at RT

Set up and run the real-time PCR instrument

- Place the reaction plate in the RT-PCR instrument
- Use fast cycling mode:

Table 3 Fast cycling mode (primer T_m ≥60°C)

Step	Temperature	Duration	Cycles
UDG activation	50°C	2 minutes	Hold
Dual-Lock™ DNA polymerase	95°C	2 minutes	Hold
Denature	95°C	1 second[1] or 3 seconds[2]	40
Anneal/extend	60°C	30 seconds	

[1] When using a QuantStudio™ Real-Time PCR System or a ViiA™ 7 Real-Time PCR System.
[2] When using a 7500 Fast Real-Time PCR System, StepOnePlus™ Real-Time PCR System, or StepOne™ Real-Time PCR System.

For all the qPCR experiments the following primer mix and components were used

Prepare cDNAs:
Already ready (1: 10 dilution)

Prepare primer mixes:

Component	1 well
Master Mix SYBR Green	5 µL
Primers (both together at a concentration of 5 uM each)	0.6 (final concentration 300 nM)
Nuclease-free water	3.4
DNA Template	Add 1 µL in each well
TOTAL VOLUME PER WELL	10 µL

Mix well and share 9 µL of primer mix to each well (with the step-pipette!)
Then mix well cDNA and add 1 µL of cDNA per well (change pipette every time!)

MACS culture of microglia from lesioned adult mice -ATAC seq

Protocol adapted from Miltenyi Biotech

Performed with:
Experiment date:

Things to do before:

- Bring the animals from Animal house to killing room.
- Bring the stereoscope inside the hood of killing room
- Anesthetize the animals with Ket /Xyl 0.5-1 ml per animal.
- Prepare the perfusion pump with 1XPBS
- Try to arrange for brain matrix if possible.
- Prepare the 100X DNase buffer (250 mM MgCl2, 50mM CaCl2 in dH20) (27 mg of Cacl2+157.3mg of MgCl2) in 5 ml of dH20
- Prepare 100X DNase solution (reconstitute lyophilized powder in 1 ml of HBSS buffer without Cacl2, MgCl2)
- Make 100 ul of aliquots at -20 deg C.
- Prepare enzyme mix 1 and 2 according to the table below. (for 1 Brain). Label the C tubes

Enzyme P	Buffer Z	Buffer Y	Enzyme A
50 ul	1900ul	20 ul	10 ul

Procedure:

Tissue dissociation:

- Perfuse the animal with 1XPBS and take out the brain tissue in a dish with DPBS with ice
- Dissect the region where there are 4-5 lesions with the help of Stereoscope
- Take a small chunk from the brain tissue with intact white matter as a positive control.
- With the help of forceps transfer the brain tissue into their respective C tube containing enzyme mix 1.
- Add enzyme mix 2.
- Transfer the tubes to the water bath and incubate them for 30 min
- After 15 min triturate gently with 1ml Pipette
- After 25 min triturate harshly
- Centrifuge 10 min 300 g.
- Prepare 50ml Falcon tubes with 70µm Cell strainer and moisten with DPBs
- Resuspend the pellet in 5 ml DPBS
- Pipette cell solution onto Cell strainer.
- Wash Cell strainer by pipetting 5ml of DPBS onto it
- Discard Cell strainer and centrifuge cell suspension at 300xg for 15min at 4°C (1200rpm centrifuge 4°C room)
- Aspirate supernatant completely

Debris removal:

- Always use pre-cooled buffers and solutions (4°C)

	Debris removal Solution	D-PBS	Overlay(D-PBS)	Reagent tube
20-100mg	450ul	1550ul	2ml	5ml
1 brain	**900ul**	**3100ul**	**4ml**	**15ml**
2 brains	1800ul	6200ul	4ml	15 ml

- Re-suspend cell pellet carefully with the appropriate volume of cold D-PBS according to the table appropriate reagent tube. Do not vortex.
- Add appropriate volume of cold Debris Removal Solution.
- Mix well
- Overlay very gently with an appropriate amount of cold D-PBS according to the table above

Note: Pipette very slowly to ensure that the D-PBS phase overlays the cell suspension and phases are not mixed.

- Centrifuge at 4 °C and 3000×g for 10 minutes with full acceleration and full brake.

Note: If centrifuges give suboptimal centrifugation, the acceleration and brake can be reduced.

- Three phases are formed. Aspirate the two top phases completely and discard them. (Achtung! Do not discard the bottom layer after seeing the cell pellet, u can lose a no of cells in the procedure)
- Fill up with cold D-PBS. (~10ml)
- Gently invert the tube three times. Do not vortex!
- Centrifuge at 4 °C and 1000×g for 10 minutes with full acceleration and full brake. Aspirate supernatant completely.

- Proceed for red blood cell removal.

Red blood cell removal:

- Dilute Red Blood Cell Removal Solution (10x) 1:10 with ddH2O (0.8ml in 7.2 ml ddH20)
- Do not use deionized water or DPBS for dilution!
- Store the prepared 1x Red Blood Cell Removal Solution at 2-8°C. Discard unused solution at the end of the day
- Add 500 ul of red blood cell removal solution (800 ul in case of perfusion failed and animal has to be sacrificed by decapitation, in that case there is lot of blood in brain)
- Incubate for 10 min in the refrigerator
- Add 10 ml of cold DPBS
- Centrifuge at 4°C and 300xg (1200rpm) for 10 min. Aspirate supernatant completely

Magnetic Antibody Labelling

- Resuspend pellet with 100 µl Serum media (DMEM/FCS) in order to avoid non-specific binding
- Add Micro-beads 10 µl and flick the tube
- Incubate solution for 15 min in the refrigerator
- Add 3ml of serum media
- Centrifuge at 4°C and 300xg (1200rpm) for 10 min. Aspirate supernatant completely and suspend in 0.5ml DPBS
- Equilibrate MS columns attached to the magnet with 0.5ml DPBS
- Place 15ml Falcon tubes stacked in ice under the columns to collect flow through
- Pipette cell suspension onto the MS Column
- Flush falcon tube with 0.5ml DPBS and pipette it also onto the column after reservoir is empty
- Wash columns 2x with 0.5ml DPBS
- Elute cells by detaching the columns from the magnet and placing them on a suitable collection tube (15 ml)

DNase treatment and storage

- Elute with 1 ml of serum media (DMEM /FCS). For both control and lesions cells
- Count the number of cells ;(ensure that the number of cells is between (100,00-50000) cells)
- Add 5 ml of (DMEM/FCS) media
- Add 1:100 volume of 100X DNase buffer (so in 5 ml 0.05 ml =50ul)
- Add 1:100 volume of 100X DNase solution to media (so in 5ml 0.05 ml= 50 ul). Mix by inverting the tubes several times.
- Loosen the lid on the conical tube, incubate at 37 deg C for 30 min
- Spin the cells, (1000 g 10 min), wash one time with 1 X PBS. Transfer to the desired centrifuge tube.
- Spin at 10000 rpm for 5 min to pellet the cells and then remove supernatant at 4 deg.
- Resuspend the cells in 500 ul of growth media plus 5% DMSO (For example: 500 ul of growth media +25ul of DMSO).
- For 8 tubes (prepare 4ml of serum media + 200 ul of DMSO)
- Freeze the cells at a slow cooling rate to minimize cell lysis in Mr. frosty container - put in -80 deg.
- Next day, transfer the tubes to desired storage box
- Ship the samples to the collaborator in dry ice!

MACS culture of microglia from adult mice -CHIP seq

Protocol adapted from Miltenyi Biotech

Date this was run:
Sample this protocol was run on:

Things to do before:

- Bring the animals from Animal house to killing room
- Animals were sacrificed with CO2.
- Use DPBS without calcium and Magnesium (pre-cooled on ice)
- Prepare MACS buffer fresh
- To prepare MACS buffer 0.34 ml of 30 percent BSA (Stock-Sigma) in 20ul of DPBS, since Miltenyi recommends to use 0.5 BSA stock solution at a ratio of (1:20).
- Prepare 1.25 M Glycine (Fresh). Prepare 5 ml in molecular Biology grade water; molecular weight - 75.07g/mol
  therefore, add 0.4691875 g of glycine in 5 ml of Water ~470mg
- Prepare PIC from Diagenode before -
- The Diagenode P.I.C. should be dissolved in 400 µl of molecular biology water to obtain a 25x stock concentration (Make 100ul of aliquots and freeze (stable in -20 deg for 4 months). Avoid freeze and thaw cycles
- In 10 ml of HBSS add complete 400ul of PIC prepared (fresh)
- In 5 ml of HBSS add 200 ul of PIC
- Prepare enzyme mix 1 and enzyme mix 2 according to the table below (for 1 Brain). Label the C tubes
- Bring the enzyme mix 1 and enzyme mix 2 and bring them on ice with clean forceps (Forceps will be needed to transfer the brain in C tubes)

Enzyme P	Buffer Z	Buffer Y	Enzyme A
50 ul	1900ul	20 ul	10 ul

- Bring them inside the hood in ice
- In one C tube max 20g to 500mg of brain tissue could be used. I have tried 800 mg (2 adult /12 -13 months old -in 1 C tube)
- Use 1.5 ml tubes (which are low retention - usually the tubes used in RNA isolation)

Protocol:

Tissue dissociation:

- With the help of forceps transfer the brain tissue into their respective C tube containing enzyme mix 1.
- Add enzyme mix 2.
- Run the appropriate gentleMACS Program: 20–100 mg:
  37C_ABDK_02
  For two brains run 37C_ABDK_01
- Centrifuge 10 min 300 g.
- Prepare 50ml Falcon tubes with 70µm Cell strainer and moisten with DPBs.
- Resuspend the pellet in 5 ml DPBS
- Pipette cell solution onto Cell strainer.
- Wash Cell strainer by pipetting 5ml of DPBS onto it
- Discard Cell strainer and centrifuge cell suspension at 300xg for 15min at 4°C (1200rpm centrifuge 4°C room)
- Aspirate supernatant completely.

Debris removal:

- Always use pre-cooled buffers and solutions (4°C)

	Debris removal Solution	D-PBS	Overlay(D-PBS)	Reagent tube
20-100mg	450ul	1550ul	2ml	5ml
1 brain	**900ul**	**3100ul**	**4ml**	**15ml**
2 brains	1800ul	6200ul	4ml	15 ml

- Re-suspend cell pellet carefully with the appropriate volume of cold D-PBS according to the table appropriate reagent tube. Do not vortex.
- Add appropriate volume of cold Debris Removal Solution.
- Mix well
- Overlay very gently with an appropriate amount of cold D-PBS according to the table above

Note: Pipette very slowly to ensure that the D-PBS phase overlays the cell suspension and phases are not mixed.

- Centrifuge at 4 °C and 3000×g for 10 minutes with full acceleration and full brake.

Note: If centrifuges give suboptimal centrifugation, the acceleration and brake can be reduced.

- Three phases are formed. Aspirate the two top phases completely and discard them. (Achtung! Do not discard the bottom layer after seeing the cell pellet, u can lose a no of cells in the procedure)
- Fill up with cold D-PBS. (~10ml)
- Gently invert the tube three times. Do not vortex!
- Centrifuge at 4 °C and 1000×g for 10 minutes with full acceleration and full brake. Aspirate supernatant completely.
- Proceed for red blood cell removal.

Red blood cell removal:

- Dilute Red Blood Cell Removal Solution (10x) 1:10 with ddH2O (0.8ml in 7.2 ml ddH20)
- Do not use deionized water or DPBS for dilution!
- Store the prepared 1x Red Blood Cell Removal Solution at 2-8°C. Discard unused solution at the end of the day
- Add 500 ul of red blood cell removal solution (800 ul in case of perfusion failed and animal has to be sacrificed by decapitation, in that case there is lot of blood in brain)
- Incubate for 10 min in the refrigerator
- Add 10 ml of cold DPBS
- Centrifuge at 4°C and 300xg (1200rpm) for 10 min. Aspirate supernatant completely

Magnetic Antibody Labelling

- Resuspend cell pellet carefully in 90 µL of MACS buffer or DPBS per 10^7 total cells by pipetting slowly up and down. (used 500ul), the cell count comes around 1x107 cells
- Do not vortex
- Add 10 µL of CD11b (Microglia) Microbeads, human and mouse for 10^7 cells (add 20 ul of beads)
- Incubate solution for 15 min in the refrigerator
- Add 3ml of DPBS
- Centrifuge at 4°C and 1000g for 10 min. Aspirate supernatant completely and suspend in 0.5ml DPBS
- Equilibrate MS columns attached to the magnet with 0.5ml DPBS
- Place 15ml Falcon tubes stacked in ice under the columns to collect flow through
- Pipette cell suspension onto the MS Column
- Flush falcon tube with 0.5ml DPBS and pipette it also onto the column after reservoir is empty
- Wash columns 3x with 0.5ml DPBS
- Elute cells by detaching the columns from the magnet and placing them on a suitable collection tube
- For Chip - flush with 1 ml of DPBS in low retention tubes (RNA tubes 1.5ml) - and count the number of cells, transfer to 1.5 ml tube.

Fixation and Quenching

- Open a fresh ampoule of 16% formaldehyde and add 62.5 ul of it in the tube (final concentration ~1 %) and invert the tubes two to three times to ensure complete mixing
- The cells were fixed in formaldehyde for 10 min (this time point was chosen based on shearing validation
- Add 115ul of glycine to the sample
- Mix by inversion of the tube four to five times. Incubate for 5 minutes at room temperature to stop the fixation. Work on ice from this point onwards.
- Centrifuge at 3000x g for 10 minutes at 4°C. We recommend the use of a swing-out rotor with soft settings for deceleration (Centrifuge used is of fixed rotor).
- Aspirate the supernatant slowly and leave approximately 30 µl of the solution. Do not disturb the pellet. Take care to not remove these cross-linked cells.
- Wash the cross-linked cells with 1 ml of ice cold HBSS containing protease inhibitor cocktail. In 5 ml of HBSS add 200 ul of PIC
- Add 1 ml of HBSS and invert the tube four to five times to resuspend the cells
- Centrifuge at 3000 x g for 10 minutes at 4°C (in a swing-out rotor with soft settings for deceleration)
- Discard all the supernatant (no liquid should be left) and keep the cell pellet on ice. Proceed directly to -80°C for up to 2 months
- Send the samples for sequencing to Diagenode

Shearing profiles

Control samples C1 and C3 with 2-3 brains pooled in each replicate; 8 cycles of shearing on fixed cells (10 min with formaldehyde)

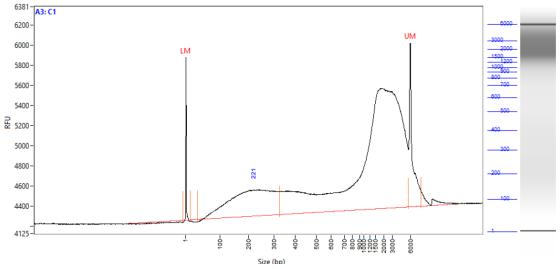

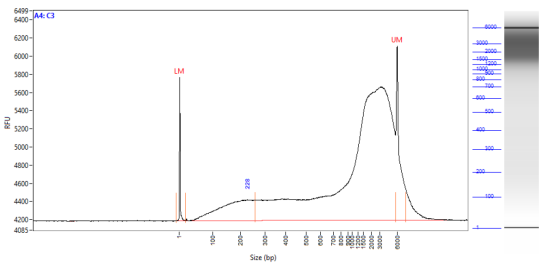

BCG treated samples from mice B1 and B3 with 2-3 brains pooled in each replicate; 8 cycles of shearing on fixed cells (10 min with formaldehyde)

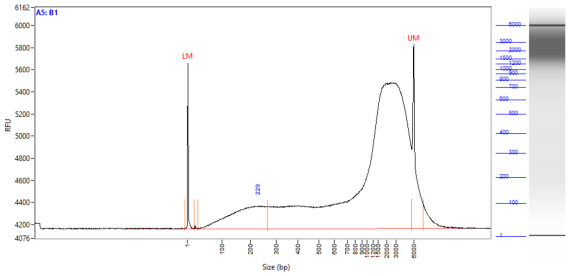

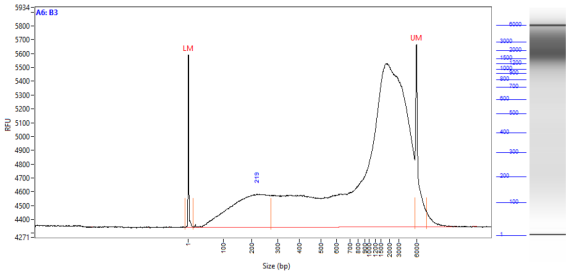

3. Custom made Macros in Fiji and R scripts

The macros in FIJI for analyzing

- Consecutive lesion areas in one demyelinated area
- Percentage of area covered and intensity of different signals
- Signal from Fluorescent in situ hybridization

have been adapted from (Bosch-Queralt *et al.*, 2021, 2022)

The R scripts used for analyzing

- snRNA seq dataset
- ATAC seq dataset
- Chip seq dataset
- RNA seq dataset

Have been adapted from the publically available pipelines for analyzing high end sequencing datasets and platforms such as GALAXY and are available on special request from the authors

References

Agrawal, A. and Gupta, S. (2011) 'Impact of aging on dendritic cell functions in humans', *Ageing research reviews*, 10(3), pp. 336–345. Available at: https://doi.org/10.1016/J.ARR.2010.06.004.

Aguzzi, A., Barres, B.A. and Bennett, M.L. (2013) 'Microglia: Scapegoat, Saboteur, or Something Else?', *Science*, 339(6116), pp. 156–161. Available at: https://doi.org/10.1126/SCIENCE.1227901.

Ajami, B. *et al.* (2007) 'Local self-renewal can sustain CNS microglia maintenance and function throughout adult life', *Nature Neuroscience 2007 10:12*, 10(12), pp. 1538–1543. Available at: https://doi.org/10.1038/nn2014.

Ajami, B. *et al.* (2011) 'Infiltrating monocytes trigger EAE progression, but do not contribute to the resident microglia pool', *Nature Neuroscience 2011 14:9*, 14(9), pp. 1142–1149. Available at: https://doi.org/10.1038/nn.2887.

Al-Chalabi, A., Van Den Berg, L.H. and Veldink, J. (2016) 'Gene discovery in amyotrophic lateral sclerosis: implications for clinical management', *Nature Reviews Neurology 2016 13:2*, 13(2), pp. 96–104. Available at: https://doi.org/10.1038/nrneurol.2016.182.

Alliot, F., Godin, I. and Pessac, B. (1999) 'Microglia derive from progenitors, originating from the yolk sac, and which proliferate in the brain', *Developmental Brain Research*, 117(2), pp. 145–152. Available at: https://doi.org/10.1016/S0165-3806(99)00113-3.

Alvarez, E. *et al.* (2001) 'Age-related changes in membrane lipid composition, fluidity and respiratory burst in rat peritoneal neutrophils', *Clinical and experimental immunology*, 124(1), pp. 95–102. Available at: https://doi.org/10.1046/J.1365-2249.2001.01490.X.

Amit, I., Winter, D.R. and Jung, S. (2015) 'The role of the local environment and epigenetics in shaping macrophage identity and their effect on tissue homeostasis', *Nature Immunology 2015 17:1*, 17(1), pp. 18–25. Available at: https://doi.org/10.1038/ni.3325.

Arifuzzaman, S. *et al.* (2017) 'Selective inhibition of EZH2 by a small molecule inhibitor regulates microglial gene expression essential for inflammation', *Biochemical Pharmacology*, 137, pp. 61–80. Available at: https://doi.org/10.1016/J.BCP.2017.04.016.

Arts, R.J.W., Novakovic, B., *et al.* (2016) 'Glutaminolysis and Fumarate Accumulation Integrate Immunometabolic and Epigenetic Programs in Trained Immunity', *Cell metabolism*, 24(6), pp. 807–819. Available at: https://doi.org/10.1016/J.CMET.2016.10.008.

Arts, R.J.W., Carvalho, A., *et al.* (2016a) 'Immunometabolic Pathways in BCG-Induced Trained Immunity', *Cell Reports*, 17(10), pp. 2562–2571. Available at: https://doi.org/10.1016/j.celrep.2016.11.011.

Arts, R.J.W. *et al.* (2018a) 'BCG Vaccination Protects against Experimental Viral Infection in Humans through the Induction of Cytokines Associated with Trained Immunity', *Cell Host and Microbe*, 23(1), pp. 89-100.e5. Available at: https://doi.org/10.1016/j.chom.2017.12.010.

Arts, R.J.W., Joosten, L.A.B. and Netea, M.G. (2016) 'Immunometabolic circuits in trained immunity', *Seminars in immunology*, 28(5), pp. 425–430. Available at: https://doi.org/10.1016/J.SMIM.2016.09.002.

Asai, H. *et al.* (2015) 'Depletion of microglia and inhibition of exosome synthesis halt tau propagation', *Nature Neuroscience 2015 18:11*, 18(11), pp. 1584–1593. Available at: https://doi.org/10.1038/nn.4132.

Asare, Y. *et al.* (2020) 'Histone Deacetylase 9 Activates IKK to Regulate Atherosclerotic Plaque Vulnerability', *Circulation Research*, 127(6), pp. 811–823. Available at: https://doi.org/10.1161/CIRCRESAHA.120.316743.

Askew, K. *et al.* (2017) 'Coupled Proliferation and Apoptosis Maintain the Rapid Turnover of Microglia in the Adult Brain', *Cell Reports*, 18(2), pp. 391–405. Available at: https://doi.org/10.1016/J.CELREP.2016.12.041.

Bailey, K.L. *et al.* (2019) 'Aging leads to dysfunctional innate immune responses to TLR2 and TLR4 agonists', *Aging Clinical and Experimental Research*, 31(9), pp. 1185–1193. Available at: https://doi.org/10.1007/S40520-018-1064-0/METRICS.

Bambouskova, M. *et al.* (2018) 'Electrophilic properties of itaconate and derivatives regulate the IκBζ-ATF3 inflammatory axis', *Nature*, 556(7702), pp. 501–504. Available at: https://doi.org/10.1038/S41586-018-0052-Z.

Baranzini, S.E. *et al.* (2010) 'Genome, epigenome and RNA sequences of monozygotic twins discordant for multiple sclerosis', *Nature*, 464(7293), pp. 1351–1356. Available at: https://doi.org/10.1038/NATURE08990.

Barnett, D.W. *et al.* (2011) 'BamTools: a C++ API and toolkit for analyzing and managing BAM files', *Bioinformatics*, 27(12), pp. 1691–1692. Available at: https://doi.org/10.1093/BIOINFORMATICS/BTR174.

Bekkering, S. *et al.* (2018) 'Metabolic Induction of Trained Immunity through the Mevalonate Pathway', *Cell*, 172(1–2), pp. 135-146.e9. Available at: https://doi.org/10.1016/J.CELL.2017.11.025.

Bektas, A. *et al.* (2018) 'Aging, Inflammation and the Environment', *Experimental gerontology*, 105, p. 10. Available at: https://doi.org/10.1016/J.EXGER.2017.12.015.

Belbasis, L. *et al.* (2015) 'Environmental risk factors and multiple sclerosis: an umbrella review of systematic reviews and meta-analyses', *The Lancet. Neurology*, 14(3), pp. 263–

273. Available at: https://doi.org/10.1016/S1474-4422(14)70267-4.

Ben-Nun, A. *et al.* (2014) 'From classic to spontaneous and humanized models of multiple sclerosis: Impact on understanding pathogenesis and drug development', *Journal of Autoimmunity*, 54, pp. 33–50. Available at: https://doi.org/10.1016/J.JAUT.2014.06.004.

Bennett, M.L. *et al.* (2016) 'New tools for studying microglia in the mouse and human CNS', *Proceedings of the National Academy of Sciences of the United States of America*, 113(12), pp. E1738–E1746. Available at: https://doi.org/10.1073/PNAS.1525528113/SUPPL_FILE/PNAS.1525528113.SD01.XLSX.

von Bernhardi, R. (2007) 'Glial cell dysregulation: a new perspective on Alzheimer disease', *Neurotoxicity Research 2007 12:4*, 12(4), pp. 215–232. Available at: https://doi.org/10.1007/BF03033906.

von Bernhardi, R. *et al.* (2015) 'Role of TGFβ signaling in the pathogenesis of Alzheimer's disease', *Frontiers in Cellular Neuroscience*, 9(OCTOBER), p. 426. Available at: https://doi.org/10.3389/FNCEL.2015.00426/BIBTEX.

von Bernhardi, R., Eugenín-von Bernhardi, L. and Eugenín, J. (2015) 'Microglial cell dysregulation in brain aging and neurodegeneration', *Frontiers in Aging Neuroscience*, 7(JUN), p. 124. Available at: https://doi.org/10.3389/FNAGI.2015.00124/BIBTEX.

Von Bernhardi, R., Tichauer, J. and Eugenín-von Bernhardi, L. (2011) 'Proliferating culture of aged microglia for the study of neurodegenerative diseases', *Journal of Neuroscience Methods*, 202(1), pp. 65–69. Available at: https://doi.org/10.1016/J.JNEUMETH.2011.08.027.

Von Bernhardi, R., Tichauer, J.E. and Eugenín, J. (2010) 'Aging-dependent changes of microglial cells and their relevance for neurodegenerative disorders', *Journal of Neurochemistry*, 112(5), pp. 1099–1114. Available at: https://doi.org/10.1111/J.1471-4159.2009.06537.X.

Beutler, B. (2004) 'Innate immunity: an overview', *Molecular Immunology*, 40(12), pp. 845–859. Available at: https://doi.org/10.1016/J.MOLIMM.2003.10.005.

Bieber, A.J., Ure, D.R. and Rodriguez, M. (2005) 'Genetically dominant spinal cord repair in a murine model of chronic progressive multiple sclerosis', *Journal of neuropathology and experimental neurology*, 64(1), pp. 46–57. Available at: https://doi.org/10.1093/JNEN/64.1.46.

Bilbo, S.D. (2010) 'Early-life infection is a vulnerability factor for aging-related glial alterations and cognitive decline', *Neurobiology of Learning and Memory*, 94(1), pp. 57–64. Available at: https://doi.org/10.1016/J.NLM.2010.04.001.

Bistoni, F. *et al.* (1988) 'Immunomodulation by a low-virulence, agerminative variant of Candida albicans. Further evidence for macrophage activation as one of the effector mechanisms of nonspecific anti-infectious protection', *Journal of medical and veterinary mycology : bi-monthly publication of the International Society for Human and Animal Mycology*, 26(5), pp. 285–299. Available at: https://doi.org/10.1080/02681218880000401.

Blakemore, W.F. and Franklin, R.J.M. (2008) 'Remyelination in experimental models of toxin-induced demyelination', *Current Topics in Microbiology and Immunology*, 318, pp. 193–212. Available at: https://doi.org/10.1007/978-3-540-73677-6_8/COVER.

Blanchard, F. *et al.* (2002) 'FR901228, an inhibitor of histone deacetylases, increases the cellular responsiveness to IL-6 type cytokines by enhancing the expression of receptor proteins', *Oncogene 2002 21:41*, 21(41), pp. 6264–6277. Available at: https://doi.org/10.1038/sj.onc.1205777.

Bleve, A. *et al.* (2022) 'Immunosenescence, Inflammaging, and Frailty: Role of Myeloid Cells in Age-Related Diseases', *Clinical Reviews in Allergy & Immunology 2021 64:2*, 64(2), pp. 123–144. Available at: https://doi.org/10.1007/S12016-021-08909-7.

Boeger, H. *et al.* (2003) 'Nucleosomes unfold completely at a transcriptionally active promoter', *Molecular Cell*, 11(6), pp. 1587–1598. Available at: https://doi.org/10.1016/S1097-2765(03)00231-4.

Bogie, J.F.J. *et al.* (2020) 'Stearoyl-CoA desaturase-1 impairs the reparative properties of macrophages and microglia in the brain', *Journal of Experimental Medicine*, 217(5). Available at: https://doi.org/10.1084/JEM.20191660/133840.

Bonilla, F.A. and Oettgen, H.C. (2010) 'Adaptive immunity', *Journal of Allergy and Clinical Immunology*, 125(2 SUPPL. 2), pp. S33–S40. Available at: https://doi.org/10.1016/j.jaci.2009.09.017.

Bosch-Queralt, M. *et al.* (2021) 'Diet-dependent regulation of TGFβ impairs reparative innate immune responses after demyelination', *Nature Metabolism*, 3(2), pp. 211–227. Available at: https://doi.org/10.1038/s42255-021-00341-7.

Bosch-Queralt, M. *et al.* (2022) 'A fluorescence microscopy-based protocol for volumetric measurement of lysolecithin lesion-associated de- and re-myelination in mouse brain', *STAR Protocols*, 3(1), p. 101141. Available at: https://doi.org/10.1016/J.XPRO.2022.101141.

de Bree, C.L.C.J. *et al.* (2018) 'The impact of sex hormones on BCG-induced trained immunity', *Journal of Leukocyte Biology*, 104(3), pp. 573–578. Available at: https://doi.org/10.1002/JLB.5MA0118-027R.

Buenrostro, J.D. *et al.* (2013) 'Transposition of native chromatin for fast and sensitive epigenomic profiling of open chromatin, DNA-binding proteins and nucleosome position', *Nature methods*, 10(12), pp. 1213–1218. Available at: https://doi.org/10.1038/NMETH.2688.

Burg, T. *et al.* (2021) 'Histone deacetylase inhibition regulates lipid homeostasis in a mouse model of amyotrophic lateral sclerosis', *International Journal of Molecular Sciences*, 22(20), p. 11224. Available at: https://doi.org/10.3390/IJMS222011224/S1.

Butovsky, O. *et al.* (2013) 'Identification of a unique TGF-β–dependent molecular and functional signature in microglia', *Nature Neuroscience 2013 17:1*, 17(1), pp. 131–143. Available at: https://doi.org/10.1038/nn.3599.

Butovsky, O. *et al.* (2015) 'Targeting miR-155 restores abnormal microglia and attenuates disease in SOD1 mice', *Annals of Neurology*, 77(1), pp. 75–99. Available at: https://doi.org/10.1002/ANA.24304.

Calder, P.C. (2015) 'Marine omega-3 fatty acids and inflammatory processes: Effects, mechanisms and clinical relevance', *Biochimica et Biophysica Acta (BBA) - Molecular and Cell Biology of Lipids*, 1851(4), pp. 469–484. Available at: https://doi.org/10.1016/J.BBALIP.2014.08.010.

Callender, L.A. *et al.* (2018) 'Human CD8+ EMRA T cells display a senescence-associated secretory phenotype regulated by p38 MAPK', *Aging Cell*, 17(1), p. e12675. Available at: https://doi.org/10.1111/ACEL.12675.

Calvanese, V. *et al.* (2009) 'The role of epigenetics in aging and age-related diseases', *Ageing research reviews*, 8(4), pp. 268–276. Available at: https://doi.org/10.1016/J.ARR.2009.03.004.

Camelo, S. *et al.* (2005) 'Transcriptional therapy with the histone deacetylase inhibitor trichostatin A ameliorates experimental autoimmune encephalomyelitis', *Journal of neuroimmunology*, 164(1–2), pp. 10–21. Available at: https://doi.org/10.1016/J.JNEUROIM.2005.02.022.

Cantuti-Castelvetri, L. *et al.* (2018) 'Defective cholesterol clearance limits remyelination in the aged central nervous system', *Science*, 359(6376), pp. 684–688. Available at: https://doi.org/10.1126/SCIENCE.AAN4183/SUPPL_FILE/AAN4183_CANTUTI-CATSTELVETRI_SM.PDF.

Cao, Q. *et al.* (2014) 'Histone deacetylase 9 represses cholesterol efflux and alternatively activated macrophages in atherosclerosis development', *Arteriosclerosis, Thrombosis, and Vascular Biology*, 34(9), pp. 1871–1879. Available at: https://doi.org/10.1161/ATVBAHA.114.303393/-/DC1.

Castrillo, A. and Tontonoz, P. (2004) 'NUCLEAR RECEPTORS IN MACROPHAGE BIOLOGY: At the Crossroads of Lipid Metabolism and Inflammation', *https://doi.org/10.1146/annurev.cellbio.20.012103.134432*, 20, pp. 455–480. Available at: https://doi.org/10.1146/ANNUREV.CELLBIO.20.012103.134432.

Chastain, E.M.L. *et al.* (2011) 'The role of antigen presenting cells in multiple sclerosis', *Biochimica et Biophysica Acta (BBA) - Molecular Basis of Disease*, 1812(2), pp. 265–274. Available at: https://doi.org/10.1016/J.BBADIS.2010.07.008.

Chawla, A. *et al.* (2001) 'A PPARγ-LXR-ABCA1 Pathway in Macrophages Is Involved in Cholesterol Efflux and Atherogenesis', *Molecular Cell*, 7(1), pp. 161–171. Available at: https://doi.org/10.1016/S1097-2765(01)00164-2.

Chen, P.S. *et al.* (2007) 'Valproic acid and other histone deacetylase inhibitors induce microglial apoptosis and attenuate lipopolysaccharide-induced dopaminergic neurotoxicity', *Neuroscience*, 149(1), pp. 203–212. Available at: https://doi.org/10.1016/J.NEUROSCIENCE.2007.06.053.

Chen, T. *et al.* (2019) 'Butyrate suppresses demyelination and enhances remyelination', *Journal of Neuroinflammation*, 16(1), pp. 1–13. Available at: https://doi.org/10.1186/S12974-019-1552-Y/FIGURES/7.

Cheng, S.C. *et al.* (2014a) 'mTOR- and HIF-1α-mediated aerobic glycolysis as metabolic basis for trained immunity', *Science (New York, N.Y.)*, 345(6204). Available at: https://doi.org/10.1126/SCIENCE.1250684.

Chinetti, G. *et al.* (2001) 'PPAR-α and PPAR-γ activators induce cholesterol removal from human macrophage foam cells through stimulation of the ABCA1 pathway', *Nature Medicine 2001 7:1*, 7(1), pp. 53–58. Available at: https://doi.org/10.1038/83348.

Chitu, V. *et al.* (2016) 'Emerging Roles for CSF-1 Receptor and its Ligands in the Nervous System', *Trends in Neurosciences*, 39(6), pp. 378–393. Available at: https://doi.org/10.1016/J.TINS.2016.03.005.

Chitu, V. and Stanley, E.R. (2017) 'Regulation of Embryonic and Postnatal Development by the CSF-1 Receptor', *Current Topics in Developmental Biology*, 123, pp. 229–275. Available at: https://doi.org/10.1016/BS.CTDB.2016.10.004.

Cho, S.H. *et al.* (2015) 'SIRT1 Deficiency in Microglia Contributes to Cognitive Decline in Aging and Neurodegeneration via Epigenetic Regulation of IL-1β', *Journal of Neuroscience*, 35(2), pp. 807–818. Available at: https://doi.org/10.1523/JNEUROSCI.2939-14.2015.

Ciarlo, E. *et al.* (2020) 'Trained Immunity Confers Broad-Spectrum Protection Against Bacterial Infections', *The Journal of infectious diseases*, 222(11), pp. 1869–1881. Available at: https://doi.org/10.1093/INFDIS/JIZ692.

Civil, R.H., Warren, K.S. and Mahmoud, A.A.F. (1978) 'Conditions for bacille Calmette-Guérin-induced resistance to infection with Schistosoma mansoni in mice', *The Journal of infectious diseases*, 137(5), pp. 550–555. Available at: https://doi.org/10.1093/INFDIS/137.5.550.

Clark, I.A., Allison, A.C. and Cox, F.E. (1976) 'Protection of mice against Babesia and Plasmodium with BCG', *Nature*, 259(5541), pp. 309–311. Available at: https://doi.org/10.1038/259309A0.

Colonna, M. and Butovsky, O. (2017) 'Microglia Function in the Central Nervous System During Health and Neurodegeneration', *https://doi.org/10.1146/annurev-immunol-051116-052358*, 35, pp. 441–468. Available at: https://doi.org/10.1146/ANNUREV-IMMUNOL-051116-052358.

Colonna, M. and Wang, Y. (2016) 'TREM2 variants: new keys to decipher Alzheimer disease pathogenesis', *Nature Reviews Neuroscience 2016 17:4*, 17(4), pp. 201–207. Available at: https://doi.org/10.1038/nrn.2016.7.

Consonni, F.M. *et al.* (2019) 'Myeloid-Derived Suppressor Cells: Ductile Targets in Disease', *Frontiers in immunology*, 10(MAY). Available at: https://doi.org/10.3389/FIMMU.2019.00949.

Conway, G.D. *et al.* (2012) 'Histone deacetylase activity is required for human oligodendrocyte progenitor differentiation', *Glia*, 60(12), pp. 1944–1953. Available at: https://doi.org/10.1002/GLIA.22410.

Copray, S. *et al.* (2009) 'Epigenetic mechanisms facilitating oligodendrocyte development, maturation and aging', *Glia*, 57(15), p. 1579. Available at: https://doi.org/10.1002/GLIA.20881.

Corces, M.R. *et al.* (2017) 'An improved ATAC-seq protocol reduces background and enablesinterrogation of frozen tissues', *Nature methods*, 14(10), p. 959. Available at: https://doi.org/10.1038/NMETH.4396.

Cordes, T. *et al.* (2016) 'Immunoresponsive Gene 1 and Itaconate Inhibit Succinate Dehydrogenase to Modulate Intracellular Succinate Levels', *The Journal of biological chemistry*, 291(27), pp. 14274–14284. Available at: https://doi.org/10.1074/JBC.M115.685792.

Cornejo, F. and von Bernhardi, R. (2016) 'Age-Dependent Changes in the Activation and Regulation of Microglia', *Advances in experimental medicine and biology*, 949, pp. 205–226. Available at: https://doi.org/10.1007/978-3-319-40764-7_10.

Cossu, D. *et al.* (2017) 'Altered humoral immunity to mycobacterial antigens in Japanese patients affected by inflammatory demyelinating diseases of the central nervous system', *Scientific Reports*, 7(1). Available at: https://doi.org/10.1038/S41598-017-03370-Z.

Cossu, D. *et al.* (2021) 'PARKIN modifies peripheral immune response and increases neuroinflammation in active experimental autoimmune encephalomyelitis (EAE)', *Journal of neuroimmunology*, 359. Available at: https://doi.org/10.1016/J.JNEUROIM.2021.577694.

da Costa, J.P. *et al.* (2016) 'A synopsis on aging-Theories, mechanisms and future prospects', *Ageing research reviews*, 29, pp. 90–112. Available at: https://doi.org/10.1016/J.ARR.2016.06.005.

Costet, P. *et al.* (2000) 'Sterol-dependent transactivation of the ABC1 promoter by the liver X receptor/retinoid X receptor', *Journal of Biological Chemistry*, 275(36), pp. 28240–28245. Available at: https://doi.org/10.1074/jbc.M003337200.

Courtney, R. and Landreth, G.E. (2016) 'LXR Regulation of Brain Cholesterol: From Development to Disease', *Trends in endocrinology and metabolism: TEM*, 27(6), pp. 404–414. Available at: https://doi.org/10.1016/J.TEM.2016.03.018.

Creyghton, M.P. *et al.* (2010) 'Histone H3K27ac separates active from poised enhancers and predicts developmental state', *Proceedings of the National Academy of Sciences of the United States of America*, 107(50), pp. 21931–21936. Available at: https://doi.org/10.1073/PNAS.1016071107/SUPPL_FILE/ST01.XLSX.

Cummins, C.L. and Mangelsdorf, D.J. (2006) 'Liver X receptors and cholesterol homoeostasis: spotlight on the adrenal gland', *Biochemical Society transactions*, 34(Pt 6), pp. 1110–1113. Available at: https://doi.org/10.1042/BST0341110.

Cunha, M.I. *et al.* (2020a) 'Pro-inflammatory activation following demyelination is required for myelin clearance and oligodendrogenesis', *Journal of Experimental Medicine*, 217(5). Available at: https://doi.org/10.1084/jem.20191390.

Cunliffe, V.T. and Casaccia-Bonnefil, P. (2006) 'Histone deacetylase 1 is essential for oligodendrocyte specification in the zebrafish CNS', *Mechanisms of development*, 123(1), pp. 24–30. Available at: https://doi.org/10.1016/J.MOD.2005.10.005.

Cunningham, C. *et al.* (2005) 'Central and systemic endotoxin challenges exacerbate the local inflammatory response and increase neuronal death during chronic neurodegeneration', *The Journal of neuroscience : the official journal of the Society for Neuroscience*, 25(40), pp. 9275–9284. Available at: https://doi.org/10.1523/JNEUROSCI.2614-05.2005.

Curtiss, L.K. (2000) 'ApoE in Atherosclerosis', *Arteriosclerosis, Thrombosis, and Vascular Biology*, 20(8), pp. 1852–1853. Available at: https://doi.org/10.1161/01.ATV.20.8.1852.

D'Haeseleer, P. (2006) 'What are DNA sequence motifs?', *Nature Biotechnology 2006 24:4*, 24(4), pp. 423–425. Available at: https://doi.org/10.1038/nbt0406-423.

Dani, N. *et al.* (2021) 'A cellular and spatial map of the choroid plexus across brain ventricles and ages', *Cell*, 184(11), pp. 3056-3074.e21. Available at: https://doi.org/10.1016/J.CELL.2021.04.003.

Das, A., Chai, J.C., Kim, S.H., Park, K.S., *et al.* (2015) 'Dual RNA Sequencing Reveals the Expression of Unique Transcriptomic Signatures in Lipopolysaccharide-Induced BV-2 Microglial Cells', *PLOS ONE*, 10(3), p. e0121117. Available at: https://doi.org/10.1371/JOURNAL.PONE.0121117.

Das, A., Chai, J.C., Kim, S.H., Lee, Y.S., *et al.* (2015) 'Transcriptome sequencing of microglial cells stimulated with TLR3 and TLR4 ligands', *BMC Genomics*, 16(1), pp. 1–21. Available at: https://doi.org/10.1186/S12864-015-1728-5/FIGURES/9.

Datta, M. *et al.* (2018a) 'Histone Deacetylases 1 and 2 Regulate Microglia Function during Development, Homeostasis, and Neurodegeneration in a Context-Dependent Manner', *Immunity*, 48(3), pp. 514-529.e6.

Available at: https://doi.org/10.1016/j.immuni.2018.02.016.

Davalos, D. *et al.* (2005) 'ATP mediates rapid microglial response to local brain injury in vivo', *Nature Neuroscience 2005 8:6*, 8(6), pp. 752–758. Available at: https://doi.org/10.1038/nn1472.

Deczkowska, A. *et al.* (2018) 'Disease-Associated Microglia: A Universal Immune Sensor of Neurodegeneration', *Cell*, 173(5), pp. 1073–1081. Available at: https://doi.org/10.1016/J.CELL.2018.05.003.

Dobin, A. *et al.* (2013) 'STAR: ultrafast universal RNA-seq aligner', *Bioinformatics*, 29(1), pp. 15–21. Available at: https://doi.org/10.1093/BIOINFORMATICS/BTS635.

Domínguez-Andrés, J. *et al.* (2019) 'The Itaconate Pathway Is a Central Regulatory Node Linking Innate Immune Tolerance and Trained Immunity', *Cell metabolism*, 29(1), pp. 211-220.e5. Available at: https://doi.org/10.1016/J.CMET.2018.09.003.

Domínguez-Andrés, J. *et al.* (2020) 'Advances in understanding molecular regulation of innate immune memory', *Current opinion in cell biology*, 63, pp. 68–75. Available at: https://doi.org/10.1016/J.CEB.2019.12.006.

Domínguez-Andrés, J., Joosten, L.A. and Netea, M.G. (2019a) 'Induction of innate immune memory: the role of cellular metabolism', *Current opinion in immunology*, 56, pp. 10–16. Available at: https://doi.org/10.1016/J.COI.2018.09.001.

Donohoe, D.R. and Bultman, S.J. (2012a) 'Metaboloepigenetics: interrelationships between energy metabolism and epigenetic control of gene expression', *Journal of cellular physiology*, 227(9), pp. 3169–3177. Available at: https://doi.org/10.1002/JCP.24054.

Donohoe, D.R. and Bultman, S.J. (2012b) 'Metaboloepigenetics: Interrelationships between energy metabolism and epigenetic control of gene expression', *Journal of Cellular Physiology*, 227(9), pp. 3169–3177. Available at: https://doi.org/10.1002/JCP.24054.

Dresselhaus, E. *et al.* (2018) 'Class I HDAC inhibition is a novel pathway for regulating astrocytic apoE secretion', *PLOS ONE*, 13(3), p. e0194661. Available at: https://doi.org/10.1371/JOURNAL.PONE.0194661.

Duffy, D. and Rader, D.J. (2009) 'Update on strategies to increase HDL quantity and function', *Nature reviews. Cardiology*, 6(7), pp. 455–463. Available at: https://doi.org/10.1038/NRCARDIO.2009.94.

Durham, B.S., Grigg, R. and Wood, I.C. (2017) 'Inhibition of histone deacetylase 1 or 2 reduces induced cytokine expression in microglia through a protein synthesis independent mechanism', *Journal of Neurochemistry*, 143(2), pp. 214–224. Available at: https://doi.org/10.1111/JNC.14144.

Ek, M. *et al.* (2001) 'Pathway across the blood–brain barrier', *Nature 2001 410:6827*, 410(6827), pp. 430–431. Available at: https://doi.org/10.1038/35068632.

Eljaschewitsch, E. *et al.* (2006) 'The Endocannabinoid Anandamide Protects Neurons during CNS Inflammation by Induction of MKP-1 in Microglial Cells', *Neuron*, 49(1), pp. 67–79. Available at: https://doi.org/10.1016/J.NEURON.2005.11.027.

Emery, B. (2010) 'Regulation of oligodendrocyte differentiation and myelination', *Science (New York, N.Y.)*, 330(6005), pp. 779–782. Available at: https://doi.org/10.1126/SCIENCE.1190927.

Esteller, M. (2008) 'Epigenetics in Cancer', *https://doi.org/10.1056/NEJMra072067*, 358(11), pp. 1148–1159. Available at: https://doi.org/10.1056/NEJMRA072067.

Fantin, A. *et al.* (2010) 'Tissue macrophages act as cellular chaperones for vascular anastomosis downstream of VEGF-mediated endothelial tip cell induction', *Blood*, 116(5), pp. 829–840. Available at: https://doi.org/10.1182/BLOOD-2009-12-257832.

Fanucchi, S. *et al.* (2019) 'Immune genes are primed for robust transcription by proximal long noncoding RNAs located in nuclear compartments', *Nature genetics*, 51(1), pp. 138–150. Available at: https://doi.org/10.1038/S41588-018-0298-2.

Ferguson, R. and Simes, A. (1949) 'BCG vaccination of Indian infants in Saskatchewan', *Tubercle*, 30(1), pp. 5–11. Available at: https://doi.org/10.1016/S0041-3879(49)80055-9.

Fielding, C.J. and Fielding, P.E. (1995) 'Molecular physiology of reverse cholesterol transport.', *Journal of Lipid Research*, 36(2), pp. 211–228. Available at: https://doi.org/10.1016/S0022-2275(20)39898-9.

Fleiss, B. *et al.* (2012) 'Neuroprotection by the histone deacetylase inhibitor trichostatin A in a model of lipopolysaccharide-sensitised neonatal hypoxic-ischaemic brain injury', *Journal of Neuroinflammation*, 9(1), pp. 1–15. Available at: https://doi.org/10.1186/1742-2094-9-70/FIGURES/8.

Franceschi, C. *et al.* (2000) 'Inflamm-aging. An evolutionary perspective on immunosenescence', *Annals of the New York Academy of Sciences*, 908, pp. 244–254. Available at: https://doi.org/10.1111/J.1749-6632.2000.TB06651.X.

Franceschi, C. *et al.* (2018) 'Inflammaging: a new immune–metabolic viewpoint for age-related diseases', *Nature Reviews Endocrinology 2018 14:10*, 14(10), pp. 576–590. Available at: https://doi.org/10.1038/s41574-018-0059-4.

Franceschi, C., Santoro, A. and Capri, M. (2020) 'The complex relationship between Immunosenescence and Inflammaging: Special issue on the New Biomedical Perspectives', *Seminars in Immunopathology*, 42(5), p. 517. Available at: https://doi.org/10.1007/S00281-020-00823-Y.

Frank, M.G. *et al.* (2006) 'mRNA up-regulation of MHC II and pivotal pro-inflammatory genes in normal brain aging', *Neurobiology of Aging*, 27(5), pp. 717–722. Available at:

https://doi.org/10.1016/J.NEUROBIOLAGING.2005.03.013.

Frank, M.G. *et al.* (2007) 'Microglia serve as a neuroimmune substrate for stress-induced potentiation of CNS pro-inflammatory cytokine responses', *Brain, behavior, and immunity*, 21(1), pp. 47–59. Available at: https://doi.org/10.1016/J.BBI.2006.03.005.

Franklin, R.J.M. and Ffrench-Constant, C. (2008) 'Remyelination in the CNS: from biology to therapy', *Nature Reviews Neuroscience 2008 9:11*, 9(11), pp. 839–855. Available at: https://doi.org/10.1038/nrn2480.

Franklin, R.J.M. and Ffrench-Constant, C. (2017) 'Regenerating CNS myelin — from mechanisms to experimental medicines', *Nature Reviews Neuroscience 2017 18:12*, 18(12), pp. 753–769. Available at: https://doi.org/10.1038/nrn.2017.136.

Frost, J.L. and Schafer, D.P. (2016) 'Microglia: Architects of the Developing Nervous System', *Trends in Cell Biology*, 26(8), pp. 587–597. Available at: https://doi.org/10.1016/J.TCB.2016.02.006.

Füger, P. *et al.* (2017) 'Microglia turnover with aging and in an Alzheimer's model via long-term in vivo single-cell imaging', *Nature Neuroscience 2017 20:10*, 20(10), pp. 1371–1376. Available at: https://doi.org/10.1038/nn.4631.

Fujiwara, S. *et al.* (2019) 'High Quality ATAC-Seq Data Recovered from Cryopreserved Breast Cell Lines and Tissue', *Scientific Reports 2019 9:1*, 9(1), pp. 1–11. Available at: https://doi.org/10.1038/s41598-018-36927-7.

Fulop, T. *et al.* (2004) 'Signal transduction and functional changes in neutrophils with aging', *Aging cell*, 3(4), pp. 217–226. Available at: https://doi.org/10.1111/J.1474-9728.2004.00110.X.

Fulop, T. *et al.* (2016) 'From inflamm-aging to immune-paralysis: a slippery slope during aging for immune-adaptation', *Biogerontology*, 17(1), pp. 147–157. Available at: https://doi.org/10.1007/S10522-015-9615-7/METRICS.

Fulop, T. *et al.* (2018) 'Immunosenescence and inflamm-aging as two sides of the same coin: Friends or Foes?', *Frontiers in Immunology*, 8(JAN), p. 1960. Available at: https://doi.org/10.3389/FIMMU.2017.01960/BIBTEX.

Fulop, T. *et al.* (2021) 'Immunology of Aging: the Birth of Inflammaging', *Clinical Reviews in Allergy & Immunology 2021 64:2*, 64(2), pp. 109–122. Available at: https://doi.org/10.1007/S12016-021-08899-6.

Gan, L. and Mucke, L. (2008) 'Paths of Convergence: Sirtuins in Aging and Neurodegeneration', *Neuron*, 58(1), pp. 10–14. Available at: https://doi.org/10.1016/J.NEURON.2008.03.015.

Gao, Z. *et al.* (2013) 'Reciprocal modulation between microglia and astrocyte in reactive gliosis following the CNS injury', *Molecular neurobiology*, 48(3), pp. 690–701. Available at: https://doi.org/10.1007/S12035-013-8460-4.

Garly, M.L. *et al.* (2003) 'BCG scar and positive tuberculin reaction associated with reduced child mortality in West Africa: A non-specific beneficial effect of BCG?', *Vaccine*, 21(21–22), pp. 2782–2790. Available at: https://doi.org/10.1016/S0264-410X(03)00181-6.

Ge, Z. *et al.* (2013) 'Vorinostat, a histone deacetylase inhibitor, suppresses dendritic cell function and ameliorates experimental autoimmune encephalomyelitis', *Experimental neurology*, 241(1), pp. 56–66. Available at: https://doi.org/10.1016/J.EXPNEUROL.2012.12.006.

Gearing, K.L. *et al.* (1993) 'Interaction of the peroxisome-proliferator-activated receptor and retinoid X receptor.', *Proceedings of the National Academy of Sciences*, 90(4), pp. 1440–1444. Available at: https://doi.org/10.1073/PNAS.90.4.1440.

Giera, S. *et al.* (2018) 'Microglial transglutaminase-2 drives myelination and myelin repair via GPR56/ADGRG1 in oligodendrocyte precursor cells', *eLife*, 7. Available at: https://doi.org/10.7554/ELIFE.33385.

Ginhoux, F. *et al.* (2010) 'Fate mapping analysis reveals that adult microglia derive from primitive macrophages', *Science*, 330(6005), pp. 841–845. Available at: https://doi.org/10.1126/SCIENCE.1194637/SUPPL_FILE/GINHOUX.SOM.PDF.

Ginhoux, F. and Guilliams, M. (2016) 'Tissue-Resident Macrophage Ontogeny and Homeostasis', *Immunity*, 44(3), pp. 439–449. Available at: https://doi.org/10.1016/J.IMMUNI.2016.02.024.

Godbout, J.P. *et al.* (2005) 'Exaggerated neuroinflammation and sickness behavior in aged mice following activation of the peripheral innate immune system', *FASEB journal : official publication of the Federation of American Societies for Experimental Biology*, 19(10), pp. 1329–1331. Available at: https://doi.org/10.1096/FJ.05-3776FJE.

Godoy, M.C.P. *et al.* (2008) 'Central and systemic IL-1 exacerbates neurodegeneration and motor symptoms in a model of Parkinson's disease', *Brain : a journal of neurology*, 131(Pt 7), pp. 1880–1894. Available at: https://doi.org/10.1093/BRAIN/AWN101.

Goldberg, E.L., Shaw, A.C. and Montgomery, R.R. (2020) 'How Inflammation Blunts Innate Immunity in Aging', *Interdisciplinary Topics in Gerontology and Geriatrics*, 43, pp. 1–17. Available at: https://doi.org/10.1159/000504480.

Goldmann, T. *et al.* (2013) 'A new type of microglia gene targeting shows TAK1 to be pivotal in CNS autoimmune inflammation', *Nature Neuroscience 2013 16:11*, 16(11), pp. 1618–1626. Available at: https://doi.org/10.1038/nn.3531.

Goldmann, T. *et al.* (2016) 'Origin, fate and dynamics of macrophages at central nervous system interfaces', *Nature Immunology 2016 17:7*, 17(7), pp. 797–805. Available at: https://doi.org/10.1038/ni.3423.

Goldmann, T. and Prinz, M. (2013) 'Role of microglia in CNS autoimmunity', *Clinical & developmental*

immunology, 2013. Available at: https://doi.org/10.1155/2013/208093.

Goll, M.G. and Bestor, T.H. (2005) 'Eukaryotic cytosine methyltransferases', *Annual review of biochemistry*, 74, pp. 481–514. Available at: https://doi.org/10.1146/ANNUREV.BIOCHEM.74.010904.153721.

Gomez Perdiguero, E. *et al.* (2014) 'Tissue-resident macrophages originate from yolk-sac-derived erythro-myeloid progenitors', *Nature 2014 518:7540*, 518(7540), pp. 547–551. Available at: https://doi.org/10.1038/nature13989.

Gong, T. *et al.* (2019) 'DAMP-sensing receptors in sterile inflammation and inflammatory diseases', *Nature Reviews Immunology 2019 20:2*, 20(2), pp. 95–112. Available at: https://doi.org/10.1038/s41577-019-0215-7.

Gosselin, D. *et al.* (2014) 'Environment Drives Selection and Function of Enhancers Controlling Tissue-Specific Macrophage Identities', *Cell*, 159(6), pp. 1327–1340. Available at: https://doi.org/10.1016/J.CELL.2014.11.023.

Greenhalgh, A.D. *et al.* (2018) 'Peripherally derived macrophages modulate microglial function to reduce inflammation after CNS injury', *PLoS biology*, 16(10). Available at: https://doi.org/10.1371/JOURNAL.PBIO.2005264.

Griciuc, A. *et al.* (2013) 'Alzheimer's Disease Risk Gene CD33 Inhibits Microglial Uptake of Amyloid Beta', *Neuron*, 78(4), pp. 631–643. Available at: https://doi.org/10.1016/J.NEURON.2013.04.014.

Guerreiro, R. *et al.* (2013) 'TREM2 Variants in Alzheimer's Disease ', *New England Journal of Medicine*, 368(2), pp. 117–127. Available at: https://doi.org/10.1056/NEJMOA1211851/SUPPL_FILE/NEJMOA1211851_DISCLOSURES.PDF.

Hagemeyer, N. *et al.* (2017) 'Microglia contribute to normal myelinogenesis and to oligodendrocyte progenitor maintenance during adulthood', *Acta Neuropathologica*, 134(3), pp. 441–458. Available at: https://doi.org/10.1007/S00401-017-1747-1/FIGURES/5.

Hamilton, J.A. *et al.* (2007) 'Brain uptake and utilization of fatty acids, lipids and lipoproteins: application to neurological disorders', *Journal of molecular neuroscience : MN*, 33(1), pp. 2–11. Available at: https://doi.org/10.1007/S12031-007-0060-1.

Hammond, T.R. *et al.* (2014) 'Astrocyte-derived Endothelin-1 inhibits remyelination through Notch activation', *Neuron*, 81(3), p. 588. Available at: https://doi.org/10.1016/J.NEURON.2013.11.015.

Hammond, T.R. *et al.* (2019) 'Single-Cell RNA Sequencing of Microglia throughout the Mouse Lifespan and in the Injured Brain Reveals Complex Cell-State Changes', *Immunity*, 50(1), pp. 253-271.e6. Available at: https://doi.org/10.1016/J.IMMUNI.2018.11.004.

Han, R.F. and Pan, J.G. (2006) 'Can intravesical bacillus Calmette-Guérin reduce recurrence in patients with superficial bladder cancer? A meta-analysis of randomized trials', *Urology*, 67(6), pp. 1216–1223. Available at: https://doi.org/10.1016/J.UROLOGY.2005.12.014.

Harris, M.A. *et al.* (2008) 'The Gene Ontology project in 2008', *Nucleic Acids Research*, 36(Database issue), p. D440. Available at: https://doi.org/10.1093/NAR/GKM883.

Hashimoto, D. *et al.* (2013) 'Tissue-Resident Macrophages Self-Maintain Locally throughout Adult Life with Minimal Contribution from Circulating Monocytes', *Immunity*, 38(4), pp. 792–804. Available at: https://doi.org/10.1016/J.IMMUNI.2013.04.004.

Hayflick, L. and Moorhead, P.S. (1961) 'The serial cultivation of human diploid cell strains', *Experimental Cell Research*, 25(3), pp. 585–621. Available at: https://doi.org/10.1016/0014-4827(61)90192-6.

Hazeldine, J. and Lord, J.M. (2015a) 'Innate immunesenescence: underlying mechanisms and clinical relevance', *Biogerontology*, 16(2), pp. 187–201. Available at: https://doi.org/10.1007/S10522-014-9514-3/METRICS.

He, H.H. *et al.* (2010) 'Nucleosome dynamics define transcriptional enhancers', *Nature Genetics 2010 42:4*, 42(4), pp. 343–347. Available at: https://doi.org/10.1038/ng.545.

Hefendehl, J.K. *et al.* (2014) 'Homeostatic and injury-induced microglia behavior in the aging brain', *Aging Cell*, 13(1), pp. 60–69. Available at: https://doi.org/10.1111/ACEL.12149.

Van Der Heijden, C.D.C.C. *et al.* (2018) 'Epigenetics and Trained Immunity', *Antioxidants & redox signaling*, 29(11), pp. 1023–1040. Available at: https://doi.org/10.1089/ARS.2017.7310.

Heinz, S. *et al.* (2010) 'Simple Combinations of Lineage-Determining Transcription Factors Prime cis-Regulatory Elements Required for Macrophage and B Cell Identities', *Molecular Cell*, 38(4), pp. 576–589. Available at: https://doi.org/10.1016/j.molcel.2010.05.004.

Henikoff, S. (2008) 'Nucleosome destabilization in the epigenetic regulation of gene expression', *Nature Reviews Genetics 2007 9:1*, 9(1), pp. 15–26. Available at: https://doi.org/10.1038/nrg2206.

Hinks, G.L. and Franklin, R.J.M. (2000) 'Delayed changes in growth factor gene expression during slow remyelination in the CNS of aged rats', *Molecular and cellular neurosciences*, 16(5), pp. 542–556. Available at: https://doi.org/10.1006/MCNE.2000.0897.

Hirsch-Reinshagen, V. *et al.* (2004) 'Deficiency of ABCA1 impairs apolipoprotein E metabolism in brain', *Journal of Biological Chemistry*, 279(39), pp. 41197–41207. Available at: https://doi.org/10.1074/jbc.M407962200.

Holtman, I.R. *et al.* (2015a) 'Induction of a common microglia gene expression signature by aging and

neurodegenerative conditions: a co-expression meta-analysis', *Acta neuropathologica communications*, 3(1), p. 31. Available at: https://doi.org/10.1186/S40478-015-0203-5/FIGURES/6.

Holtman, I.R. *et al.* (2015b) 'Induction of a common microglia gene expression signature by aging and neurodegenerative conditions: a co-expression meta-analysis', *Acta neuropathologica communications*, 3, p. 31. Available at: https://doi.org/10.1186/s40478-015-0203-5.

Hong, C. and Tontonoz, P. (2014) 'Liver X receptors in lipid metabolism: opportunities for drug discovery', *Nature reviews. Drug discovery*, 13(6), pp. 433–444. Available at: https://doi.org/10.1038/NRD4280.

Hoshiko, M. *et al.* (2012) 'Deficiency of the Microglial Receptor CX3CR1 Impairs Postnatal Functional Development of Thalamocortical Synapses in the Barrel Cortex', *Journal of Neuroscience*, 32(43), pp. 15106–15111. Available at: https://doi.org/10.1523/JNEUROSCI.1167-12.2012.

Van Hove, H. *et al.* (2019) 'A single-cell atlas of mouse brain macrophages reveals unique transcriptional identities shaped by ontogeny and tissue environment', *Nature Neuroscience 2019 22:6*, 22(6), pp. 1021–1035. Available at: https://doi.org/10.1038/s41593-019-0393-4.

Hsing, C.H. *et al.* (2015) 'Histone deacetylase inhibitor trichostatin a ameliorated endotoxin-induced neuroinflammation and cognitive dysfunction', *Mediators of Inflammation*, 2015. Available at: https://doi.org/10.1155/2015/163140.

Huang, J.K. *et al.* (2010) 'Retinoid X receptor gamma signaling accelerates CNS remyelination', *Nature Neuroscience 2010 14:1*, 14(1), pp. 45–53. Available at: https://doi.org/10.1038/nn.2702.

Hyeon, J.K. *et al.* (2007) 'Histone deacetylase inhibitors exhibit anti-inflammatory and neuroprotective effects in a rat permanent ischemic model of stroke: multiple mechanisms of action', *The Journal of pharmacology and experimental therapeutics*, 321(3), pp. 892–901. Available at: https://doi.org/10.1124/JPET.107.120188.

Irvine, K.A. and Blakemore, W.F. (2006) 'Age increases axon loss associated with primary demyelination in cuprizone-induced demyelination in C57BL/6 mice', *Journal of neuroimmunology*, 175(1–2), pp. 69–76. Available at: https://doi.org/10.1016/J.JNEUROIM.2006.03.002.

Ito, K. *et al.* (2002) 'A molecular mechanism of action of theophylline: Induction of histone deacetylase activity to decrease inflammatory gene expression', *Proceedings of the National Academy of Sciences*, 99(13), pp. 8921–8926. Available at: https://doi.org/10.1073/PNAS.132556899.

Jeffery, N.D. and Blakemore, W.F. (1995a) 'Remyelination of mouse spinal cord axons demyelinated by local injection of lysolecithin', *Journal of neurocytology*, 24(10), pp. 775–781. Available at: https://doi.org/10.1007/BF01191213.

Jeffery, N.D. and Blakemore, W.F. (1995b) 'Remyelination of mouse spinal cord axons demyelinated by local injection of lysolecithin', *Journal of neurocytology*, 24(10), pp. 775–781. Available at: https://doi.org/10.1007/BF01191213.

Jensen, C.J., Massie, A. and De Keyser, J. (2013) 'Immune Players in the CNS: The Astrocyte', *Journal of Neuroimmune Pharmacology 2013 8:4*, 8(4), pp. 824–839. Available at: https://doi.org/10.1007/S11481-013-9480-6.

Ji, H. *et al.* (2023) 'High-Resolution RNA Sequencing from PFA-Fixed Microscopy Sections', *Methods in molecular biology (Clifton, N.J.)*, 2616, pp. 205–212. Available at: https://doi.org/10.1007/978-1-0716-2926-0_16/COVER.

Joseph, S.B. *et al.* (2003) 'Reciprocal regulation of inflammation and lipid metabolism by liver X receptors', *Nature Medicine 2003 9:2*, 9(2), pp. 213–219. Available at: https://doi.org/10.1038/nm820.

Kaikkonen, M.U. *et al.* (2013) 'Remodeling of the Enhancer Landscape during Macrophage Activation Is Coupled to Enhancer Transcription', *Molecular Cell*, 51(3), pp. 310–325. Available at: https://doi.org/10.1016/J.MOLCEL.2013.07.010.

Kannan, V. *et al.* (2013) 'Histone deacetylase inhibitors suppress immune activation in primary mouse microglia', *Journal of neuroscience research*, 91(9), pp. 1133–1142. Available at: https://doi.org/10.1002/JNR.23221.

Kaufmann, E. *et al.* (2018) 'BCG Educates Hematopoietic Stem Cells to Generate Protective Innate Immunity against Tuberculosis', *Cell*, 172(1–2), pp. 176-190.e19. Available at: https://doi.org/10.1016/J.CELL.2017.12.031.

Kaya, T. *et al.* (2022) 'CD8+ T cells induce interferon-responsive oligodendrocytes and microglia in white matter aging', *Nature Neuroscience 2022 25:11*, 25(11), pp. 1446–1457. Available at: https://doi.org/10.1038/s41593-022-01183-6.

Kelly, R.D.W. and Cowley, S.M. (2013) 'The physiological roles of histone deacetylase (HDAC) 1 and 2: complex co-stars with multiple leading parts', *Biochemical Society Transactions*, 41(3), pp. 741–749. Available at: https://doi.org/10.1042/BST20130010.

Keren-Shaul, H. *et al.* (2017a) 'A Unique Microglia Type Associated with Restricting Development of Alzheimer's Disease', *Cell*, 169(7), pp. 1276-1290.e17. Available at: https://doi.org/10.1016/J.CELL.2017.05.018.

Kierdorf, K. *et al.* (2013) 'Microglia emerge from erythromyeloid precursors via Pu.1- and Irf8-dependent pathways', *Nature Neuroscience 2013 16:3*, 16(3), pp. 273–280. Available at: https://doi.org/10.1038/nn.3318.

Klappacher, G.W. and Glass, C.K. (2002) 'Roles of peroxisome proliferator-activated receptor gamma in lipid homeostasis and inflammatory responses of macrophages', *Current opinion in lipidology*, 13(3), pp. 305–312. Available at: https://doi.org/10.1097/00041433-200206000-00011.

Kleinnijenhuis, J. *et al.* (2012a) 'Bacille Calmette-Guerin

induces NOD2-dependent nonspecific protection from reinfection via epigenetic reprogramming of monocytes', *Proceedings of the National Academy of Sciences of the United States of America*, 109(43), pp. 17537–17542. Available at: https://doi.org/10.1073/PNAS.1202870109.

Klinger, D. *et al.* (2021) 'Bladder Cancer Immunotherapy by BCG Is Associated with a Significantly Reduced Risk of Alzheimer's Disease and Parkinson's Disease', *Vaccines*, 9(5). Available at: https://doi.org/10.3390/VACCINES9050491.

Knutson, S.K. *et al.* (2008) 'Liver-specific deletion of histone deacetylase 3 disrupts metabolic transcriptional networks', *The EMBO Journal*, 27(7), pp. 1017–1028. Available at: https://doi.org/10.1038/EMBOJ.2008.51.

Kopper, T.J. and Gensel, J.C. (2018) 'Myelin as an inflammatory mediator: Myelin interactions with complement, macrophages, and microglia in spinal cord injury', *Journal of Neuroscience Research*, 96(6), pp. 969–977. Available at: https://doi.org/10.1002/JNR.24114.

Kornberg, R.D. (1974) 'Chromatin structure: A repeating unit of histones and DNA', *Science*, 184(4139), pp. 868–871. Available at: https://doi.org/10.1126/SCIENCE.184.4139.868/ASSET/F767CB17-9373-448B-A058-D0598FEFAF69/ASSETS/SCIENCE.184.4139.868.FP.PNG.

Kotter, M.R. *et al.* (2006a) 'Myelin impairs CNS remyelination by inhibiting oligodendrocyte precursor cell differentiation', *The Journal of neuroscience : the official journal of the Society for Neuroscience*, 26(1), pp. 328–332. Available at: https://doi.org/10.1523/JNEUROSCI.2615-05.2006.

Koval, E.D. *et al.* (2013) 'Method for widespread microRNA-155 inhibition prolongs survival in ALS-model mice', *Human Molecular Genetics*, 22(20), pp. 4127–4135. Available at: https://doi.org/10.1093/HMG/DDT261.

Van De Kraats, C. *et al.* (2014) 'Oxysterols and cholesterol precursors correlate to magnetic resonance imaging measures of neurodegeneration in multiple sclerosis', *Multiple sclerosis (Houndmills, Basingstoke, England)*, 20(4), pp. 412–417. Available at: https://doi.org/10.1177/1352458513499421.

Kühtreiber, W.M. *et al.* (2018) 'Long-term reduction in hyperglycemia in advanced type 1 diabetes: the value of induced aerobic glycolysis with BCG vaccinations', *NPJ vaccines*, 3(1). Available at: https://doi.org/10.1038/S41541-018-0062-8.

Kumar, H., Kawai, T. and Akira, S. (2011) 'Pathogen Recognition by the Innate Immune System', *https://doi.org/10.3109/08830185.2010.529976*, 30(1), pp. 16–34. Available at: https://doi.org/10.3109/08830185.2010.529976.

Laffitte, B.A. *et al.* (2001) 'LXRs control lipid-inducible expression of the apolipoprotein E gene in macrophages and adipocytes', *Proceedings of the National Academy of Sciences*, 98(2), pp. 507–512. Available at: https://doi.org/10.1073/PNAS.98.2.507.

Lambertsen, K.L. *et al.* (2009) 'Microglia protect neurons against ischemia by synthesis of tumor necrosis factor', *The Journal of neuroscience : the official journal of the Society for Neuroscience*, 29(5), pp. 1319–1330. Available at: https://doi.org/10.1523/JNEUROSCI.5505-08.2009.

Lampron, A. *et al.* (2015) 'Inefficient clearance of myelin debris by microglia impairs remyelinating processes', *Journal of Experimental Medicine*, 212(4), pp. 481–495. Available at: https://doi.org/10.1084/JEM.20141656/VIDEO-1.

Lampron, A., Pimentel-Coelho, P.M. and Rivest, S. (2013) 'Migration of Bone Marrow-Derived Cells Into the Central Nervous System in Models of Neurodegeneration', *Journal of Comparative Neurology*, 521(17), pp. 3863–3876. Available at: https://doi.org/10.1002/CNE.23363.

Lampropoulou, V. *et al.* (2016) 'Itaconate Links Inhibition of Succinate Dehydrogenase with Macrophage Metabolic Remodeling and Regulation of Inflammation', *Cell metabolism*, 24(1), pp. 158–166. Available at: https://doi.org/10.1016/J.CMET.2016.06.004.

Langfelder, P. and Horvath, S. (2008) 'WGCNA: An R package for weighted correlation network analysis', *BMC Bioinformatics*, 9(1), pp. 1–13. Available at: https://doi.org/10.1186/1471-2105-9-559/FIGURES/4.

Langmead, B. and Salzberg, S.L. (2012) 'Fast gapped-read alignment with Bowtie 2', *Nature methods*, 9(4), p. 357. Available at: https://doi.org/10.1038/NMETH.1923.

Larbi, A. *et al.* (2006) 'Differential role of lipid rafts in the functions of CD4+ and CD8+ human T lymphocytes with aging', *Cellular Signalling*, 18(7), pp. 1017–1030. Available at: https://doi.org/10.1016/J.CELLSIG.2005.08.016.

Larsen, E.S. *et al.* (2020) 'Bacillus Calmette-Guérin immunotherapy for bladder cancer: a review of immunological aspects, clinical effects and BCG infections', *APMIS : acta pathologica, microbiologica, et immunologica Scandinavica*, 128(2). Available at: https://doi.org/10.1111/APM.13011.

Lassmann, H. (2010) 'Axonal and neuronal pathology in multiple sclerosis: what have we learnt from animal models', *Experimental neurology*, 225(1), pp. 2–8. Available at: https://doi.org/10.1016/J.EXPNEUROL.2009.10.009.

Lassmann, H. and Bradl, M. (2016) 'Multiple sclerosis: experimental models and reality', *Acta Neuropathologica 2016 133:2*, 133(2), pp. 223–244. Available at: https://doi.org/10.1007/S00401-016-1631-4.

Lavin, Y. *et al.* (2014) 'Tissue-Resident Macrophage Enhancer Landscapes Are Shaped by the Local Microenvironment', *Cell*, 159(6), pp. 1312–1326. Available at: https://doi.org/10.1016/J.CELL.2014.11.018.

Lavrnja, I. *et al.* (2017) 'Expression profiles of cholesterol

metabolism-related genes are altered during development of experimental autoimmune encephalomyelitis in the rat spinal cord', *Scientific reports*, 7(1). Available at: https://doi.org/10.1038/S41598-017-02638-8.

LeBoeuf, M. *et al.* (2010) 'Hdac1 and Hdac2 act redundantly to control p63 and p53 functions in epidermal progenitor cells', *Developmental cell*, 19(6), pp. 807–818. Available at: https://doi.org/10.1016/J.DEVCEL.2010.10.015.

Lee, C.K. *et al.* (2004) 'Evidence for nucleosome depletion at active regulatory regions genome-wide', *Nature Genetics 2004 36:8*, 36(8), pp. 900–905. Available at: https://doi.org/10.1038/ng1400.

Lee, H.T. *et al.* (2014) 'Transcription-related element gene expression pattern differs between microglia and macrophages during inflammation', *Inflammation Research*, 63(5), pp. 389–397. Available at: https://doi.org/10.1007/S00011-014-0711-Y/FIGURES/5.

Lee, J. *et al.* (2008) 'Mycobacterium bovis Bacille Calmette-Guérin Infection in the CNS Suppresses Experimental Autoimmune Encephalomyelitis and Th17 Responses in an IFN-gamma-independent Manner', *Journal of immunology (Baltimore, Md. : 1950)*, 181(9), p. 6201. Available at: https://doi.org/10.4049/JIMMUNOL.181.9.6201.

Letiembre, M. *et al.* (2007) 'Innate immune receptor expression in normal brain aging', *Neuroscience*, 146(1), pp. 248–254. Available at: https://doi.org/10.1016/J.NEUROSCIENCE.2007.01.004.

LEVINE, M.I. and SACKETT, M.F. (1946) 'Results of BCG immunization in New York City', *American review of tuberculosis*, 53, pp. 517–532. Available at: https://doi.org/10.1164/ART.1946.53.6.517.

Li, W.W. *et al.* (2006) 'Females remyelinate more efficiently than males following demyelination in the aged but not young adult CNS', *Experimental neurology*, 202(1), pp. 250–254. Available at: https://doi.org/10.1016/J.EXPNEUROL.2006.05.012.

Li, X. *et al.* (2007) 'SIRT1 deacetylates and positively regulates the nuclear receptor LXR', *Molecular cell*, 28(1), pp. 91–106. Available at: https://doi.org/10.1016/J.MOLCEL.2007.07.032.

Li, X. *et al.* (2022) 'Maladaptive innate immune training of myelopoiesis links inflammatory comorbidities', *Cell*, 185(10), pp. 1709-1727.e18. Available at: https://doi.org/10.1016/J.CELL.2022.03.043.

Liao, Y., Smyth, G.K. and Shi, W. (2014) 'featureCounts: an efficient general purpose program for assigning sequence reads to genomic features', *Bioinformatics (Oxford, England)*, 30(7), pp. 923–930. Available at: https://doi.org/10.1093/BIOINFORMATICS/BTT656.

Libert, S. and Guarente, L. (2013) 'Metabolic and Neuropsychiatric Effects of Calorie Restriction and Sirtuins', *https://doi.org/10.1146/annurev-physiol-030212-183800*, 75, pp. 669–684. Available at: https://doi.org/10.1146/ANNUREV-PHYSIOL-030212-183800.

Liggett, T. *et al.* (2010) 'Methylation patterns of cell-free plasma DNA in relapsing-remitting multiple sclerosis', *Journal of the neurological sciences*, 290(1–2), pp. 16–21. Available at: https://doi.org/10.1016/J.JNS.2009.12.018.

Lippens, C. *et al.* (2018) 'Extended freeze-dried BCG instructed pDCs induce suppressive tregs and dampen EAE', *Frontiers in Immunology*, 9(NOV), p. 2777. Available at: https://doi.org/10.3389/FIMMU.2018.02777/BIBTEX.

Liu, G.Y. and Sabatini, D.M. (2020) 'mTOR at the nexus of nutrition, growth, ageing and disease', *Nature Reviews Molecular Cell Biology 2020 21:4*, 21(4), pp. 183–203. Available at: https://doi.org/10.1038/s41580-019-0199-y.

Liu, P.S. *et al.* (2017) 'α-ketoglutarate orchestrates macrophage activation through metabolic and epigenetic reprogramming', *Nature immunology*, 18(9), pp. 985–994. Available at: https://doi.org/10.1038/NI.3796.

Liu, Z. *et al.* (2007) 'Chronic Treatment With Minocycline Preserves Adult New Neurons and Reduces Functional Impairment After Focal Cerebral Ischemia', *Stroke*, 38(1), pp. 146–152. Available at: https://doi.org/10.1161/01.STR.0000251791.64910.CD.

Lloyd, A.F. *et al.* (2019) 'Central nervous system regeneration is driven by microglia necroptosis and repopulation', *Nature neuroscience*, 22(7), pp. 1046–1052. Available at: https://doi.org/10.1038/S41593-019-0418-Z.

Lloyd, A.F. and Miron, V.E. (2019a) 'The pro-remyelination properties of microglia in the central nervous system', *Nature Reviews Neurology 2019 15:8*, 15(8), pp. 447–458. Available at: https://doi.org/10.1038/s41582-019-0184-2.

López-Otín, C. *et al.* (2013) 'The Hallmarks of Aging', *Cell*, 153(6), p. 1194. Available at: https://doi.org/10.1016/J.CELL.2013.05.039.

Love, M.I., Huber, W. and Anders, S. (2014) 'Moderated estimation of fold change and dispersion for RNA-seq data with DESeq2', *Genome biology*, 15(12). Available at: https://doi.org/10.1186/S13059-014-0550-8.

Love, S. (2006) 'Demyelinating diseases', *Journal of Clinical Pathology*, 59(11), p. 1151. Available at: https://doi.org/10.1136/JCP.2005.031195.

Loving, B.A. and Bruce, K.D. (2020) 'Lipid and Lipoprotein Metabolism in Microglia', *Frontiers in Physiology*, 11, p. 393. Available at: https://doi.org/10.3389/FPHYS.2020.00393/BIBTEX.

Lu, L.F. *et al.* (2015) 'A Single miRNA-mRNA Interaction Affects the Immune Response in a Context- and Cell-Type-Specific Manner', *Immunity*, 43(1), pp. 52–64. Available at: https://doi.org/10.1016/J.IMMUNI.2015.04.022.

Lun, A.T.L. and Smyth, G.K. (2016) 'csaw: a Bioconductor package for differential binding analysis of ChIP-seq data using sliding windows', *Nucleic acids research*, 44(5), p. e45. Available at: https://doi.org/10.1093/NAR/GKV1191.

De Maeyer, R.P.H. and Chambers, E.S. (2021a) 'The impact of ageing on monocytes and macrophages', *Immunology Letters*, 230, pp. 1–10. Available at: https://doi.org/10.1016/J.IMLET.2020.12.003.

Marin-Husstege, M. *et al.* (2002) 'Histone deacetylase activity is necessary for oligodendrocyte lineage progression', *The Journal of neuroscience : the official journal of the Society for Neuroscience*, 22(23), pp. 10333–10345. Available at: https://doi.org/10.1523/JNEUROSCI.22-23-10333.2002.

Martin, M. (2011) 'Cutadapt removes adapter sequences from high-throughput sequencing reads', *EMBnet.journal*, 17(1), pp. 10–12. Available at: https://journal.embnet.org/index.php/embnetjournal/article/view/200/479 (Accessed: 2 March 2023).

Mass, E. *et al.* (2016) 'Specification of tissue-resident macrophages during organogenesis', *Science*, 353(6304). Available at: https://doi.org/10.1126/SCIENCE.AAF4238/SUPPL_FILE/MASS.SM.PDF.

Mastorakos, P. and McGavern, D. (2019) 'The anatomy and immunology of vasculature in the central nervous system', *Science Immunology*, 4(37). Available at: https://doi.org/10.1126/SCIIMMUNOL.AAV0492.

Mastronardi, F.G. *et al.* (2006) 'Increased citrullination of histone H3 in multiple sclerosis brain and animal models of demyelination: a role for tumor necrosis factor-induced peptidylarginine deiminase 4 translocation', *The Journal of neuroscience : the official journal of the Society for Neuroscience*, 26(44), pp. 11387–11396. Available at: https://doi.org/10.1523/JNEUROSCI.3349-06.2006.

Masuda, T. *et al.* (2019) 'Spatial and temporal heterogeneity of mouse and human microglia at single-cell resolution', *Nature*, 566(7744), pp. 388–392. Available at: https://doi.org/10.1038/S41586-019-0924-X.

Matsuzaki, G. *et al.* (2021a) 'Mycobacterium bovis BCG-mediated suppression of Th17 response in mouse experimental autoimmune encephalomyelitis', *Immunopharmacology and immunotoxicology*, 43(2), pp. 203–211. Available at: https://doi.org/10.1080/08923973.2021.1878215.

Mattei, D. *et al.* (2017) 'Maternal immune activation results in complex microglial transcriptome signature in the adult offspring that is reversed by minocycline treatment', *Translational Psychiatry 2017 7:5*, 7(5), pp. e1120–e1120. Available at: https://doi.org/10.1038/tp.2017.80.

Maxfield, F.R. and Tabas, I. (2005) 'Role of cholesterol and lipid organization in disease', *Nature*, 438(7068), pp. 612–621. Available at: https://doi.org/10.1038/NATURE04399.

Mayya, V. *et al.* (2019) 'Cutting Edge: Synapse Propensity of Human Memory CD8 T Cells Confers Competitive Advantage over Naive Counterparts', *Journal of immunology (Baltimore, Md. : 1950)*, 203(3), pp. 601–606. Available at: https://doi.org/10.4049/JIMMUNOL.1801687.

McDonald, W.I. *et al.* (2001) 'Recommended diagnostic criteria for multiple sclerosis: guidelines from the International Panel on the diagnosis of multiple sclerosis', *Annals of neurology*, 50(1), pp. 121–127. Available at: https://doi.org/10.1002/ANA.1032.

McGinnis, C.S., Murrow, L.M. and Gartner, Z.J. (2019) 'DoubletFinder: Doublet Detection in Single-Cell RNA Sequencing Data Using Artificial Nearest Neighbors', *Cell Systems*, 8(4), pp. 329-337.e4. Available at: https://doi.org/10.1016/j.cels.2019.03.003.

McGuire, P.J. (2019) 'Mitochondrial Dysfunction and the Aging Immune System', *Biology 2019, Vol. 8, Page 26*, 8(2), p. 26. Available at: https://doi.org/10.3390/BIOLOGY8020026.

Michan, S. and Sinclair, D. (2007) 'Sirtuins in mammals: insights into their biological function', *Biochemical Journal*, 404(1), pp. 1–13. Available at: https://doi.org/10.1042/BJ20070140.

Mills, E.L. *et al.* (2018) 'Itaconate is an anti-inflammatory metabolite that activates Nrf2 via alkylation of KEAP1', *Nature*, 556(7699), pp. 113–117. Available at: https://doi.org/10.1038/NATURE25986.

Minhas, P.S. *et al.* (2019) 'Macrophage de novo NAD+ synthesis specifies immune function in aging and inflammation', *Nature immunology*, 20(1), pp. 50–63. Available at: https://doi.org/10.1038/S41590-018-0255-3.

Miron, V.E. *et al.* (2013a) 'M2 microglia and macrophages drive oligodendrocyte differentiation during CNS remyelination', *Nature Neuroscience 2013 16:9*, 16(9), pp. 1211–1218. Available at: https://doi.org/10.1038/nn.3469.

Mitro, N. *et al.* (2007) 'Insights in the regulation of cholesterol 7α-hydroxylase gene reveal a target for modulating bile acid synthesis', *Hepatology*, 46(3), pp. 885–897. Available at: https://doi.org/10.1002/HEP.21819.

Mitroulis, I. *et al.* (2018a) 'Modulation of Myelopoiesis Progenitors Is an Integral Component of Trained Immunity', *Cell*, 172(1–2), pp. 147-161.e12. Available at: https://doi.org/10.1016/J.CELL.2017.11.034.

Mitroulis, I. *et al.* (2018b) 'Modulation of Myelopoiesis Progenitors Is an Integral Component of Trained Immunity', *Cell*, 172(1–2), pp. 147-161.e12. Available at: https://doi.org/10.1016/J.CELL.2017.11.034.

Moorlag, S.J.C.F.M. *et al.* (2019) 'Non-specific effects of BCG vaccine on viral infections', *Clinical microbiology and infection : the official publication of the European Society of Clinical Microbiology and Infectious Diseases*, 25(12), pp. 1473–1478. Available at: https://doi.org/10.1016/J.CMI.2019.04.020.

Morabito, S. *et al.* (2021) 'Single-nucleus chromatin accessibility and transcriptomic characterization of Alzheimer's disease', *Nature genetics*, 53(8), pp. 1143–1155. Available at: https://doi.org/10.1038/S41588-021-00894-Z.

Mossadegh-Keller, N. *et al.* (2013) 'M-CSF instructs myeloid lineage fate in single haematopoietic stem cells', *Nature 2013 497:7448*, 497(7448), pp. 239–243. Available at: https://doi.org/10.1038/nature12026.

Mrdjen, D. *et al.* (2018) 'High-Dimensional Single-Cell Mapping of Central Nervous System Immune Cells Reveals Distinct Myeloid Subsets in Health, Aging, and Disease', *Immunity*, 48(2), pp. 380-395.e6. Available at: https://doi.org/10.1016/J.IMMUNI.2018.01.011.

Müller, L., Di Benedetto, S. and Pawelec, G. (2019) 'The immune system and its dysregulation with aging', *Subcellular Biochemistry*, 91, pp. 21–43. Available at: https://doi.org/10.1007/978-981-13-3681-2_2/COVER.

Munro, D.A.D., Movahedi, K. and Priller, J. (2022) 'Macrophage compartmentalization in the brain and cerebrospinal fluid system', *Science Immunology*, 7(69). Available at: https://doi.org/10.1126/SCIIMMUNOL.ABK0391.

Murphy, A.J. *et al.* (2011) 'ApoE regulates hematopoietic stem cell proliferation, monocytosis, and monocyte accumulation in atherosclerotic lesions in mice', *The Journal of clinical investigation*, 121(10), pp. 4138–4149. Available at: https://doi.org/10.1172/JCI57559.

Natoli, G. and Ostuni, R. (2019) 'Adaptation and memory in immune responses', *Nature immunology*, 20(7), pp. 783–792. Available at: https://doi.org/10.1038/S41590-019-0399-9.

Neher, J.J. and Cunningham, C. (2019) 'Priming Microglia for Innate Immune Memory in the Brain', *Trends in Immunology*. Elsevier Ltd, pp. 358–374. Available at: https://doi.org/10.1016/j.it.2019.02.001.

Netea, M.G. *et al.* (2015) 'Innate immune memory: a paradigm shift in understanding host defense', *Nature Immunology 2015 16:7*, 16(7), pp. 675–679. Available at: https://doi.org/10.1038/ni.3178.

Netea, M.G. *et al.* (2016a) 'Trained immunity: A program of innate immune memory in health and disease', *Science*, 352(6284), p. 427. Available at: https://doi.org/10.1126/SCIENCE.AAF1098/ASSET/1906CC7D-18B2-4A5A-865D-40C50CB78907/ASSETS/GRAPHIC/352_AAF1098_FA.JPEG.

Netea, M.G. *et al.* (2020a) 'Defining trained immunity and its role in health and disease', *Nature Reviews Immunology 2020 20:6*, 20(6), pp. 375–388. Available at: https://doi.org/10.1038/s41577-020-0285-6.

Netea, M.G., Quintin, J. and Van Der Meer, J.W.M. (2011a) 'Trained immunity: a memory for innate host defense', *Cell host & microbe*, 9(5), pp. 355–361. Available at: https://doi.org/10.1016/J.CHOM.2011.04.006.

Netea, M.G., Quintin, J. and Van Der Meer, J.W.M. (2011b) 'Trained immunity: A memory for innate host defense', *Cell Host and Microbe*, 9(5), pp. 355–361. Available at: https://doi.org/10.1016/j.chom.2011.04.006.

Neumann, H., Kotter, M.R. and Franklin, R.J.M. (2009) 'Debris clearance by microglia: an essential link between degeneration and regeneration', *Brain : a journal of neurology*, 132(Pt 2), pp. 288–295. Available at: https://doi.org/10.1093/BRAIN/AWN109.

Nimmerjahn, A., Kirchhoff, F. and Helmchen, F. (2005) 'Neuroscience: Resting microglial cells are highly dynamic surveillants of brain parenchyma in vivo', *Science*, 308(5726), pp. 1314–1318. Available at: https://doi.org/10.1126/SCIENCE.1110647/SUPPL_FILE/1110647S9.MOV.

Niraula, A., Sheridan, J.F. and Godbout, J.P. (2016) 'Microglia Priming with Aging and Stress', *Neuropsychopharmacology 2017 42:1*, 42(1), pp. 318–333. Available at: https://doi.org/10.1038/npp.2016.185.

Norata, G.D. *et al.* (2015) 'The Cellular and Molecular Basis of Translational Immunometabolism', *Immunity*, 43(3), pp. 421–434. Available at: https://doi.org/10.1016/J.IMMUNI.2015.08.023.

Norden, D.M. and Godbout, J.P. (2013) 'Microglia of the Aged Brain: Primed to be Activated and Resistant to Regulation', *Neuropathology and applied neurobiology*, 39(1), p. 19. Available at: https://doi.org/10.1111/J.1365-2990.2012.01306.X.

Novakovic, B. *et al.* (2016) 'β-Glucan Reverses the Epigenetic State of LPS-Induced Immunological Tolerance', *Cell*, 167(5), pp. 1354-1368.e14. Available at: https://doi.org/10.1016/J.CELL.2016.09.034.

O'Connor, R.A., Wittmer, S. and Dalton, D.K. (2005) 'Infection-induced apoptosis deletes bystander CD4+ T cells: a mechanism for suppression of autoimmunity during BCG infection', *Journal of autoimmunity*, 24(2), pp. 93–100. Available at: https://doi.org/10.1016/J.JAUT.2005.01.005.

Odegaard, J.I. *et al.* (2007) 'Macrophage-specific PPARγ controls alternative activation and improves insulin resistance', *Nature 2007 447:7148*, 447(7148), pp. 1116–1120. Available at: https://doi.org/10.1038/nature05894.

Olah, M. *et al.* (2012) 'Identification of a microglia phenotype supportive of remyelination', *Glia*, 60(2), pp. 306–321. Available at: https://doi.org/10.1002/GLIA.21266.

Old, L.J., Clarke, D.A. and Benacerraf, B. (1959) 'Effect of Bacillus Calmette-Guérin Infection on Transplanted Tumours in the Mouse', *Nature 1959 184:4682*, 184(4682), pp. 291–292. Available at: https://doi.org/10.1038/184291a0.

P. Chou, J. and B. Effros, R. (2013) 'T cell replicative senescence in human aging', *Current pharmaceutical design*, 19(9), pp. 1680–1698. Available at: https://doi.org/10.2174/138161213805219711.

Pace JL, Russell SW, Torres BA, Johnson HM, Gray PW. Recombinant mouse gamma interferon induces the priming

step in macrophage activation for tumor cell killing. J Immunol. 1983 May;130(5):2011-3. PMID: 6403616.

Pal, S. and Tyler, J.K. (2016) 'Epigenetics and aging', *Science Advances*, 2(7). Available at: https://doi.org/10.1126/SCIADV.1600584.

Palin, K. *et al.* (2008a) 'Systemic inflammation switches the inflammatory cytokine profile in CNS Wallerian degeneration', *Neurobiology of disease*, 30(1), pp. 19–29. Available at: https://doi.org/10.1016/J.NBD.2007.11.012.

Paolicelli, R.C. *et al.* (2011) 'Synaptic pruning by microglia is necessary for normal brain development', *Science*, 333(6048), pp. 1456–1458. Available at: https://doi.org/10.1126/SCIENCE.1202529/SUPPL_FILE/PAOLICELLI.SOM.PDF.

Paolillo, A. *et al.* (2003) 'The effect of Bacille Calmette-Guérin on the evolution of new enhancing lesions to hypointense T1 lesions in relapsing remitting MS', *Journal of neurology*, 250(2), pp. 247–248. Available at: https://doi.org/10.1007/S00415-003-0967-6.

Park, S.Y. and Kim, J.S. (2020) 'A short guide to histone deacetylases including recent progress on class II enzymes', *Experimental & Molecular Medicine 2020 52:2*, 52(2), pp. 204–212. Available at: https://doi.org/10.1038/s12276-020-0382-4.

Patel, J.R. and Klein, R.S. (2011) 'Mediators of oligodendrocyte differentiation during remyelination', *FEBS letters*, 585(23), pp. 3730–3737. Available at: https://doi.org/10.1016/J.FEBSLET.2011.04.037.

Patil, V.S., Zhou, R. and Rana, T.M. (2014) 'Gene regulation by non-coding RNAs', *http://dx.doi.org/10.3109/10409238.2013.844092*, 49(1), pp. 16–32. Available at: https://doi.org/10.3109/10409238.2013.844092.

Pearl, R. (1928) 'On the Pathological Relations Between Cancer and Tuberculosis.', *https://doi.org/10.3181/00379727-26-4143*, 26(1), pp. 73–75. Available at: https://doi.org/10.3181/00379727-26-4143.

Pedre, X. *et al.* (2011) 'Changed histone acetylation patterns in normal-appearing white matter and early multiple sclerosis lesions', *The Journal of neuroscience : the official journal of the Society for Neuroscience*, 31(9), pp. 3435–3445. Available at: https://doi.org/10.1523/JNEUROSCI.4507-10.2011.

Penkov, S. *et al.* (2019) 'Immunometabolic Crosstalk: An Ancestral Principle of Trained Immunity?', *Trends in immunology*, 40(1), pp. 1–11. Available at: https://doi.org/10.1016/J.IT.2018.11.002.

Perdiguero, E.G. and Geissmann, F. (2015) 'The development and maintenance of resident macrophages', *Nature Immunology 2016 17:1*, 17(1), pp. 2–8. Available at: https://doi.org/10.1038/ni.3341.

Perry, V.H. (2007) 'Stress primes microglia to the presence of systemic inflammation: Implications for environmental influences on the brain', *Brain, Behavior, and Immunity*, 21(1), pp. 45–46. Available at: https://doi.org/10.1016/J.BBI.2006.08.004.

Perry, V.H. and Holmes, C. (2014) 'Microglial priming in neurodegenerative disease', *Nature reviews. Neurology*, 10(4), pp. 217–224. Available at: https://doi.org/10.1038/NRNEUROL.2014.38.

Perry, V.H., Matyszak, M.K. and Fearn, S. (1993) 'Altered antigen expression of microglia in the aged rodent CNS', *Glia*, 7(1), pp. 60–67. Available at: https://doi.org/10.1002/GLIA.440070111.

Perry, V.H., Nicoll, J.A.R. and Holmes, C. (2010) 'Microglia in neurodegenerative disease', *Nature Reviews Neurology*, pp. 193–201. Available at: https://doi.org/10.1038/nrneurol.2010.17.

Petroff, S.A. and Branch, A. (1928) 'Bacillus Calmette-Guérin (B.C.G.): Animal Experimentation and Prophylactic Immunization of Children', *American journal of public health and the nation's health*, 18(7), pp. 843–864. Available at: https://doi.org/10.2105/AJPH.18.7.843-B.

Phillips, M.C. (2014) 'Molecular mechanisms of cellular cholesterol efflux', *The Journal of biological chemistry*, 289(35), pp. 24020–24029. Available at: https://doi.org/10.1074/JBC.R114.583658.

Plantier, L. *et al.* (2012) 'Activation of sterol-response element-binding proteins (SREBP) in alveolar type II cells enhances lipogenesis causing pulmonary lipotoxicity', *Journal of Biological Chemistry*, 287(13), pp. 10099–10114. Available at: https://doi.org/10.1074/jbc.M111.303669.

Plemel, J.R. *et al.* (2018) 'Mechanisms of lysophosphatidylcholine-induced demyelination: A primary lipid disrupting myelinopathy', *Glia*, 66(2), pp. 327–347. Available at: https://doi.org/10.1002/GLIA.23245.

Plemel, J.R. *et al.* (2020) 'Microglia response following acute demyelination is heterogeneous and limits infiltrating macrophage dispersion', *Science advances*, 6(3). Available at: https://doi.org/10.1126/SCIADV.AAY6324.

Pont-Lezica, L. *et al.* (2014) 'Microglia shape corpus callosum axon tract fasciculation: functional impact of prenatal inflammation', *European Journal of Neuroscience*, 39(10), pp. 1551–1557. Available at: https://doi.org/10.1111/EJN.12508.

Prinz, M. *et al.* (2011) 'Heterogeneity of CNS myeloid cells and their roles in neurodegeneration', *Nature neuroscience*, 14(10), pp. 1227–1235. Available at: https://doi.org/10.1038/NN.2923.

Przanowski, P. *et al.* (2014) 'The signal transducers Stat1 and Stat3 and their novel target Jmjd3 drive the expression of inflammatory genes in microglia', *Journal of Molecular Medicine*, 92(3), pp. 239–254. Available at: https://doi.org/10.1007/S00109-013-1090-5/FIGURES/8.

Pu, A., Stephenson, E.L. and Yong, V.W. (2018) 'The

extracellular matrix: Focus on oligodendrocyte biology and targeting CSPGs for remyelination therapies', *Glia*, 66(9), pp. 1809–1825. Available at: https://doi.org/10.1002/GLIA.23333.

Püntener, U. *et al.* (2012) 'Long-term impact of systemic bacterial infection on the cerebral vasculature and microglia', *Journal of Neuroinflammation*, 9(1), pp. 1–13. Available at: https://doi.org/10.1186/1742-2094-9-146/FIGURES/7.

Qi, X. *et al.* (2017) 'Long non-coding RNA SNHG14 promotes microglia activation by regulating miR-145-5p/PLA2G4A in cerebral infarction', *Neuroscience*, 348, pp. 98–106. Available at: https://doi.org/10.1016/J.NEUROSCIENCE.2017.02.002.

Radman-Livaja, M. and Rando, O.J. (2010) 'Nucleosome positioning: How is it established, and why does it matter?', *Developmental Biology*, 339(2), pp. 258–266. Available at: https://doi.org/10.1016/J.YDBIO.2009.06.012.

Rafalski, V.A. *et al.* (2013) 'Expansion of oligodendrocyte progenitor cells following SIRT1 inactivation in the adult brain', *Nature cell biology*, 15(6), pp. 614–624. Available at: https://doi.org/10.1038/NCB2735.

Raj, D.D.A. *et al.* (2014) 'Priming of microglia in a DNA-repair deficient model of accelerated aging', *Neurobiology of aging*, 35(9), pp. 2147–2160. Available at: https://doi.org/10.1016/J.NEUROBIOLAGING.2014.03.025.

Ramaglia, V. *et al.* (2012) 'C3-dependent mechanism of microglial priming relevant to multiple sclerosis', *Proceedings of the National Academy of Sciences of the United States of America*, 109(3), pp. 965–970. Available at: https://doi.org/10.1073/PNAS.1111924109.

Ramírez, F. *et al.* (2014) 'deepTools: a flexible platform for exploring deep-sequencing data', *Nucleic Acids Research*, 42(Web Server issue), p. W187. Available at: https://doi.org/10.1093/NAR/GKU365.

Rando, T.A. (2006) 'Stem cells, ageing and the quest for immortality', *Nature*, 441(7097), pp. 1080–1086. Available at: https://doi.org/10.1038/NATURE04958.

Ransohoff, R.M. (2016a) 'A polarizing question: do M1 and M2 microglia exist?', *Nature Neuroscience 2016 19:8*, 19(8), pp. 987–991. Available at: https://doi.org/10.1038/nn.4338.

Ransohoff, R.M. (2016b) 'How neuroinflammation contributes to neurodegeneration', *Science*, 353(6301), pp. 777–783. Available at: https://doi.org/10.1126/SCIENCE.AAG2590.

Rawji, K.S. *et al.* (2018) 'Deficient Surveillance and Phagocytic Activity of Myeloid Cells Within Demyelinated Lesions in Aging Mice Visualized by Ex Vivo Live Multiphoton Imaging', *The Journal of neuroscience : the official journal of the Society for Neuroscience*, 38(8), pp. 1973–1988. Available at: https://doi.org/10.1523/JNEUROSCI.2341-17.2018.

Repa, J.J. *et al.* (2000) 'Regulation of Absorption and ABC1-Mediated Efflux of Cholesterol by RXR Heterodimers', *Science*, 289(5484), pp. 1524–1529. Available at: https://doi.org/10.1126/SCIENCE.289.5484.1524.

Ricote, M. *et al.* (1998) 'The peroxisome proliferator-activated receptor-γ is a negative regulator of macrophage activation', *Nature 1998 391:6662*, 391(6662), pp. 79–82. Available at: https://doi.org/10.1038/34178.

Rigamonti, E. *et al.* (2005) 'Liver X receptor activation controls intracellular cholesterol trafficking and esterification in human macrophages', *Circulation research*, 97(7), pp. 682–9. Available at: https://doi.org/10.1161/01.RES.0000184678.43488.9F.

Ristori, G. *et al.* (2014a) 'Effects of Bacille Calmette-Guerin after the first demyelinating event in the CNS', *Neurology*, 82(1), pp. 41–48. Available at: https://doi.org/10.1212/01.WNL.0000438216.93319.AB.

Ristori, G. *et al.* (2018) 'Bridging the gap between vaccination with Bacille Calmette-Guérin (BCG) and immunological tolerance: the cases of type 1 diabetes and multiple sclerosis', *Current Opinion in Immunology*, 55, pp. 89–96. Available at: https://doi.org/10.1016/J.COI.2018.09.016.

Robinson, J.T. *et al.* (2011) 'Integrative genomics viewer', *Nature biotechnology*, 29(1), pp. 24–26. Available at: https://doi.org/10.1038/NBT.1754.

Rodrigues, A. *et al.* (2007) 'Revaccination with Bacillus Calmette-Guerin (BCG) vaccine does not reduce morbidity from malaria in African children', *Tropical medicine & international health : TM & IH*, 12(2), pp. 224–229. Available at: https://doi.org/10.1111/J.1365-3156.2006.01766.X.

Rodrigues, L.P. *et al.* (2021) 'Hallmarks of aging and immunosenescence: Connecting the dots', *Cytokine & growth factor reviews*, 59, pp. 9–21. Available at: https://doi.org/10.1016/J.CYTOGFR.2021.01.006.

Rosenberg, A.B. *et al.* (2018) 'Single-cell profiling of the developing mouse brain and spinal cord with split-pool barcoding', *Science*, 360(6385), pp. 176–182. Available at: https://doi.org/10.1126/SCIENCE.AAM8999/SUPPL_FILE/PAPV2.PDF.

ROSENTHAL, S.R. *et al.* (1961) 'BCG vaccination in tuberculous households', *The American review of respiratory disease*, 84, pp. 690–704. Available at: https://doi.org/10.1164/ARRD.1961.84.5P1.690.

Rossi, D.J., Brady, J.D. and Mohr, C. (2007) 'Astrocyte metabolism and signaling during brain ischemia', *Nature neuroscience*, 10(11), pp. 1377–1386. Available at: https://doi.org/10.1038/NN2004.

Roth, T.L. *et al.* (2013) 'Transcranial amelioration of inflammation and cell death after brain injury', *Nature 2013 505:7482*, 505(7482), pp. 223–228. Available at: https://doi.org/10.1038/nature12808.

Ruckh, J.M. *et al.* (2012) 'Rejuvenation of regeneration in the aging central nervous system', *Cell stem cell*, 10(1), pp. 96–103. Available at: https://doi.org/10.1016/J.STEM.2011.11.019.

Saeed, S. *et al.* (2014a) 'Epigenetic programming of monocyte-to-macrophage differentiation and trained innate immunity', *Science*, 345(6204). Available at: https://doi.org/10.1126/SCIENCE.1251086/SUPPL_FILE/SAEED_SM.PDF.

Safaiyan, S. *et al.* (2016) 'Age-related myelin degradation burdens the clearance function of microglia during aging', *Nature Neuroscience 2016 19:8*, 19(8), pp. 995–998. Available at: https://doi.org/10.1038/nn.4325.

Safaiyan, S. *et al.* (2021) 'White matter aging drives microglial diversity', *Neuron*, 109(7), pp. 1100-1117.e10. Available at: https://doi.org/10.1016/J.NEURON.2021.01.027.

Sahasrabuddhe, V. and Ghosh, H.S. (2022) 'Cx3Cr1-Cre induction leads to microglial activation and IFN-1 signaling caused by DNA damage in early postnatal brain', *Cell reports*, 38(3). Available at: https://doi.org/10.1016/J.CELREP.2021.110252.

Sawcer, S. *et al.* (2011a) 'Genetic risk and a primary role for cell-mediated immune mechanisms in multiple sclerosis', *Nature 2011 476:7359*, 476(7359), pp. 214–219. Available at: https://doi.org/10.1038/nature10251.

Schaafsma, W. *et al.* (2015) 'Long-lasting pro-inflammatory suppression of microglia by LPS-preconditioning is mediated by RelB-dependent epigenetic silencing', *Brain, Behavior, and Immunity*, 48, pp. 205–221. Available at: https://doi.org/10.1016/J.BBI.2015.03.013.

Schafer, D.P. *et al.* (2012) 'Article Microglia Sculpt Postnatal Neural Circuits in an Activity and Complement-Dependent Manner'. Available at: https://doi.org/10.1016/j.neuron.2012.03.026.

Schafer, D.P. and Stevens, B. (2015) 'Microglia Function in Central Nervous System Development and Plasticity', *Cold Spring Harbor Perspectives in Biology*, 7(10), p. a020545. Available at: https://doi.org/10.1101/CSHPERSPECT.A020545.

Schindelin, J. *et al.* (2012) 'Fiji: an open-source platform for biological-image analysis', *Nature Methods 2012 9:7*, 9(7), pp. 676–682. Available at: https://doi.org/10.1038/nmeth.2019.

Schuitemaker, A. *et al.* (2012) 'Microglial activation in healthy aging', *Neurobiology of Aging*, 33(6), pp. 1067–1072. Available at: https://doi.org/10.1016/J.NEUROBIOLAGING.2010.09.016.

Schwartz, K., Lawn, R.M. and Wade, D.P. (2000) 'ABC1 Gene Expression and ApoA-I-Mediated Cholesterol Efflux Are Regulated by LXR', *Biochemical and Biophysical Research Communications*, 274(3), pp. 794–802. Available at: https://doi.org/10.1006/BBRC.2000.3243.

Seto, E. and Yoshida, M. (2014) 'Erasers of Histone Acetylation: The Histone Deacetylase Enzymes', *Cold Spring Harbor Perspectives in Biology*, 6(4). Available at: https://doi.org/10.1101/CSHPERSPECT.A018713.

Sewell, D.L. *et al.* (2003) 'Infection with Mycobacterium bovis BCG diverts traffic of myelin oligodendroglial glycoprotein autoantigen-specific T cells away from the central nervous system and ameliorates experimental autoimmune encephalomyelitis', *Clinical and diagnostic laboratory immunology*, 10(4), pp. 564–572. Available at: https://doi.org/10.1128/CDLI.10.4.564-572.2003.

Shalova, I.N. *et al.* (2015) 'Human Monocytes Undergo Functional Re-programming during Sepsis Mediated by Hypoxia-Inducible Factor-1α', *Immunity*, 42(3), pp. 484–498. Available at: https://doi.org/10.1016/J.IMMUNI.2015.02.001.

Shaw, A.C., Goldstein, D.R. and Montgomery, R.R. (2013) 'Age-dependent dysregulation of innate immunity', *Nature Reviews Immunology 2013 13:12*, 13(12), pp. 875–887. Available at: https://doi.org/10.1038/nri3547.

Shein, N.A. *et al.* (2009) 'Histone deacetylase inhibitor ITF2357 is neuroprotective, improves functional recovery, and induces glial apoptosis following experimental traumatic brain injury', *FASEB journal : official publication of the Federation of American Societies for Experimental Biology*, 23(12), pp. 4266–4275. Available at: https://doi.org/10.1096/FJ.09-134700.

Shein, N.A. and Shohami, E. (2011) 'Histone deacetylase inhibitors as therapeutic agents for acute central nervous system injuries', *Molecular medicine (Cambridge, Mass.)*, 17(5–6), pp. 448–456. Available at: https://doi.org/10.2119/MOLMED.2011.00038.

Shen, S. *et al.* (2008a) 'Age-dependent epigenetic control of differentiation inhibitors is critical for remyelination efficiency', *Nature neuroscience*, 11(9), pp. 1024–1034. Available at: https://doi.org/10.1038/NN.2172.

Shen, S., Li, J. and Casaccia-Bonnefil, P. (2005) 'Histone modifications affect timing of oligodendrocyte progenitor differentiation in the developing rat brain', *The Journal of cell biology*, 169(4), pp. 577–589. Available at: https://doi.org/10.1083/JCB.200412101.

Sheng, J.G., Mrak, R.E. and Griffin, W.S.T. (1998) 'Enlarged and phagocytic, but not primed, interleukin-1 alpha-immunoreactive microglia increase with age in normal human brain', *Acta neuropathologica*, 95(3), pp. 229–234. Available at: https://doi.org/10.1007/S004010050792.

Sierra, A. *et al.* (2007a) 'Microglia derived from aging mice exhibit an altered inflammatory profile', *Glia*, 55(4), pp. 412–424. Available at: https://doi.org/10.1002/GLIA.20468.

Sim, F.J. *et al.* (2002) 'The age-related decrease in CNS remyelination efficiency is attributable to an impairment of both oligodendrocyte progenitor recruitment and

differentiation', *The Journal of neuroscience : the official journal of the Society for Neuroscience*, 22(7), pp. 2451–2459. Available at: https://doi.org/10.1523/JNEUROSCI.22-07-02451.2002.

Smith, K.J., Blakemore, W.F. and McDonald, W.I. (1979) 'Central remyelination restores secure conduction', *Nature*, 280(5721), pp. 395–396. Available at: https://doi.org/10.1038/280395A0.

Smith, M.E. (2001) 'Phagocytic properties of microglia in vitro: implications for a role in multiple sclerosis and EAE', *Microscopy research and technique*, 54(2), pp. 81–94. Available at: https://doi.org/10.1002/JEMT.1123.

Smrkovski, L.L. (1981) 'Effect of route of Mycobacterium bovis BCG administration on induction of suppression of sporozoite immunity in rodent malaria', *Infection and immunity*, 31(1), pp. 408–412. Available at: https://doi.org/10.1128/IAI.31.1.408-412.1981.

Solana, R. *et al.* (2012) 'Innate immunosenescence: Effect of aging on cells and receptors of the innate immune system in humans', *Seminars in Immunology*, 24(5), pp. 331–341. Available at: https://doi.org/10.1016/J.SMIM.2012.04.008.

Stephan, A.H., Barres, B.A. and Stevens, B. (2012) 'The Complement System: An Unexpected Role in Synaptic Pruning During Development and Disease', *https://doi.org/10.1146/annurev-neuro-061010-113810*, 35, pp. 369–389. Available at: https://doi.org/10.1146/ANNUREV-NEURO-061010-113810.

van Strien, M.E. *et al.* (2011) 'Tissue transglutaminase activity is involved in the differentiation of oligodendrocyte precursor cells into myelin-forming oligodendrocytes during CNS remyelination', *Glia*, 59(11), pp. 1622–1634. Available at: https://doi.org/10.1002/GLIA.21204.

Suh, H.S. *et al.* (2010) 'Histone deacetylase inhibitors suppress the expression of inflammatory and innate immune response genes in human microglia and astrocytes', *Journal of Neuroimmune Pharmacology*, 5(4), pp. 521–532. Available at: https://doi.org/10.1007/S11481-010-9192-0/TABLES/1.

Sun, D. *et al.* (2017) 'LncRNA GAS5 inhibits microglial M2 polarization and exacerbates demyelination', *EMBO reports*, 18(10), pp. 1801–1816. Available at: https://doi.org/10.15252/EMBR.201643668.

Supek, F. *et al.* (2011) 'REVIGO Summarizes and Visualizes Long Lists of Gene Ontology Terms', *PLOS ONE*, 6(7), p. e21800. Available at: https://doi.org/10.1371/JOURNAL.PONE.0021800.

Suuronen, T. *et al.* (2003) 'Regulation of microglial inflammatory response by histone deacetylase inhibitors', *Journal of neurochemistry*, 87(2), pp. 407–416. Available at: https://doi.org/10.1046/J.1471-4159.2003.02004.X.

Swinnen, N. *et al.* (2013) 'Complex invasion pattern of the cerebral cortex bymicroglial cells during development of the mouse embryo', *Glia*, 61(2), pp. 150–163. Available at: https://doi.org/10.1002/GLIA.22421.

Swiss, V.A. *et al.* (2011) 'Identification of a gene regulatory network necessary for the initiation of oligodendrocyte differentiation', *PloS one*, 6(4). Available at: https://doi.org/10.1371/JOURNAL.PONE.0018088.

Takahashi, K., Rochford, C.D.P. and Neumann, H. (2005) 'Clearance of apoptotic neurons without inflammation by microglial triggering receptor expressed on myeloid cells-2', *The Journal of experimental medicine*, 201(4), pp. 647–657. Available at: https://doi.org/10.1084/JEM.20041611.

Tang, Y. *et al.* (2013) 'Jmjd3 is essential for the epigenetic modulation of microglia phenotypes in the immune pathogenesis of Parkinson's disease', *Cell Death & Differentiation 2014 21:3*, 21(3), pp. 369–380. Available at: https://doi.org/10.1038/cdd.2013.159.

Tannahill, G.M. *et al.* (2013) 'Succinate is an inflammatory signal that induces IL-1β through HIF-1α', *Nature*, 496(7444), pp. 238–242. Available at: https://doi.org/10.1038/NATURE11986.

Tay, T.L. *et al.* (2017) 'A new fate mapping system reveals context-dependent random or clonal expansion of microglia', *Nature Neuroscience 2017 20:6*, 20(6), pp. 793–803. Available at: https://doi.org/10.1038/nn.4547.

Thomas, R., Wang, W. and Su, D.M. (2020) 'Contributions of Age-Related Thymic Involution to Immunosenescence and Inflammaging', *Immunity & Ageing 2020 17:1*, 17(1), pp. 1–17. Available at: https://doi.org/10.1186/S12979-020-0173-8.

Tontonoz, P. *et al.* (1998) 'PPARγ Promotes Monocyte/Macrophage Differentiation and Uptake of Oxidized LDL', *Cell*, 93(2), pp. 241–252. Available at: https://doi.org/10.1016/S0092-8674(00)81575-5.

Tremblay, M.È. *et al.* (2012) 'Effects of aging and sensory loss on glial cells in mouse visual and auditory cortices', *Glia*, 60(4), pp. 541–558. Available at: https://doi.org/10.1002/GLIA.22287.

Trunz, B.B., Fine, P. and Dye, C. (2006) 'Effect of BCG vaccination on childhood tuberculous meningitis and miliary tuberculosis worldwide: a meta-analysis and assessment of cost-effectiveness', *Lancet (London, England)*, 367(9517), pp. 1173–1180. Available at: https://doi.org/10.1016/S0140-6736(06)68507-3.

Ueno, M. *et al.* (2013) 'Layer V cortical neurons require microglial support for survival during postnatal development', *Nature Neuroscience 2013 16:5*, 16(5), pp. 543–551. Available at: https://doi.org/10.1038/nn.3358.

Vallejo, A.N. (2005) 'CD28 extinction in human T cells: altered functions and the program of T-cell senescence', *Immunological Reviews*, 205(1), pp. 158–169. Available at: https://doi.org/10.1111/J.0105-2896.2005.00256.X.

Vaughan, D.W. and Peters, A. (1974) 'Neuroglial cells in the cerebral cortex of rats from young adulthood to old age: An electron microscope study', *Journal of Neurocytology*, 3(4),

pp. 405–429. Available at: https://doi.org/10.1007/BF01098730/METRICS.

Venkateswaran, A. *et al.* (2000) 'Control of cellular cholesterol efflux by the nuclear oxysterol receptor LXRα', *Proceedings of the National Academy of Sciences*, 97(22), pp. 12097–12102. Available at: https://doi.org/10.1073/PNAS.200367697.

Verma, D. *et al.* (2017) 'Anti-mycobacterial activity correlates with altered DNA methylation pattern in immune cells from BCG-vaccinated subjects', *Scientific reports*, 7(1). Available at: https://doi.org/10.1038/S41598-017-12110-2.

Vetvicka, V., Sima, P. and Vannucci, L. (2021) 'Trained Immunity as an Adaptive Branch of Innate Immunity', *International Journal of Molecular Sciences*, 22(19), p. 10684. Available at: https://doi.org/10.3390/IJMS221910684.

Voß, E.V. *et al.* (2012) 'Characterisation of microglia during de- and remyelination: can they create a repair promoting environment?', *Neurobiology of disease*, 45(1), pp. 519–528. Available at: https://doi.org/10.1016/J.NBD.2011.09.008.

Wake, H. *et al.* (2009) 'Resting microglia directly monitor the functional state of synapses in vivo and determine the fate of ischemic terminals', *The Journal of neuroscience : the official journal of the Society for Neuroscience*, 29(13), pp. 3974–3980. Available at: https://doi.org/10.1523/JNEUROSCI.4363-08.2009.

Wang, J. *et al.* (2017) 'Long Noncoding RNA H19 Promotes Neuroinflammation in Ischemic Stroke by Driving Histone Deacetylase 1–Dependent M1 Microglial Polarization', *Stroke*, 48(8), pp. 2211–2221. Available at: https://doi.org/10.1161/STROKEAHA.117.017387.

Wang, L. *et al.* (2002) 'Liver X receptors in the central nervous system: from lipid homeostasis to neuronal degeneration', *Proceedings of the National Academy of Sciences of the United States of America*, 99(21), pp. 13878–13883. Available at: https://doi.org/10.1073/PNAS.172510899.

Wang, P. *et al.* (2018) 'Sodium butyrate triggers a functional elongation of microglial process via Akt-small RhoGTPase activation and HDACs inhibition', *Neurobiology of Disease*, 111, pp. 12–25. Available at: https://doi.org/10.1016/J.NBD.2017.12.006.

Wang, S. *et al.* (1998) 'Notch receptor activation inhibits oligodendrocyte differentiation', *Neuron*, 21(1), pp. 63–75. Available at: https://doi.org/10.1016/S0896-6273(00)80515-2.

Welch, J.D. *et al.* (2019) 'Single-Cell Multi-omic Integration Compares and Contrasts Features of Brain Cell Identity', *Cell*, 177(7), pp. 1873-1887.e17. Available at: https://doi.org/10.1016/j.cell.2019.05.006.

Wen, Y., Yu, Y. and Fu, X. (2017) 'LncRNA Gm4419 contributes to OGD/R injury of cerebral microglial cells via IκB phosphorylation and NF-κB activation', *Biochemical and Biophysical Research Communications*, 487(4), pp. 923–929. Available at: https://doi.org/10.1016/J.BBRC.2017.05.005.

Wendeln, A.-C. *et al.* (2018) 'innate_memory_microglia_Nat2018', *Nature*, 556(7701), pp. 332–338. Available at: http://www.nature.com/articles/s41586-018-0023-4.

White, F.A. *et al.* (1992) 'JC virus DNA is present in many human brain samples from patients without progressive multifocal leukoencephalopathy', *Journal of virology*, 66(10), pp. 5726–5734. Available at: https://doi.org/10.1128/JVI.66.10.5726-5734.1992.

Williams, A. *et al.* (2007) 'Semaphorin 3A and 3F: key players in myelin repair in multiple sclerosis?', *Brain : a journal of neurology*, 130(Pt 10), pp. 2554–2565. Available at: https://doi.org/10.1093/BRAIN/AWM202.

Witschkowski, J. *et al.* (2020) 'BCG Provides Short-Term Protection from Experimental Cerebral Malaria in Mice', *Vaccines*, 8(4), pp. 1–15. Available at: https://doi.org/10.3390/VACCINES8040745.

Wolswijk, G. (1998) 'Chronic stage multiple sclerosis lesions contain a relatively quiescent population of oligodendrocyte precursor cells', *The Journal of neuroscience : the official journal of the Society for Neuroscience*, 18(2), pp. 601–609. Available at: https://doi.org/10.1523/JNEUROSCI.18-02-00601.1998.

Wolswijk, G. and Noble, M. (1992) 'Cooperation between PDGF and FGF converts slowly dividing O-2Aadult progenitor cells to rapidly dividing cells with characteristics of O-2Aperinatal progenitor cells', *The Journal of cell biology*, 118(4), pp. 889–900. Available at: https://doi.org/10.1083/JCB.118.4.889.

Wu, C.Y. *et al.* (2013) 'Expression of angiotensin II and its receptors in activated microglia in experimentally induced cerebral ischemia in the adult rats', *Molecular and cellular biochemistry*, 382(1–2), pp. 47–58. Available at: https://doi.org/10.1007/S11010-013-1717-4.

Xuan, A. *et al.* (2012) 'Neuroprotective effects of valproic acid following transient global ischemia in rats', *Life sciences*, 90(11–12), pp. 463–468. Available at: https://doi.org/10.1016/J.LFS.2012.01.001.

Yamasaki, R. *et al.* (2014) 'Differential roles of microglia and monocytes in the inflamed central nervous system', *The Journal of experimental medicine*, 211(8), pp. 1533–1549. Available at: https://doi.org/10.1084/JEM.20132477.

Yan, J. *et al.* (2014) 'Obesity- and aging-induced excess of central transforming growth factor-β potentiates diabetic development via an RNA stress response', *Nature Medicine 2014 20:9*, 20(9), pp. 1001–1008. Available at: https://doi.org/10.1038/nm.3616.

Yanes, R.E. *et al.* (2019) 'Metabolic reprogramming in memory CD4 T cell responses of old adults', *Clinical Immunology*, 207, pp. 58–67. Available at:

https://doi.org/10.1016/J.CLIM.2019.07.003.

Ye, F. *et al.* (2009) 'HDAC1 and HDAC2 regulate oligodendrocyte differentiation by disrupting the beta-catenin-TCF interaction', *Nature neuroscience*, 12(7), pp. 829–838. Available at: https://doi.org/10.1038/NN.2333.

Yin, Z. *et al.* (2017) 'Immune hyperreactivity of Aβ plaque-associated microglia in Alzheimer's disease', *Neurobiology of aging*, 55, pp. 115–122. Available at: https://doi.org/10.1016/J.NEUROBIOLAGING.2017.03.021.

Yu, Z. *et al.* (2015) 'MSX3 Switches Microglia Polarization and Protects from Inflammation-Induced Demyelination', *The Journal of neuroscience : the official journal of the Society for Neuroscience*, 35(16), pp. 6350–6365. Available at: https://doi.org/10.1523/JNEUROSCI.2468-14.2015.

Yvan-Charvet, L. *et al.* (2010) 'ATP-binding cassette transporters and HDL suppress hematopoietic stem cell proliferation', *Science (New York, N.Y.)*, 328(5986), pp. 1689–1693. Available at: https://doi.org/10.1126/SCIENCE.1189731.

Zawislak, C.L. *et al.* (2013) 'Stage-specific regulation of natural killer cell homeostasis and response against viral infection by microRNA-155', *Proceedings of the National Academy of Sciences of the United States of America*, 110(17), pp. 6967–6972. Available at: https://doi.org/10.1073/PNAS.1304410110.

Zhang, B. *et al.* (2008) 'HDAC inhibitor increases histone H3 acetylation and reduces microglia inflammatory response following traumatic brain injury in rats', *Brain research*, 1226, pp. 181–191. Available at: https://doi.org/10.1016/J.BRAINRES.2008.05.085.

Zhang, H. *et al.* (2011) 'Central nervous system remyelination in culture — A tool for multiple sclerosis research', *Experimental Neurology*, 230(1), pp. 138–148. Available at: https://doi.org/10.1016/J.EXPNEUROL.2011.04.009.

Zhang, X. *et al.* (2018) 'Macrophage/microglial Ezh2 facilitates autoimmune inflammation through inhibition of Socs3', *Journal of Experimental Medicine*, 215(5), pp. 1365–1382. Available at: https://doi.org/10.1084/JEM.20171417.

Zhang, Y. *et al.* (2001) 'Regulation of Lipoprotein Lipase by the Oxysterol Receptors, LXRα and LXRβ', *Journal of Biological Chemistry*, 276(46), pp. 43018–43024. Available at: https://doi.org/10.1074/jbc.M107823200.

Zhang, Y. *et al.* (2008) 'Model-based analysis of ChIP-Seq (MACS)', *Genome Biology*, 9(9), pp. 1–9. Available at: https://doi.org/10.1186/GB-2008-9-9-R137/FIGURES/3.

Zhang, Z.Y. *et al.* (2007) 'Global hypomethylation defines a sub-population of reactive microglia/macrophages in experimental traumatic brain injury', *Neuroscience Letters*, 429(1), pp. 1–6. Available at: https://doi.org/10.1016/J.NEULET.2007.09.061.

Zhao, C. and Dahlman-Wright, K. (2009) 'Liver X receptor in cholesterol metabolism.', *The Journal of Endocrinology*, 204(3), pp. 233–240. Available at: https://doi.org/10.1677/JOE-09-0271.

Zhao, C., Li, W.W. and Franklin, R.J.M. (2006) 'Differences in the early inflammatory responses to toxin-induced demyelination are associated with the age-related decline in CNS remyelination', *Neurobiology of aging*, 27(9), pp. 1298–1307. Available at: https://doi.org/10.1016/J.NEUROBIOLAGING.2005.06.008.

Zhou, Y. *et al.* (2020) 'Human and mouse single-nucleus transcriptomics reveal TREM2-dependent and TREM2-independent cellular responses in Alzheimer's disease', *Nature medicine*, 26(1), pp. 131–142. Available at: https://doi.org/10.1038/S41591-019-0695-9.

Zorzella-Pezavento, S.F.G. *et al.* (2013) 'BCG and BCG/DNAhsp65 Vaccinations Promote Protective Effects without Deleterious Consequences for Experimental Autoimmune Encephalomyelitis', *Clinical and Developmental Immunology*, 2013. Available at: https://doi.org/10.1155/2013/721383.

Zuo, Z. *et al.* (2017) 'Immunization with Bacillus Calmette-Guérin (BCG) alleviates neuroinflammation and cognitive deficits in APP/PS1 mice via the recruitment of inflammation-resolving monocytes to the brain', *Neurobiology of Disease*, 101, pp. 27–39. Available at: https://doi.org/10.1016/j.nbd.2017.02.001.

List of figures

Abstract

Abstract 1.1: Graphical Abstract

Introduction

Illustration 1.5: Microglia /macrophages at the lesion site in the CNS

Illustration 2.5: Pro-regenerative functions of microglia

Illustration 3.2: Contrasting functions of HDACs in glial cells during neurodegeneration

Illustration 5.2: Epigenetic reprogramming in trained immunity

Illustration 6.1: Overview of lipid metabolism in microglia / macrophages

Hypothesis

Hypothesis 1.1: Illustration to explain the working hypothesis

Results

Figure 1.1: Quality control analysis of snRNA seq experiment

Figure 1.2: Characterization of microglia clusters

Figure 1.3: Single-nucleus RNA-seq to examine distinct cellular response in young and aged white matter (WM) after demyelinating injury

Figure 1.4: Distinct microglia response in young and aged mice post demyelinating injury

Figure 2.1: Epigenomic analysis of young and aged microglia after demyelinating injury

Figure 2.2: Epigenomic analysis of young and aged microglia after demyelinating injury

Figure 3.1: H3K27ac and H3K4me3 epigenetic marks are enriched in the microglia of aged mice treated with BCG

Figure 4.1: BCG immunization promotes lesion recovery after demyelinating injury in aged mice

Figure 4.2: BCG immunization promotes lesion recovery after demyelinating injury in aged mice

Figure 4.3: BCG treatment increases activation and cytokine expression after demyelinating injury

Figure 5.1: Quality control of differential analysis between BCG and Saline (control)

Figure 5.2: Differential transcriptomic analysis of lesions isolated from BCG-treated mice vs. control

Figure 6.1: Differential transcriptomic analysis of lesions isolated from BCG-treated mice vs. control

Figure 6.2: Genetic ablation of HDAC1 and HDAC 2 from aged microglia improves lipid clearance and activation

Figure 7.1: Trained immune response by BCG is abolished in Cx3cr1-HDAC1,2 depleted, aged mice

Appendix

Appendix 1.1: Innate immune training of microglia restores CNS lesion recovery in aged mice

List of tables

Table 1: Resource table

Table 2: Sequence details of all primers used for genotyping

Table 3: Sequence details of all primers used for RT-qPCR analysis

Table 4: The following thermocycler steps were performed to amplify the *Cx3cr1* ^{creERT2}gene

Table 5: The following thermocycler steps were performed to amplify the *HDAC1* ^{flox} gene

Table 6: The following thermocycler steps were performed to amplify the *HDAC2* ^{flox} gene

List of abbreviations

ABCA1: ATP- binding cassete transporter A1
ABCG1: ATP- binding cassete transporter G1
AD: Alzheimer's disease
ADEM: Acute disseminated encephalomyelitis
AHL: Acute hemorrhagic leukoencephalitis
ALS: Amylotropic lateral sclerosis
APP: Amyloid precursor protein
APOA1: Apolipoprotein A1
APOC: Apolipoprotein C
APOE: Apolipoprotein E
ARG1: Arginase1
ATAC seq- Assay for transposase accessible chromatin using sequencing
ATF3: Activating transcription factor 3
BAM: Border associated macrophages
BBB: Blood brain barrier
BCG: Bacillus Calmette Guerin
BCS: Bovine calf serum
BMDMs: Bone marrow derived macrophages
BSA: Bovine serum albumin
CD4: Cluster of differentiation 4
CD8: Cluster of differentiation 8
CD11b: Cluster of differentiation 11b
CD11c: Cluster of differentiation 11c
CD14: Cluster of differentiation 14
CD16: Cluster of differentiation 16
CD28: Cluster of differentiation 28
CD32: Cluster of differentiation 32
CD33: Cluster of differentiation 33
CD36: Cluster of differentiation 36
CD68: Cluster of differentiation 68
CD131: Cluster of differentiation 131
CD206: Cluster of differentiation 206
CCl12: Chemokine (C-C motif) ligand 12
CCR2: Chemokine receptor 2
CE: Cholesterol esters
CHIP seq: Chromatin immunoprecipitation using sequencing
CLEC7A: C-type lectin domain containing 7A
CNS: Central nervous system
CoA: Coenzyme
COX2: Cyclooxygenase2
CPM: Central pontine myelitis
CYP7A1: Cholesterol 7 alpha-hydroxylase
CR2: Complement receptor 2
CR3: Complement receptor 3
CR5: Complement receptor 5
CSF: Cerebrospinal fluid
CSF1R: Colony stimulating factor 1
CX3CR1: CX3C chemokine receptor 1, also known as fractalkine receptor or G protein coupled receptor 13
DAM: Disease associated microglia
DCs: Dendritic cells
DEG: Differentially expressed genes
DNMTs: DNA methyl transferases
Dpi: days post injection
EAE : Experimental auto-immune encephalomyelitis
EMPs : Erythromyeloid precursor cells
EPM: Extra pontine myelitis
ER: Endoplasmic reticulum
EZH2: Enhancer of zeste homolog 2
FDA: Food and drug administration
fMLP: formyl-methionine-leucine phenyl-alanine
GFP: Green fluorescent protein
GM-CSF: Granulocyte-macrophage colony-stimulating factor
GO: Gene ontology
H2A: Histone 2A
H2B: Histone 2B
H3: Histone 3
H4: Histone 4
H3K4me3: Tri-methylation at the 4th lysine residue of the histone H3 protein
H3K4me1: Mono-methylation at the 4th lysine Residue of the histone H3 protein
H3K27ac: Acetylation of the lysine residue at N-terminal position 27 of the histone H3 protein
H3K27me3: Tri-methylation at the 27th lysine residue of the histone H3 protein
HATs: Histone acetyltransferases
HDAC1: Histone deacetylase 1
HDAC2: Histone deacetylase 2
HDAC3: Histone deacetylase 3
HDAC4: Histone deacetylase 4
HDAC5: Histone deacetylase 5
HDAC6: Histone deacetylase 6
HDAC7: Histone deacetylase 7
HDAC8: Histone deacetylase 8
HDAC9: Histone deacetylase 9
HDAC10: Histone deacetylase 10
HDAC11: Histone deacetylase 11
HDL: High density lipoprotein
HDMs: Histone demethylases
HGF: Hepatocyte growth factor
HIF-1: Hypoxia-inducible factor 1
HIV: Human immunodeficiency virus
HMG-CoA: β-hydroxy β-methylglutaryl-CoA
HMTs: Histone methyl transferases
HSCs: Hematopoietic stem cells

HSP: Heat shock protein
HSPCs: Hematopoietic stem and progenitor cells
IBA1: Ionized calcium binding adapter molecule 1, also known as allograft inflammatory factor 1, AIF1
IFNγ: Interferon-γ
IGF-1: Insulin growth factor 1
IIM: Innate immune memory
IL-1: Interleukin 1
IL-2: Interleukin 2
IL-4: Interleukin 4
IL-6: Interleukin 6
IL-1β: Interleukin 1β
IL-3: Interleukin 3
IL-10: Interleukin 10
IL-12: Interleukin 12
IL-17: Interleukin 17
ILCs: Innate lymphoid cells
iNMF: Integrative non-matrix factorization
iNOS: inducible nitric oxide synthase
i.p.: intra peritoneal
IRM: Injury responsive microglia
i.v: intra venous
IPL: Immune gene priming lncRNA
IRG1: Immune responsive gene 1
ITGAX: Integrin subunit alpha X
JMJD3: Jumonji domain 3
KEGG: Kyoto encyclopedia of genes and genomes
Klra2: Killer cell lectin-like receptor 2
KO: Knock out
LAMP1: Lysosomal- associated membrane protein 1
LDL: Low density lipoprotein
LDLr: Low density lipoprotein receptor
LIGER: Linked inference of Genomic Experimental relationships
LLC: Lysolecithin
LncRNA : long non-coding RNA
LPC : Lyso-phosphatidylcholine
LPS : Lipopolysaccharide
lps: line per second
LPL : Lipoprotein lipase
LXR: Liver X receptor
Lys: Lysine
MAC2: also known as galectin 3
MCMV: Murine cytomegalovirus
MDM: Monocyte derived macrophages
MDSCs: Myeloid derived suppressor cells
MEF2C: Myocyte specific enhancer factor 2C
MHCII: Major histocompatibility complex II
MIA: Maternal immune activation
miRNA: micro RNA
MKP1: Mitogen activated protein kinase Phosphatase-1
MPP: Multipotent progenitor population
MRI: Magnetic resonance imaging
MS: Multiple Sclerosis
TCA: Tricarboxylic acid
MTOR: Mammalian target of rapamycin
NAD: Nicotinamide adenine dinucleotide
NK cells: Natural killer cells
NOX-A: NADPH oxidase A
NCoR1: Nuclear receptor co-repressor 1
NOD1: Nucleotide-binding oligomerization domain containing protein 1
NOD2: Nucleotide-binding oligomerization domain containing protein 2
NLR: NOD like receptor
NPC1: Niemann Pick Disease Type C intracellular cholesterol transporter 1
NPC1: Niemann Pick Disease Type C intracellular cholesterol transporter 2
NRF2: Nuclear factor erythroid 2- related factor 2
NVU: Neurovascular unit
OPCs: Oligodendrocyte precursor cells
PBS: Phosphate buffer saline
PD: Parkinson's disease
PDGF: Platelet derived growth factor
PFA: Paraformaldehyde
PI3K: Phosphoinositide 3 kinase
PLs: Phospholipids
PLIN 2: Perilipin 2
PML: Progressive multifocal leukoencephalopathy
PPAR: Peroxisome Proliferator Activator receptor
PRC2: Polycomb repressive complex 2
PRR: Pattern recognition receptors
PVMs: Perivascular macrophages
RLR: Rig-like receptors
RNAPII: RNA polymerase
ROS: Reactive oxygen species
RXR: Retinoid X receptor
SAHA: Suberoylanilide hydroxamic acid
SB: Sodium Butyrate
SIRT1: Sirtuin1
SMRT: Silencing mediator of retinoic acid and thyroid hormone receptor
snRNA seq: Single nucleus RNA sequencing
SOCS1: Suppressor of cytokine signaling 1
SOD1: Superoxide dismutase 1
SRII: Scavenger receptor II
SR-A: Scavenger receptor A
SRE: Sterol regulatory elements
SREBF1: Sterol regulatory element binding transcription factor 1
SREBF2: Sterol regulatory element binding transcription factor 2
SREBP: sterol regulatory element- binding protein
STAT1: Signal transducer and activator of transcription 1
STAT3: Signal transducer and activator of transcription 3
TADs: Topologically associated domains
TBI: Traumatic brain injury

TF: transcription factors
TG: Triglycerides
TGFβ: Transforming growth factor-β
Th1: T helper cell 1
Th17: T helper cell 17
TLR1: Toll-like receptor 1
TLR2: Toll-like receptor 2
TLR3: Toll-like receptor 3
TLR4: Toll-like receptor 4
TLR5: Toll-like receptor 5
TMEM119- Transmembrane protein 119
TNFα- Tumor necrosis factor-α
TREM2: Triggering receptor expressed on myeloid cells 2
TSA: Trichostatin A
TSS: transcription start site
VPA: Valproic acid
YS: Yolk Sac
WGCNA: Weighted gene co-expression network analysis

List of publications

1. **Vini Tiwari,** Bharat Prajapati, Yaw Asare, Alkmini Damkou, Hao Ji, Garyfallia Gouna, Jakub Mieczkowski, Qing Wang, Riki Kawaguchi, Marco Prinz, Mikael Simons '*Innate immune training rejuvenates myeloid responses in the aging central nervous system'* **Immunity (***in revision***)**

2. Felicitas Selter, Tatiana Hetzel, Karla Alex*, Katharina Braun*, Samuel Camenzind*, Rita Dodaro*, Svea Jörgensen*, Erich Linder*, Sara Capas Peneda*, Eva Reihs*, **Vini Tiwari***, Zorana Todorovic*, Hannes Kahrass, Marcel Mertz '*From Ethical Presumptions to conducting animal research to publishing results and back again- Towards a more complete account of Animal research Ethics'* **Nature ethics (***in manuscript preparation***) *** equal contribution

3. Mar Bosch-Queralt, **Vini Tiwari**, Alkmini Damkou, Lenka Vaculčiaková, Ioannis Alexopoulos, Mikael Simons '*A fluorescence microscopy-based protocol for volumetric measurement of lysolecithin lesion- associated de- and remyelination in mouse brain.'* **Star Protocols, 2022** Doi*: https://star-protocols.cell.com/protocols/1407*

4. Horst Penkert, Alix Bertrand, **Vini Tiwari,** Stephan Breimann, Stephan A. Müller, Paul M. Jordan, Mathias J. Gerl, Christian Klose, Dmitrij Frishman, Ludovico Cantuti-Castelvetri, Mar Bosch-Queralt, Ilya Levental, Stefan F. Lichtenthaler, Oliver Werz, Mikael Simons "*Proteomic and lipidomic profiling of demyelinating lesions identifies lipid mediators as modulators in inflammation resolution."* **Cell reports, 2021** Doi: *https://doi.org/10.1016/j.celrep.2021.109898*

5. K.G. Rolland, H. S. Pandey, O. M. Rostand, **V. Tiwari**, K. Diane, P. Singh, D. A. Joseph, P. Seth "*Cytoprotective action of Griffonia simplicifolia (DC.) Baill. against the oxidative stress caused by hydrogen peroxide (H2O2) on neurons and astrocytes*". **GSC Biological and Pharmaceutical Sciences, 2018** Doi*: https://doi.org/10.30574/gscbps.2018.5.2.0093*

Acknowledgements

Although only my name appears on the cover of this dissertation, numerous individuals and institutions have contributed significantly to its completion. I would like to express my heartfelt gratitude to all those who have played a part in making this thesis possible and have made my graduate experience a cherished one. Their unwavering support, guidance, and encouragement have been invaluable throughout my research journey.

First and foremost, I am deeply grateful to my Ph.D. advisor, Prof. Mikael Simons, for giving me the opportunity to work in his lab for my doctoral thesis, delving into the fascinating realm of epigenetic regulation in glia in central nervous system regeneration. I am immensely thankful for his exceptional mentorship, insightful feedback, and continuous support. His expertise, patience, and dedication have been instrumental in shaping this research and fostering my growth as a research scholar. I would like to extend my sincere thanks to the members of my thesis committee, Prof. Martin Kerschensteiner and Prof. Axel Imhof, for their valuable feedback, constructive criticism, and scholarly guidance. Their expertise in their respective fields has significantly enriched the quality of this work. I would also like to express my appreciation to the Graduate School of Systemic Neurosciences at Ludwig Maximilian Universität (GSN-LMU) for providing access to valuable resources, facilities, a conducive research environment, and a wonderful neuroscience community.

Acknowledgment is also due to the financial support provided by TUM, TRR, and SyNergy. Their generous funding has not only enabled me to carry out this research but also provided opportunities to attend conferences and workshops, further enhancing my academic and professional development.

Special gratitude is extended to all the collaborators and colleagues who made immense contributions to this study. I would like to express my heartfelt thanks to Bharat for his invaluable role in teaching me bioinformatic analysis, starting from the basics and guiding me through advanced techniques. I am deeply grateful for his unwavering support, advice, and his expertise in critical dataset analysis. You have not only been an exceptional mentor but also a wonderful friend. Thank you for your extraordinary patience in addressing my never-ending scientific curiosities about analysis. I am also thankful to Yaw for his technical expertise in intravenous injections and enriching discussions on epigenetics. His help and valuable advice made my project run smoothly and efficiently. I express my gratitude to Alkmini, Hao, and Gary for their extremely helpful and patient contributions to this project with their technical expertise. I would also like to thank Katarzyna B Leszczynska, Jakub Mieczkowski, Qing Wang, Riki Kawaguchi, Zechuan Shi, and Vivek Swarup for our fruitful collaboration on high-end sequencing. I am grateful to Prof. Marco Prinz and Ori Staszewski for sharing the HDAC1,2 mouse line, and to Prof. Martin Dichgans and Prof. Ozgun Gökce for their technical feedback and valuable advice. Finally, I want to express my sincere appreciation to the hardworking staff at our animal facility, including Vanessa, Krystyna, Ekrem, Ljiljana, Michelle, Peggy, Steffi, Claudia, Anne, and Manu, for their help and patience, which made working in the facility pleasant and hassle-free and EM facility.

I am grateful to all my colleagues in the lab and beyond for their unwavering support in every possible way. Special thanks to Mar for being an excellent mentor and providing valuable technical feedback, support and advice. I would like to thank Ludo and Minou for their support and willingness to answer

my numerous technical questions throughout my PhD. I am also grateful to Chaitali and Martina Arends for not only assisting me in the lab but also helping me settle in Germany. Thank you, Shima and Maria, for sharing the office space and engaging in insightful conversations. I extend my gratitude to Horst and Alix for sharing their clinical research experience and giving me the opportunity to contribute to their project. Although my interactions with Sebastian and Minhui were brief, I am grateful for their willingness to share their Ph.D. experiences when I was just starting out in the lab. Your insights and guidance were invaluable in those early days. Thank you, Giannis, for developing the macros for lab use. We continue to rely on them for image analysis, and they have been tremendously helpful. I consider myself fortunate to have had all of you as colleagues during the initial years of my Ph.D. journey.

Many more people accompanied me during these years. My wonderful lab colleagues who joined after me also became my friends. Thank you, Alkmini, Jianping, Gary, Lennart, Martin, Shreeya and Swathi, for your positive energy, helpful nature, and for initiating our lab dinners and afternoon lunches at the Mensa. It was a joy to share our lab experiences and more with all of you.

Thankyou Lili, for lending an ear to my complaints and endless queries about GSN, and for pushing me to finish my PhD. I am truly impressed by your long working hours and patience, Seiji and Johanna; there is much to learn from you. Nico, thank you for your patience and vision. Lastly, special thanks to the colleagues who recently joined us, Stefan, Lena, Taisiia, Yan, Simona, and Ruoqing. Your arrival has brought new cheerful energy to our team and fostered a wonderful collaborative environment.

Living abroad presents unique challenges. I am tremendously grateful to Jana for her assistance in helping me settle in Germany. She has been incredibly helpful in extending my residence permits and work contracts, and has always been patient with me whenever I struggled to understand German documents. Additionally, I would like to express my gratitude to UNIKUM student housing for providing me with a delightful and tranquil 5-year stay in Martinsried. I am also thankful to Herr and Frau Berger for generously offering their furnished apartment when I was in search of new housing during my submission of thesis.

Throughout these years, I have made new friends and acquaintances who have nurtured my vision and outlook on life. I am deeply grateful to all of them, with a special mention of Kasturi, Anagh, Varsha, Sreyashi, and Anuradha. Thank you all for the intellectual stimulation, insightful discussions, emotional support, and for staying in touch throughout these years. Your presence and camaraderie have made this research experience more enjoyable and fulfilling. Finally, I would like to express my gratitude to all the unnamed individuals who have contributed to this research in some way but are not explicitly mentioned in this acknowledgment. Your support has been deeply appreciated.

Most importantly, none of this would have been possible without the love and affection of my parents. Thank you, Mummy and Papa, for being a constant source of encouragement, support, and strength throughout these years. Especially during the years when the COVID pandemic gripped the world, and travel was not an option, your constant motivation helped me focus on my research. I am at a loss for words to express the sacrifices you have made without expecting anything in return. I miss you and love you with all my heart.

The most beautiful part of my PhD journey was meeting the love of my life, soon to be my husband, Dr. Ankur Sharma, a brilliant scientist and a wonderful partner. You have made me a better thinker, a better researcher, and a better person in every way. Despite being more than 6000 km away, your

viewpoint, hardworking nature, and dedication has inspired me. You have helped me develop the art of patience. We have shared every moment of joy, happiness, sadness, anger, fear, non-sensical talks, scientific discussions, and research execution. Thank you for believing in me, supporting me, and never giving up on me. I look forward to collaborating and spending the next beautiful years of my life with you.

I dedicate this thesis to my love and my wonderful parents. You are my world.

Affidavit / Eidesstattliche Versicherung

I hereby confirm that the dissertation "Innate immune training restores pro-reparative myeloid functions for remyelination in aged central nervous system" is the result of my own work and that I have only used sources or materials listed and specified in the dissertation.

Hiermit versichere ich an Eides statt, dass ich die vorliegende Dissertation " Innate immune training restores pro-reparative myeloid functions for remyelination in aged central nervous system" selbstständig angefertigt habe, mich außer der angegebenen keiner weiteren Hilfsmittel bedient und alle Erkenntnisse, die aus dem Schrifttum ganz oder annähernd übernommen sind, als solche kenntlich gemacht und nach ihrer Herkunft unter Bezeichnung der Fundstelle einzeln nachgewiesen habe.

München, 26 June 2023 Vini Tiwari

Author contributions

We hereby declare that the following authors contributed to the results of this study in the following manner:

1. Bharat Prajapati helped in bioinformatic analysis for snRNA seq, ATAC seq, Chip Seq and Bulk RNA sequencing
2. Yaw Asare performed intravenous BCG injections in mice
3. Alkmini Damkou performed immunohistochemistry and image acquisition of the samples from BCG immunized and HDAC1,2 KO animals for Cholesterol crystals. In addition, she performed RNA scope experiments for Abca1, Abcg1, Nr1h2 combined with Immunohistochemistry in BCG treated and HDAC1,2 KO mice.
4. Hao Ji processed the samples for library preparation for Bulk RNA seq from PFA fixed lesioned tissue from mouse brain and sequencing and quality control analysis was performed by BGI, China
5. Garyfallia Gouna performed immunohistochemistry for Plin2 in BCG immunized and HDAC1,2 mice. In addition, she helped with stereotactic LPC mouse surgery for one batch of animals
6. Katarzyna B. Leszczyńska and Jakub Mieczkowski processed the samples for ATAC seq experiment and performed sequencing and quality control analysis.
7. Qing Wang and Riki Kawaguchi processed the samples for snRNA seq experiment and performed sequencing and quality control analysis.
8. Zechuan Shi and Vivek Swarup provided technical guidance on Bioinformatic analysis of snRNA seq experiment.
9. Diagenode processed the samples for Chip sequencing and performed quality control analysis.
10. Marco Prinz assisted in providing Cx3cr1 HDAC1,2 KO mice for this study.
11. Martin Dichgans, and Ozgun Gökce provided technical feedback on the overall project.

All other experiments, sample preparations, sample processing, sample analysis, statistical analysis, bioinformatic analysis and data visualization were performed by Vini Tiwari.

Yours Sincerely,

Vini Tiwari Prof. Mikael Simons München, 26 June 2023